Cellular Functions of *myo*-Inositol-Derived Signaling Molecules in Yeast and Plants during Abiotic and Biotic Stresses

Dissertation

der Mathematisch-Naturwissenschaftlichen Fakultät

der Eberhard Karls Universität Tübingen

zur Erlangung des Grades eines

Doktors der Naturwissenschaften

(Dr. rer. nat.)

vorgelegt von

Philipp Johnen

aus Malsch

Tübingen

2019

Gedruckt mit Genehmigung der Mathematisch-Naturwissenschaftlichen Fakultät der Eberhard Karls Universität Tübingen.

Tag der mündlichen Qualifikation:	29.10.2019
Dekan:	Prof. Dr. Wolfgang Rosenstiel
1. Berichterstatter:	Prof. Dr. Gabriel Schaaf
2. Berichterstatter:	Prof. Dr. Klaus Harter
3. Berichterstatter:	Prof. Dr. Edgar Peiter

Danksagung

Nun ist es wirklich an der Zeit Danke zu sagen!

Zuerst möchte ich mich gerne bei Gabriel bedanken. Deine Betreuung war herausragend! Du hast mir den Freiraum gegeben die Projekte eigenständig zu entwickeln und bist mir immer zur Seite gestanden. Ich habe so viel, auf so vielen Ebenen von Dir gelernt. Danke!

Bei der Landesgraduiertenförderung und der Studienstiftung des deutschen Volkes möchte ich mich recht herzlich für die Förderung meiner Forschungsvorhaben bedanken.

Natürlich möchte ich dem Lab Schaaf für die super Atmosphäre, die Hilfe und Unterstützung danken. Danke Deb, Frank, Marília und Philipp G. für die tollen Gespräche und für den immer willkommenen Input (wie oft haben wir überlegt, was Sfh1 denn nun macht). Natürlich möchte ich mich bei Simone, Frank, Jonas und Rosa für die tatkräftige Unterstützung bedanken. Auch den zahlreichen KollaboratorInnen gilt ein großer Dank.

Ein herzlicher Dank geht auch an meine KollegInnen am ZMBP. Ich bin sehr froh, dass ich meine Doktorarbeit an so einem herausragenden Institut machen durfte. Danke Klaus, Claudia, Christopher, Georg, Katharina, Christina und Farid für Euren Input. Dank auch an (alphabetische Reihenfolge) Abhi, Arvid, Corinna, Philipp R., Stephi und Tobi, mann haben wir viel gelacht!

Ein sehr besonderer Dank geht an meine Familie. Mama und Papa vielen Dank, dass ihr immer an mich glaubt, mich unterstützt und für mich da seid!

Last but not least, Margaux ich kann gar nicht in Worte fassen, was Du mir bedeutest! Danke für das Zuhören, Input geben, Meinung sagen, gut Zureden, auf den Boden der Tatsachen zurückholen, Ermuntern, Motivieren, Relativieren, Helfen und all das was ich hier vergessen habe. Was haben wir eine schöne Zeit zusammen!

Naja und das Kleinste zum Schluss. Danke Jan und Mats. Ihr macht jeden Feierabend zu einem kleinen, schönen Abenteuer!

Table of contents

1 Zusammenfassung

Myo-Inositol (Ins)-Derivate sind an einer Reihe von zellulären Prozessen beteiligt. Neben der Rolle als kompatibles Solut bildet Ins das Grundgerüst für eine Vielzahl von Molekülen, welche als Signalmoleküle agieren können. Sowohl lösliche, als auch unlösliche Ins-derivate sind an verschiedenen zellulären Signalwegen beteiligt, von denen einige essential sind. Obwohl zahlreiche Funktionen dieser Molekülklasse in Hefe und Säugetieren beschrieben wurden (z.B. bei Signalweiterleitung bei Phosphatmangel oder der Insulinsignaltransduktion), fängt man in Pflanzen gerade erst an die Rolle dieser Molekülklasse zu verstehen. In meiner Doktorarbeit habe ich die Rolle von Ins-basierten Signalmolekülen bei abiotischem und biotischem Stress untersucht.

Weltweit stellt Aluminium (Al) eine der schwerwiegendsten, abiotischen Einschränkungen für die Getreideproduktion dar. Im Manuskript, Johnen et al., untersuchten wir die Rolle von Ins-basierten Signalmolekülen bei Al-Stress. Wir zeigen, dass die ektopische Expression der Sec14 Homologe, *AtSFH5* und *ScSFH1*, im Modelorganismus Hefe robust Al-Toleranz erzeugt und dass dies sehr wahrscheinlich nicht durch eine Veränderung der Al-Aufnahme oder intrazellulären Kompartimentierung von Al bewirkt wird. Des Weiteren zeigen wir, dass *ScSFH1* (*2μ*) Expression die negative Ladung der Plasmamembran (PM) erhöht, dass in Pflanzen und Hefen eine Erhöhung der Biosynthese von negativ geladenen Phospholipid-spezies zu erhöhter Al-Toleranz führt und dass Al die Lokalisation von ladungsabhängig zur PM-rekrutierter Proteine ändert. Zusammengenommen weisen die Ergebnisse darauf hin, dass die Ladung der PM einen primären Angriffspunkt der Al-Toxizität darstellt. Genetische, zellbiologische und biochemische Experimente weisen darauf hin, dass AtSFH5 und ScSfh1 durch einen *in vivo* Phospholipid-Transfer entweder Menge oder Deprotonierungszustand und damit Aktivität von Phosphatidylinositol-4-Phosphat an der PM erhöhen, und dass dies die beobachtete erhöhte Al-Toleranz verursacht.

Humanpathogene Pilze verursachen invasive Pilzerkrankungen, welche mit sehr hohen Mortalitätsraten assoziiert sind. Zur Behandlung solcher Pilzerkrankungen stehen allerdings nur drei Klassen von Antimykotika zur Verfügung. Daher ist die Entwicklung neuartiger Wirkstoffe dringend nötig. In Pries, Nöcker, Khan, Johnen, Hong et al. (2018) beschreiben wir zwei Chemotypen, Picolinamide und Benzamide, als hochspezifische Inhibitoren von ScSec14 im Modellorganismus *Saccharomyces cerevisiae*, welche Leitstrukturen für die Entwicklung neuer Antimykotika darstellen. Die Identifizierung des Wirkortes gelang durch

eine Kombination von chemogenomischer Profilerstellung, sowie genetischen und biochemischen Experimenten. Die präsentierte Ko-Kristallstruktur eines ScSec14 Proteins mit gebundenem Wirkstoff, stellt die erste ScSec14-Inhibitor-Struktur dar und dient als ideale Grundlage für die effektive Entwicklung neuer Pilzmedikamente.

Inositolpyrophosphate (PP-InsPs) sind eine spezielle Klasse von Ins-Derivaten in denen eine oder mehrere energiereiche Diphosphat- (oder Pyrophosphat-) Gruppen vorhanden sind. In tierischen Systemen und in Hefe wurde gezeigt, dass diese Moleküle bei einer Vielzahl bedeutender zellulärer Prozesse beteiligt sind. Im Gegensatz dazu war die Rolle dieser Molekülklasse in Pflanzen zu Beginn meiner Doktorarbeit weitestgehend unbekannt. In Laha et al. 2015 und Laha et al. 2016, beschreiben wir zwei Proteine in *Arabidopsis thaliana*, AtVIH1 und AtVIH2, als funktionale PPIP5K Homologe, welche die Biosynthese des Ins-PP $InsP_8$ katalysieren. Basierend auf einer Reihe von Experimenten, in denen wir die Toleranz von Pflanzen mit gestörter $InsP_8$ Biosynthese gegenüber herbivoren Fraßfeinden und pilzlichen Pflanzenpathogenen untersuchten, konnten wir zeigen, dass $InsP_8$ eine Rolle bei der pflanzlichen Immunantwort spielt. Konkret zeigen unsere Ergebnisse, dass $InsP_8$ bei der Jasmonsäure (JA)-abhängigen Pathogenantwort beteiligt ist. Hierbei konnten wir zeigen, dass Methyl-JA-Behandlung zur spezifischen Erhöhung von $InsP_8$ in Pflanzen führt und dass Pflanzenlinien mit erniedrigten $InsP_8$ Gehalten erhöhte Konzentrationen aktiver JA-Spezies aufweisen. Zusammen mit diesen Erkenntnissen, weisen Ask1-AtCOI1-AtJAZ1 Re-konstitutionsversuche, Yeast 2-hybrid (Y2H) Studien und *in silico* Docking-Experimente darauf hin, dass der SCF^{AtCOI1} Ko-Rezeptorkomplex $InsP_8$ direkt binden kann und dadurch die JA-Ko-Rezeptor-vermittelte Signalweiterleitung reguliert wird.

Zusammengenommen zeigen die hier präsentierten Ergebnisse die Bedeutung von Ins-basierten Signalmoleküle bei der Reaktion von Pflanzen und Hefe auf abiotischen und biotischen Stress, und erweitern unser Verständnis über die Rolle dieser einzigartigen Molekülklasse.

2 Summary

Myo-Inositol (Ins)-derived molecules are involved in many cellular processes. Besides the role as compatible solute, Ins represents the building block for a variety of molecules, which function as signaling molecules. Cells utilize insoluble (lipid-bound) and soluble Ins derivatives for diverse signal transduction pathways, many of them essential for cell survival. In yeast and mammalian cells, Ins-derived signaling molecules are involved in many processes, such as phosphate starvation or insulin signaling. In plants first insights in the roles of this class of molecules are just emerging. In this work, I address the roles of Ins-derived signaling molecules during abiotic and biotic stress in *Saccharomyces cerevisiae* and *Arabidopsis thaliana*.

In the presented manuscript (Johnen et al., in preparation) the role of Ins derivatives in overcoming aluminum (Al) toxicity, representing a major abiotic limitation for crop production worldwide, was investigated. We report that the ectopic expression of *AtSFH5* and *ScSFH1*, encoding proteins, which belong to the ScSec14 lipid transfer protein family, mediates Al tolerance in the model organism yeast, likely independent from the uptake or compartmentalisation of Al. We show that through expression of *ScSFH1* the negative charge of the plasma membrane (PM) is increased suggesting PM charge as an early toxicity target for Al. This idea is corroborated by yeast and plant genetics, as well as by cell biological analyses, showing that at physiological relevant Al concentrations proper membrane targeting of proteins is impaired and that an increase or a decrease of the PM charge led to higher or lower Al tolerance in yeast and plants, respectively. Based on a combination of cell biological, genetic and biochemical experiments, we propose a model in which AtSFH5 and ScSfh1 mediate in vivo phospholipid transfer, resulting in either increased levels or increased deprotonation state (and thus activity) of phosphatidyl inositol-4-phosphate (PtdIns(4)P) at the PM, thereby leading to an increase in negative PM charge and Al tolerance.

Human fungal pathogens cause invasive fungal infections, which are associated with high morbidity and mortality rates. With only three classes of antifungal drugs in therapeutic use there is a lack of diversity of antifungal agents. In Pries, Nöcker, Khan, Johnen, Hong et al. (2018), we identified two chemotypes, the picolinamides and the benzamides, as specific ScSec14 inhibitors in *S. cerevisiae*, representing lead structures for the development of antifungal drugs. This finding is based on chemogenomic profiling in yeast and is confirmed by genetic and biochemical evidence. The presented co-crystal structure of ScSec14 bound to

a compound belonging to the picolinamide chemotype represents the first structure of inhibitor-bound Sec14 and lays the groundwork for developing new antifungal drugs.

Inositol pyrophosphates (PP-InsPs) are a specific class of Ins derivatives containing one or more high-energy diphosphate (or pyrophosphate) groups. In mammals and yeast these molecules are involved in a variety of cellular processes. In contrast to that, in plants insights in the biosynthesis or the roles of this class of molecules remained elusive at the onset of this work. In Laha et al. (2015) and Laha et al. (2016) we identified two proteins of *A. thaliana*, AtVIH1 and AtVIH2, as functional PPIP5K homologs catalyzing the biosynthesis of the PP-InsP $InsP_8$ *in planta*. Based on a series of bioassays investigating the performance of herbivores and fungal pathogens on plant mutant lines defective inositol polyphosphate biosynthesis, we provide evidence that $InsP_8$ plays a role in tuning the Jasmonic acid (JA)-dependent pathogen defense. Furthermore, it is presented that methyl-JA treatment led to an increase of $InsP_8$ and did not have a major effect on other inositol polyphosphate species. Even though mutant lines with decreased $InsP_8$ levels are more susceptible to plant pathogens, the levels of active JA species are increased compared to wild type plants. Based these findings, combined with Ask1-AtCOI1-AtJAZ reconstitution assays, yeast 2-hyrbid (Y2H) studies and *in silico* docking experiments, we propose that coincidence detection of active JA species and $InsP_8$ by the $SCF1^{AtCOI1}$-AtJAZ co-receptor complex regulates JA signaling and is thereby regulating JA-related plant defenses.

Collectively, the presented data in this work highlight the importance of Ins-derived signaling molecules during abiotic and biotic stress in yeast and plants, and expand our knowledge of the roles of this exciting class of molecules.

3 List of publications

Accepted manuscripts

1. **VIH2 Regulates the Synthesis of Inositol Pyrophosphate InsP8 and Jasmonate-Dependent Defenses in Arabidopsis.**

   Laha, D., Johnen, P.*, Azevedo, C.*, Dynowski, M., Weiss, M., Capolicchio, S., Mao, H., Iven, T., Steenbergen, M., Freyer, M., Gaugler, P., de Campos, M. K., Zheng, N., Feussner, I., Jessen, H. J., Van Wees, S. C., Saiardi, A. and Schaaf, G.

   *These authors contributed equally to this work

   Plant Cell. 2015 Apr;27(4):1082-97. doi: 10.1105/tpc.114.135160.

2. **Inositol Polyphosphate Binding Specificity of the Jasmonate Receptor Complex.**

   Laha, D.*, Parvin, N.*, Dynowski, M., Johnen, P., Mao, H., Bitters, S. T., Zheng, N. and Schaaf, G.

   *These authors contributed equally to this work.

   Plant Physiol. 2016 Aug;171(4):2364-70. doi: 10.1104/pp.16.00694.

3. **Target Identification and Mechanism of Action of Picolinamide and Benzamide Chemotypes with Antifungal Properties.**

   Pries, V.*, Nöcker, C.*, Khan, D.*, Johnen, P.*, Hong, Z.*, Tripathi, A., Keller, A. L., Fitz, M., Perruccio, F., Filipuzzi, I., Thavam, S., Aust, T., Riedl, R., Ziegler, S., Bono, F., Schaaf, G., Bankaitis, V. A., Waldmann, H. and Hoepfner, D.

   *These authors contributed equally to this work.

   Cell Chem Biol. 2018 Mar 15;25(3):279-290.e7. doi: 10.1016/j.chembiol.2017.12.007.

Manuscript (not yet submitted)

1. **Al-tolerance mediated by SEC14-type lipid transfer proteins reveals that membrane charge is both a primary target of Al-toxicity and a tool to increase Al-tolerance in yeast and plants.**

   Johnen, P., Winklbauer, E. M., Herrmann, D., Pankalla, S., Fitz, M., Hagenberg, J., Enderle, B., Martín, H., González, G., Nishimura, T., Krieger, N., Bitters, S.T., Ackermann, F., Richter, S., Stierhof, Y.D., von Wirén, N., Stefan, C.J., Molina, M. and Schaaf, G.

4 Personal contributions

4.1 VIH2 Regulates the Synthesis of Inositol Pyrophosphate $InsP_8$ and Jasmonate-Dependent Defenses in Arabidopsis (Laha et al, 2015).

In this accepted research article, I am listed as second author. For this work, isolated the *vih2-4* mutant line used in Figure 4, 5 and S4 and S6. As biological replicate from data obtained in my master thesis, I performed bioassays with *Pieris rapae* and *Mamestra brassicae* mentioned in Figure 5A and 5B as independent repetition. I performed bioassays with *Botrytis cinerea* and *Alternaria brassicicola*, shown in Figure S6C and D. I performed qPCR analyses as independent repetitions for data shown in Figure 5E. I carried out the statistical analyses of above-mentioned bioassays presented in Figure 5I. Together with Laha, D., I performed plant cultivation and harvesting for measurements of JA-species shown in Figure 5C, 5D and S6A. Together with Laha D, I cloned different mutant variants of AtCOI1 shown in Figure 6.

Laha, D., Van Wees, S. C., Saiardi, A. and Schaaf, G. designed research.

Laha, D. and Schaaf, S. wrote the manuscript.

Laha, D., Johnen, P., Azevedo, C., Dynowski, M., Weiss, M., Zheng, N., Feussner, I., Jessen, H. J., Van Wees, S. C., Saiardi, A. and Schaaf, G revised the article.

4.2 Inositol Polyphosphate Binding Specificity of the Jasmonate Receptor Complex Laha, Parvin et al., 2016).

In this accepted scientific correspondence, I am listed as third author. For this work, I performed bioassays with *Alternaria brassicicola* and *Botrytis cinerea* shown in Figure 1F, S1A and S1B. Additionally I performed protein stability assays of AtCOI1 variants shown in Figure S3. Further, I performed statistical analysis of bioassays shown in Figure 1F, S1A and S1B. Further, I wrote the methods section for the bioassays.

Laha, D., Parvin N. and Schaaf, S. designed research.

Laha, D. and Schaaf, S. wrote the manuscript.

Laha, D., Dynowski, M., Johnen, P., Zheng, N. and Schaaf, G. revised the article.

4.3 Target Identification and Mechanism of Action of Picolinamide and Benzamide Chemotypes with Antifungal Properties (Pries, Nöcker, Khan, Johnen, Hong et al., 2018).

In this accepted research article, I am listed as equally contributing first author. I performed toxicity assays in yeast with ScSec14 and ScSFH1* activation alleles shown in Figure 1F. Further, I performed yeast growth with different mutant versions of ScSec14 shown in Figure S6. Further together with Keller, A.L. and Fitz, M., I expressed and purified ScSec14 protein in *Escherichia coli* and performed protein crystallization trails. Together with Hong Z., I collected diffraction data of obtained crystals at the Swiss Light Source in Villigen. Based on obtained structural data Figure 4D, 4E, S3, S4 and S5 were generated. Further, I wrote the Methods sections for protein purification for crystallization.

Pries, V., Khan, D., Johnen P., Fillipuzze, I., Tripathi, A., Riedl, R. and Sava, Z., designed and performed genetic experiments. Nöcker, C. and Thavam, S. designed, synthesized and analyzed compounds. Johnen P., Keller, A.L. and Fitz, M. conducted crystallization experiments, Hong Z. and Bono F. determined and analyzed the structure, Tripathi A. and Perruccio, F. generated docking poses, Tripathi, A. developed the SAR, conducted the MD simulations, structure-based design, and MedChem Transformation of new analogs. Khan. D. purified Sec14p and the various mutant derivatives and performed the in vitro lipid transfer experiments. Pries V., Bono, F., Schaaf G., Bankaitis, V. and Waldmann, H. and Hoepfner, D. conceived the study, analyzed data, prepared figures and wrote the manuscript.

4.4 Al-tolerance mediated by SEC14-type lipid transfer proteins reveals that membrane charge is both a primary target of Al-toxicity and a tool to increase Al-tolerance in yeast and plants (Johnen et al., in preparation).

In this manuscript I am listed as first author. For this work, I performed yeast growth assays and drew cartoons shown in Figure 1A, 1C, 2A, 2E, 3A, 3B, 4F, 5G, 5K-N, 7A, 8C, 8D, S1E, S2A, S3A, S5B, S7B and S7F. Further, I performed microscopy and subsequent analyses shown in Figure 2H, 2I, 4B-E, 4G, 4H, 5H, 5I, 5L, 7B, 7E, 7G, 8A, 8B, 8F, 8G, 9F-K, S3H, S4A-E, S6B-F, S6H, S7A, S7C, S8A and S8B. Moreover, I drew cartoons for and performed the following experiments, ScMss4 kinase stimulation

assays assays, PtdIns(4,5)P_2 release assays and PL transfer assays with respective analyses of protein stability shown in Figure 3C, 3D, 3F, 3G, 5A, 6A-D and S3C-G. Furthermore, I performed SAX-HPLC-based PIP analysis shown in 3H. Additionally, I performed TLC-based PL analysis shown in Figure 4A, 5C-F and S6A. Furthermore, I performed *in silico* BH-Score analyses shown in Figure 8E. Together with Pankalla S., I performed plant growth assays shown in Figure 9A-E and 9L. Additionally, I drew models shown in Figure 10A, 10B, 11A and 11B.

Johnen, P., Winklbauer E.M. and Schaaf, S. designed research.

Johnen, P. wrote the manuscript.

Schaaf, G. revised the article.

5 Introduction

5.1 Inositols

Inositol and its derivatives represent a variety of different bioactive molecules involved in diverse biological processes, such as cellular signaling, osmoregulation or nutrient storage (Dickson and Hille, 2019; Heilmann and Heilmann, 2015; Michell, 2011; Raboy, 2003). Inositols are cyclohexanehexols with $C_6H_2O_6$ as empirical formula. Their core structure is an all-carbon ring of six carbons each linked to a hydroxyl group. There are 9 isomers of inositol: *myo*- *scyllo*-, *muco*-, D-*chiro*-, L-*chiro*-, *neo*-, *allo*-, *epi*-, and *cis*-inositol. Among these nine isomers, six (*myo*-, *scyllo*-, *epi*-, D-*chiro*-, *neo*- and *muco*- inositol) are found in nature (Michell, 2008). Compared to the other biological relevant isomers, *myo*-inositol (Ins) is representing the far most abundant isomer (Michell, 2008). Ins derivatives are used among all three domains of life, Archaea, Bacteria and Eukarya. In contrast to ubiquitous use and diverse roles in archaea and eukaryotes, only a few bacterial species use Ins and its derivatives (Fahey, 2001; Michell, 2008).

Ins is synthesized from the glycolytic metabolite glucose-6-P (Glc6P). First, the NAD^+-dependent enzyme *myo*-inositol-3-phosphate synthase (MIPS) catalyzes the cyclization of D-Glc6P resulting in D-inositol-3-phosphate (Ins(3)P) (Majumder et al., 1997). Second, the phosphate on the third position is cleaved by inositol monophosphatase (InsPase) resulting in Ins (Chen and Charalam.Fc, 1966). Additional to the Ins synthesis, the uptake of Ins from the environment through Na^+- or H^+-coupled symporters is utilized by different organisms (Wright and Turk, 2004). Dependent on the type of cell, the uptake is tightly regulated by Ins abundance in the environment (Nunez and Henry, 2006) and is in some cases essential for cell survival (Eagle et al., 1957). Based on following parameters: synthesis, uptake and usage of Ins and its derivatives in Archaea, Bacteria and Eukarya, the *MIPS* and *InsPase* genes likely orginated in the Archaea or alternatively in the common ancestor of Archaea and Eukarya (Michell, 2008). In Bacteria, genes necessary for Ins synthesis probably evolved by lateral transfer from Archeae or Eukarya (Michell, 2008).

5.2 Ins derivatives

The importance of Ins in many cellular signaling pathways is linked to the occurrence of the high number of its different derivatives (Michell, 2008). The family of Ins derivatives can be grouped into soluble and insoluble members.

5.2.1 Insoluble Ins derivatives

Members of insoluble Ins derivatives are represented by different lipids with an Ins or Ins derivative containing head group (Michell, 2008). There are two different classes of Ins-containing lipids: i) glycerophospholipids, such as archaetidyl inositol and phosphatidyl inositol and ii) sphingolipids, such as inositol phosphoceramide or mannose inositol phosphoceramide (Michell, 2008). Interestingly, these molecules can act as signal molecules in numerous signaling pathways (De Craene et al., 2017; Dickson, 2010). The best-understood class of Ins-containing lipids is the class of phosphoinositides (PIPs), along with phosphatidylinositol (PtdIns) representing the precursor molecule. PtdIns is synthesized by a class of enzymes with PtdIns synthase (Mamode Cassim et al.) activity, which catalyzes the PtdIns synthesis from cytidine diphosphate diacylglycerol (CDP-DAG) and Ins (Nikawa et al., 1987; Nikawa and Yamashita, 1984). The Ins head group of PtdIns can be phosphorylated at different positions resulting in different PtdIns isomers with a variety of biological activities. So far seven different PIP isomers were identified in nature, which are generated by interplay between kinases and phosphatases regulating Ins phosphorylation at specific positions (De Craene et al., 2017). Enzymes of the PtdIns 3-kinase type III family (*Saccharomyces cerevisiae*: ScVps34, *Homo sapiens*: HsVPS34 and *Arabidopsis thaliana*: AtVPS34) are able to phosphorylate PtdIns at the third position of the Ins ring resulting in PtdIns(3)P (Lee et al., 2008a; Schu et al., 1993; Volinia et al., 1995). PtdIns(3)P is the substrate for a class of PtdIns(3)P 5-kinases (*S. cerevisiae*: ScFab1, *H. sapiens*: HsPIKfyve and *A. thaliana*: AtFAB1a-d) resulting in PtdIns(3,5)P_2 (Bak et al., 2013; Gary et al., 1998; Sbrissa et al., 2000). PtdIns 4-kinases (*S. cerevisiae*: ScStt4, ScPik1, *H. sapiens*: HsPI4Kα, β or *A. thaliana*: PI4Kα1, α2, β1, β2 and γ1-8) phosphorylate the Ins head group of PtdIns on the fourth position resulting in PtdIns(4)P (De Craene et al., 2017; Flanagan et al., 1993; Stevenson et al., 1998; Yoshida et al., 1994). PtdIns(4)P represents the substrate for PtdIns(4) 5-kinases (*S. cerevisiae*: ScMss4, *H. sapiens*: HsPIP5Kiα,β,γ, and *A.thaliana*: AtPIPK5K1-11), which phosphorylate PtdIns(4)P at the fifth position resulting in PtdIns(4,5)P_2 (De Craene et al., 2017; Desrivieres et al., 1998; Mueller-Roeber and Pical, 2002). Furthermore, PtdIns(3,4)P_2 and PtdIns(3,4,5)P_3 can be generated by phosphorylation of the third position of PtdIns(4)P or PtdIns(4,5)P_2 (*S. cerevisiae*: not identified, *H. sapiens*: HsPI3Kα-δ and *A. thaliana*: not identified, (Dickson and Hille, 2019). Interestingly, both PtdIns(3,4)P_2 and PtdIns(3,4,5)P_3 isomers have only been identified in mammalian cells and fission yeast, but have not been found in baker's yeast or plants (Divecha and Halstead, 2004). Recently, the

very low abundant PtdIns(5)P obtained more attention in regard of cellular signaling in mammals (Shisheva, 2013) and was also described in plants (Ndamukong et al., 2010). However, the main biosynthetic route for PtdIns(5)P is still under debate since it is not clear if it mainly occurs via phosphorylation of PtdIns by PtdIns 5-OH kinase or through degradation of PtdIns(4,5P)$_2$ or PtdIns(3,5)P$_2$ by specific PIP phosphatases. Together this shows that not only the synthesis of PIPs via specific kinases is an important process in the PIP biogenesis but also that the degradation of PIPs through PIP phosphatases, removing phosphates at specific positions, is an important factor in PIP homeostasis. In yeast and mammalian organisms, specific phosphatases for the third, fourth and fifth position of the Ins head group are described showing that a complex organization of PIPs evolved in these organism (Liu and Bankaitis, 2010). Also plant genomes contain genes encoding for different PIP phosphatases. However their specificity or regulation is still poorly understood (Munnik and Testerink, 2009).

A hallmark and an essential feature for the different PIPs are their cellular distribution. PtdIns is produced at the endoplasmic reticulum (ER) but abundant in all cellular membranes (Bell and Coleman, 1980). In contrast, PtdIns(3)P mainly decorates endosomal membranes. PtdIns(3,5)P2 is mainly found in membranes of multi vesicular bodies/late endosomes and at vacuolar/lysosomal membranes. PtdIns(4)P is located at the trans-Golgi network (TGN) and the plasma membrane (PM). Whereas so far PtdIns(4,5)P$_2$, PtdIns(3,4)P$_2$ and PtdIns(3,4,5)P$_3$ appears to be mainly located at the PM (Posor et al., 2015).

Cellular PIP distribution is partially mediated by the localization of PtdIns/PIP kinases, PIP phosphatases and vesicular trafficking (Sleight, 1987). Even though, spontaneous transfer of phospholipids (PLs) is considered too slow to be of physiological relevance (Sleight, 1987), a class of proteins, the so-called lipid transfer proteins (LTP), evolved to facilitate transfer of PLs (e.g. also PtdIns or PIPs) between membranes through the cytosol (Bankaitis et al., 2010). Thus, LTPs add another layer of complexity for the regulation of the PL/PIP distribution in the cell. Interestingly, LTPs were shown to be important to establish PIP domains in membranes, e.g. for establishing a PtdIns(4,5)P$_2$ domain at tip growing root hairs essential for proper root hair formation (Ghosh et al., 2015). The underlying LTP for tip localization of PtdIns(4,5)P$_2$ in root hairs is a member of the Secretory 14 (Sec14) family. The name giving member of this family, ScSec14, is involved in increasing PtdIns(4)P at the TGN, which is essential for vesicle formation at the TGN (Fang et al., 1996). Based on the observations that ScSec14 transfers phosphatidyl choline (PtdCho) and PtdIns membrane

bilayers *in vitro* (Bankaitis et al., 1990; Phillips et al., 1999) and that its transfer capabilities of PtdCho and PtdIns has to reside in *cis* (Schaaf et al., 2008), two models for ScSec14 function were proposed: i) the vectorial transfer from PtdIns to the TGN using PtdCho as counter substrate and ii) the presentation of PtdIns to the TGN localized PtdIns 4-kinase ScPik1 through a heterotypic exchange with PtdCho, increasing local PtdIns(4)P synthesis. Till today it is unclear which mechanism reflects the physiological relevant scenario. Recently, another family of LTPs was in the intense focus of research. The family of oxysterol-binding protein related proteins (ORP) is proposed to mediate phosphatidyl serine (PtdSer) and sterol transfer from their origin of biosynthesis, the ER, to the PM fueled by PtdIns(4)P through a heterotypic exchange (Chung et al., 2015; de Saint-Jean et al., 2011; Maeda et al., 2013). Taken together, organisms developed a complex network for the spatiotemporal regulation of PIPs.

So it is not surprising that spatiotemporal regulation of PIPs is crucial for many fundamental cellular processes, such as endocytosis, exocytosis, cell division, cell polarity and many more (Dickson and Hille, 2019; Heilmann, 2016; Heilmann and Heilmann, 2015). Interestingly, involvement of PIPs in the majority of named processes occurs among all eukaryotes (Dickson and Hille, 2019). Looking at the unicellular organism *S. cerevisiae* with its, compared to higher eukaryotes, simple PIP metabolism, the importance of PIPs becomes clear, since each of the three kinases responsible for PtdIns(4)P or PtdIns(4,5)P_2 (ScPik1, ScStt4 and ScMss4) are essential (Desrivieres et al., 1998; Flanagan et al., 1993; Yoshida et al., 1994). Interestingly, even though PIP metabolism is largely similar between yeast, plants and mammals, it also differs in terms of abundance/existence of PIP isomers, e.g. proposed lack of PtdIns(3,4)P_2 and PtdIns(3,4,5)P_3 in baker's yeast and plants or the, compared to yeast and mammalian cells, very low level PtdIns(4,5)P_2 found in the plant PM (Krishnamoorthy et al., 2014). This suggests that different organisms evolved different ways for utilizing the PIP code in the cellular context. Taken together, the spatiotemporal regulation of PIP is essential for cell survival and involved in numerous cellular processes. But how is this PIP code read and processed by cells?

There are three principles described how the PIP code is translated to cellular signaling: i) PIP-binding triggering allosteric changes in target proteins. An example is PtdIns(4,5)P_2-regulated ions channels, which open upon PtdIns(4,5)P_2 binding (Hansen, 2015). ii) Recruitment of proteins to certain membranes either by stereospecific interaction of protein domains with PIP head group or by recruiting proteins containing basic hydrophobic (BH)

domains by affecting overall negative charge of the target membranes. Based on the PIP composition, PIPs are involved in the establishment of specific protein pools at different membranes. Examples for stereospecific PIP-binding motifs are manifold: different pleckstrin homology (PH) domains that mainly bind to PtdIns(4)P, PtdIns(4,5)P_2 or PtdIns(3,4)P_2; FYVE (Fab1, YOTB, Vac1 and EEA1) domains that bind to PtdIns(3)P; β-propellers that bind polyphosphoinositides (PROPPIN) domains that bind to PtdIns(3,5)P_2 or plant homeodomain (PHD) fingers (Streb et al., 1983; Takai et al., 1979) that bind to PtdIns(5)P (Lemmon, 2008). Proteins containing BH domains are manifold, as well. Prominent examples are the HsMARK1 kinase (Moravcevic et al., 2010) and AtPINOID (AtPID) (Simon et al., 2016). iii) PIPs can act as precursor for soluble 2nd messenger molecules. The most famous example for this mechanism is PtdIns(4,5)P_2, representing the precursor for diacylglycerol (DAG) and inositol(1,4,5)P_3 (catalyzed by phospholipase C, PLC) as 2nd messenger molecules involved in Ca^{2+}- and protein kinase c (PKC)-signaling in mammalian cells (Streb et al., 1983).

5.2.2 Soluble Ins derivatives

The example that PtdIns(4,5)P_2 acting as precursor for Ins(1,4,5)P_3 shows that insoluble and soluble Ins derivates are biosynthetically linked. However, two independent biosynthetic routes were described for soluble InsPs: i) the lipid-dependent route generates soluble inositol phosphates (InsPs) by PLC-mediated hydrolysis of PtdIns(4,5)P_2, resulting in the Ins(1,4,5)P_3 isomer representing the precursor for higher phosphorylated InsP species (Tsui and York, 2010) and ii) lipid-independent route, which synthesize the precursor Ins(3)P through the MIPS-dependent synthesis from Glc6P. For biosynthesis of higher phosphorylated InsPs the latter route was only described in slime molds (*Dictyostelium discoideum*) and duckweed (*Spirodela polyrhiza*) (Brearley and Hanke, 1996; Stephens and Irvine, 1990). Till today, the lipid-independent synthesis of InsPs remains poorly understood (Sparvoli and Cominelli, 2015). In contrast, the lipid-dependent InsP biosynthesis pathway is well described. Starting with Ins(1,4,5)P_3 as substrate a dual-specificity InsP_3/InsP_4 6-/3-kinase (*S. cerevisiae*: ScIpk1, *H. sapiens*: HsIPMK and *A. thaliana*: AtIPK2α and β) generates Ins(1,3,4,5,6)P_5 with Ins(1,3,4,5)P4 and Ins(1,4,5,6)P_4 as intermediates (Nalaskowski et al., 2002; Odom et al., 2000; Stevenson-Paulik et al., 2002). Ins(1,3,4,5,6)P_5 represents the substrate for the inositol polyphosphate kinase 1 (IPK1) family (*S. cerevisiae*: ScIpk1, *H. sapiens*: HsIPK1 and *A. thaliana*: AtIPK1), which phosphorylates at the second position resulting in Ins(1,2,3,4,5,6)P_6, a fully phosphorylated Ins ring (Ives et al., 2000; Stevenson-Paulik et al.,

2002; Verbsky et al., 2002). Additionally, in plants and mammalian cells an alternative route for $InsP_6$ biosynthesis was discovered. The Ins(1,3,4)P_3 5/6-kinase family (*H. sapiens*: HsITPK1 and *A. thaliana*: AtIPK1-3) generate Ins(1,3,4,5,6)P_5 from Ins(1,3,4,)P_3 (Shi et al., 2003; Sweetman et al., 2006; Sweetman et al., 2007; Verbsky et al., 2005; Wilson and Majerus, 1997), which is a generated by a phosphate activity of an the inositol polyphosphate 5-phosphatase on Ins(1,3,4,5)P_4 (Tsui and York, 2010). Ins(1,3,4,5,6)P_5 can further be phosphorylated by IPK1 kinases to obtain $InsP_6$. In addition to above mentioned InsP species other isomers exist, which are generated by phosphorylation or dephosphorylation events resulting in a network of more than 20 isomers (Irvine and Schell, 2001). On top of this variety of InsP isomers, in the early 90s the striking discovery of the existence of InsPs with a higher anionic charge than $InsP_6$, referred to as inositol pyrophosphates (PP-InsPs), made by (Menniti et al., 1993; Stephens et al., 1993), increased the family of inositol polyphosphates even further. Two classes of enzymes were described, which mainly are responsible for the biosynthesis of PP-InsPs: The first class, which generates 5PP-$InsP_5$, 5PP-IP_4 or 5PP-IP_3 from $InsP_6$, $InsP_5$ or $InsP_4$ respectively, are members of the $InsP_6$ kinase (IP6K) family (*S. cerevisiae*: ScKcs1, *H. sapiens*: HsIP6K1-3 and *A. thaliana*: not identified). These kinases are able to phosphorylate the already phosphorylated fifth position of $InsP_6$, $InsP_5$ or $InsP_4$ resulting in a pyrophosphate (di-phosphate) moiety at position 5 (5PP-InsPx, (Saiardi et al., 1999; Saiardi et al., 2001). The second class of enzymes are the PP-InsP5 kinases (PPIP5Ks, (IP6Ks, *S. cerevisiae*: ScVip1, *H. sapiens*: HsPPIP5K1/2 and *A. thaliana*: not characterized at the onset of this work), which pyrophosphorylate $InsP_6$ or 5PP-$InsP_5$ at the first position resulting in either 1PP-$InsP_5$ and 1,5PP-$InsP_5$ (Mulugu et al., 2007). Since 5PP-InsP5 represents the main substrate for PPIP5Ks and 1PP-InsP5 is preferentially degraded by diphosphoinositol-polyphosphate phosphohydrolases (*S. cerevisiae*: ScDdp1, *H. sapiens*: DIPP1-4 and *A. thaliana*: not characterized) 5PP-$InsP_5$ and 1,5PP-$InsP_5$ represent the most abundant PP-InsP species in the cell (Safrany et al., 1998). In addition to that, at least *in vitro*, IP6Ks generate tri-phosphate containing molecules (Draskovic et al., 2008; Saiardi et al., 2001). Given the number of the different, phosphate-rich InsP and PP-InsP species, cells consume an immense amount of energy maintaining this network, especially when considering their high turnover rates (Menniti et al., 1993).

For what reasons did cells develop this complex network of InsP and PP-InsP species? i) Soluble derivatives of Ins or Ins itself are used as compatible solutes for protecting cellular processes under osmotic stress situations (Yancey, 2005). ii) $InsP_6$ is used as storage molecule

of phosphate and (Raboy, 2003). iii) InsP and PP-InsPs are involved in the cellular signaling network: InsP isomers can bind proteins specifically resulting in regulation through e.g. allosteric changes (e.g. IP3R representing a Ca^{2+} channel allosterically opened by InsP(1,4,5)P_3 (Hamada et al., 2017), acting as co-factor regulating enzymatic activity (e.g. $InsP_6$ represents the co-factor for the HsADAR2 required for its enzymatic activity mediating in RNA editing (Macbeth et al., 2005) or it might act as ligand/co-ligand, e.g. 1PP-$InsP_5$ was suggested to influence interactions between ScPho80-ScPho85 and ScPho81 involved in the yeast phosphate starvation signaling (Lee et al., 2008b). Interestingly, in plants $InsP_5$ and $InsP_6$ have been suggested to act as co-ligand for regulating interaction between Jasmonate (JA) receptor complex $SCF^{CORONATINE\ INSENSITIVE\ 1}$ (SCF^{COI1})-mediated JASMONATE ZIM-domain (JAZ) (Sheard et al., 2010) and Auxin (IAA) receptor complex $SCF^{TRANSPORT\ INHIBITOR\ RESPONSE\ 1}$ (SCF^{TIR1}) and AUX/IAA (Tan et al., 2007), respectively. iv) PP-InsPs are also proposed to mediate non-enzymatic pyrophosphorylation of proteins via the phosphorylation of an already phosphorylated serine residue (Bhandari et al., 2007). However, the existence and relevance *in vivo* remains controversial (Marmelstein et al., 2018). Taken together, these examples show how cells developed different ways to utilize InsPs and PP-InsPs.

Summarizing the current knowledge of PIPs, InsPs and PP-InsPs clearly shows the importance of the class of Ins-derived molecules. Studying the homeostasis and utilization of them is an exciting, but challenging task and will deepen our knowledge of how complex signaling networks emerged and how interplay of different classes of molecules lay the ground work achieving single cell survival or development of tissues and whole organisms.

6 Objectives

Ins and Ins derivatives are present in all three domains of life, in Archaea, Bacteria and Eukarya. Especially, eukaryotic organisms developed a complex network of Ins-derived molecules consisting of PIPs, InsPs, PP-InPs and other Ins derivatives. Eukaryotic cells utilize this network of molecules for a great variety of processes and its proper regulation is essential for cell survival. Ins-derived molecules often function as signaling molecules regulating diverse cellular signal transduction pathways. Given that Ins derivatives are rich in phosphate and exhibit high turnover rates, the maintenance of the PIP, InsP and PP-IP molecular network is energy costly. Especially during stress situations organisms have to economize their energy consumption. Thus, using a combination of genetics, cell biology and biochemistry in the model organisms *S. cerevisiae* and *A. thaliana*, I aimed to get more insights in the role of Ins-derived signaling molecules in different abiotic and biotic stress situations.

i) Aluminum (Al) toxicity represents one of the biggest abiotic limitations to crop production worldwide. In acidic soils Al becomes soluble and is taken up by the plant subsequently leading to root shortening and loss of yields. Even though, effects of Al toxicity in plants are extensively studied, little is known about cellular targets of Al. Previous work in the Schaaf lab hinted to an involvement of PIPs in an Al tolerance phenotype identified in yeast. The aim of the first part of my thesis was to understand the molecular basis of the identified Al tolerance phenotype in yeast and investigate whether the findings can be applied to plants.

ii) Invasive fungal infections (IFIs) are associated with high mortality rates exceeding death cases caused by tuberculosis or malaria. However, only three compound classes are on the market, which poses a great risk for the development of drug resistant fungal pathogens. Previous findings in the Hoepfner lab at the Novartis Institutes for BioMedical Research (NIBR) led to the identification of two small-molecule inhibitor classes putatively targeting ScSec14, which is essential for cell viability. The aim of the second part of my thesis was to characterize the site of action of identified compounds on a structural level. I expect that these findings will help to evaluate and develop ScSec14 inhibitors as antifungal drugs.

iii) In mammals, the energy-rich class of PP-InsPs is involved in the regulation of signaling networks triggered by different stress situations. However, the biosynthesis and roles of this class of molecules were not yet addressed in plants at the onset of my work. Thus, the aim of the third part of my thesis was to investigate the biosynthesis and identify roles of PP-InsPs *in planta*.

7 Results and discussion

7.1 Abiotic stress

7.1.1 Aluminum-induced Change of Membrane Charge and Lipid Accessibility alters Aluminum Tolerance in Yeast and Plants

Johnen, P., Winklbauer, E. M., Herrmann, D., Pankalla S., Fitz, M., Hagenberg, J., Enderle, B., Martín, H., González, G., Nishimura, T., Krieger, N., Bitters, S.T., Ackermann, F., Richter, S., Stierhof, Y.D., von Wirén, N., Stefan, C.J., Molina, M. and Schaaf, G.

Manuscript in preparation.

7.1.1.1 Summary of results

Stress conditions, caused by drought, heat, salinity or metal toxicity, co-occurring in the field, represent abiotic factors, which can dramatically limit crop production (Lamaoui et al., 2018; Mittler, 2006). Al, the most abundant metal in the earth crust, represents a serious factor for limitations to crop production worldwide (Panda et al., 2009). Al becomes soluble in acidic soils, representing approximately one-third of all arable land. Soluble Al is taken up by plant roots and probably together with Al in the apoplast leads to a dramatic root growth inhibition (Horst et al., 2010; Vonuexkull and Mutert, 1995; Wood et al., 2000). Limitations of crop production in acidic soils are severely influenced by Al toxicity. In spite of intense research for unraveling Al tolerance mechanisms in plants, direct cellular targets for Al causing primary toxicity remain widely elusive. With the work presented in this thesis (manuscript Johnen, et al., in preparation), we propose the charge of the plant PM, mainly driven by a combination of PIPs and phosphatidyl serine, (PtdSer, Platre et al., 2018 and Simon et al., 2016) as a primary cellular toxicity target for Al. This finding is based on a yeast screen and subsequent experiments, which identified that ectopic expression of two members of the ScSec14 LTP family, AtSFH5 and ScSfh1, led to a dramatic increase in Al tolerance in the model organism *S. cerevisiae*. Further analysis led to the model that increased phosphatidyl ethanolamine (PtdEtn) at the PM might increase the levels or accessibility of PtdIns(4)P at the PM, along with an overall increase of electronegative charge. Our data suggest that changes in the lipid composition at the PM might be mediated by a heterotypic exchange of PtdEtn with PtdCho. Microscopic analyses suggested that this transfer might occur between lipid droplets

(LD) monolayer membranes and the PM or between different pools of the PM. Furthermore, we were able to show that abundance of negatively charged PIPs and negatively charged phospholipids (PLs) correlate with Al tolerance and sensitivity in yeast, respectively. Moreover, the same correlation was identified by studying *A. thaliana* mutant lines altered in the metabolism of the negatively charged PLs PtdIns(4)P, PtdIns(4,5)P_2 and PtdSer. Furthermore, Al treatment resulted in a disruption of proper PM targeting mediated by stereospecific lipid binding domains and of charge-dependent membrane recruitment. Based on these findings, we propose that PM charge represents a direct cellular target of Al.

7.1.1.2 Discussion

7.1.1.2.1 Role of PIPs and other negatively charged PLs in the plant Al tolerance

In detail, we show that a conditional increase of the PtdIns(4)P 5-kinase (PI5K) AtPIP5K3 led to an increase of Al tolerance in *A. thaliana*. The observed increases were between 7% and 20 % increase of relative primary root growth. One problem of this approach is that the global increase of PtdIns(4,5)P_2 causes pleiotropic effects in plants (Ischebeck et al., 2013; Kusano et al., 2008). Thus, it will be important to see if a conditional increase of PtdIns(4,5)P_2 or other negatively charged lipids via the expression of lipid biosynthetic genes by promoters regulated by Al abundance, will increase Al tolerance without affecting general plant development. Moreover, it will be important to use Al-induced promoters only active in the root transition zone, which is described as part of the root with the highest Al accumulation. Since Al is linked to several neurodegenerative diseases (Kawahara and Kato-Negishi, 2011), it will be further interesting to test the effects of Al treatment on membrane targeting in mammalian cells, especially on different neuronal cell types.

Furthermore, we were able to show that Al treatment changed the localization of AtPIN FORMED 2 (AtPIN2), which was shown to be regulated by the AtPINOID (AtPID) kinase (Friml et al., 2004; Sukumar et al., 2009). Interestingly, it was proposed that biosynthesis and transport of IAA represent major factors in Al-induced root shortening (Wang et al., 2016; Yang et al., 2014). In the same line it was shown that PIN trafficking is influenced by PtdIns(4,5)P_2 since in a *atpip5k1 atpip5k2* double mutant PIN cycling is disrupted (Ischebeck et al., 2013). Since PIPs directly regulate membrane trafficking in plants (Ischebeck et al., 2013; Lin et al., 2019) it will be interesting to dissect if mislocalization of AtPIN2 during Al treatment is caused by deranged membrane trafficking and/or AtPID localization. One way to address this question would be to enhance PM recruitment of AtPID by e.g. increasing the

positive charge of the basic hydrophobic domain of AtPID (Barbosa et al., 2016) or by fusing a charge independent membrane anchor to AtPID, and to observe if PIN2 localization under Al conditions is altered and is affecting overall root growth behavior. Interestingly, another class of kinases (AtD6PKs) involved in regulation of PIN activity was also shown to harbor a basic hydrophobic (BH) domain (Barbosa et al., 2016). So in future it will be interesting to test the effect of Al on this class of proteins as well.

Moreover, our work shows that membrane targeting of several tested proteins is disturbed after Al treatment. The *Arabidopsis* genome encodes for at least 70 proteins containing putative lipid binding domains mediating stereospecific PL binding (van Leeuwen et al., 2004). On top of this number, the *Arabidopsis* genome encodes proteins containing BH domains mediating charge-dependent membrane recruitment. Unfortunately, up to date there is no analysis available estimating the number of BH domain in *Arabidopsis*. In general in plants, except for proteins directly involved in the metabolism and organization of PLs (Ghosh et al., 2015; Stevenson et al., 1998), little is known about the importance of membrane recruitment by lipid binding domains or BH domain-containing proteins. So in future, there is a desperate need for identification and the functional characterization of plant membrane binding domains to understand the relevance of PL homeostasis in plants. In the same line, it is important to note that the PIP composition of the plant PM differs from yeast and mammalian cells. It was proposed that the PtdIns(4,5)P_2 content of the PM is substantially lower than that of the yeast or mammalian PM (Krishnamoorthy et al., 2014). Furthermore, it is stunning that in contrast to yeast, in which PtdSer represents the main driving force for the negative charge of the PM (Yeung et al., 2008), in plants PtdIns(4)P seems to represent the most important factor (Platre et al., 2018; Simon et al., 2016). In contrast to the classical view on PM-localized PtdIns(4)P only representing the precursor molecule of PtdIns(4,5)P_2, recent evidence suggest that PtdIns(4)P acts as independent signaling molecule (Hammond et al., 2012; Yamamoto et al., 2018). Based on the high level of PtdIns(4)P relative to PtdIns(4,5)P_2 at the plant PM membrane, it will be very interesting to identify differences in the utilization of the two PIPs in comparison to yeast and mammals.

7.1.1.2.2 Aluminum tolerance and cell wall integrity

Furthermore, our results show that AtSFH5-/ScSfh1-mediated Al tolerance requires an intact cell wall integrity (CWI) pathway in yeast and we suggest that increased accessibility of PtdIns(4)P mediates proper localization of essential signaling components of the CWI pathway under Al stress conditions. We also show that Al alone triggers CWI signaling.

Furthermore, we confirmed the reports that described mutants in the CWI pathway to be more sensitive to Al stress (Kakimoto et al., 2005; Schott and Gardner, 1997). Together this data suggests that modulating the composition of the cell wall is an important factor for Al tolerance. This is in accordance to the finding that Al treatment leads to a fast rigidification of the cell wall (Kopittke et al., 2015) and leads to changes in the cell wall composition (Tabuchi and Matsumoto, 2001). Interestingly, the yeast CWI pathway is not conserved in plants. Insights in CWI signaling of plants are just emerging (Voxeur and Hofte, 2016; Wolf, 2017). The *Catharanthus roseus* receptor-like kinase like family, brassinosteroid (BR) signaling and the class of *AtWALL ASSOCIATED KINASEs* (*AtWAKs*) were suggested to be involved in regulating CWI in plants (Kohorn and Kohorn, 2012; Voxeur and Hofte, 2016). Interestingly, the finding that overexpression of *AtWALL ASSOCIATED KINASE 1* (*AtWAK1*) encoding a protein suggested as pectin receptor (Kohorn and Kohorn, 2012) increased Al tolerance in *Arabidopsis* (Sivaguru et al., 2003) suggested a link between CWI and Al tolerance in plants. In future, it will be of great interest to unravel the CWI pathway in plants and to understand its relation to Al stress for finding possibilities to enhance Al tolerance of plants. Additionally, it will be interesting to see if PIPs or other lipids are involved in CWI signaling in plants as well.

7.1.1.2.3 Putative effect of interlipid contacts on PtdIns(4)P accessibility

We propose that PtdEtn is influencing accessibility of PtdIns(4)P at the PM. This is based on the following findings: i) *ScSFH1* (*2μ*) expression significantly increased PM association of the PtdIns(4)P fluorescent lipid-associated reporter (FLARE) GFP-2xPH^{Osh2}, ii) PtdIns(4)P levels are not majorly influenced by *ScSFH1* overexpression, iii) *ScSFH1* overexpression enhanced PtdEtn biosynthesis, iv) a pharmacological approach suggested that *ScSFH1* overexpression increased PtdEtn at the PM, v) preliminary data suggesting that localization of the independent PtdIns(4)P FLARE mCherry-LpP4C is not affected by *ScSFH1* (*2μ*) expression (data not shown) and vi) preliminary results suggesting mutant yeast strains with decreased PtdEtn showed a decrease in PM association of GFP-2xPH^{Osh2}, whereas mCherry-LpP4C was not affected (data not shown). Together these results let us to propose a model in which PtdEtn abundance changes accessibility of PtdIns(4)P for specific PtdIns(4)P binding domains. For the following reasons this is an interesting finding. First, it would show that lipid binding domains, proposed to bind the same PL can have different affinities or can be influenced by the lipid environment and second, it would open the possibility that PtdEtn can affect PtdIns(4)P accessibility without changing PtdIns(4)P levels. Interestingly, for

phosphatidic acid (PtdOH) it was shown that PtdEtn can change its protonation state (Kooijman et al., 2005), thus decreasing its pKa value. Based on this as working hypothesis, we propose that PtdEtn can not only influence the protonation state of PtdOH but also that of PtdIns(4)P. Further we propose that certain lipid binding domains are sensitive to PtdEtn-mediated changes in lipid protonation states and some are insensitive. This further opens the question if the protonation state of PLs other than PtdOH and PtdIns(4)P is influenced by PtdEtn and if pH changes in the cytosol, caused by stress treatments, affect membrane binding of certain lipid binding domains. In future, it will be of great importance to test these hypotheses. The first hypothesis might be addressed by studying the influence of PtdEtn on the pKa value of PtdIns(4)P (and other negatively charged lipids) in artificial liposomes, using nuclear magnetic resonance (NMR) analysis to determine the protonation state of PtdIns(4)P in the presence of PtdEtn. The second hypothesis might be addressed by surface plasmon resonance spectroscopy (SPR) using liposomes containing a fixed PtdIns(4)P concentration, phosphatidyl choline (PtdCho) as structure giving lipid and increasing amounts of PtdEtn. The latter setup would allow us to determine binding affinities of different recombinant lipid binding domains, such as the $2xPH^{ScOsh2}$ or the LcP4C binding domains.

7.1.1.2.4 Membranes putatively involved in AtSFH5-/ScSfh1-mediated PtdEtn transfer

Change in PtdIns(4)P accessibility is not only mediated by overexpression of *ScSFH1* but also by expression of the plant ScSec14 homolog *AtSFH5*. Interestingly, AtSFH5 mainly contains two domains: the SEC14 and the Nlj16 domain. The latter was shown to play a role in lipid-dependent protein recruitment (Ghosh et al., 2015). Using fluorescence microscopy and correlative light and electron microscopy (CLEM), we show that a functional eGFP-AtSFH5 fusion localized to LDs close to the PM and to the PM itself. Localization studies in combination with a PtdIns(4,5)P_2 FLARE suggested localization of eGFP-AtSFH5 at contact sites of the PM and LDs, which are not yet described in yeast or other organisms. These findings gave rise to the working hypothesis that PtdEtn transfer might be mediated between the PM and LDs. Together with the idea that PtdEtn might influence the protonation state of several PM localized lipids this opens the questions if the lipid transfer between LDs and the PM might establish a fast buffer system for lipid accessibility at the PM. This would mean that the monolayer of lipid droplets might represent a storage organelle for PtdEtn and maybe other PLs, which are quickly accessible via lipid transfer proteins. To test this hypothesis, it will be important to test different FLAREs in the *Δare1 Δare2 Δdga1 Δlro1* quadruple mutant

strain completely devoid of LDs and identify lipid transfer proteins endogenously involved in this mechanism.

7.1.1.2.5 Lipid transfer proteins in plants

Our findings suggest a role for AtSFH5 in yeast. However, *A. thaliana atsfh5* (*Atsfh5*) knock out plants did not show any developmental phenotypes or increased sensitivity to Al (our unpublished data). Moreover, expression of *ScSFH1* or overexpression of *AtSFH5* in *A. thaliana* did not increase Al tolerance (our unpublished data). These observations suggest that AtSFH5 might mediate different functions in yeast and plants. The observation that *atsfh5* knock out plants show no obvious defects, suggest that there is redundancy with other AtSFH homologs.

In general, the *Arabidopsis* genome encodes for a variety of lipid transfer homologs. Based on homology, there are 32 proteins with ScSec14 domains, 35 proteins with StAR-related lipid transfer (START) domains and 12 oxysterol binding proteins-related proteins (ORPs) (Kf de Campos and Schaaf, 2017; Schrick et al., 2014; Umate, 2011). Except of a handful of studies addressing the functions of these proteins, very little is known about their importance in plants (Ghosh and Bankaitis, 2011; Huang et al., 2016; Peterman et al., 2004; Schrick et al., 2014; Skirpan et al., 2006; Suzuki et al., 2016). The arguably best-studied plant ScSec14 is AtSFH1. It is shown to regulate PtdIns(4,5)P_2 clustering at the tip of root hairs and is essential for proper root hair formation (Ghosh et al., 2015). It was proposed that this spatial regulation of PtdIns(4,5)P_2 through AtSFH1 is achieved by a combination of AtPIP5K stimulation and oligomerization of AtSFH1 tetramers upon PtdIns(4,5)P_2-mediated neutralization of the AtSFH1^{Nlj16} domain. However, one question still await clarification: Is AtSFH1 stimulating AtPIP5K3? In this line it is interesting to consider our model for AtSFH5 (a Nlj16 domain containing protein very similar in architecture as AtSFH1), which proposes that this SEC14 protein regulates PtdIns(4)P accessibility, and to address the question whether PtdIns(4,5)P_2 accessibility might be changed AtSFH1. Future studies will be necessary for addressing these questions and the general importance of lipid transfer proteins in plants.

7.2 Biotic stress

7.2.1 Target Identification and Mechanism of Action of Picolinamide and Benzamide Chemotypes with Antifungal Properties

Pries, V.*, Nöcker, C.*, Khan, D.*, Johnen, P.*, Hong, Z.*, Tripathi, A., Keller, A. L., Fitz, M., Perruccio, F., Filipuzzi, I., Thavam, S., Aust, T., Riedl, R., Ziegler, S., Bono, F., Schaaf, G., Bankaitis, V. A., Waldmann, H. and Hoepfner, D.

*These authors contributed equally to this work.

7.2.1.1 Summary of results

Invasive fungal infections (IFIs) are associated with high morbidity and mortality rates, and exceed death cases caused by malaria or tuberculosis (Brown et al., 2012). In general, IFIs are no major threat for humans with a healthy immune system. However, for premature infants, patients with advanced age, patients receiving immunosuppressive or suffer from immunosuppressive infections IFIs represent a serious threat, which is reflected in the high IFI-associated morbidity rates (Pfaller et al., 2006). Currently, there are only three compound classes in therapeutic use (azoles, polyenes, and echinocandins). However, for several reasons, such as development of fungal resistances, they are only modestly effective. In Pries, Nöcker, Khan, Johnen, Hong, et al. (2018) we describe two new chemotypes, the picolinamides and benzamides, both of them representing arylamides, as promising leads for the development of new antifungal drugs. Chemogenomic profiling using a small-molecule inhibitor compound archive (Richie et al., 2013) identified a picolinamide-containing compound as inhibitor for *S. cerevisiae* growth not showing any cytotoxicity against human HCT116 cells. Subsequent haploinsufficiency profiling (HIP) and homozygous profiling (HOP) at sub-lethal compound concentrations identified ScSec14 as single putative SMI target. Through performing structure activity relationship (SAR) analysis with a small compound collection besides the picolinamides we identified benzamide chemotypes as potent *S. cerevisiae* growth inhibitors. Subsequent genetic and biochemical analysis revealed ScSec14 as sole target for the identified picolinamide and benzamide compounds. By a directed evolution approach amino acids putatively involved in compound binding were identified and these were confirmed by compound sensitivity growth assays and a co-crystal structure of ScSec14 in complex with the picolinamide compound ~{N}-(1,3-benzodioxol-5-ylmethyl)-5-bromanyl-3-fluoranyl-pyridine-2-carboxamide. Subsequent analysis of the growth inhibitory effects of the two most potent compounds on clinical relevant pathogens

revealed inhibitory effects on growth of *Candida albican*, *C. glabrata* and *Aspergillus brasiliensis* (albeit with a relatively weak effect compared to the positive control Posaconazole). Taken together, the detailed understanding of the site of action of the identified compounds lays the groundwork for the development of more potent SMIs targeting pathogenic Sec14 homologs.

7.2.1.2 Discussion

7.2.1.2.1 Inhibition potency of picolinamides and benzamides on pathogenic ScSec14 homologs

Our study identified presented compounds as effective and highly specific inhibitors for ScSec14. However, inhibitory effects on growth of pathogenic fungi were low. Testing *in vitro* growth inhibition evaluates mitotic growth and does not necessarily correlate with the lack of activity as antifungal agent. First there is still lack of detailed understanding of Sec14 in pathogens and Sec14 proteins were reported to be involved in yeast dimorphism, sporulation and sustaining mycelial growth (Rudge et al., 2004) (Chayakulkeeree et al., 2011; Lopez et al., 1994; Monteoliva et al., 1996; Phillips et al., 2006) representing processes involved in fungal pathogenicity but not in mitotic growth. The sequence homology of pathogenic ScSec14 homologs ranges from 45% to 86%. In our study, we show that the presented compounds did not affect the closely related ScSfh1 (64% similarity). This result suggests that the compounds are highly specific for the ScSec14 but not for closely related homologs even though amino acids of the lipid-binding cavity are highly conserved in Sec14 homologs. Together these observations show that for the development of an efficient antifungal drug based on inhibition of ScSec14 function there is need of the development of more potent Sec14 inhibitors. Interestingly, two other studies identified independent classes of ScSec14 inhibitors (Filipuzzi et al., 2016; Nile et al., 2014). The structural information of the independent inhibitors together with the presented co-crystal structure and our *in silico* analysis with suggestions for inhibitor improvements lay the basis for the development of more potent Sec14 inhibitors with higher antifungal activity. Additionally, structural information of pathogenic Sec14 homologs would be valuable for developing more Sec14-inhibitors for a wide range of Sec14 homologs.

7.2.1.2.2 HOP result as source for understanding ScSec14 function in *S. cerevisiae*

The HOP identified known synthetic interaction with ScSec14. Given the high specificity of the presented inhibitor for ScSec14, the HOP results revealed independent negative synthetic interactions. Thus presented results are a valuable source for further understanding ScSec14 roles in *S. cerevisiae*.

7.2.1.2.3 Development of resistances

As shown in our study, single amino acid changes are sufficient for developing resistant versions of ScSec14. This questions Sec14 as attractive drug target. However, it was shown that ScSec14 by-pass mutant strains showed a deranged lipid metabolism, which likely goes along with reduced fitness and might explain why the relevant residues that render Sec14 susceptible against the inhibitors appear to be conserved in different species. In future, it will be important to test whether amino acid substitutions in ScSec14 causing inhibitor resistance also influence overall fitness of yeast. Furthermore, it was shown that in azole-resistant *C. albicans* strains *ScSFH3* (*PDR16*), a member of the Sec14-family, is overexpressed and increasing azole resistance. Thus, co-treatment of Sec14 inhibitors with antifungal drugs belonging to the azole class might lead to more efficient antifungal treatments.

Taken together, future studies will be necessary to evaluate the potential of Sec14 inhibitors as new class of antifungal drugs.

7.2.2 VIH2 Regulates the Synthesis of Inositol Pyrophosphate $InsP_8$ and Jasmonate-Dependent Defenses in Arabidopsis

Laha, D., Johnen, P., Azevedo, C.*, Dynowski, M., Weiss, M., Capolicchio, S., Mao, H., Iven, T., Steenbergen, M., Freyer, M., Gaugler, P., de Campos, M. K., Zheng, N., Feussner, I., Jessen, H. J., Van Wees, S. C., Saiardi, A. and Schaaf, G.*

**These authors contributed equally to this work*

7.2.2.1 Summary of results

In mammals and in yeast, PP-InsPs act as signal molecules and are described in a variety of signaling pathways. Furthermore, the biosynthesis of these molecules is well understood in mammalian and *S. cerevisiae*. In contrast, the biosynthetic route and possible roles of PP-InsPs in plants remain elusive. In Laha et al (2015) we show that PIP5K homologs, involved in $InsP_8$ biosynthesis in yeast and mammals, are widespread in plants. We identified two PPIP5K homologs in *A. thaliana*, AtVIH1 and AtVIH2. Functional analyses of AtVIH1 and AtVIH2 in *vip1Δ* yeast knock out strain showed that the ATP-Grasp kinase domain is functional and structurally conserved. Expression analysis of different plant tissues revealed ubiquitous expression of *AtVIH2* in all tested tissues, but showed that expression of *AtVIH1* was restricted to pollen. Analysis of $InsP_8$ levels of independent *vih2* knock out lines revealed a severe decrease of $InsP_8$ levels showing that AtVIH2 is involved in PP-InsP homeostasis *in planta*. InsPs where previously linked to the Jasmonate (JA)-regulated plant defense response. Interestingly, analysis of inositol polyphosphate levels after methyl-JA treatment revealed a strong increase in $InsP_8$ levels and no or mild effects on other inositol polyphosphate isomers. Furthermore, this increase was absent in *vih2* mutant plants showing that the methyl-JA mediated $InsP_8$ increase was AtVIH2-dependent. Interestingly, independent *vih2* mutant lines showed a decreased resistance to the insect herbivores *Pieris rapae* and *Mamestra brassica*, as well as to the necrotrophic fungi *Botrytis cinerea* and *Alternaria brassicicola,* all of which plants try to contain by JA-dependent defenses. Moreover, we showed that after wounding, active JA species were even increased in *vih2* mutant plants. Together these data suggested that $InsP_8$ is involved perception of active JA. Yeast 2-hybrid (Y2H) analysis and InsP/PP-InsP binding assays with the JA-co-receptor complex, SCF^{AtCOI1}/AtJAZ, led us to propose a model in which direct binding of InsP8 to the SCF^{AtCOI1}-AtJAZ co-receptor complex activates JA-signaling thereby fine tuning the immune response to plant pathogens.

7.2.3 Inositol Polyphosphate Binding Specificity of the Jasmonate Receptor Complex

Laha, D., Parvin, N.*, Dynowski, M., Johnen, P., Mao, H., Bitters, S. T., Zheng, N. and Schaaf, G.*

**These authors contributed equally to this work*

7.2.3.1 Summary of results

InsPs and PP-InsP were suggested to play a role in the JA-dependent SCF^{AtCOI1}-AtJAZ-mediated immune response (Laha et al., 2015; Mosblech et al., 2011; Sheard et al., 2010). By competitive and direct binding assays using recombinant Ask1-AtCOI1 and AtJAZ, we show that disitinct $InsP_5$ isomers and $InsP_6$ exhibit different binding affinities for the Ask1-AtCOI1/AtJAZ co-receptor complex. We observed the following order of $InsP_x$ binding affinities, $InsP_5$ [3-OH] ≥ $InsP_6$ > $InsP_5$ [4-OH] > $InsP_5$ [2-OH] > $InsP_5$ [5-OH] > $InsP_5$ [6-OH] > $InsP_5$ [1-OH]. Our results further indicate that different AtJAZ are not affecting binding affinities to different InsP isomers. Interestingly, $InsP_5$ [2-OH], which was previously suggested to positively regulate SCF^{AtCOI1}-AtJAZ mediated JA signaling (Mosblech et al., 2011), exhibited lower binding affinities than $InsP_6$. The previous proposition that $InsP_5$ [2-OH] is involved in SCF^{COI1}-JAZ mediated JA signaling was based on Y2H results and the observation that *ipk1-1* mutant plants were more tolerance to *Plutella xylostella* caterpillars (Mosblech et al., 2011). Interestingly, our observation that *ipk1-1* plants are more susceptible to the necrotrophic pathogens *B. cinerea* and *A. brassicicola*, which plants contain by JA-dependent defenses, suggested that $InsP_5$ [2-OH] does not generally increase JA-related pathogen responses. Further analysis by *in silico* docking experiments using available structural data of the co-receptor complex (Sheard et al., 2010) suggested that both $InsP_5$ or $InsP_8$ are able to influence the elliptical shape of the Leu-rich repeat (LRR) solenoid of AtCOI1 important for hormone binding and likely for binding of the JAZ degron to the carboxy-terminal of the LRR domain. However, the *in silico* analysis suggested $InsP_8$ as superior ligand. Mutational analysis of AtCOI1 followed by Y2H studies further suggested that, in contrast to $InsP_8$, $InsP_5$ is unlikely to play a role in AtCOI-AtJAZ interaction.

7.2.3.2 Discussion

7.2.3.2.1 Influence of $InsP_8$ on plant defenses

Together the two publications related to InsPs and PP-InsPs presented in my thesis indicate a role of $InsP_8$ in JA-related plant defenses mediated by the SCF^{COI1}-JAZ co-receptor complex. Pathogen performance phenotypes presented in these studies only report susceptibility of plants with reduced $InsP_8$. Interestingly, we also showed that overexpression of the *AtVIH2* kinase domain led to an increased tolerance towards herbivores and necrotrophic fungi. This finding also resulted in filing a patent (C12N 15/82). This is a very promising finding for a possible application of our findings to crops. In future it will be very interesting to evaluate pathogen tolerance along with other important traits, such as germination rate and yield, for crops with altered $InsP_8$ levels. Moreover, given the reported antagonism between JA-related defenses on SA-related defense responses (Caarls et al., 2015) it will be important to include a wide range of plant pathogens including bacterial biotrophs.

The finding that misregulation of InsPs have different effects on JA-related defenses, raises the question whether InsPs and PP-InsPs fine tune the immune response triggered by different pathogens. In this regard it would be very interesting to test tolerance of *ipk1-1* and *vih2* mutant plants with different herbivores and necrotrophic pathogens. Interestingly, recently it was shown that the *Xanthomonas campestris*, a biotrophic pathogen infecting pepper and tomato, developed an effector acting as 1-phytase on $InsP_6$ thereby increasing $InsP_5$ [1-OH] maybe changing JA-related signaling (Bluher et al., 2017). However, whether or in which way increased $InsP_5$ [1-OH] and/or decreased $InsP_6$ might affect SCF^{AtCOI1}-AtJAZ mediated signaling needs to be further elucidated.

To further strengthen the involvement of InsPs and PP-InsPs in JA-related defenses following lines of experiments are needed. i) The analysis of protein degradation of different AtJAZ homologs in plant lines with defects in the InsP and PP-InsP homeostasis and ii) crossings of *coi1* mutant lines with lines with defects in the InsP or PP-InsP homeostasis and the subsequent testing of pathogen resistance of double mutant lines to investigate whether the signaling molecules also regulate plant defenses independent of the JA-receptor.

7.2.3.2.2 Intracellular concentration of InsPs and PP-InsPs

Furthermore, to understand the involvement of different inositol polyphosphate on SCF^{COI1}-JAZ co-receptor activity it would be of high interest to develop Förster resonance energy

transfer (FRET)-based InsP/PP-InsP sensors based on domains specific for different inositol polyphosphate isomers, e.g. based on the AtCOI1-AtJAZ interaction or other PP-InsP binding proteins. This would enable studies of InsP/PP-InsP dynamics in living cells and would certainly revolutionize the field of soluble inositol polyphosphates.

7.2.3.2.3 Developmental roles of $InsP_8$

AtCOI1-mediated JA signaling not only affects plant defenses, but also the plant developmental program (Huang et al., 2017). Interestingly, *vih2* mutant plants did not show major differences in development. This suggests that $InsP_8$ is not involved in the developmental program mediated by AtCOI1. However, in *vih2* mutant plants there is still a residual amount of InsP8 detectable.

Interestingly, recently a preprint by the Hothorn lab (Zhu et al. 2018, BioRXiv) shows that *vih1 vih2* double mutants exhibit a severe developmental phenotype. The *vih1 vih2* double mutant plants also showed a phosphate hyperaccumulation. The authors propose that $InsP_8$ is binding to SPX domains, present in many proteins involved in the phosphate starvation response (PSR, Liu et al., 2018), and thereby influences PSR of plants. Interestingly, Zhu et al. (2018, BioRXiv) showed that phosphate hyperaccumulation in *vih1-2 vih2-4* indeed can be rescued to wild type level by generating a higher order mutant line with PHOSPHATE STARVATION RESPONSE 1 (PHR1) and *PHR1-LIKE 1* (*PHL1*, the *vih1-2 vih2-4 phr1 phl1* quadruple mutant line). In contrast to the phosphate hyperaccumulation, the developmental phenotypes could only be partially rescued suggesting roles of $InsP_8$ beyond PSR in developmental processes. Thus in future, it will be important to dissect phenotypes originating from defects in the PSR or originating from the involvement of $InsP_8$ in other developmental pathways. To test this it will be interesting to study the phenotypes of the *vih1-2 vih2-4 phr1 phl1* quadruple mutant lines.

The SCF^{AtCOI1}-AtJAZ co-receptor complex is structurally very similar to the SCF^{AtTIR1}-AtAUX/IAA IAA receptor complex. Interestingly, insect-derived $InsP_6$ was co-crystalized with the receptor complex. Given the similarity to SCF^{AtCOI1}-AtJAZ and the idea that different InsPs and PP-InsPs regulate JA perception, it will be interesting to address if the auxin perception is influenced by different inositol polyphosphates.

7.2.3.2.4 InsP6K in plants

Furthermore, the identity of InsP6Ks in plants remains elusive. The identification of the InsP6K of plants and the subsequent analysis of mutant plants will deepen our knowledge of the roles of PP-InsPs in plants. To identify plant InsP6Ks a screen with a plant cDNA in the *kcs1Δ* yeast strain should be performed.

7.2.3.2.5 PP-InsP binding domains in plants

Except of the proposed binding of SPX domains to PP-InsPs no other PP-InsP binding domain has been identified in plants. Therefore, performing pull down from plant protein extracts with biotinylated, non-hydrolysable PP-InsP isomers coupled with mass spectrometry for protein identification (comparable to Wu et al., 2016) would be a straightforward approach to identify new PP-InsP binding domains. This would certainly expand our understanding of PP-InsP utilization in plants. Based on the variety of functions of PP-InPs revealed by studying different organisms,it will be interesting to test the involvement of this class of molecules in e.g. energy homeostasis, lipid homeostasis, regulation of protein membrane recruitment, protein pyrophosphorylations and its physiological roles in plants.

7.2.3.2.6 Biosynthesis of InsPs and PP-InsPs

To understand the physiological roles of InsPs and PP-InsPs a wider knowledge of the two different routes of biosynthesis of InsPs is needed. The importance of the lipid-independent route for the biosynthesis of higher InsPs suggested by Brearley and Hanke (1996) still needs clarification. Furthermore, the influence of the lipid or the lipid-independent pathway on different InsP isomers remains elusive. Studying the abundance of the different InsP and PP-InsP isomers in mutant plants with alteration in PIP homeostasis or defects in the lipid-independent biosynthesis will clarify the importance of the proposed two biosynthetic routes. In summary, research of PP-InsPs in plants is just gaining momentum and the near future will bring new interesting insights into the role PP-InsP and in their homeostasis.

Taken together, my PhD thesis covered a variety of aspects and roles of *myo*-inositol-derived signaling molecules and thereby layed the foundation for subsequent analyses of this exciting class of molecules.

8 References

Bak, G., Lee, E.J., Lee, Y., Kato, M., Segami, S., Sze, H., Maeshima, M., Hwang, J.U., and Lee, Y. (2013). Rapid structural changes and acidification of guard cell vacuoles during stomatal closure require phosphatidylinositol 3,5-bisphosphate. The Plant cell *25*, 2202-2216.

Bankaitis, V.A., Aitken, J.R., Cleves, A.E., and Dowhan, W. (1990). An essential role for a phospholipid transfer protein in yeast Golgi function. Nature *347*, 561-562.

Bankaitis, V.A., Mousley, C.J., and Schaaf, G. (2010). The Sec14 superfamily and mechanisms for crosstalk between lipid metabolism and lipid signaling. Trends Biochem Sci *35*, 150-160.

Barbosa, I.C.R., Shikata, H., Zourelidou, M., Heilmann, M., Heilmann, I., and Schwechheimer, C. (2016). Phospholipid composition and a polybasic motif determine D6 PROTEIN KINASE polar association with the plasma membrane and tropic responses. Development *143*, 4687-4700.

Bell, R.M., and Coleman, R.A. (1980). Enzymes of glycerolipid synthesis in eukaryotes. Annu Rev Biochem *49*, 459-487.

Bhandari, R., Saiardi, A., Ahmadibeni, Y., Snowman, A.M., Resnick, A.C., Kristiansen, T.Z., Molina, H., Pandey, A., Werner, J.K., Juluri, K.R.*, et al.* (2007). Protein pyrophosphorylation by inositol pyrophosphates is a posttranslational event. Proceedings of the National Academy of Sciences of the United States of America *104*, 15305-15310.

Bluher, D., Laha, D., Thieme, S., Hofer, A., Eschen-Lippold, L., Masch, A., Balcke, G., Pavlovic, I., Nagel, O., Schonsky, A.*, et al.* (2017). A 1-phytase type III effector interferes with plant hormone signaling. Nat Commun *8*, 2159.

Brearley, C.A., and Hanke, D.E. (1996). Metabolic evidence for the order of addition of individual phosphate esters in the myo-inositol moiety of inositol hexakisphosphate in the duckweed Spirodela polyrhiza L. Biochem J *314 (Pt 1)*, 227-233.

Brown, G.D., Denning, D.W., Gow, N.A.R., Levitz, S.M., Netea, M.G., and White, T.C. (2012). Hidden Killers: Human Fungal Infections. Sci Transl Med *4*.

Caarls, L., Pieterse, C.M., and Van Wees, S.C. (2015). How salicylic acid takes transcriptional control over jasmonic acid signaling. Front Plant Sci *6*, 170.

Chayakulkeeree, M., Johnston, S.A., Oei, J.B., Lev, S., Williamson, P.R., Wilson, C.F., Zuo, X.M., Leal, A.L., Vainstein, M.H., Meyer, W.*, et al.* (2011). SEC14 is a specific requirement for secretion of phospholipase B1 and pathogenicity of Cryptococcus neoformans. Molecular Microbiology *80*, 1088-1101.

Chen, I.W., and Charalam.Fc (1966). Biochemical Studies on Inositol .9. D-Inositol 1-Phosphate as Intermediate in Biosynthesis of Inositol from Glucose 6-Phosphate and Characteristics of 2 Reactions in This Biosynthesis. J Biol Chem *241*, 2194-&.

Chung, J., Torta, F., Masai, K., Lucast, L., Czapla, H., Tanner, L.B., Narayanaswamy, P., Wenk, M.R., Nakatsu, F., and De Camilli, P. (2015). PI4P/phosphatidylserine countertransport at ORP5-and ORP8-mediated ER-plasma membrane contacts. Science *349*, 428-432.

Couso, I., Evans, B.S., Li, J., Liu, Y., Ma, F.F., Diamond, S., Allen, D.K., and Umen, J.G. (2016). Synergism between Inositol Polyphosphates and TOR Kinase Signaling in Nutrient Sensing, Growth Control, and Lipid Metabolism in Chlamydomonas. The Plant cell *28*, 2026-2042.

De Craene, J.O., Bertazzi, D.L., Bar, S., and Friant, S. (2017). Phosphoinositides, Major Actors in Membrane Trafficking and Lipid Signaling Pathways. Int J Mol Sci *18*.

de Saint-Jean, M., Delfosse, V., Douguet, D., Chicanne, G., Payrastre, B., Bourguet, W., Antonny, B., and Drin, G. (2011). Osh4p exchanges sterols for phosphatidylinositol 4-phosphate between lipid bilayers. Journal of Cell Biology *195*, 965-978.

Desrivieres, S., Cooke, F.T., Parker, P.J., and Hall, M.N. (1998). MSS4, a phosphatidylinositol-4-phosphate 5-kinase required for organization of the actin cytoskeleton in Saccharomyces cerevisiae. J Biol Chem *273*, 15787-15793.

Dickson, E.J., and Hille, B. (2019). Understanding phosphoinositides: rare, dynamic, and essential membrane phospholipids. Biochem J *476*, 1-23.

Dickson, R.C. (2010). Roles for sphingolipids in Saccharomyces cerevisiae. Adv Exp Med Biol *688*, 217-231.

Divecha, N., and Halstead, J.R. (2004). Of yeast and men - The evolution of PtdIns(3,4,5)P-3 synthesis. EMBO reports *5*, 865-866.

Draskovic, P., Saiardi, A., Bhandari, R., Burton, A., Ilc, G., Kovacevic, M., Snyder, S.H., and Podobnik, M. (2008). Inositol hexakisphosphate kinase products contain diphosphate and triphosphate groups. Chem Biol *15*, 274-286.

Eagle, H., Oyama, V.I., Levy, M., and Freeman, A.E. (1957). Myo-Inositol as an essential growth factor for normal and malignant human cells in tissue culture. J Biol Chem *226*, 191-205.

Fahey, R.C. (2001). Novel thiols of prokaryotes. Annu Rev Microbiol *55*, 333-356.

Fang, M., Kearns, B.G., Gedvilaite, A., Kagiwada, S., Kearns, M., Fung, M.K., and Bankaitis, V.A. (1996). Kes1p shares homology with human oxysterol binding protein and participates in a novel regulatory pathway for yeast Golgi-derived transport vesicle biogenesis. Embo J *15*, 6447-6459.

Filipuzzi, I., Cotesta, S., Perruccio, F., Knapp, B., Fu, Y., Studer, C., Pries, V., Riedl, R., Helliwell, S.B., Petrovic, K.T.*, et al.* (2016). High-Resolution Genetics Identifies the Lipid Transfer Protein Sec14p as Target for Antifungal Ergolines. Plos Genet *12*.

Flanagan, C.A., Schnieders, E.A., Emerick, A.W., Kunisawa, R., Admon, A., and Thorner, J. (1993). Phosphatidylinositol 4-kinase: gene structure and requirement for yeast cell viability. Science *262*, 1444-1448.

Friml, J., Yang, X., Michniewicz, M., Weijers, D., Quint, A., Tietz, O., Benjamins, R., Ouwerkerk, P.B., Ljung, K., Sandberg, G.*, et al.* (2004). A PINOID-dependent binary switch in apical-basal PIN polar targeting directs auxin efflux. Science *306*, 862-865.

Gary, J.D., Wurmser, A.E., Bonangelino, C.J., Weisman, L.S., and Emr, S.D. (1998). Fab1p is essential for PtdIns(3)P 5-kinase activity and the maintenance of vacuolar size and membrane homeostasis. Journal of Cell Biology *143*, 65-79.

Ghosh, R., and Bankaitis, V.A. (2011). Phosphatidylinositol transfer proteins: Negotiating the regulatory interface between lipid metabolism and lipid signaling in diverse cellular processes. Biofactors *37*, 290-308.

Ghosh, R., de Campos, M.K., Huang, J., Huh, S.K., Orlowski, A., Yang, Y., Tripathi, A., Nile, A., Lee, H.C., Dynowski, M.*, et al.* (2015). Sec14-nodulin proteins and the patterning of phosphoinositide landmarks for developmental control of membrane morphogenesis. Mol Biol Cell *26*, 1764-1781.

Hamada, K., Miyatake, H., Terauchi, A., and Mikoshiba, K. (2017). IP3-mediated gating mechanism of the IP3 receptor revealed by mutagenesis and X-ray crystallography. Proceedings of the National Academy of Sciences of the United States of America *114*, 4661-4666.

Hammond, G.R., Fischer, M.J., Anderson, K.E., Holdich, J., Koteci, A., Balla, T., and Irvine, R.F. (2012). PI4P and PI(4,5)P2 are essential but independent lipid determinants of membrane identity. Science *337*, 727-730.

Hansen, S.B. (2015). Lipid agonism: The PIP2 paradigm of ligand-gated ion channels. Biochimica et biophysica acta *1851*, 620-628.

Heilmann, I. (2016). Phosphoinositide signaling in plant development. Development *143*, 2044-2055.

Heilmann, M., and Heilmann, I. (2015). Plant phosphoinositides-complex networks controlling growth and adaptation. Biochimica et biophysica acta *1851*, 759-769.

Horst, W.J., Wang, Y., and Eticha, D. (2010). The role of the root apoplast in aluminium-induced inhibition of root elongation and in aluminium resistance of plants: a review. Annals of botany *106*, 185-197.

Huang, H., Liu, B., Liu, L.Y., and Song, S.S. (2017). Jasmonate action in plant growth and development. J Exp Bot *68*, 1349-1359.

Huang, J., Ghosh, R., Tripathi, A., Lonnfors, M., Somerharju, P., and Bankaitis, V.A. (2016). Two-ligand priming mechanism for potentiated phosphoinositide synthesis is an evolutionarily conserved feature of Sec14-like phosphatidylinositol and phosphatidylcholine exchange proteins. Mol Biol Cell *27*, 2317-2330.

Irvine, R.F., and Schell, M.J. (2001). Back in the water: the return of the inositol phosphates. Nat Rev Mol Cell Biol *2*, 327-338.

Ischebeck, T., Werner, S., Krishnamoorthy, P., Lerche, J., Meijon, M., Stenzel, I., Lofke, C., Wiessner, T., Im, Y.J., Perera, I.Y*., et al.* (2013). Phosphatidylinositol 4,5-bisphosphate influences PIN polarization by controlling clathrin-mediated membrane trafficking in Arabidopsis. The Plant cell *25*, 4894-4911.

Ives, E.B., Nichols, J., Wente, S.R., and York, J.D. (2000). Biochemical and functional characterization of inositol 1,3,4,5, 6-pentakisphosphate 2-kinases. J Biol Chem *275*, 36575-36583.

Jiang, C., Liu, L., Li, X., Han, R., Wei, Y., and Yu, Y. (2018). Insights into aluminum-tolerance pathways in Stylosanthes as revealed by RNA-Seq analysis. Sci Rep.

Kakimoto, M., Kobayashi, A., Fukuda, R., Ono, Y., Ohta, A., and Yoshimura, E. (2005). Genome-wide screening of aluminum tolerance in Saccharomyces cerevisiae. Biometals *18*, 467-474.

Kawahara, M., and Kato-Negishi, M. (2011). Link between Aluminum and the Pathogenesis of Alzheimer's Disease: The Integration of the Aluminum and Amyloid Cascade Hypotheses. Int J Alzheimers Dis *2011*, 276393.

Kf de Campos, M., and Schaaf, G. (2017). The regulation of cell polarity by lipid transfer proteins of the SEC14 family. Current opinion in plant biology *40*, 158-168.

Kohorn, B.D., and Kohorn, S.L. (2012). The cell wall-associated kinases,WAKs, as pectin receptors. Frontiers in Plant Science *3*.

Kooijman, E.E., Carter, K.M., van Laar, E.G., Chupin, V., Burger, K.N.J., and de Kruijff, B. (2005). What makes the bioactive lipids phosphatidic acid and lysophosphatidic acid so special? Biochemistry-Us *44*, 17007-17015.

Kopittke, P.M., Moore, K.L., Lombi, E., Gianoncelli, A., Ferguson, B.J., Blamey, F.P.C., Menzies, N.W., Nicholson, T.M., McKenna, B.A., Wang, P*., et al.* (2015). Identification of the Primary Lesion of Toxic Aluminum in Plant Roots. Plant physiology *167*, 1402-1411.

Krishnamoorthy, P., Sanchez-Rodriguez, C., Heilmann, I., and Persson, S. (2014). Regulatory roles of phosphoinositides in membrane trafficking and their potential impact on cell-wall synthesis and re-modelling. Annals of botany *114*, 1049-1057.

Kusano, H., Testerink, C., Vermeer, J.E.M., Tsuge, T., Shimada, H., Oka, A., Munnik, T., and Aoyama, T. (2008). The Arabidopsis phosphatidylinositol phosphate 5-kinase PIP5K3 is a key regulator of root hair tip growth. The Plant cell *20*, 367-380.

Laha, D., Johnen, P., Azevedo, C., Dynowski, M., Weiss, M., Capolicchio, S., Mao, H., Iven, T., Steenbergen, M., Freyer, M*., et al.* (2015). VIH2 Regulates the Synthesis of Inositol Pyrophosphate InsP8 and Jasmonate-Dependent Defenses in Arabidopsis. The Plant cell *27*, 1082-1097.

Laha, D., Parvin, N., Dynowski, M., Johnen, P., Mao, H., Bitters, S.T., Zheng, N., and Schaaf, G. (2016). Inositol Polyphosphate Binding Specificity of the Jasmonate Receptor Complex. Plant physiology *171*, 2364-2370.

Lamaoui, M., Jemo, M., Datla, R., and Bekkaoui, F. (2018). Heat and Drought Stresses in Crops and Approaches for Their Mitigation. Front Chem *6*.

Lee, Y., Bak, G., Choi, Y., Chuang, W.I., Cho, H.T., and Lee, Y. (2008a). Roles of phosphatidylinositol 3-kinase in root hair growth. Plant physiology *147*, 624-635.

Lee, Y.S., Huang, K., Quiocho, F.A., and O'Shea, E.K. (2008b). Molecular basis of cyclin-CDK-CKI regulation by reversible binding of an inositol pyrophosphate. Nat Chem Biol *4*, 25-32.

Lemmon, M.A. (2008). Membrane recognition by phospholipid-binding domains. Nat Rev Mol Cell Biol *9*, 99-111.

Lin, F., Krishnamoorthy, P., Schubert, V., Hause, G., Heilmann, M., and Heilmann, I. (2019). A dual role for cell plate-associated PI4Kbeta in endocytosis and phragmoplast dynamics during plant somatic cytokinesis. Embo J.

Liu, N., Shang, W., Li, C., Jia, L., Wang, X., Xing, G., and Zheng, W. (2018). Evolution of the SPX gene family in plants and its role in the response mechanism to phosphorus stress. Open Biol *8*.

Liu, Y., and Bankaitis, V.A. (2010). Phosphoinositide phosphatases in cell biology and disease. Prog Lipid Res *49*, 201-217.

Lopez, M.C., Nicaud, J.M., Skinner, H.B., Vergnolle, C., Kader, J.C., Bankaitis, V.A., and Gaillardin, C. (1994). A Phosphatidylinositol Phosphatidylcholine Transfer Protein Is Required for Differentiation of the Dimorphic Yeast Yarrowia-Lipolytica from the Yeast to the Mycelial Form. Journal of Cell Biology *125*, 113-127.

Luo, H.B.R., Huang, Y.E., Chen, J.M.C., Saiardi, A., Iijima, M., Ye, K.Q., Huang, Y.F., Nagata, E., Devreotes, P., and Snyder, S.H. (2003). Inositol pyrophosphates mediate chemotaxis in Dictyostelium via pleckstrin homology domain-PtdIns (3,4,5)P3 interactions. Cell *114*, 559-572.

Macbeth, M.R., Schubert, H.L., VanDemark, A.P., Lingam, A.T., Hill, C.P., and Bass, B.L. (2005). Inositol hexakisphosphate is bound in the ADAR2 core and required for RNA editing. Science *309*, 1534-1539.

Maeda, K., Anand, K., Chiapparino, A., Kumar, A., Poletto, M., Kaksonen, M., and Gavin, A.C. (2013). Interactome map uncovers phosphatidylserine transport by oxysterol-binding proteins. Nature *501*, 257-+.

Majumder, A.L., Johnson, M.D., and Henry, S.A. (1997). 1L-myo-inositol-1-phosphate synthase. Bba-Lipid Lipid Met *1348*, 245-256.

Mamode Cassim, A., Gouguet, P., Gronnier, J., Laurent, N., Germain, V., Grison, M., Boutte, Y., Gerbeau-Pissot, P., Simon-Plas, F., and Mongrand, S. (2019). Plant lipids: Key players of plasma membrane organization and function. Prog Lipid Res *73*, 1-27.

Marmelstein, A.M., Morgan, J.A.M., Penkert, M., Rogerson, D.T., Chin, J.W., Krause, E., and Fiedler, D. (2018). Pyrophosphorylation via selective phosphoprotein derivatization. Chem Sci *9*, 5929-5936.

Menniti, F.S., Miller, R.N., Putney, J.W., Jr., and Shears, S.B. (1993). Turnover of inositol polyphosphate pyrophosphates in pancreatoma cells. J Biol Chem *268*, 3850-3856.

Michell, R.H. (2008). Inositol derivatives: evolution and functions. Nat Rev Mol Cell Biol *9*, 151-161.

Michell, R.H. (2011). Inositol and its derivatives: their evolution and functions. Advances in enzyme regulation *51*, 84-90.

Mittler, R. (2006). Abiotic stress, the field environment and stress combination. Trends Plant Sci *11*, 15-19.

Monteoliva, L., Sanchez, M., Pla, J., Gil, C., and Nombela, C. (1996). Cloning of Candida albicans SEC14 gene homologue coding for a putative essential function. Yeast *12*, 1097-1105.

Moravcevic, K., Mendrola, J.M., Schmitz, K.R., Wang, Y.H., Slochower, D., Janmey, P.A., and Lemmon, M.A. (2010). Kinase associated-1 domains drive MARK/PAR1 kinases to membrane targets by binding acidic phospholipids. Cell *143*, 966-977.

Mosblech, A., Thurow, C., Gatz, C., Feussner, I., and Heilmann, I. (2011). Jasmonic acid perception by COI1 involves inositol polyphosphates in Arabidopsis thaliana. The Plant journal : for cell and molecular biology *65*, 949-957.

Mueller-Roeber, B., and Pical, C. (2002). Inositol phospholipid metabolism in Arabidopsis. Characterized and putative isoforms of inositol phospholipid kinase and phosphoinositide-specific phospholipase C. Plant physiology *130*, 22-46.

Mulugu, S., Bai, W.L., Fridy, P.C., Bastidas, R.J., Otto, J.C., Dollins, D.E., Haystead, T.A., Ribeiro, A.A., and York, J.D. (2007). A conserved family of enzymes that phosphorylate inositol hexakisphosphate. Science *316*, 106-109.

Munnik, T., and Testerink, C. (2009). Plant phospholipid signaling: "in a nutshell". Journal of lipid research *50*, S260-S265.

Nalaskowski, M.M., Deschermeier, C., Fanick, W., and Mayr, G.W. (2002). The human homologue of yeast ArgRIII protein is an inositol phosphate multikinase with predominantly nuclear localization. Biochem J *366*, 549-556.

Ndamukong, I., Jones, D.R., Lapko, H., Divecha, N., and Avramova, Z. (2010). Phosphatidylinositol 5-phosphate links dehydration stress to the activity of ARABIDOPSIS TRITHORAX-LIKE factor ATX1. Plos One *5*, e13396.

Nikawa, J., Kodaki, T., and Yamashita, S. (1987). Primary Structure and Disruption of the Phosphatidylinositol Synthase Gene of Saccharomyces-Cerevisiae. J Biol Chem *262*, 4876-4881.

Nikawa, J., and Yamashita, S. (1984). Molecular cloning of the gene encoding CDPdiacylglycerol-inositol 3-phosphatidyl transferase in Saccharomyces cerevisiae. Eur J Biochem *143*, 251-256.

Nile, A.H., Tripathi, A., Yuan, P.H., Mousley, C.J., Suresh, S., Wallace, I.M., Shah, S.D., Pohlhaus, D.T., Temple, B., Nislow, C*., et al.* (2014). PITPs as targets for selectively interfering with phosphoinositide signaling in cells. Nat Chem Biol *10*, 76-U123.

Nunez, L.R., and Henry, S.A. (2006). Regulation of 1D-myo-inositol-3-phosphate synthase in yeast. Sub-cellular biochemistry *39*, 135-156.

Odom, A.R., Stahlberg, A., Wente, S.R., and York, J.D. (2000). A role for nuclear inositol 1,4,5-trisphosphate kinase in transcriptional control. Science *287*, 2026-2029.

Panda, S.K., Baluska, F., and Matsumoto, H. (2009). Aluminum stress signaling in plants. Plant Signal Behav *4*, 592-597.

Peterman, T.K., Ohol, Y.M., McReynolds, L.J., and Luna, E.J. (2004). Patellin1, a novel Sec14-like protein, localizes to the cell plate and binds phosphoinositides. Plant physiology *136*, 3080-3094; discussion 3001-3082.

Pfaller, M.A., Pappas, P.G., and Wingard, J.R. (2006). Invasive fungal pathogens: Current epidemiological trends. Clin Infect Dis *43*, S3-S14.

Phillips, S.E., Ile, K.E., Boukhelifa, M., Huijbregts, R.P., and Bankaitis, V.A. (2006). Specific and nonspecific membrane-binding determinants cooperate in targeting

phosphatidylinositol transfer protein beta-isoform to the mammalian trans-Golgi network. Mol Biol Cell *17*, 2498-2512.

Phillips, S.E., Sha, B.D., Topalof, L., Xie, Z.G., Alb, J.G., Klenchin, V.A., Swigart, P., Cockcroft, S., Martin, T.F.J., Luo, M.*, et al.* (1999). Yeast Sec14p deficient in phosphatidylinositol transfer activity is functional in vivo. Mol Cell *4*, 187-197.

Platre, M.P., Noack, L.C., Doumane, M., Bayle, V., Simon, M.L.A., Maneta-Peyret, L., Fouillen, L., Stanislas, T., Armengot, L., Pejchar, P.*, et al.* (2018). A Combinatorial Lipid Code Shapes the Electrostatic Landscape of Plant Endomembranes. Dev Cell *45*, 465-480 e411.

Posor, Y., Eichhorn-Grunig, M., and Haucke, V. (2015). Phosphoinositides in endocytosis. Biochimica et biophysica acta *1851*, 794-804.

Pries, V., Nocker, C., Khan, D., Johnen, P., Hong, Z., Tripathi, A., Keller, A.L., Fitz, M., Perruccio, F., Filipuzzi, I., et al. (2018). Target Identification and Mechanism of Action of Picolinamide and Benzamide Chemotypes with Antifungal Properties. Cell Chem Biol 25, 279-290 e277.

Raboy, V. (2003). myo-Inositol-1,2,3,4,5,6-hexakisphosphate. Phytochemistry *64*, 1033-1043.

Richie, D.L., Thompson, K.V., Studer, C., Prindle, V.C., Aust, T., Riedl, R., Estoppey, D., Tao, J.S., Sexton, J.A., Zabawa, T.*, et al.* (2013). Identification and Evaluation of Novel Acetolactate Synthase Inhibitors as Antifungal Agents. Antimicrob Agents Ch *57*, 2272-2280.

Rudge, S.A., Sciorra, V.A., Iwamoto, M., Zhou, C., Strahl, T., Morris, A.J., Thorner, J., and Engebrecht, J. (2004). Roles of phosphoinositides and of Spo14p (phospholipase D)-generated phosphatidic acid during yeast sporulation. Mol Biol Cell *15*, 207-218.

Safrany, S.T., Caffrey, J.J., Yang, X.N., Bembenek, M.E., Moyer, M.B., Burkhart, W.A., and Shears, S.B. (1998). A novel context for the 'MutT' module, a guardian of cell integrity, in a diphosphoinositol polyphosphate phosphohydrolase. Embo J *17*, 6599-6607.

Saiardi, A. (2016). Protein pyrophosphorylation: moving forward. Biochem J *473*, 3765-3768.

Saiardi, A., Erdjument-Bromage, H., Snowman, A.M., Tempst, P., and Snyder, S.H. (1999). Synthesis of diphosphoinositol pentakisphosphate by a newly identified family of higher inositol polyphosphate kinases. Current biology : CB *9*, 1323-1326.

Saiardi, A., Nagata, E., Luo, H.R., Snowman, A.M., and Snyder, S.H. (2001). Identification and characterization of a novel inositol hexakisphosphate kinase. J Biol Chem *276*, 39179-39185.

Sbrissa, D., Ikonomov, O.C., and Shisheva, A. (2000). PIKfyve lipid kinase is a protein kinase: Downregulation of 5 '-phosphoinositide product formation by autophosphorylation. Biochemistry-Us *39*, 15980-15989.

Schaaf, G., Ortlund, E.A., Tyeryar, K.R., Mousley, C.J., Ile, K.E., Garrett, T.A., Ren, J., Woolls, M.J., Raetz, C.R., Redinbo, M.R.*, et al.* (2008). Functional anatomy of phospholipid binding and regulation of phosphoinositide homeostasis by proteins of the sec14 superfamily. Mol Cell *29*, 191-206.

Schott, E.J., and Gardner, R.C. (1997). Aluminum-sensitive mutants of Saccharomyces cerevisiae. Molecular & general genetics : MGG *254*, 63-72.

Schrick, K., Bruno, M., Khosla, A., Cox, P.N., Marlatt, S.A., Roque, R.A., Nguyen, H.C., He, C., Snyder, M.P., Singh, D.*, et al.* (2014). Shared functions of plant and mammalian StAR-related lipid transfer (START) domains in modulating transcription factor activity. Bmc Biol *12*, 70.

Schu, P.V., Takegawa, K., Fry, M.J., Stack, J.H., Waterfield, M.D., and Emr, S.D. (1993). Phosphatidylinositol 3-kinase encoded by yeast VPS34 gene essential for protein sorting. Science *260*, 88-91.

Sheard, L.B., Tan, X., Mao, H.B., Withers, J., Ben-Nissan, G., Hinds, T.R., Kobayashi, Y., Hsu, F.F., Sharon, M., Browse, J.*, et al.* (2010). Jasmonate perception by inositol-phosphate-potentiated COI1-JAZ co-receptor. Nature *468*, 400-U301.

Shi, J., Wang, H., Wu, Y., Hazebroek, J., Meeley, R.B., and Ertl, D.S. (2003). The maize low-phytic acid mutant lpa2 is caused by mutation in an inositol phosphate kinase gene. Plant physiology *131*, 507-515.

Shisheva, A. (2013). PtdIns5P: news and views of its appearance, disappearance and deeds. Arch Biochem Biophys *538*, 171-180.

Simon, M.L.A., Platre, M.P., Marques-Bueno, M.M., Armengot, L., Stanislas, T., Bayle, V., Caillaud, M.C., and Jaillais, Y. (2016). A PtdIns(4)P-driven electrostatic field controls cell membrane identity and signalling in plants. Nat Plants *2*.

Sivaguru, M., Ezaki, B., He, Z.H., Tong, H., Osawa, H., Baluska, F., Volkmann, D., and Matsumoto, H. (2003). Aluminum-induced gene expression and protein localization of a cell wall-associated receptor kinase in Arabidopsis. Plant physiology *132*, 2256-2266.

Skirpan, A.L., Dowd, P.E., Sijacic, P., Jaworski, C.J., Gilroy, S., and Kao, T.H. (2006). Identification and characterization of PiORP1, a Petunia oxysterol-binding-protein related protein involved in receptor-kinase mediated signaling in pollen, and analysis of the ORP gene family in Arabidopsis. Plant Mol Biol *61*, 553-565.

Sleight, R.G. (1987). Intracellular lipid transport in eukaryotes. Annu Rev Physiol *49*, 193-208.

Sparvoli, F., and Cominelli, E. (2015). Seed Biofortification and Phytic Acid Reduction: A Conflict of Interest for the Plant? Plants (Basel) *4*, 728-755.

Stephens, L., Radenberg, T., Thiel, U., Vogel, G., Khoo, K.H., Dell, A., Jackson, T.R., Hawkins, P.T., and Mayr, G.W. (1993). The detection, purification, structural characterization, and metabolism of diphosphoinositol pentakisphosphate(s) and bisdiphosphoinositol tetrakisphosphate(s). J Biol Chem *268*, 4009-4015.

Stephens, L.R., and Irvine, R.F. (1990). Stepwise phosphorylation of myo-inositol leading to myo-inositol hexakisphosphate in Dictyostelium. Nature *346*, 580-583.

Stevenson, J.M., Perera, I.Y., and Boss, W.F. (1998). A phosphatidylinositol 4-kinase pleckstrin homology domain that binds phosphatidylinositol 4-monophosphate. J Biol Chem *273*, 22761-22767.

Stevenson-Paulik, J., Odom, A.R., and York, J.D. (2002). Molecular and biochemical characterization of two plant inositol polyphosphate 6-/3-/5-kinases. J Biol Chem *277*, 42711-42718.

Streb, H., Irvine, R.F., Berridge, M.J., and Schulz, I. (1983). Release of Ca2+ from a nonmitochondrial intracellular store in pancreatic acinar cells by inositol-1,4,5-trisphosphate. Nature *306*, 67-69.

Sukumar, P., Edwards, K.S., Rahman, A., DeLong, A., and Muday, G.K. (2009). PINOID Kinase Regulates Root Gravitropism through Modulation of PIN2-Dependent Basipetal Auxin Transport in Arabidopsis. Plant physiology *150*, 722-735.

Suzuki, T., Matsushima, C., Nishimura, S., Higashiyama, T., Sasabe, M., and Machida, Y. (2016). Identification of Phosphoinositide-Binding Protein PATELLIN2 as a Substrate of Arabidopsis MPK4 MAP Kinase during Septum Formation in Cytokinesis. Plant Cell Physiol *57*, 1744-1755.

Sweetman, D., Johnson, S., Caddick, S.E., Hanke, D.E., and Brearley, C.A. (2006). Characterization of an Arabidopsis inositol 1,3,4,5,6-pentakisphosphate 2-kinase (AtIPK1). Biochem J *394*, 95-103.

Sweetman, D., Stavridou, I., Johnson, S., Green, P., Caddick, S.E.K., and Brearley, C.A. (2007). Arabidopsis thaliana inositol 1,3,4-trisphosphate 5/6-kinase 4 (AtITPK4) is an

outlier to a family of ATP-grasp fold proteins from Arabidopsis. Febs Lett *581*, 4165-4171.

Szijgyarto, Z., Garedew, A., Azevedo, C., and Saiardi, A. (2011). Influence of inositol pyrophosphates on cellular energy dynamics. Science *334*, 802-805.

Tabuchi, A., and Matsumoto, H. (2001). Changes in cell-wall properties of wheat (Triticum aestivum) roots during aluminum-induced growth inhibition. Physiol Plant *112*, 353-358.

Takai, Y., Kishimoto, A., Kikkawa, U., Mori, T., and Nishizuka, Y. (1979). Unsaturated Diacylglycerol as a Possible Messenger for the Activation of Calcium-Activated, Phospholipid Dependent Protein-Kinase System. Biochem Bioph Res Co *91*, 1218-1224.

Tan, X., Calderon-Villalobos, L.I.A., Sharon, M., Zheng, C.X., Robinson, C.V., Estelle, M., and Zheng, N. (2007). Mechanism of auxin perception by the TIR1 ubiquitin ligase. Nature *446*, 640-645.

Tsui, M.M., and York, J.D. (2010). Roles of inositol phosphates and inositol pyrophosphates in development, cell signaling and nuclear processes. Advances in enzyme regulation *50*, 324-337.

Umate, P. (2011). Oxysterol binding proteins (OSBPs) and their encoding genes in Arabidopsis and rice. Steroids *76*, 524-529.

van Leeuwen, W., Okresz, L., Bogre, L., and Munnik, T. (2004). Learning the lipid language of plant signalling. Trends Plant Sci *9*, 378-384.

Verbsky, J.W., Chang, S.C., Wilson, M.P., Mochizuki, Y., and Majerus, P.W. (2005). The pathway for the production of inositol hexakisphosphate in human cells. J Biol Chem *280*, 1911-1920.

Verbsky, J.W., Wilson, M.P., Kisseleva, M.V., Majerus, P.W., and Wente, S.R. (2002). The synthesis of inositol hexakisphosphate. Characterization of human inositol 1,3,4,5,6-pentakisphosphate 2-kinase. J Biol Chem *277*, 31857-31862.

Volinia, S., Dhand, R., Vanhaesebroeck, B., MacDougall, L.K., Stein, R., Zvelebil, M.J., Domin, J., Panaretou, C., and Waterfield, M.D. (1995). A human phosphatidylinositol 3-kinase complex related to the yeast Vps34p-Vps15p protein sorting system. Embo J *14*, 3339-3348.

Vonuexkull, H.R., and Mutert, E. (1995). Global Extent, Development and Economic-Impact of Acid Soils. Plant Soil *171*, 1-15.

Voxeur, A., and Hofte, H. (2016). Cell wall integrity signaling in plants: "To grow or not to grow that's the question". Glycobiology *26*, 950-960.

Wang, S.Y., Ren, X.Y., Huang, B.R., Wang, G., Zhou, P., and An, Y. (2016). Aluminium-induced reduction of plant growth in alfalfa (Medicago sativa) is mediated by interrupting auxin transport and accumulation in roots. Sci Rep-Uk *6*.

Wilson, M.P., and Majerus, P.W. (1997). Characterization of a cDNA encoding Arabidopsis thaliana inositol 1,3,4-trisphosphate 5/6-kinase. Biochem Biophys Res Commun *232*, 678-681.

Wolf, S. (2017). Plant cell wall signalling and receptor-like kinases. Biochem J *474*, 471-492.

Wood, S., Sebastian, K., and Scherr, S.J. (2000). Agroecosystems pilot analysis of global ecosystems (Washington, DC: World Resources Institute).

Wright, E.M., and Turk, E. (2004). The sodium/glucose cotransport family SLC5. Pflugers Arch *447*, 510-518.

Wu, M., Chong, L.S., Perlman, D.H., Resnick, A.C., and Fiedler, D. (2016). Inositol polyphosphates intersect with signaling and metabolic networks via two distinct mechanisms. Proceedings of the National Academy of Sciences of the United States of America *113*, E6757-E6765.

Yamamoto, W., Wada, S., Nagano, M., Aoshima, K., Siekhaus, D.E., Toshima, J.Y., and Toshima, J. (2018). Distinct roles for plasma membrane PtdIns(4)P and PtdIns(4,5)P2 during receptor-mediated endocytosis in yeast. J Cell Sci *131*.

Yancey, P.H. (2005). Organic osmolytes as compatible, metabolic and counteracting cytoprotectants in high osmolarity and other stresses. J Exp Biol *208*, 2819-2830.

Yang, Z.B., Geng, X., He, C., Zhang, F., Wang, R., Horst, W.J., and Ding, Z. (2014). TAA1-regulated local auxin biosynthesis in the root-apex transition zone mediates the aluminum-induced inhibition of root growth in Arabidopsis. The Plant cell *26*, 2889-2904.

Yeung, T., Gilbert, G.E., Shi, J., Silvius, J., Kapus, A., and Grinstein, S. (2008). Membrane phosphatidylserine regulates surface charge and protein localization. Science *319*, 210-213.

Yoshida, S., Ohya, Y., Goebl, M., Nakano, A., and Anraku, Y. (1994). A novel gene, STT4, encodes a phosphatidylinositol 4-kinase in the PKC1 protein kinase pathway of Saccharomyces cerevisiae. J Biol Chem *269*, 1166-1172.

9 Appendix

9.1 VIH2 Regulates the Synthesis of Inositol Pyrophosphate InsP8 and Jasmonate-Dependent Defenses in Arabidopsis.

9.2 Inositol Polyphosphate Binding Specificity of the Jasmonate Receptor Complex.

9.3 Target Identification and Mechanism of Action of Picolinamide and Benzamide Chemotypes with Antifungal Properties.

9.4 Al-tolerance mediated by SEC14-type lipid transfer proteins reveals that membrane charge is both a primary target of Al-toxicity and a tool to increase Al-tolerance in yeast and plants.

9.1 Laha et al., 2015

VIH2 Regulates the Synthesis of Inositol Pyrophosphate InsP8 and Jasmonate-Dependent Defenses in Arabidopsis.

Laha, D., Johnen, P.*, Azevedo, C.*, Dynowski, M., Weiss, M., Capolicchio, S., Mao, H., Iven, T., Steenbergen, M., Freyer, M., Gaugler, P., de Campos, M. K., Zheng, N., Feussner, I., Jessen, H. J., Van Wees, S. C., Saiardi, A. and Schaaf, G.

*These authors contributed equally to this work

Plant Cell. 2015 Apr;27(4):1082-97. doi: 10.1105/tpc.114.135160.

The Plant Cell, Vol. 27: 1082–1097, April 2015, www.plantcell.org

VIH2 Regulates the Synthesis of Inositol Pyrophosphate $InsP_8$ and Jasmonate-Dependent Defenses in Arabidopsis[OPEN]

Debabrata Laha,[a] Philipp Johnen,[a,1] Cristina Azevedo,[b,1] Marek Dynowski,[c] Michael Weiß,[d] Samanta Capolicchio,[e] Haibin Mao,[f] Tim Iven,[g] Merel Steenbergen,[h] Marc Freyer,[a] Philipp Gaugler,[a] Marília K.F. de Campos,[a] Ning Zheng,[f] Ivo Feussner,[g] Henning J. Jessen,[e] Saskia C.M. Van Wees,[h] Adolfo Saiardi,[b] and Gabriel Schaaf[a,2]

[a] Center for Plant Molecular Biology, University of Tübingen, 72076 Tübingen, Germany
[b] Medical Research Council Laboratory for Molecular Cell Biology, University College London, London WC1E 6BT, United Kingdom
[c] Zentrum für Datenverarbeitung, University of Tübingen, 72074 Tübingen, Germany
[d] Department of Biology, University of Tübingen, 72076 Tübingen, Germany
[e] Department of Chemistry, University of Zürich, 8057 Zurich, Switzerland
[f] Department of Pharmacology, Howard Hughes Medical Institute, University of Washington, Seattle, Washington 98195
[g] Department of Plant Biochemistry, Georg-August-University Göttingen, 37077 Göttingen, Germany
[h] Plant-Microbe Interactions, Department of Biology, Utrecht University, 3508 TB Utrecht, The Netherlands

ORCID IDs: 0000-0002-7823-5489 (D.L.); 0000-0002-4512-9508 (P.J.); 0000-0002-1025-9484 (H.J.J.); 0000-0001-9022-4515 (G.S.)

Diphosphorylated inositol polyphosphates, also referred to as inositol pyrophosphates, are important signaling molecules that regulate critical cellular activities in many eukaryotic organisms, such as membrane trafficking, telomere maintenance, ribosome biogenesis, and apoptosis. In mammals and fungi, two distinct classes of inositol phosphate kinases mediate biosynthesis of inositol pyrophosphates: Kcs1/IP6K- and Vip1/PPIP5K-like proteins. Here, we report that PPIP5K homologs are widely distributed in plants and that *Arabidopsis thaliana* VIH1 and VIH2 are functional PPIP5K enzymes. We show a specific induction of inositol pyrophosphate $InsP_8$ by jasmonate and demonstrate that steady state and jasmonate-induced pools of $InsP_8$ in Arabidopsis seedlings depend on VIH2. We identify a role of VIH2 in regulating jasmonate perception and plant defenses against herbivorous insects and necrotrophic fungi. In silico docking experiments and radioligand binding-based reconstitution assays show high-affinity binding of inositol pyrophosphates to the F-box protein COI1-JAZ jasmonate coreceptor complex and suggest that coincidence detection of jasmonate and $InsP_8$ by COI1-JAZ is a critical component in jasmonate-regulated defenses.

INTRODUCTION

Inositol polyphosphates became an intense focus of research with the discovery that *myo*- inositol 1,4,5-trisphosphate ($InsP_3$) mobilizes Ca^{2+} in a receptor-dependent fashion from intracellular stores in pancreatic cells (Streb et al., 1983). The stereochemistry of D-*myo*-inositol suggested that the inositol ring represents a 6-bit signaling scaffold with the potential to "encode" 64 unique signaling states (York, 2006). In plants, $InsP_3$ has been associated with a wide range of cellular functions, such as guard cell physiology (Blatt et al., 1990; Gilroy et al., 1990; Burnette et al., 2003; Han et al., 2003), drought tolerance (Knight et al., 1997; Perera et al., 2008), heat shock responses (Liu et al., 2006), blue light perception (Chen et al., 2008), root gravitropism (Wang et al., 2009; Zhang et al., 2011), response to mechanical wounding (Mosblech et al., 2008), and pollen dormancy (Y. Wang et al., 2012). However, the role of $InsP_3$ and other inositol phosphates in plant signaling remains controversial as no inositol phosphate receptor has been identified to date (Munnik and Vermeer, 2010; Munnik and Nielsen, 2011; Gillaspy, 2013).

Recent discoveries that $InsP_6$ binds to the auxin receptor complex TIR1/IAA (Tan et al., 2007) and $InsP_5$ binds to the jasmonate receptor complex COI1/JAZ (Sheard et al., 2010) suggest that inositol polyphosphates are involved in plant hormone perception. COI1 is the F-box component of a SKP1-CUL1-F-box protein (SCF) ubiquitin E3 ligase complex that recruits Jasmonate ZIM-domain (JAZ) transcriptional repressors upon binding to the bioactive jasmonic acid (JA) conjugate JA-Ile. This triggers polyubiquitylation and subsequent degradation of the JAZ repressors by the 26S proteasome (Chini et al., 2007; Thines et al., 2007; Katsir et al., 2008; Sheard et al., 2010). JAZ degradation relieves repression of *MYC2* and other transcription factors, thus permitting the expression of jasmonate-responsive genes (Chini et al., 2007). Mass spectrometry and NMR analyses revealed that inositol-1,2,4,5,6-pentakisphosphate [Ins(1,2,4,5,6)P_5] copurified with Arabidopsis SKP1 homolog (ASK1)-COI1 expressed in insect cells (Sheard et al., 2010). Although ligand binding based reconstitution assays suggested that Ins(1,2,4,5,6)P_5 potentiates jasmonate receptor assembly in vitro, its physiological role remains unclear. Two studies that analyzed *Arabidopsis thaliana* backgrounds altered in inositol polyphosphate metabolism provide evidence that this class of molecules contributes to COI1

[1] These authors contributed equally to this work.
[2] Address correspondence to gabriel.schaaf@zmbp.uni-tuebingen.de.
The author responsible for distribution of materials integral to the findings presented in this article in accordance with the policy described in the Instructions for Authors (www.plantcell.org) is: Gabriel Schaaf (gabriel.schaaf@zmbp.uni-tuebingen.de).
[OPEN]Articles can be viewed online without a subscription.
www.plantcell.org/cgi/doi/10.1105/tpc.114.135160

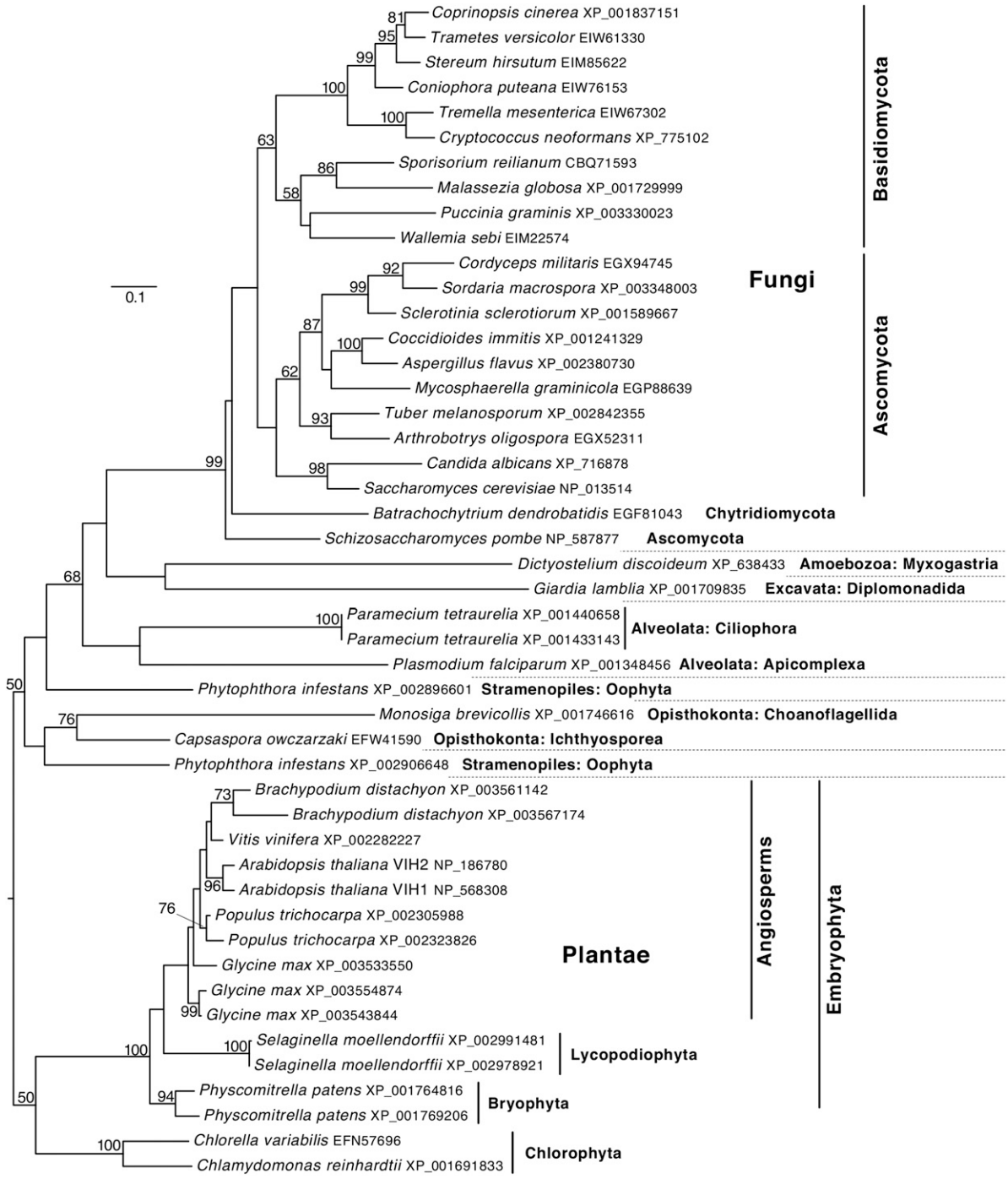

Figure 1. Vip1/PPIP5K Homologs Are Ubiquitous in Plants.

BLAST search analyses were performed employing the protein sequence of the *Saccharomyces cerevisiae* Vip1 ATP-grasp kinase domain (residues 1 to 535) as a search template. The tree was estimated from an alignment of ATP-grasp kinase domains of the encoded proteins using maximum likelihood. Branch support was calculated from 10,000 bootstrap replicates, and values below 50% are omitted. Branch lengths are given in terms of expected numbers of amino acid substitutions per site.

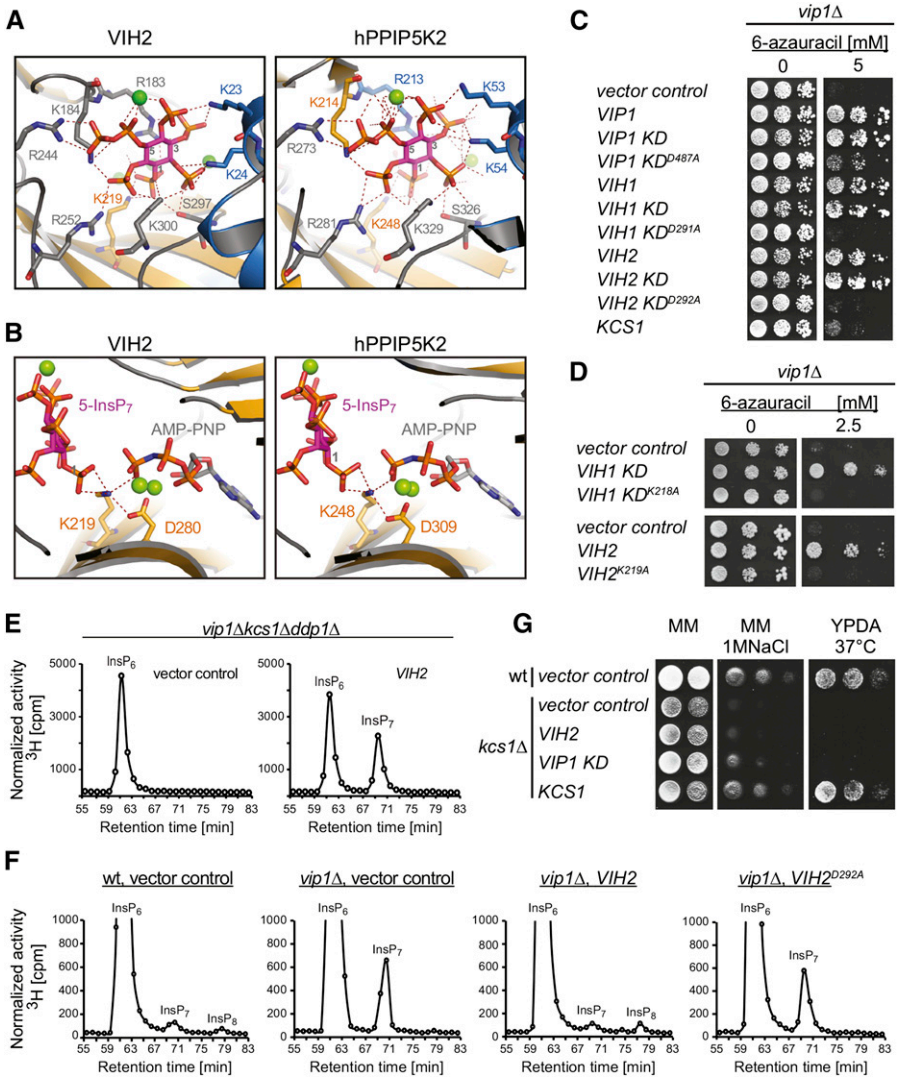

Figure 2. VIH1 and VIH2 Are Functional Vip1-Type PPIP5 Kinases.

(A) and **(B)** Structural model of the VIH2 ATP-grasp kinase domain (left) and the hPPIP5K2 ATP-grasp kinase domain (PDB ID: 3T9D, right) depicting the 5-InsP_7 binding sites and key catalytic residues. Residues coordinating substrate via polar contacts are shown as sticks, polar interactions are highlighted by dashed lines, α-helices are rendered in blue, β-sheets in orange, substrate (5-InsP_7) is rendered in magenta, and Mg^{2+} ions are presented as green spheres. Three carbon atoms on the inositol ring are numbered. The ATP analog AMP-PNP (in **[B]**) is depicted with gray carbon and orange and red phosphate groups.

(C) and **(D)** Complementation of *vip1*Δ-associated growth defects in yeast by ectopic expression of inositol pyrophosphate synthetases. The *vip1*Δ yeast strain transformed with episomal pDR195(*URA3*) plasmids carrying either *VIP1*, *VIH1*, or *VIH2*, sequences encoding their respective ATP-grasp kinase domains (*KD*) or designated kinase domain mutants, or carrying *KCS1* were spotted in 8-fold serial dilutions onto uracil-free minimal medium in presence or absence of 6-azauracil, as indicated. Rescue on medium supplemented with 6-azauracil (right) reports Vip1 activity.

(E) and **(F)** Normalized HPLC profiles of inositol phosphates of extracts from designated [^{3}H] inositol-labeled yeast transformants. Extracts were resolved by Partisphere SAX HPLC and fractions collected each minute for subsequent determination of radioactivity as indicated. Changes in elution times in independent experiments were observed and can be explained by subtle changes in column properties or column change. Experiments were repeated three times with similar results.

(G) Complementation assays of *kcs1*Δ-associated growth defects on high salt by ectopic expression inositol pyrophosphate synthetases. Wild-type (wt) or *kcs1*Δ yeast transformants (both DDY1810 background) carrying designated plasmids were spotted in 8-fold serial dilutions onto solid minimal media (MM, uracil deficient CSM media with YNB and appropriate supplements) in presence or absence of NaCl and onto solid YPDA media incubated at 37°C.

function during the plants wound response (Mosblech et al., 2008, 2011).

The discovery of diphosphoinositol polyphosphates, also referred to as inositol pyrophosphates, in amoebae, mammals, and yeast (Stephens et al., 1991; Menniti et al., 1993; Saiardi et al., 2000b) revealed an even higher complexity of this family of signaling molecules. In these organisms, inositol pyrophosphates regulate many cellular processes, including stress responses, membrane trafficking, telomere maintenance, ribosome biogenesis, cytoskeletal dynamics, insulin signaling, apoptosis, phosphate homeostasis, and neutrophil activation (Barker et al., 2009; Burton et al., 2009; Shears, 2009; Chakraborty et al., 2011; Wundenberg and Mayr, 2012). Two distinct classes of inositol pyrophosphate synthetases have been described: inositol hexakisphosphate kinases (also termed IP6Ks or Kcs1-like proteins) and diphosphoinositol pentakisphosphate kinases (PPIP5K or IP7K/Vip1-like proteins). IP6Ks phosphorylate the phosphate in the 5-position of $InsP_6$ and $Ins(1,3,4,5,6)P_5$ ($InsP_5$) and can use the resulting inositol pyrophosphates as substrates to generate more complex molecules containing two or more additional pyrophosphate moieties (Saiardi et al., 2000a, 2001; Draskovic et al., 2008). In contrast, PPIP5Ks phosphorylate the phosphate in the 1-position of both 5-$InsP_7$ and $InsP_6$, leading to the formation of the $InsP_8$ isomer 1,5$(PP)_2$-$InsP_4$ (1,5-$InsP_8$) and the $InsP_7$ isomer 1PP-$InsP_5$ (1-$InsP_7$), respectively (Mulugu et al., 2007; Lin et al., 2009; H. Wang et al., 2012).

The existence of inositol species more polar than $InsP_6$ has been reported in *Spirodela polyrrhiza* (Flores and Smart, 2000), barley (*Hordeum vulgare*; Brearley and Hanke, 1996; Dorsch et al., 2003), guard cells of intact guard cells of potato (*Solanum tuberosum*; Lemtiri-Chlieh et al., 2000), and in extracts of Arabidopsis and maize (*Zea mays*; Desai et al., 2014). In the later study, the authors addressed a possible involvement of Arabidopsis Vip1 homologs in the synthesis of inositol pyrophosphates by performing yeast complementation assays (Desai et al., 2014). Based on these assays, the authors proposed a function of Arabidopsis Vip1 homologs as IP6K enzymes with a possible role in $InsP_7$ biosynthesis. However, plants with altered Vip1 functions have not been investigated and the physiological role(s) of Vip1 proteins and inositol pyrophosphates in plants await clarification.

Here, we show that plant genomes of phylogenetically diverse taxa encode Vip1 homologs that appear to have evolved from a single common ancestor. We also provide evidence that $InsP_7$ and $InsP_8$ are readily detected in Arabidopsis extracts. The Vip1 homologs VIH1 and VIH2 are functional PPIP5Ks, and VIH2 is critical for $InsP_8$ production in Arabidopsis seedlings. Our data further suggest that VIH2-dependent inositol pyrophosphates represent key cofactors of the COI1-JAZ receptor complex, thereby playing an important role in jasmonate perception and jasmonate-regulated defenses.

Note that in a previous published work (Desai et al., 2014), which was published during the preparation of this article, Arabidopsis homologs of yeast Vip1 were named AtVIP1 and AtVIP2 (corresponding to VIH2 and VIH1, respectively). Because VIP1 is already in use for an unrelated protein (Arabidopsis VirE2 Interacting Protein 1, encoded by At1g43700), we propose to use the gene symbol *VIH* (*VIP1* homolog) registered at the TAIR database (see http://www.arabidopsis.org).

RESULTS

Vip1/PPIP5K Homologs Are Widespread in Plants

BLAST searching with the N-terminal ATP-grasp kinase domain of Vip1 as the query sequence allowed us to identify genes encoding putative Vip1/PPIP5K proteins in all available plant genomes, including diverse taxa such as green algae (Chlorophyta), mosses (Bryophyta), lycopods, and monocot and eudicot angiosperms, suggesting that PPIP5Ks play important basic functions in all plants. Phylogenetic analysis of the N-terminal ATP-grasp kinase domain of selected proteins, with a focus on plants and fungi, reflects major monophyletic groups as currently accepted (Keeling et al., 2009; Blackwell et al., 2012) (Figure 1). According to the maximum likelihood tree (Figure 1), all of the plant homologs are derived from a single ancestral gene, with subsequent gene duplications in the individual lineages.

The N-Terminal ATP-Grasp Kinase Domain in Arabidopsis Vip1 Homologs Has a Two-Domain Architecture and Is Structurally Conserved

We named the Arabidopsis Vip1 homologs identified in our BLAST search VIH1 and VIH2 (Vip1 homolog), respectively. Protein sequence comparison suggests that both proteins possess a two-domain architecture conserved in members of the Vip1/PPIP5K family, with an N-terminal ATP-grasp kinase domain and a C-terminal phosphatase-like domain (Supplemental Figure 1A). A model of the VIH2 kinase domain based on the crystal structure of human diphosphoinositol pentakisphosphate kinase 2 (hPPIP5K2) predicts the nucleotide analog AMP-PNP to be coordinated between two sets of antiparallel β-sheets as it has been described for hPPIP5K2 (H. Wang et al., 2012) (Supplemental Figure 1B). $InsP_7$ is coordinated exclusively by VIH2 lysine and arginine residues with the exception of one serine residue (as in hPPIP5K2), a hallmark of PPIP5K enzymes (H. Wang et al., 2012). Importantly, all protein-substrate interactions, including residues involved in the phosphotransfer reaction are conserved: VIH2 (hPPIP5K2) residues that coordinate the substrate are Lys-23 (Lys-53), Lys-24 (Lys-54), Arg-183 (Arg-213), Lys-184 (Lys-214), Lys-219 (Lys-248), Arg-244 (Arg-273), Arg-252 (Arg-281), Ser-297 (Ser-326), and Lys-300 (Lys-329) (Figures 2A and 2B) (H. Wang et al., 2012). These residues are also conserved in the VIH1 polypeptide (Supplemental Figure 1C). Collectively, these results suggest Arabidopsis VIH proteins execute Vip1/PPIP5K-like activities.

VIH1 and VIH2 Complement *vip1*Δ- but Not *kcs1*Δ-Associated Defects in Yeast

To address the function of VIH more directly, we investigated consequences of heterologous VIH expression in yeast. A previously identified *vip1*Δ-associated growth defect on 6-azauracil in yeast (Osada et al., 2012) was rescued by Arabidopsis VIH1 and VIH2, suggesting that these proteins execute Vip1-like activities in vivo (Figure 2C). In contrast, ectopic overexpression of Kcs1 under similar conditions failed to cause growth complementation of the single *vip1*Δ strain (Figure 2C). Rescue of this yeast strain was also observed by expression of the N-terminal

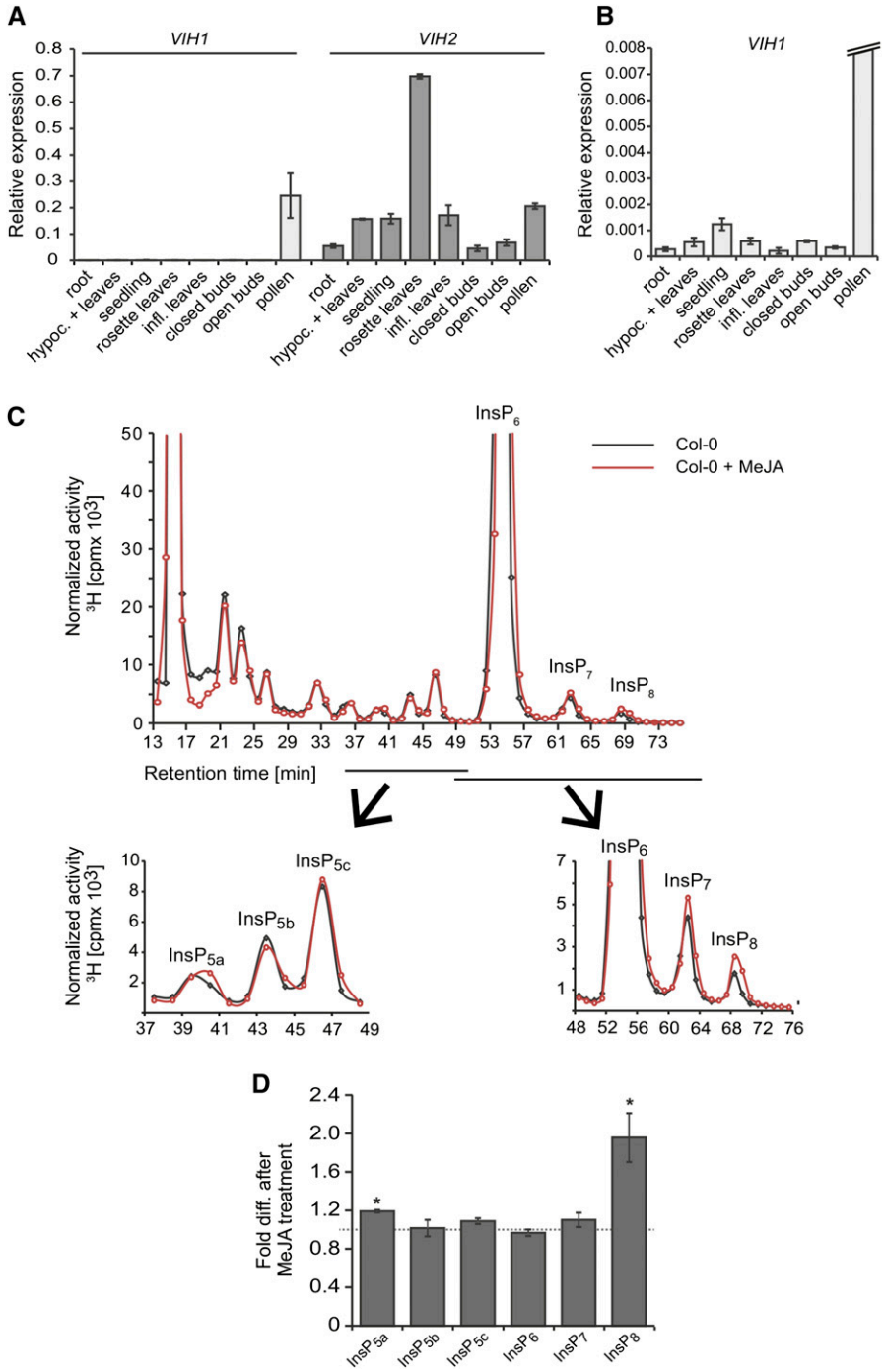

Figure 3. Expression Analyses Suggest Specialized Functions of *VIH1* and *VIH2*, and Inositol Pyrophosphates Can Be Detected in Arabidopsis Extracts and Are Regulated by Jasmonate.

(A) and **(B)** qPCR analyses of *VIH* expression in Col-0 plants using cDNA prepared from RNA extracts of different plant tissues as indicated. Averages of triplicate reactions ± SD are shown. β-*TUBULIN* was used as reference gene. Transcript levels of *VIH1* and *VIH2* are presented relative to β-*TUBULIN* transcript. The experiment was repeated three times with similar results.

(C) and **(D)** MeJA increases $InsP_8$ level. Normalized HPLC profiles **(C)** of 3-week old [^{3}H] inositol-labeled Col-0 seedlings that were untreated (solid gray line) or treated for 4 h with 50 μM MeJA (solid red lines). Treated and nontreated plants were harvested simultaneously to avoid daytime-dependent differences in inositol polyphosphate homeostasis. The experiment was repeated with similar results, and representative results from one experiment are shown. For relative amounts of respective species **(D)**, averages of fold differences after MeJA treatment of three independent experiments ± SE are

kinase domains of Vip1, VIH1, and VIH2, indicating that the 6-azauracil sensitivity of *vip1*Δ is caused by loss of Vip1 kinase activity and, importantly, that VIH1 and VIH2 possess a functional Vip1-like ATP-grasp kinase domain. This idea is supported by the finding that kinase catalytic dead mutant Vip1^{D487A} (Mulugu et al., 2007) and the corresponding mutant proteins VIH1^{D291A} and VIH2^{D292A} failed to rescue *vip1*Δ-associated growth defects on 6-azauracil (Figure 2C). In the context of the hPPIP5K2 enzyme, another residue, Lys-248, interacts with both the 1-phosphate of 5-InsP_7 and the γ-phosphate of ATP and therefore plays an essential function in the catalytic cycle of 5-InsP_7 phosphorylation and the specificity of the phosphotransfer reaction (Figure 2B) (H. Wang et al., 2012). This residue is conserved in plant Vip1 homologs and our structural model suggests that the corresponding Arabidopsis VIH2 residue K219 interacts with substrate and cofactor in a similar manner (Figure 2B).

In agreement with this idea, mutant polypeptides VIH1-KD^{K218A} and VIH2^{K219A} are dysfunctional (Figure 2D). All proteins, including catalytic dead mutants, were correctly expressed (Supplemental Figures 2A and 2B). We further investigated consequences of VIH2 expression on inositol polyphosphate metabolism in different yeast strains. We expressed VIH2 in a *vip1*Δ *kcs1*Δ *ddp1*Δ triple mutant yeast strain, which lacks inositol pyrophosphates and is devoid of Ddp1 (diadenosine-and-diphosphoinositol-polyphosphate-phosphohydrolase)-dependent inositol pyrophosphatase activity, thus facilitating the detection of inositol pyrophosphates synthesized by ectopically expressed kinases (Safrany et al., 1998; Mulugu et al., 2007). VIH2 expression in this background resulted in a robust InsP_7 peak that eluted at a retention time identical to the 1-InsP_7 peak in transformants ectopically expressing Vip1 (Figure 2E; Supplemental Figure 2D), supporting recent observations by Desai et al. (2014). However, these results did not address whether VIH proteins have Vip1/PPIP5K or Kcs1/IP6K-like activities.

Therefore, we expressed VIH2 in single *vip1*Δ or *kcs1*Δ mutant backgrounds. Because of a preference of Vip1 to phosphorylate 5-InsP_7 to 1,5-InsP_8, *vip1*Δ yeast cells accumulate the non-metabolized substrate 5-InsP_7 (Azevedo et al., 2009; Onnebo and Saiardi, 2009; Padmanabhan et al., 2009) (Figure 2F). Levels of 1-InsP_7 and 1,5-InsP_8 are generally low in wild-type yeast due to the activity of Ddp1 (Safrany et al., 1998; Mulugu et al., 2007). As apparent from a robust rescue of (i.e., decrease in) 5-InsP_7 levels, expression of VIH2 complemented *vip1*Δ-associated defects in inositol pyrophosphate homeostasis in a kinase-dependent manner (Figure 2F; Supplemental Figure 2C). We also investigated the consequences of ectopic expression of Kcs1, Vip1, and VIH2 in a *kcs1*Δ single mutant yeast strain. While ectopic expression of Kcs1 complemented a previously described growth defect of *kcs1*Δ cells on 1 M NaCl at 37°C, ectopic expression of Vip1 and VIH2 under similar conditions failed to do so. This is in agreement with the idea that VIH2 does not have Kcs1/IP6K-like activities (Figure 2G). We also found that overexpression of Vip1 kinase activity in *kcs1*Δ cells causes production of InsP_7 and InsP_8 (Supplemental Figure 2E). Based on previous in vitro studies (Losito et al., 2009), these species are likely to represent 1-InsP_7 and 1,3-InsP_8 or 1PPP-InsP_7. Likewise, ectopic expression of VIH2 caused peaks with identical chromatographic mobilities (Supplemental Figure 2E). Collectively, these data suggest that VIH2 executes Vip1/PPIP5K but not Kcs1/IP6K-like activities in yeast.

Levels of the Inositol Pyrophosphate InsP_8 Are Regulated by Methyl Jasmonate and Depend on VIH2

Quantitative PCR (qPCR) analyses showed expression of *VIH1* to be restricted mainly to pollen (Figures 3A and 3B). *VIH2* expression, on the other hand, was ubiquitous and especially strong in rosette leaves (Figure 3A), suggesting specialized functions of both isoforms. To investigate VIH2 functions in planta, we analyzed inositol polyphosphates in 3-week-old seedlings of wild-type (Columbia-0 [Col-0]) and *vih2* mutant plants. HPLC runs of [^{3}H]-inositol-labeled Col-0 plant extracts showed a similar profile as reported previously (Stevenson-Paulik et al., 2005), with a robust peak at a retention time identical to the [^{3}H]-InsP_6 standard (Figure 3C; Supplemental Figure 3A). However, in contrast to this previous report, we also detected two additional peaks more anionic than InsP_6 that eluted at elution times expected for InsP_7 and InsP_8, respectively (Figure 3C), supporting recent findings by Desai et al. (2014).

Inositol phosphates have been implicated in the wound response (Mosblech et al., 2008, 2011; Sheard et al., 2010), a process that is regulated by the oxylipin JA and related signaling molecules (collectively referred to as jasmonates), as well as by the stress hormone abscisic acid (ABA) (Vos et al., 2013). Therefore, we explored the role of jasmonates and ABA in the regulation of inositol pyrophosphates. Treatment of Col-0 seedlings with methyl jasmonate (MeJA) caused a 2-fold increase in InsP_8, but only had subtle effects on other inositol polyphosphate species (as exemplified for various InsP_5 species; Figures 3C and 3D). A time-course experiment with MeJA-treated plants showed an almost 2-fold increase in levels of InsP_8 already after 15 min, which remained stable for the course of 3 h. In contrast, InsP_7 levels were not affected by MeJA treatment (Supplemental Figures 3C and 3D). Very different effects were observed in ABA-treated plants: ABA induced increases in both InsP_7 and InsP_8 in a dose-dependent manner (Supplemental Figure 3E).

To investigate the potential role of VIH2 in inositol pyrophosphate homeostasis, we analyzed two independent T-DNA insertion lines (*vih2-3* and *vih2-4*) that lack *VIH2* transcript (Supplemental Figures 4A and 4B). Overall incorporation of [^{3}H]-*myo*-inositol was not affected in these mutants (Supplemental

Figure 3. (continued).

shown. Asterisks indicate statistical differences (Student's *t* test; *P < 0.02).The isomeric identity of InsP_{5b} is unknown in Arabidopsis seedlings. Based on chromatographic mobilities presented in a previous study on seedlings of Col-0 plants and *ipk1-1* plants (Stevenson-Paulik et al., 2005), and comparison with chromatographic mobilities of inositol polyphosphates in the same *ipk1-1* line on our HPLC (Supplemental Figures 8A and 8B), InsP_{5a} represents Ins(1,3,4,5,6)P_5 and InsP_{5c} represents Ins(1,2,4,5,6)P_5 or its enatiomer Ins(2,3,4,5,6)P_5.

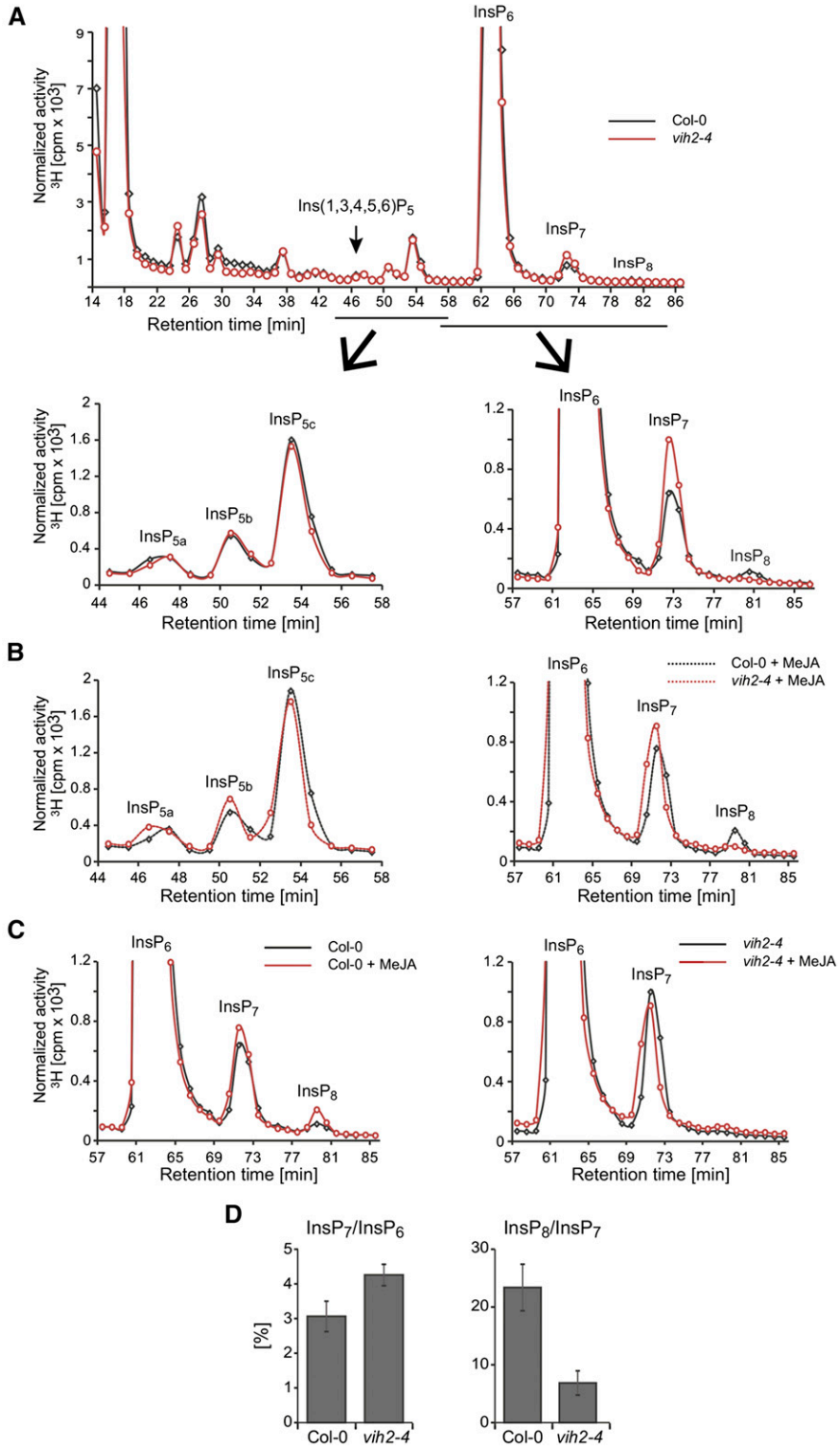

Figure 4. Bulk Steady State and Jasmonate-Induced Pools of $InsP_8$ in Arabidopsis Seedlings Depend on VIH2.

Normalized HPLC profiles (**[A]** to **[C]**) or relative amounts **(D)** of inositol phosphate species of 3-week-old [^{3}H] inositol-labeled Col-0 (solid black line) and *vih2-4* seedlings. In **(B)** and **(C)**, plants were treated with 50 μM MeJA and harvested after 30 min together with nontreated plants. Extracts were resolved by Partisphere SAX HPLC and fractions collected each minute for subsequent determination of radioactivity. The experiment was repeated

Figure 4C). HPLC profiles of *vih2* plants were similar to those of wild-type plants but showed a robust reduction of $InsP_8$ with a concomitant increase in $InsP_7$, suggesting that, like Vip1 in yeast, Arabidopsis VIH2 catalyzes the conversion of $InsP_7$ to $InsP_8$ (Figures 4A and 4D; Supplemental Figures 5A to 5C). Small residual levels of $InsP_8$ in *vih2* plants remained completely insensitive to MeJA, independent of the exposure time (30 min MeJA in Figures 4B and 4C; 4 h MeJA in Supplemental Figure 5D). In summary, these results show that in seedlings, $InsP_8$ levels are upregulated by MeJA treatment and that both bulk/steady state and MeJA-induced pools of $InsP_8$ depend on VIH2.

VIH2 Plays a Critical Role in Jasmonate-Regulated Defenses

We examined the functional role of VIH2 in the defense against Brassicaceae specialist *Pieris rapae* (small white butterfly) and the generalist *Mamestra brassicae* (cabbage moth) by monitoring larval development in a no-choice setup in which larvae are contained and allowed to only graze on one specific genotype. Both *P. rapae* and *M. brassicae* larvae feeding on *vih2* plants showed a significant weight increase compared with larvae feeding on Col-0 plants (Figures 5A and 5B), suggesting that VIH2 plays a role in activating defenses that interfere with insect herbivore development.

To examine whether decreased herbivore resistance was caused by compromised jasmonate production or perception, we analyzed jasmonates and jasmonate-responsive gene expression. To our surprise, upon mechanical wounding, *vih2* mutants exhibited increased levels of JA and bioactive conjugates such as JA-Leu/Ile and JA-Val compared with Col-0 (Figures 5C and 5D; Supplemental Figure 6A), an observation that is counterintuitive to decreased insect herbivore resistance in these plants. However, expression of *VSP2*, a marker gene of the MYC branch of JA signaling known to be induced by jasmonates and herbivores, was reduced in *vih2* plants after infestation with *P. rapae* larvae relative to Col-0 plants (Figure 5E; Supplemental Figure 6B). Similar results were obtained for *MYC2* expression (Figure 5E). These findings are in agreement with a reduced resistance of *vih2* plants in the performance assays. The observation that MYC-branch marker gene expression in *vih2* plants was reduced despite an increase in jasmonates suggests a defect in jasmonate perception. Supporting a defect in jasmonate-regulated defenses, *vih2* plants were also found to be more susceptible to the necrotrophic fungi *Botrytis cinerea* and *Alternaria brassicicola* (Supplemental Figures 6C and 6D).

Inositol Pyrophosphates Bind to the ASK1-COI1-JAZ Jasmonate Receptor Complex

To further investigate the role of VIH2 in jasmonate perception, we performed molecular docking of Ins(1,2,4,5,6)P_5, which copurified with ASK1-COI1 from insect cells (Sheard et al., 2010), and 1,5-$InsP_8$ into the proposed inositol polyphosphate binding pocket of the ASK1-COI1-JAZ1-JA-Ile complex. Poses with the highest scores (shown in Figures 6A and 6B) predict that the concave surface of the COI1 solenoid fold surrounds and binds molecules at overlapping, yet distinct, sites. An intricate network of basic COI1 residues (Lys-79, Lys-81, Arg-85, Arg-120, Arg-121, Arg-409, and Arg-440) and JAZ1 residue Arg-206 are predicted to coordinate Ins(1,2,4,5,6)P_5 and 1,5-$InsP_8$ (Figures 6A and 6B). The 1,5-$InsP_8$ molecule is predicted to be additionally stabilized by COI1 residues His-118, Arg-346, Tyr-382, and Lys-492, which coordinate the 1-β-phosphate, the 3-phosphate, the 3-phosphate, and the 5-β-phosphate of 1,5-$InsP_8$, respectively. We investigated the involvement of three of these residues (His-118, Arg-346, and Lys-492; highlighted in Figure 6B) in COI1-JAZ1 interaction in a yeast two-hybrid system. These residues are positioned as an almost equilateral triangle (distance of respective coordinating groups: His-118, Lys-492, 13.01 Å; His-118-Arg-346, 13.06 Å; and Lys-492-Arg-346, 13.57 Å) and for geometrical reasons and assuming rigid ligand binding, not all three residues can interact with Ins(1,2,4,5,6)P_5 or other $InsP_5$ isomers (not containing diphosphobonds) simultaneously. Individual substitution of these amino acids (predicted to specifically coordinate 1,5-$InsP_8$) by Ile completely abolished COI1-JAZ1 interaction, even though protein stability was not (His-118I and Lys-492I) or only mildly (Arg-346I) affected (Figures 6C and 6D). These results suggest a critical role of $InsP_8$ rather than $InsP_5$ isomers in COI1-JAZ1 complex formation.

To investigate whether inositol pyrophosphate can bind directly to the COI1-JAZ1 complex, we performed binding assays of ASK1-COI1-JAZ1 with radiolabeled [^{3}H]-$InsP_5$, [^{3}H]-$InsP_6$, and [^{3}H]-$InsP_7$ purified and desalted from [^{3}H]-*myo*-inositol-labeled seedlings as described in experimental procedures. Inositol polyphosphate binding was only observed in the presence of the structural JA-Ile analog coronatine, suggesting that inositol polyphosphates do not stimulate ASK1-COI1-JAZ1 complex formation in the absence of jasmonates (Figure 7A). Importantly, plant $InsP_7$ bound more efficiently than $InsP_6$, which bound more efficiently than Ins(1,3,4,5,6)P_5, indicating that inositol pyrophosphates are superior ligands of the ASK1-COI1-JAZ1 complex compared with less anionic inositol polyphosphate species (Figures 7A and 7B).

DISCUSSION

Inositol pyrophosphates have gained recent attention as signaling molecules in amoeba, yeast, and mammalian cells (Mulugu et al., 2007; Shears, 2009; Chakraborty et al., 2011; Szijgyarto et al., 2011; Wundenberg and Mayr, 2012; Pöhlmann et al., 2014). Here,

Figure 4. (continued).

with similar results, and representative results from one experiment are shown. **(B)** is a zoom-in into the $InsP_5$ (left) and $InsP_{6\text{-}8}$ (right) regions of HPLC runs with extracts of MeJA-treated Col-0 and *vih2* seedlings as indicated. For $InsP_{5a\text{-}c}$ isomer identities, see comment in Figure 3. **(C)** is a zoom-in into the $InsP_{6\text{-}8}$ regions of HPLC runs with extracts of Col-0 (left) and *vih2* (right) seedlings with or without MeJA treatment as indicated. For relative amounts **(D)**, data are presented either as $InsP_7$/$InsP_6$ ratio (a measure of IP6K activity) or as $InsP_8$/$InsP_7$ ratio (a measure of PPIP5K activity). The data represent means ± SE.

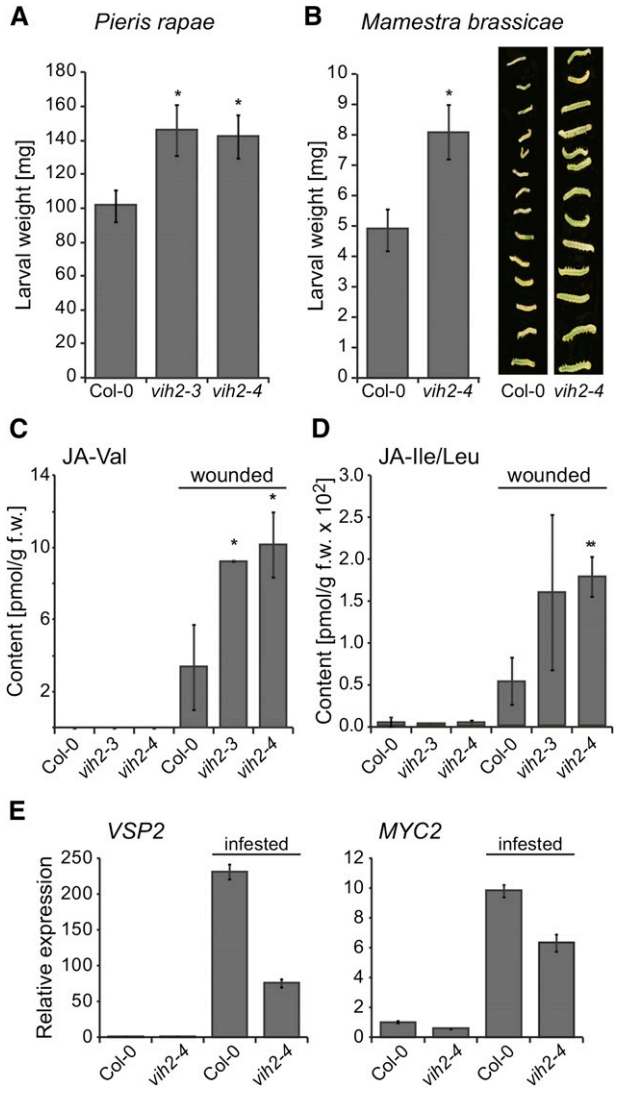

Figure 5. Arabidopsis *vih2* Lines Have Reduced Defenses against Larvae of Herbivorous Insects and Are Compromised in Jasmonate Perception.

(A) and **(B)** Larval development was monitored in a no choice setup. One caterpillar each (larval stage L1) of the Brassicaceae specialist *P. rapae* **(A)** or the generalist *M. brassicae* **(B)** was released onto a single 5-week-old plant ($n = 20$) of the designated genotype. Fresh weight of caterpillars was determined after 7 d (*P. rapae*) or 8 d (*M. brassicae*). The values represent means ± SE. Asterisks indicate statistical differences (Student's *t* test; *P < 0.02). Plant genotype-dependent size differences of *M. brassicae* larvae are also visualized by a photograph (**[B]**, right panel). Experiments were repeated with similar results.

(C) and **(D)** Determination of bioactive conjugates JA-Val and JA-Ile/Leu. Conjugate levels were determined in rosette leaves of 4-week-old plants of designated genotypes under sterile conditions and 3 h after inflecting wounding by squeezing each leaf with forceps. Data represent means of three independent biological replica ± SD. Statistical significance is indicated by asterisks (Student's *t* test; *P < 0.02 and **P < 0.005).

(E) qPCR analysis of JA-dependent genes. Gene expression was analyzed by qPCR analyses using RNA extracted from pooled leaves ($n = 5$) of 5-week-old plants of the designated genotype that were untreated or infested for 24 h by *P. rapae* larvae as indicated. *PP2AA3* was used as a reference gene. The expression value of untreated Col-0 was set to 1. Shown are means ± SE ($n = 3$). qPCR analyses were repeated with similar results.

we describe the presence of $InsP_7$ and $InsP_8$ in the model plant Arabidopsis and show that VIH2 is a functional inositol pyrophosphate synthetase responsible for $InsP_8$ production, playing a critical role in jasmonate-regulated defenses. The ubiquitous presence of Vip1/PPIP5K homologs in plants as suggested by our work supports and extends previous reports of the wide distribution of these enzymes in eukaryotic organisms and underlines the fundamental importance of inositol pyrophosphates in regulating cellular functions.

VIH Proteins Have Vip1/PPIP5K-Like Activities

A structural model of the VIH2 ATP-grasp kinase domain and complementation of defects in growth and inositol polyphosphate homeostasis of yeast *vip1* mutants indicate that VIH1 and VIH2 execute Vip1/PPIP5K-like activities and are likely to pyrophosphorylate the 1-position of $InsP_6$ and 5-$InsP_7$ in yeast (Figure 2). A recent study by Desai et al. (2014) that was published while this article was in preparation also addressed the function of Arabidopsis Vip1 homologs. Similar to the experiment shown in Figure 2E, the authors show that expression of these proteins in a yeast *vip1*Δ *kcs1*Δ *ddp1*Δ triple mutant results in $InsP_7$ production. Based on these results, the authors predicted a role of these enzymes as IP6K ($InsP_6$ kinase) enzymes. Unfortunately, this experiment does not allow discrimination between Kcs1/IP6K and Vip1/PPIP5K activities because Vip1/PPIP5K enzymes are well known to efficiently use $InsP_6$ as a substrate to produce (1-)$InsP_7$ (Mulugu et al., 2007; Lin et al., 2009; Losito et al., 2009). We therefore investigated the ability of VIH proteins to complement single mutant *kcs1*Δ or *vip1*Δ yeast phenotypes and analyzed the role of VIH2 in planta. We show that VIH proteins rescue *vip1*Δ-associated growth defects on 6-azauracil, whereas they fail to rescue *kcs1*Δ-associated growth defects (Figures 2C, 2D, and 2G). Furthermore, we show that VIH2 complements the *vip1*Δ-associated defect in $InsP_7$ to $InsP_8$ conversion (Figure 2F; Supplemental Figure 2C) and that *vih2* lines are compromised in $InsP_8$ synthesis and (similar to yeast *vip1*Δ mutants) accumulate $InsP_7$ (Figures 4B and 4D; Supplemental Figure 5). Collectively, these data provide strong evidence that in vivo VIH proteins do not execute IP6K/Kcs1-like activities as suggested by Desai et al. (2014) but PPIP5K/Vip1-like activities.

The Isomer Identity of Plant Inositol Pyrophosphates Remains Unresolved

The expression pattern of *VIH2* and the pronounced effect on seedling $InsP_8$ production observable in *vih2* plants indicate that VIH2 is the major enzyme synthesizing $InsP_8$ in Arabidopsis (Figures 3 and 4; Supplemental Figures 5A and 5B). It remains unclear, however, whether plant $InsP_7$ and $InsP_8$ have the same isomer identity as in yeast. Anion exchange HPLC

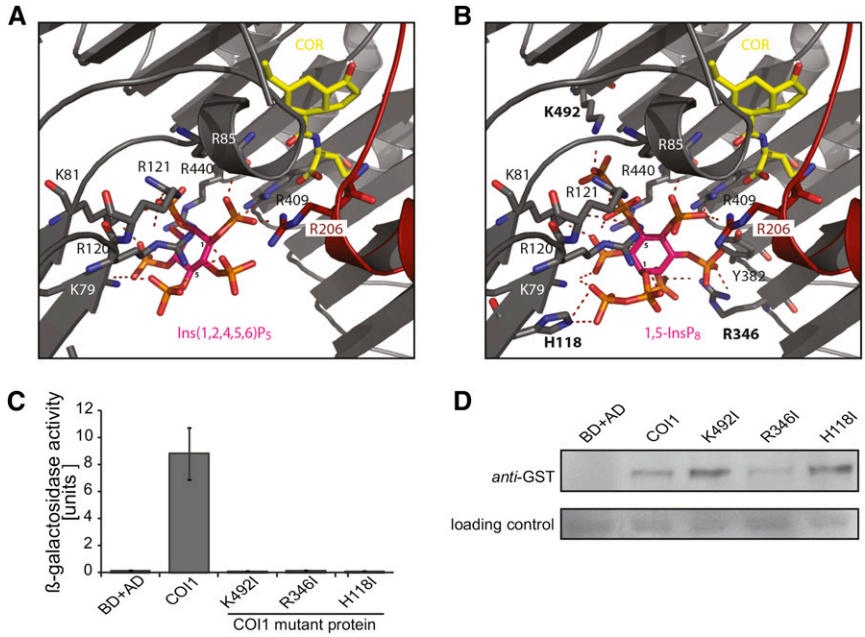

Figure 6. Structural Models of ASK1-COI1-JAZ1-Coronatine in Complex with Ins(1,2,4,5,6)P_5 or 1,5-InsP_8 and Functional Evaluation of Proposed 1,5-InsP_8 Binding Mutants Suggest a Role of InsP_8 in Jasmonate Receptor Complex Formation.

(A) and **(B)** COI1-JAZ structures containing Ins(1,2,4,5,6)P_5 or 1,5-InsP_8 as obtained from in silico docking experiments are shown. COI1 (gray ribbon), coronatine (COR) in yellow stick representation, and inositol polyphosphates (rendered as stick in magenta) are presented. Hydrogen bonds and salt bridge networks are depicted as dashed lines. Residues in bold were substituted by Ile for yeast two-hybrid studies.

(C) JAZ1 interaction with wild-type or mutant COI1 in yeast was evaluated in the presence of 50 μM coronatine by coexpression of pGBKT7-*COI1* (and mutated versions as indicated) with pGADT7-*JAZ1* in yeast strain Y187 (Clontech) and subsequent quantification of β-galactosidase-mediated hydrolysis of ortho-nitrophenyl-β-D-galactopyranoside. Values represent means of four independent biological replica ± SD.

(D) Stability of mutant COI1 protein. Immunoblots of soluble lysates prepared from tobacco (*Nicotiana benthamiana*) leaves expressing COI1 mutants (as designated) in translational fusion with N-terminal GST. Equal amounts of total protein were loaded, and COI1 was detected with antibodies against GST (Sigma-Aldrich). As a normalization control (lower panel), a representative unspecific band was chosen.

chromatography does not allow unambiguous discrimination between different inositol pyrophosphate isomers of same molecular mass. Two major observations challenge the idea that yeast and plant InsP_7 and InsP_8 isomers are identical. First, BLAST search analyses did not allow the identification of plant Kcs1/IP6K homologs, suggesting that an unknown enzyme activity is responsible for plant InsP_7 production. Second, plant-purified InsP_7 exhibits a higher binding affinity for the ASK1-COI1-JAZ1 jasmonate receptor complex than InsP_6 or InsP(1,3,4,5,6)P_5 (Figure 7B). In contrast, competition assays following a similar strategy recently employed to evaluate InsP_7 binding to human casein kinase-2 (Rao et al., 2014) showed that available

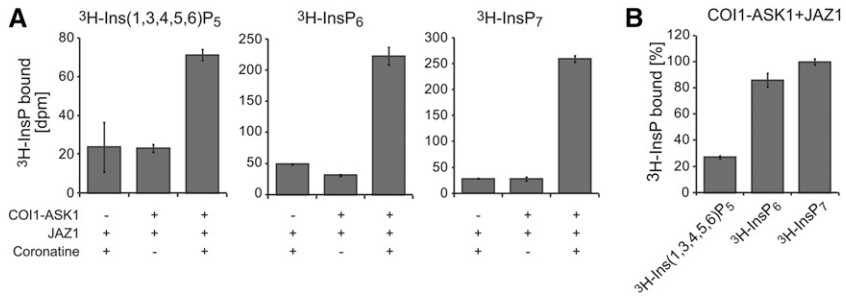

Figure 7. Plant Inositol Pyrophosphates Are Superior Ligands of the ASK1-COI1-JAZ1 Complex Compared with Less Anionic Inositol Polyphosphate Species.

Direct binding of [^{3}H]-InsP_5, [^{3}H]-InsP_6, and [^{3}H]-InsP_7 (purified and desalted from [^{3}H]-*myo*-inositol labeled seedlings of the *ipk1-1* mutant [InsP_5] or Col-0 seedlings [InsP_6 and InsP_7]) to the ASK1/COI1/His$_8$-MBP-JAZ1 jasmonate receptor complex or to individual components of the receptor complex (ASK1-COI1 or His$_8$-MBP-JAZ1) was analyzed with or without 1 μM coronatine. A total activity of 2000 dpm was used for each [^{3}H]-labeled inositol phosphate species. The average of recovered radiolabel with [^{3}H]-InsP_7 in **(B)** is set to 100%. Values show means ± SE (n = 2 or 3) of radiolabel recovered by pull-down of His$_8$-MBP-JAZ1 via metal affinity chromatography, and experiments were repeated with similar results.

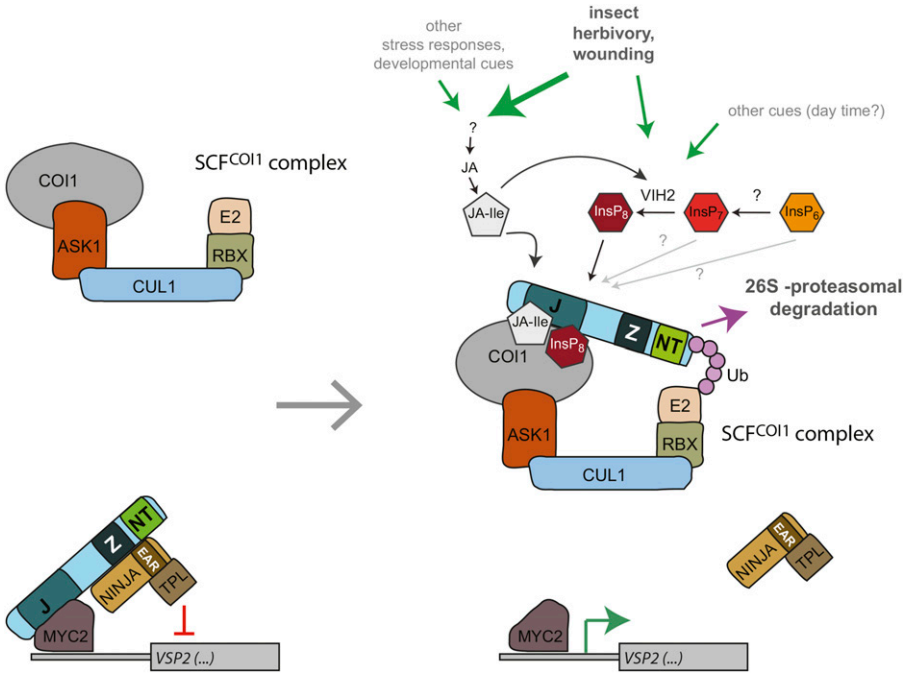

Figure 8. Model of the Role of VIH2 and $InsP_8$ in the Wound Response.

Mechanical wounding or herbivore attack stimulate the synthesis of JA and bioactive JA conjugates such as JA-Ile. Increasing jasmonate levels trigger a fast VIH2-dependent increase in $InsP_8$, which is most likely caused by posttranslational activation of the VIH2 protein. Both JA-Ile and $InsP_8$ occupy designated binding pockets in COI1-ASK1 and might work as molecular glue to recruit the JAZ repressor protein. Subsequent polyubiquitylation of JAZ by the SCF ubiquitin E3 ligase complex causes proteasomal degradation of the JAZ repressor and allows expression of jasmonate/$InsP_8$-responsive genes such as *VSP2*. The physiological role of other inositol polyphosphates on potentiating jasmonate dependent formation of the SCF^{COI1} ubiquitin E3 ligase complex remains unclear.

chemically synthesized $InsP_7$ isomers have lower affinities than $InsP_6$ (1-$InsP_7$, 5-$InsP_7$, and 6-$InsP_7$) or a similar affinity (4-$InsP_7$) for the jasmonate receptor complex (Supplemental Figures 7A to 7C). Future research will have to address purification of plant $InsP_7$ in sufficient amounts for NMR analyses or crystallography to reveal plant $InsP_7$ (and by extension $InsP_8$) isomer identity. Equally important for future studies will be the identification of the protein (s) responsible for plant $InsP_7$ synthesis.

Plant $InsP_8$ Has a Role in Resistance against Insect Herbivores and Necrotrophic Fungal Pathogens

The finding that ABA induces $InsP_7$ and $InsP_8$ production (Supplemental Figure 3E), whereas MeJA induces production of primarily $InsP_8$ and not $InsP_7$ (Figures 3C, 3D, and 4C; Supplemental Figures 3C and 3D) identifies interesting interactions between jasmonate and ABA signaling that are distinct from those reported previously (Pieterse et al., 2012). Several lines of evidence suggest that plant $InsP_8$ is responsible for the VIH2-dependent contribution to resistance against herbivores and necrotrophs: (1) *vih2*-mutant seedlings have robustly decreased levels of $InsP_8$ and exhibit a decreased resistance against larvae of herbivorous insects and necrotrophs and have a defect in jasmonate perception (Figures 4 and 5; Supplemental Figures 5 and 6); (2) MeJA treatment causes a robust and specific increase in a VIH2-dependent pool of $InsP_8$ (Figures 3 and 4; Supplemental Figures 3 and 5); (3) direct binding assays suggest that plant-derived inositol pyrophosphate ($InsP_7$) binds more efficiently to the ASK1-COI1-JAZ1 complex than less anionic inositol polyphosphates such as $InsP_6$ and Ins(1,3,4,5,6)P_5 (Figure 7B); (4) the proposed inositol polyphosphate binding pocket of the ASK1-COI1-JAZ1 jasmonate receptor complex is large enough to accommodate a single $InsP_8$ molecule (Figures 6A and 6B) and COI1 mutants designed to specifically prevent $InsP_8$ binding failed to interact with JAZ1 in yeast (Figure 6C). Unfortunately, we failed to purify sufficient amounts of plant derived $InsP_8$ to perform radioligand binding based reconstitution assays, which will be an important task for future work.

Our study does not rule out that other inositol polyphosphates may influence assembly of the jasmonate receptor complex. Ins(1,2,4,5,6)P_5, which copurified with the ASK1-COI1 complex from insect cells (Sheard et al., 2010), is an interesting candidate in this regard. However, it is unclear whether plants synthesize Ins(1,2,4,5,6)P_5 or its enantiomer Ins(2,3,4,5,6)P_5 (Stevenson-Paulik et al., 2005; Hanke et al., 2012), and a physiological significance of either species in herbivore resistance has not been established so far. Another isomer, Ins(1,3,4,5,6)P_5, that highly accumulates in *ipk1-1* plants (Supplemental Figure 8) has been implicated in the increased herbivore resistance of this plant mutant (Mosblech et al., 2011). While it remains to be shown whether this $InsP_5$ isomer has any function in ASK1-COI1-JAZ complex formation in the context of a wild-type plant, we can

exclude the possibility that it plays a role in VIH2-dependent insect herbivore resistance because Ins(1,3,4,5,6)P_5 levels did not change in *vih2* lines (Figures 4A and 4B; Supplemental Figures 5A and 5B).

Coincidence Detection of Jasmonate and Inositol Phosphates by the Jasmonate Coreceptor

Direct binding assays with [^{3}H]-Ins(1,3,4,5,6)P_5, [^{3}H]-InsP_6, and [^{3}H]-InsP_7 (Figures 7A and 7B) indicate that inositol polyphosphate binding is not sufficient for ASK1-COI1-JAZ1 assembly but still requires the presence of coronatine (or by extension JA-Ile). Combined with the previous observation that coronatine fails to trigger the formation of the ASK1-COI1-JAZ complex in the absence of inositol polyphosphate (Sheard et al., 2010), these data suggest that only coincidence detection of both inositol polyphosphate or pyrophosphate and bioactive jasmonate allows complex formation and subsequent proteasomal degradation of JAZ repressor proteins to stimulate jasmonate responsive gene expression (Figure 8). We propose that coincidence detection of two unrelated molecules might prevent an uncontrolled accidental trigger of immune responses that are known to severely affect plant growth and development (Pieterse and Dicke, 2007; Howe and Jander, 2008). This idea is in agreement with a recent finding that COI1 protein levels are strictly regulated by a dynamic balance between SCF^{COI1}-mediated stabilization and 26S proteasome-mediated degradation (Yan et al., 2013).

In addition, coincidence detection could allow differentiated immune responses. It still remains a central unanswered question how plants achieve specificity in their response to herbivore attack. It has been shown, for instance, that transcriptional responses of Arabidopsis to caterpillar (*P. rapae*) and thrips (*Frankliniella occidentalis*) infestation is primarily via COI1-dependent gene regulation, but that expression patterns of these genes are specific to one or the other insect herbivore (De Vos et al., 2005). We speculate that a differentiation in COI1-dependent responses might be in part determined by the inositol pyrophosphate signature of a given tissue under herbivore attack. It is important to note that InsP_6 also has previously been suggested to play an important role in the maintenance of basal resistance to plant pathogens. The reduction of InsP_6 in potato and Arabidopsis was correlated with increased susceptibility toward different viral infections and also caused hypersensitivity to fungal and bacterial infections in Arabidopsis (Murphy et al., 2008). In future experiments, it will be important to study whether these effects are an immediate consequence of reduced InsP_6 or whether they are caused by the reduction of InsP_6-dependent inositol pyrophosphates. Independent of this outcome, breeding strategies and biotechnological approaches to reduce InsP_6 will have to consider possible negative side effects in crop plants.

METHODS

BLAST Search and Phylogenetic Analyses

Sequence sampling focused on plants and fungi with some additions of protist species. BLAST search analyses (http://blast.ncbi.nlm.nih.gov/Blast.cgi) were performed using the N-terminal part of *Saccharomyces cerevisiae* Vip1 (residues 1 to 535), which contains the entire ATP-grasp kinase domain (Mulugu et al., 2007). The amino acid sequences were aligned using MAFFT, version 6.927b (Katoh et al., 2005). Heterogeneous alignment regions were excluded prior to phylogenetic analyses using Gblocks (Castresana, 2000), with the minimum length of a block set to five, allowing gaps in up to 50% of the sequences at a given site, a minimum number of sequences of 24 for a conserved or a flanking position, and a maximum number of contiguous nonconserved positions of eight. A phylogenetic tree was estimated using maximum likelihood (Felsenstein, 1981) with RAxML version 7.3.2 (Stamatakis, 2006a). Fast bootstrap analyses (Felsenstein, 1985; Stamatakis et al., 2008) over 10,000 rounds were run on the Web-based bioportal facility (Kumar et al., 2009) (http://www.mn.uio.no/ibv/bioportal/) with eight parallel processors, using bootstrap trees as starting trees for heuristic searches, and employing the DAYHOFF model of amino acid substitution as inferred with the ProteinModelSelection perl script (http://www.exelixis-lab.org/), accounting for rate heterogeneity by using the CAT model (Stamatakis, 2006b). The final tree was optimized using the Gamma model of rate heterogeneity (Yang, 1993).

Plants and Growth Conditions

For T-DNA insertion lines, seeds of mutant lines of *Arabidopsis thaliana* (ecotype Col-0) were obtained from The European Arabidopsis Stock Centre (http://arabidopsis.info/). The T-DNA lines used in this study are as follows: *vih2-3a* (SAIL_165_F12), *vih2-4* (GK-080A07), and *ipk1-1* (SALK_065337C). Homozygous lines were identified by PCR using T-DNA left and right border primers and gene-specific sense or antisense primers (Supplemental Table 1). The isolated homozygous progeny of the *vih2-3a* line identified by PCR-based genotyping was found to have short root hairs compared with Col-0. However, the phenotype did not cosegregate with the *vih2-3* allele in the F2 generation of a cross with the *vih1-1* T-DNA line (SAIL_543_F08), suggesting that the original *vih2-3a* plant had an additional insertion or mutation causing the root hair phenotype. Therefore, *vih2-3a* was crossed with a *VIH2* wild-type plant (Col-0 background) and F3 progeny homozygous for the *vih2-3* allele (exhibiting normal root hairs) used for further analyses. All lines analyzed in this study, including Col-0 plants, were grown in parallel for two generations under identical conditions on soil (16 h light and 8 h dark, day/night temperature 22/18°C and 120 $\mu mol^{-1}\ m^{-2}$ light intensity), and seeds of the respective last progenies were used for all analyses described in this article. For growth in sterile conditions, seeds were sterilized in 70% (v/v) ethanol and 0.05% (v/v) Triton X-100 for 30 min and washed twice in 90% (v/v) ethanol. Sterilized seeds were plated onto 0.5× MS, 1% sucrose, 0.7 to 0.8% phytagel stratified for 2 d at 4°C, and grown under conditions of 12 h light (23°C) and 12 h dark (21°C). To investigate the expression of distinct *VIH2* domains in the respective T-DNA insertion lines, qPCR analyses were performed using the primers listed in Supplemental Table 2.

Performance and Disease Assays

Plants were grown at standard growth conditions in the greenhouse as described earlier (Verhage et al., 2011). Freshly hatched larvae (L1 stage) of the Brassicaceae specialist *Pieris rapae* (small cabbage white butterfly) or the generalist *Mamestra brassicae* (cabbage moth) were released onto fully expanded rosette leaves of 5-week-old plants of the designated genotype. Individual plants of the designated genotype were infested with a single caterpillar of either *P. rapae* or *M. brassicae*. The caterpillar-challenged plants were placed in a transparent plastic container sealed with insect-proof meshes allowing adequate gas exchange and light transmission. Fresh weight of caterpillars was measured after 7 d (*P. rapae*) or 8 d (*M. brassicae*) of feeding.

Botrytis cinerea and *Alternaria brassicicola* assays were performed as previously described (Kemmerling et al., 2007; Van Wees et al., 2013).

Chemicals

Coronatine, methyl jasmonate, and abscisic acid were from Sigma-Aldrich. 2-Nitrophenyl-β-D-galactopyranoside was from Applichem. $InsP_6$ was from Sichem. 1-$InsP_7$, 4_$InsP_7$, 5-$InsP_7$, 6-$InsP_7$, and 1,5-$InsP_8$ were synthesized as recently described (Capolicchio et al., 2013, 2014). [^{3}H]-$InsP_6$ and [^{3}H]-$InsP_7$ were extracted and purified from [^{3}H]-*myo*-inositol-labeled Col-0 seedlings using a desalting protocol as described earlier (Azevedo et al., 2010). [^{3}H]-Ins(1,3,4,5,6)P_5 was purified from [^{3}H]-*myo*-inositol-labeled *ipk1-1* seedlings using the same desalting protocol. Standards were [^{3}H]-$InsP_6$ (Azevedo and Saiardi, 2006) and [^{3}H]-5-$InsP_7$ that was generated in vitro from [^{3}H]-$InsP_6$ and recombinant mammalian IP6K1 (Azevedo et al., 2010).

In Vitro Binding Assays

In vitro binding assays were performed with recombinant COI1-ASK1 and His_8-MBP-JAZ in 1:2 molar ratios. Purified and desalted [^{3}H]-$InsP_6$ was added to the reaction buffer containing 50 mM Tris-HCl, pH 7.5, 100 mM NaCl, 10 mM imidazole, 10% (v/v) glycerol, 0.1% (v/v) Tween 20, and 5 mM 2-mercaptoethanol in a total volume of 0.5 mL. Unless mentioned otherwise, [^{3}H]-$InsP_6$ at a total activity of 4000 dpm and 1 μM coronatine was added to each reaction. The reaction was incubated at room temperature (22 to 24°C) for 90 min, then 30 μL of Ni-NTA resin was added with a further incubation at 4°C for 90 min. The resin was centrifuged for 5 min at 900*g* and washed three times with ice-cold reaction buffer. Proteins were eluted with 250 mM imidazole and recovered radioactivity analyzed by scintillation counting.

Extraction and HPLC Analyses of Inositol Phosphates

Inositol polyphosphates from yeast were extracted and analyzed as described (Azevedo and Saiardi, 2006). Extraction and measurement of inositol polyphosphates from Arabidopsis seedling were performed as follows. Seedlings were grown under sterile conditions in liquid 0.5× MS with 2% sucrose for 10 d and then transferred to sucrose-free low MS semi-liquid medium (0.25 MS and 0.3% Phytagel). Labeling was started at 2 weeks of age by addition of 40 μCi mL^{-1} of [^{3}H]-*myo*-inositol (30 to 80 Ci $mmol^{-1}$ and 1 mCi mL^{-1}; Biotrend; ART-0261-5) for 2 mL liquid MS media containing 10 seedlings. After 6 d of labeling, leaves or seedlings were washed two times with ultrapure water before harvesting and freezing into liquid N_2. Inositol polyphosphates were extracted as described previously (Azevedo and Saiardi, 2006) and resolved by strong anion exchange chromatography HPLC (using the partisphere SAX 4.6 × 125 mm column; Whatman) at a flow rate of 0.5 mL min^{-1} with the gradient of buffers A (1 mM EDTA) and B [1 mM EDTA and 1.3 M $(NH_4)_2HPO_4$, pH 3.8, with H_3PO_4] following the standard protocol mentioned above. Fractions were collected each minute, mixed with scintillation cocktail (Perkin-Elmer; ULTIMA-FLO AP), and analyzed by scintillation counting. To account for differences in fresh weight and extraction efficiencies between samples, values shown are normalized activities based on the total activity of each sample. To avoid misleading results derived from unincorporated [^{3}H]-*myo*-inositol in the HPLC run, "total" activities for normalization were calculated by counting fractions from 17 min (Figures 2F and 2G; Supplemental Figures 2C and 2D), 22 min (Figure 3C; Supplemental Figures 2E, 3B, and 5A), or from 18 min (Figure 4) until the end of runs. HPLC runs within an experimental set were normalized in the following way: If sample B had less "total" activity than sample A, the equation used for normalization was −[individual data point of sample A*("total" InsP of B/"total" InsP of A)]. Results are presented as minute fractions (circle or diamond) connected by lines.

Total RNA Extraction and qPCR Analyses

Leaf samples (up to 100 mg) were harvested for total RNA extraction using the RNeasy Plant Mini Kit (Qiagen). A total of 1 μg RNA was used for cDNA preparation following DNaseI digest (Fermentas). The reverse transcription was done according to the manufacturer's instructions (Roboklon; AMV Reverse Transcriptase Native). The qPCR was performed with the SYBR Green reaction mix (Bioline; Sensimix SYBR No-ROX kit) in a Bio-Rad CFX384 real-time system. Data were analyzed using the Bio-Rad CFX Manager 2.0 (admin) system. *PP2AA3* or β-*TUBULIN* was used as a reference gene.

Yeast Two-Hybrid Assays

The full-length coding sequences of *COI1* and *JAZ1* were cloned into the yeast two-hybrid vector pGBKT7 and pGADT7, respectively, in fusion with N -terminal binding domain or activation domain. The yeast strain Y187 was transformed with individual wild-type or *COI1* mutant constructs generated by site-directed mutagenesis (see above) together with *JAZ1* construct following the standard yeast transformation protocol mentioned above. Yeast transformants were selected on solid CSM-Leu-Trp media after which single fresh colonies from independent transformants were grown overnight in liquid CSM-Leu-Trp media. JAZ1 interaction with wild-type or mutant COI1 in the presence of 50 μM coronatine was evaluated by quantification of β-galactosidase-mediated hydrolysis of ortho-nitrophenyl-β-D-galactopyranoside.

Accession Numbers

Sequence data from this article can be found in the Arabidopsis Genome Initiative or GenBank/EMBL databases under the following accession numbers: *VIH1* (At5g15070), *VIH2* (At3g01310), *MYC2* (At1g32640), *VSP2* (At5g24770), *PP2AA3* (AT1G13320), β-*TUBULIN* (*AT5G62700*), *JAZ1* (At1g19180), *COI1* (At2g39940), *IPK1* (At5g42810), *Saccharomyces cerevisiae VIP1* (YLR410W), *S. cerevisiae KCS1* (YDR017C), and *hPPIP5K2* (NM_001276277). Accession numbers for T-DNA insertion lines are as follows: *vih2-3a* (SAIL_165_F12), *vih2-4* (GK-080A07), *ipk1-1* (SALK_065337C), and *vih1-1* T-DNA line (SAIL_543_F08).

Supplemental Data

Supplemental Figure 1. Two-domain Architecture, Structural Conservation of the ATP-Grasp Domain, and Conserved Binding Residues Suggest That VIH Proteins Are Functional PPIP5 Kinases.

Supplemental Figure 2. VIH Proteins Are Functional Inositol Pyrophosphate Synthetases in Yeast.

Supplemental Figure 3. A Time-Course Experiment Reveals a Fast and Specific Induction of $InsP_8$ by MeJA.

Supplemental Figure 4. Genome Structure and Identification of *vih2*:: T-DNA Insertion Lines.

Supplemental Figure 5. Bulk Steady State and Jasmonate-Induced Pools of $InsP_8$ in Arabidopsis Seedlings Depend on VIH2.

Supplemental Figure 6. VIH2 Regulates Jasmonate Perception.

Supplemental Figure 7. Different Inositol Polyphosphates Exhibit Distinct Binding Affinities for the ASK1-COI1-JAZ Jasmonate Receptor Complex.

Supplemental Figure 8. Detection of Inositol Pyrophosphate in the *ipk1-1* Mutant Line.

Supplemental Table 1. Primer List for PCR-Based Characterization of T-DNA Insertion Lines.

Supplemental Table 2. Primer List for qPCR Analyses.

Supplemental Table 3. Primer List for Generation of pDR195-Based Yeast Episomal Expression Vectors.

Supplemental Table 4. List of Primer Sequences Used for Site-Directed Mutagenesis.

Supplemental Table 5. Primers and Plasmids Used to Generate Yeast Knockout Strains.

Supplemental Table 6. Primers Used to Clone *JAZ* Homolog into the pET28- His_8-MBP Bacterial Expression Vector

Supplemental Methods.

Supplemental References.

Supplemental Data Set 1. Text File of the Sequences and Alignment Used for the Phylogenetic Analysis Shown in Figure 1.

ACKNOWLEDGMENTS

We thank Tsuyoshi Nakagawa for Gateway binary vectors containing the *bar* gene, which was identified by Meiji Seika Kaisha, David Waugh for sharing the pDEST-HisMBP vector, Ana Pineda for providing *M. brassicae* larvae, Andreas Wachter and Martin Bayer for providing RNA, Birgit Kemmerling for providing fungal spores, and Vytas Bankaitis for the anti-Kes1 monoclonal antibody. We thank Elke Sauberzweig, Michael Fitz, and Hans van Pelt for excellent technical assistance and Junpei Takano, Sascha Laubinger, Nargis Parvin, and Kristina E. Ile for critical reading of previous versions of the article. This work was supported by Emmy Noether Grant SCHA 1274/2-1, Grants SCHA 1274/3-1 and SFB 1101/TP A05 from the Deutsche Forschungsgemeinschaft to G.S. Efforts of D.L. were also supported by the Deutscher Akademischer Austauschdienst. A.S. and C.A. are supported by the Medical Research Council (MRC) core support to the MRC/UCL Laboratory for Molecular Cell Biology University Unit (MC_U122680443). H.J.J. and S.C. are supported by the Swiss National Science Foundation (Grant PZ00P2_136816). N.Z. is a Howard Hughes Medical Institute Investigator and is supported by National Institutes of Health Grant R01CA107134. S.C.M.V.W. and M.S. were supported by Vidi Grant 11281 of the Dutch Technology Foundation STW. We dedicate this work to the memory of Laura B. Sheard. Her work greatly stimulated our interest in the regulation of jasmonate perception by inositol polyphosphates. ASK1-COI1 employed in this study was purified by her and her colleagues. Laura passed away in a tragic car accident in Seattle on November 13, 2011.

AUTHOR CONTRIBUTIONS

D.L., S.C.M.V.W., A.S., and G.S. designed the research. D.L., P.J., C.A., M.D., S.C., H.M., T.I., M.S., M.F., P.G., M.F.K.D.C, A.S., and G.S. performed the experiments. D.L., P.J., C.A., M.D., M.W., N.Z., I.F., H.J.J., S.C.M.V.W., A.S., and G.S. analyzed the data and revised the article. D.L. and G.S. wrote the article.

Received December 11, 2014; revised March 13, 2015; accepted April 3, 2015; published April 21, 2015.

REFERENCES

Azevedo, C., and Saiardi, A. (2006). Extraction and analysis of soluble inositol polyphosphates from yeast. Nat. Protoc. **1:** 2416–2422.

Azevedo, C., Burton, A., Ruiz-Mateos, E., Marsh, M., and Saiardi, A. (2009). Inositol pyrophosphate mediated pyrophosphorylation of AP3B1 regulates HIV-1 Gag release. Proc. Natl. Acad. Sci. USA **106:** 21161–21166.

Azevedo, C., Burton, A., Bennett, M., Onnebo, S.M., and Saiardi, A. (2010). Synthesis of InsP7 by the Inositol Hexakisphosphate Kinase 1 (IP6K1). Methods Mol. Biol. **645:** 73–85.

Barker, C.J., Illies, C., Gaboardi, G.C., and Berggren, P.O. (2009). Inositol pyrophosphates: structure, enzymology and function. Cell. Mol. Life Sci. **66:** 3851–3871.

Blackwell, M., Vilgalys, R., James, T.Y., and Taylor, J.W. (2012). Fungi. Eumycota: mushrooms, sac fungi, yeast, molds, rusts, smuts, etc. In The Tree of Life Web Project, http://tolweb.org/.

Blatt, M.R., Thiel, G., and Trentham, D.R. (1990). Reversible inactivation of K^+ channels of Vicia stomatal guard cells following the photolysis of caged inositol 1,4,5-trisphosphate. Nature **346:** 766–769.

Brearley, C.A., and Hanke, D.E. (1996). Inositol phosphates in barley (*Hordeum vulgare* L.) aleurone tissue are stereochemically similar to the products of breakdown of InsP6 in vitro by wheat-bran phytase. Biochem. J. **318:** 279–286.

Burnette, R.N., Gunesekera, B.M., and Gillaspy, G.E. (2003). An Arabidopsis inositol 5-phosphatase gain-of-function alters abscisic acid signaling. Plant Physiol. **132:** 1011–1019.

Burton, A., Hu, X., and Saiardi, A. (2009). Are inositol pyrophosphates signalling molecules? J. Cell. Physiol. **220:** 8–15.

Capolicchio, S., Thakor, D.T., Linden, A., and Jessen, H.J. (2013). Synthesis of unsymmetric diphospho-inositol polyphosphates. Angew. Chem. Int. Ed. Engl. **52:** 6912–6916.

Capolicchio, S., Wang, H., Thakor, D.T., Shears, S.B., and Jessen, H.J. (2014). Synthesis of densely phosphorylated bis-1,5-diphospho-myo-inositol tetrakisphosphate and its enantiomer by bidirectional P-anhydride formation. Angew. Chem. Int. Ed. Engl. **53:** 9508–9511.

Castresana, J. (2000). Selection of conserved blocks from multiple alignments for their use in phylogenetic analysis. Mol. Biol. Evol. **17:** 540–552.

Chakraborty, A., Kim, S., and Snyder, S.H. (2011). Inositol pyrophosphates as mammalian cell signals. Sci. Signal. **4:** re1.

Chen, X., Lin, W.H., Wang, Y., Luan, S., and Xue, H.W. (2008). An inositol polyphosphate 5-phosphatase functions in PHOTOTROPIN1 signaling in Arabidopis by altering cytosolic Ca^{2+}. Plant Cell **20:** 353–366.

Chini, A., Fonseca, S., Fernández, G., Adie, B., Chico, J.M., Lorenzo, O., García-Casado, G., López-Vidriero, I., Lozano, F.M., Ponce, M.R., Micol, J.L., and Solano, R. (2007). The JAZ family of repressors is the missing link in jasmonate signalling. Nature **448:** 666–671.

De Vos, M., Van Oosten, V.R., Van Poecke, R.M., Van Pelt, J.A., Pozo, M.J., Mueller, M.J., Buchala, A.J., Métraux, J.P., Van Loon, L.C., Dicke, M., and Pieterse, C.M. (2005). Signal signature and transcriptome changes of Arabidopsis during pathogen and insect attack. Mol. Plant Microbe Interact. **18:** 923–937.

Desai, M., Rangarajan, P., Donahue, J.L., Williams, S.P., Land, E.S., Mandal, M.K., Phillippy, B.Q., Perera, I.Y., Raboy, V., and Gillaspy, G.E. (2014). Two inositol hexakisphosphate kinases drive inositol pyrophosphate synthesis in plants. Plant J. **80:** 642–653.

Dorsch, J.A., Cook, A., Young, K.A., Anderson, J.M., Bauman, A.T., Volkmann, C.J., Murthy, P.P., and Raboy, V. (2003). Seed phosphorus and inositol phosphate phenotype of barley low phytic acid genotypes. Phytochemistry **62:** 691–706.

Draskovic, P., Saiardi, A., Bhandari, R., Burton, A., Ilc, G., Kovacevic, M., Snyder, S.H., and Podobnik, M. (2008). Inositol hexakisphosphate kinase products contain diphosphate and triphosphate groups. Chem. Biol. **15:** 274–286.

Felsenstein, J. (1981). Evolutionary trees from DNA sequences: a maximum likelihood approach. J. Mol. Evol. **17:** 368–376.

Felsenstein, J. (1985). Confidence limits on phylogenies: an approach using the bootstrap. Evolution **39:** 783–791.

Flores, S., and Smart, C.C. (2000). Abscisic acid-induced changes in inositol metabolism in *Spirodela polyrrhiza*. Planta **211:** 823–832.

Gillaspy, G.E. (2013). The role of phosphoinositides and inositol phosphates in plant cell signaling. Adv. Exp. Med. Biol. **991:** 141–157.

Gilroy, S., Read, N.D., and Trewavas, A.J. (1990). Elevation of cytoplasmic calcium by caged calcium or caged inositol triphosphate initiates stomatal closure. Nature **346:** 769–771.

Han, S., Tang, R., Anderson, L.K., Woerner, T.E., and Pei, Z.M. (2003). A cell surface receptor mediates extracellular Ca^{2+} sensing in guard cells. Nature **425:** 196–200.

Hanke, D.E., Parmar, P.N., Caddick, S.E., Green, P., and Brearley, C.A. (2012). Synthesis of inositol phosphate ligands of plant hormone-receptor complexes: pathways of inositol hexakisphosphate turnover. Biochem. J. **444:** 601–609.

Howe, G.A., and Jander, G. (2008). Plant immunity to insect herbivores. Annu. Rev. Plant Biol. **59:** 41–66.

Katoh, K., Kuma, K., Toh, H., and Miyata, T. (2005). MAFFT version 5: improvement in accuracy of multiple sequence alignment. Nucleic Acids Res. **33:** 511–518.

Katsir, L., Schilmiller, A.L., Staswick, P.E., He, S.Y., and Howe, G.A. (2008). COI1 is a critical component of a receptor for jasmonate and the bacterial virulence factor coronatine. Proc. Natl. Acad. Sci. USA **105:** 7100–7105.

Keeling, P., Leander, B.S., and Simpson, A. (2009). Eukaryotes. Eukaryota: Organisms with nucleated cells. In The Tree of Life Project, http://tolweb.org/Eukaryotes/3/2009.10.28.

Kemmerling, B., et al. (2007). The BRI1-associated kinase 1, BAK1, has a brassinolide-independent role in plant cell-death control. Curr. Biol. **17:** 1116–1122.

Knight, H., Trewavas, A.J., and Knight, M.R. (1997). Calcium signalling in *Arabidopsis thaliana* responding to drought and salinity. Plant J. **12:** 1067–1078.

Kumar, S., Skjaeveland, A., Orr, R.J.S., Enger, P., Ruden, T., Mevik, B.H., Burki, F., Botnen, A., and Shalchian-Tabrizi, K. (2009). AIR: A batch-oriented web program package for construction of supermatrices ready for phylogenomic analyses. BMC Bioinformatics **10:** 357.

Lemtiri-Chlieh, F., MacRobbie, E.A., and Brearley, C.A. (2000). Inositol hexakisphosphate is a physiological signal regulating the K^+-inward rectifying conductance in guard cells. Proc. Natl. Acad. Sci. USA **97:** 8687–8692.

Lin, H., Fridy, P.C., Ribeiro, A.A., Choi, J.H., Barma, D.K., Vogel, G., Falck, J.R., Shears, S.B., York, J.D., and Mayr, G.W. (2009). Structural analysis and detection of biological inositol pyrophosphates reveal that the family of VIP/diphosphoinositol pentakisphosphate kinases are 1/3-kinases. J. Biol. Chem. **284:** 1863–1872.

Liu, H.T., Gao, F., Cui, S.J., Han, J.L., Sun, D.Y., and Zhou, R.G. (2006). Primary evidence for involvement of IP3 in heat-shock signal transduction in Arabidopsis. Cell Res. **16:** 394–400.

Losito, O., Szijgyarto, Z., Resnick, A.C., and Saiardi, A. (2009). Inositol pyrophosphates and their unique metabolic complexity: analysis by gel electrophoresis. PLoS ONE **4:** e5580.

Menniti, F.S., Miller, R.N., Putney, J.W., Jr., and Shears, S.B. (1993). Turnover of inositol polyphosphate pyrophosphates in pancreatoma cells. J. Biol. Chem. **268:** 3850–3856.

Mosblech, A., Thurow, C., Gatz, C., Feussner, I., and Heilmann, I. (2011). Jasmonic acid perception by COI1 involves inositol polyphosphates in *Arabidopsis thaliana*. Plant J. **65:** 949–957.

Mosblech, A., König, S., Stenzel, I., Grzeganek, P., Feussner, I., and Heilmann, I. (2008). Phosphoinositide and inositolpolyphosphate signalling in defense responses of *Arabidopsis thaliana* challenged by mechanical wounding. Mol. Plant **1:** 249–261.

Mulugu, S., Bai, W., Fridy, P.C., Bastidas, R.J., Otto, J.C., Dollins, D.E., Haystead, T.A., Ribeiro, A.A., and York, J.D. (2007). A conserved family of enzymes that phosphorylate inositol hexakisphosphate. Science **316:** 106–109.

Munnik, T., and Vermeer, J.E. (2010). Osmotic stress-induced phosphoinositide and inositol phosphate signalling in plants. Plant Cell Environ. **33:** 655–669.

Munnik, T., and Nielsen, E. (2011). Green light for polyphosphoinositide signals in plants. Curr. Opin. Plant Biol. **14:** 489–497.

Murphy, A.M., Otto, B., Brearley, C.A., Carr, J.P., and Hanke, D.E. (2008). A role for inositol hexakisphosphate in the maintenance of basal resistance to plant pathogens. Plant J. **56:** 638–652.

Onnebo, S.M., and Saiardi, A. (2009). Inositol pyrophosphates modulate hydrogen peroxide signalling. Biochem. J. **423:** 109–118.

Osada, S., Kageyama, K., Ohnishi, Y., Nishikawa, J., Nishihara, T., and Imagawa, M. (2012). Inositol phosphate kinase Vip1p interacts with histone chaperone Asf1p in *Saccharomyces cerevisiae*. Mol. Biol. Rep. **39:** 4989–4996.

Padmanabhan, U., Dollins, D.E., Fridy, P.C., York, J.D., and Downes, C.P. (2009). Characterization of a selective inhibitor of inositol hexakisphosphate kinases: use in defining biological roles and metabolic relationships of inositol pyrophosphates. J. Biol. Chem. **284:** 10571–10582.

Perera, I.Y., Hung, C.Y., Moore, C.D., Stevenson-Paulik, J., and Boss, W.F. (2008). Transgenic Arabidopsis plants expressing the type 1 inositol 5-phosphatase exhibit increased drought tolerance and altered abscisic acid signaling. Plant Cell **20:** 2876–2893.

Pieterse, C.M., and Dicke, M. (2007). Plant interactions with microbes and insects: from molecular mechanisms to ecology. Trends Plant Sci. **12:** 564–569.

Pieterse, C.M., Van der Does, D., Zamioudis, C., Leon-Reyes, A., and Van Wees, S.C. (2012). Hormonal modulation of plant immunity. Annu. Rev. Cell Dev. Biol. **28:** 489–521.

Pöhlmann, J., Risse, C., Seidel, C., Pohlmann, T., Jakopec, V., Walla, E., Ramrath, P., Takeshita, N., Baumann, S., Feldbrügge, M., Fischer, R., and Fleig, U. (2014). The Vip1 inositol polyphosphate kinase family regulates polarized growth and modulates the microtubule cytoskeleton in fungi. PLoS Genet. **10:** e1004586.

Rao, F., et al. (2014). Inositol pyrophosphates mediate the DNA-PK/ATM-p53 cell death pathway by regulating CK2 phosphorylation of Tti1/Tel2. Mol. Cell **54:** 119–132.

Safrany, S.T., Caffrey, J.J., Yang, X., Bembenek, M.E., Moyer, M.B., Burkhart, W.A., and Shears, S.B. (1998). A novel context for the 'MutT' module, a guardian of cell integrity, in a diphosphoinositol polyphosphate phosphohydrolase. EMBO J. **17:** 6599–6607.

Saiardi, A., Caffrey, J.J., Snyder, S.H., and Shears, S.B. (2000a). The inositol hexakisphosphate kinase family. Catalytic flexibility and function in yeast vacuole biogenesis. J. Biol. Chem. **275:** 24686–24692.

Saiardi, A., Caffrey, J.J., Snyder, S.H., and Shears, S.B. (2000b). Inositol polyphosphate multikinase (ArgRIII) determines nuclear mRNA export in *Saccharomyces cerevisiae*. FEBS Lett. **468:** 28–32.

Saiardi, A., Nagata, E., Luo, H.R., Snowman, A.M., and Snyder, S.H. (2001). Identification and characterization of a novel inositol hexakisphosphate kinase. J. Biol. Chem. **276:** 39179–39185.

Sheard, L.B., et al. (2010). Jasmonate perception by inositol-phosphate-potentiated COI1-JAZ co-receptor. Nature **468:** 400–405.

Shears, S.B. (2009). Diphosphoinositol polyphosphates: metabolic messengers? Mol. Pharmacol. **76:** 236–252.

Stamatakis, A. (2006a). RAxML-VI-HPC: maximum likelihood-based phylogenetic analyses with thousands of taxa and mixed models. Bioinformatics **22:** 2688–2690.

Stamatakis, A. (2006b). Phylogenetic models of rate heterogeneity: A high performance computing perspective. In 20th International

Parallel and Distributed Processing Symposium (IPDPS), 10.1109/IPDPS.2006.1639535.

Stamatakis, A., Hoover, P., and Rougemont, J. (2008). A rapid bootstrap algorithm for the RAxML Web servers. Syst. Biol. **57:** 758–771.

Stephens, L.R., Hawkins, P.T., Stanley, A.F., Moore, T., Poyner, D.R., Morris, P.J., Hanley, M.R., Kay, R.R., and Irvine, R.F. (1991). Myo-inositol pentakisphosphates. Structure, biological occurrence and phosphorylation to myo-inositol hexakisphosphate. Biochem. J. **275:** 485–499.

Stevenson-Paulik, J., Bastidas, R.J., Chiou, S.T., Frye, R.A., and York, J.D. (2005). Generation of phytate-free seeds in Arabidopsis through disruption of inositol polyphosphate kinases. Proc. Natl. Acad. Sci. USA **102:** 12612–12617.

Streb, H., Irvine, R.F., Berridge, M.J., and Schulz, I. (1983). Release of Ca^{2+} from a nonmitochondrial intracellular store in pancreatic acinar cells by inositol-1,4,5-trisphosphate. Nature **306:** 67–69.

Szijgyarto, Z., Garedew, A., Azevedo, C., and Saiardi, A. (2011). Influence of inositol pyrophosphates on cellular energy dynamics. Science **334:** 802–805.

Tan, X., Calderon-Villalobos, L.I., Sharon, M., Zheng, C., Robinson, C.V., Estelle, M., and Zheng, N. (2007). Mechanism of auxin perception by the TIR1 ubiquitin ligase. Nature **446:** 640–645.

Thines, B., Katsir, L., Melotto, M., Niu, Y., Mandaokar, A., Liu, G., Nomura, K., He, S.Y., Howe, G.A., and Browse, J. (2007). JAZ repressor proteins are targets of the SCF(COI1) complex during jasmonate signalling. Nature **448:** 661–665.

Van Wees, S.C., Van Pelt, J.A., Bakker, P.A., and Pieterse, C.M. (2013). Bioassays for assessing jasmonate-dependent defenses triggered by pathogens, herbivorous insects, or beneficial rhizobacteria. Methods Mol. Biol. **1011:** 35–49.

Verhage, A., Vlaardingerbroek, I., Raaymakers, C., Van Dam, N.M., Dicke, M., Van Wees, S.C., and Pieterse, C.M. (2011). Rewiring of the jasmonate signaling pathway in Arabidopsis during insect herbivory. Front. Plant Sci. **2:** 47.

Vos, I.A., Verhage, A., Schuurink, R.C., Watt, L.G., Pieterse, C.M.J., and Van Wees, S.C.M. (2013). Onset of herbivore-induced resistance in systemic tissue primed for jasmonate-dependent defenses is activated by abscisic acid. Front. Plant Sci. **4:** 539.

Wang, H., Falck, J.R., Hall, T.M., and Shears, S.B. (2012). Structural basis for an inositol pyrophosphate kinase surmounting phosphate crowding. Nat. Chem. Biol. **8:** 111–116.

Wang, Y., Chu, Y.J., and Xue, H.W. (2012). Inositol polyphosphate 5-phosphatase-controlled Ins(1,4,5)P3/Ca^{2+} is crucial for maintaining pollen dormancy and regulating early germination of pollen. Development **139:** 2221–2233.

Wang, Y., Lin, W.H., Chen, X., and Xue, H.W. (2009). The role of Arabidopsis 5PTase13 in root gravitropism through modulation of vesicle trafficking. Cell Res. **19:** 1191–1204.

Wundenberg, T., and Mayr, G.W. (2012). Synthesis and biological actions of diphosphoinositol phosphates (inositol pyrophosphates), regulators of cell homeostasis. Biol. Chem. **393:** 979–998.

Yan, J., Li, H., Li, S., Yao, R., Deng, H., Xie, Q., and Xie, D. (2013). The Arabidopsis F-box protein CORONATINE INSENSITIVE1 is stabilized by SCFCOI1 and degraded via the 26S proteasome pathway. Plant Cell **25:** 486–498.

Yang, Z. (1993). Maximum-likelihood estimation of phylogeny from DNA sequences when substitution rates differ over sites. Mol. Biol. Evol. **10:** 1396–1401.

York, J.D. (2006). Regulation of nuclear processes by inositol polyphosphates. Biochim. Biophys. Acta **1761:** 552–559.

Zhang, J., et al. (2011). Inositol trisphosphate-induced Ca^{2+} signaling modulates auxin transport and PIN polarity. Dev. Cell **20:** 855–866.

VIH2 Regulates the Synthesis of Inositol Pyrophosphate $InsP_8$ and Jasmonate-Dependent Defenses in Arabidopsis

Debabrata Laha, Philipp Johnen, Cristina Azevedo, Marek Dynowski, Michael Weiß, Samanta Capolicchio, Haibin Mao, Tim Iven, Merel Steenbergen, Marc Freyer, Philipp Gaugler, Marília K.F. de Campos, Ning Zheng, Ivo Feussner, Henning J. Jessen, Saskia C.M. Van Wees, Adolfo Saiardi and Gabriel Schaaf

Plant Cell 2015;27;1082-1097; originally published online April 21, 2015;
DOI 10.1105/tpc.114.135160

9.2 Laha et al., 2016

Inositol Polyphosphate Binding Specificity of the Jasmonate Receptor Complex.

Laha, D.*, Parvin, N.*, Dynowski, M., Johnen, P., Mao, H., Bitters, S. T., Zheng, N. and Schaaf, G.

*These authors contributed equally to this work.

Plant Physiol. 2016 Aug;171(4):2364-70. doi: 10.1104/pp.16.00694.

Inositol Polyphosphate Binding Specificity of the Jasmonate Receptor Complex[1][OPEN]

Debabrata Laha[2], Nargis Parvin[2], Marek Dynowski, Philipp Johnen, Haibin Mao, Sven T. Bitters, Ning Zheng, and Gabriel Schaaf*

Center for Plant Molecular Biology (ZMBP), University of Tübingen, 72076 Tübingen, Germany (D.L., N.P., P.J., S.T.B., G.S.); Zentrum für Datenverarbeitung, University of Tübingen, 72074 Tübingen, Germany (M.D.); and Department of Pharmacology, Howard Hughes Medical Institute, University of Washington, Seattle, Washington 98195 (H.M., N.Z.)

ORCID IDs: 0000-0002-7823-5489 (D.L.); 0000-0002-7744-1408 (N.P.); 0000-0002-4512-9508 (P.J.); 0000-0002-7233-9105 (H.M.); 0000-0003-1684-2002 (S.T.B.); 0000-0001-9022-4515 (G.S.).

Recent findings that receptor complexes for auxin and jasmonate bind inositol polyphosphates stimulated the idea that plant hormone perception is regulated by inositol-derived molecules (Tan et al., 2007; Sheard et al., 2010). Inositol polyphosphates regulate critical cellular functions in eukaryotic cells (Munnik and Nielsen, 2011; Munnik and Vermeer, 2010; Gillaspy, 2013; Tsui and York, 2010; Kuo et al., 2014; Lee et al., 2015), and the discovery that these molecules bind to plant hormone receptors provides an interesting case model to study plant hormone perception. For instance, the ASK1-TIR1 component of the auxin receptor complex was copurified and cocrystallized with insect cell-derived inositol hexakisphosphate ($InsP_6$; Tan et al., 2007). TIR1 mutants defective in $InsP_6$ binding failed to interact with the IAA7 transcriptional repressor in the presence of auxin in yeast two-hybrid assays and in pull-down experiments using tagged-recombinant Aux/IAA protein (Calderón Villalobos et al., 2012), suggesting that $InsP_6$ binding might be important for auxin receptor function. Interestingly, the ASK1-COI1 component of the jasmonate receptor complex also copurified with inositol polyphosphate (Sheard et al., 2010). Here, NMR analyses revealed that insect cell-purified, nondialyzed protein contained either D- and/or L-myo-inositol-1,2,4,5,6-pentakisphosphate (Sheard et al., 2010), also referred to as Ins(1,2,4,5,6)P_5 or short $InsP_5$ [3-OH] and Ins(2,3,4,5,6)P_5 or short $InsP_5$ [1-OH], respectively. Unfortunately, NMR cannot discriminate between enantiomers; therefore, the structure of the insect-purified $InsP_5$ isomer remains unresolved. Dialyzed ASK1-COI1 protein depleted of inositol polyphosphate failed to reconstitute the jasmonate receptor complex in vitro, while addition of $InsP_5$ [3-OH] robustly stimulated complex formation (Sheard et al., 2010). Interestingly, Ins(1,4,5,6)P_4 and $InsP_6$ also stimulated complex formation, although $InsP_6$ stimulated with lower efficiency (Sheard et al., 2010). Other $InsP_5$ isomers (including the possible alternative $InsP_5$ [1-OH] enantiomer) were not tested in this study.

In plants, three $InsP_5$ species with distinct chromatographic mobilities have been identified (Stevenson-Paulik et al., 2005; Hanke et al., 2012; Laha et al., 2015; Brearley and Hanke, 1996). Among them, only the isomeric nature of the symmetrical molecule $InsP_5$ [2-OH] was determined, while the identity of the other two $InsP_5$ isomers remains unknown (Stevenson-Paulik et al., 2005; Brearley and Hanke, 1996). Independent work in amoeba and in a pancreatoma cell line showed that inositol polyphosphates can be further phosphorylated at an existing phosphate position to give rise to inositol pyrophosphates, molecules such as $InsP_7$ and $InsP_8$ that contain energy-rich diphosphate bonds and have important cellular functions in amoeba, animal, and yeast cells (Menniti et al., 1993; Stephens et al., 1993; Shears et al., 2012; Mulugu et al., 2007; Wilson et al., 2013; Thota and Bhandari, 2015). Inositol pyrophosphates have also been detected in different plant species (Desai et al., 2014; Lemtiri-Chlieh et al., 2000; Brearley and Hanke, 1996; Laha et al., 2015), and recent work suggests an important function of these molecules in regulating jasmonate-dependent responses (Laha et al., 2015).

Jasmonate perception is regulated by COI1, the F-box component of an SCF ubiquitin E3 ligase complex. COI1 recruits Jasmonate ZIM-domain (JAZ) transcriptional

[1] This work was supported by Emmy Noether Grant SCHA 1274/2-1 and SFB 1101/TP A05 from the Deutsche Forschungsgemeinschaft to G.S. Efforts of D.L. and P.J. were supported by the Deutscher Akademischer Austauschdienst and the Landesgraduiertenförderung Baden-Württemberg, respectively. N.Z. is a Howard Hughes Medical Institute Investigator and is supported by National Institutes of Health Grant R01CA107134 and the National Science Foundation.

[2] These authors contributed equally to the article.

* Address correspondence to gabriel.schaaf@zmbp.uni-tuebingen.de.

G.S. and D.L. designed the research; D.L. and N.P. performed most of the experiments; M.D. performed the molecular docking experiments; P.J. performed the immunoblot analyses and the *Botrytis* experiments; H.M. purified COI1-ASK1 from insect cells; S.T.B. helped with the analyses of the IC_{50} experiments; G.S., D.L., and N.Z. analyzed and interpreted the data; G.S. prepared the structural figures and wrote the article.

[OPEN] Articles can be viewed without a subscription.

www.plantphysiol.org/cgi/doi/10.1104/pp.16.00694

repressors upon binding to the bioactive jasmonic acid (JA) conjugate JA-Ile, resulting in polyubiquitylation and proteasomal degradation of the JAZ repressors and subsequent activation of jasmonate-dependent gene expression (Chini et al., 2007; Thines et al., 2007; Katsir et al., 2008; Pauwels and Goossens, 2011). A combinatorial approach analyzing $InsP_8$-deficient *vih2* mutant plants and using in vitro reconstitution and in silico molecular docking experiments suggested that coincidence detection (i.e. simultaneous detection) of active jasmonate and the inositol pyrophosphate $InsP_8$ by the ASK1-COI1-JAZ receptor complex is critical for the activation of defense gene expression and for defenses against insect herbivores and necrotrophic fungi (Laha et al., 2015). Another study proposed $InsP_5$ [2-OH] to be involved in jasmonate perception (Mosblech et al., 2011). Collectively, these reports raise the question whether the jasmonate receptor shows selectivity for distinct inositol polyphosphates.

COMPETITIVE BINDING ASSAYS REVEAL LARGE DIFFERENCES IN RELATIVE BINDING AFFINITIES OF DISTINCT $INSP_5$ ISOMERS TO THE JASMONATE RECEPTOR COMPLEX

To investigate inositol polyphosphate binding specificity, we performed in vitro reconstitution experiments with insect cell-purified ASK1-COI1, recombinant JAZ proteins, the JA-Ile mimic coronatine, and [^{3}H]$InsP_6$ to determine IC_{50} values (50% inhibition of radioligand binding) for different $InsP_5$ isomers. This approach was chosen because radiolabeled $InsP_5$ isomers are not commercially available. A similar strategy was recently employed to investigate relative binding affinities of mammalian casein kinase-2 to $InsP_6$, 5-$InsP_7$, and a nonhydrolyzable $InsP_7$ derivative (Rao et al., 2014). We used His_8-tagged recombinant JAZ protein to pull down ASK1-COI1 in the presence of coronatine via Ni-NTA affinity chromatography and then determined [^{3}H]$InsP_6$-derived activity (see "Supplemental Data"). For JAZ1, the following relative order of effectiveness of $InsP_6$ and the various $InsP_5$ isomers in competing with [^{3}H-$InsP_6$] binding was observed (Fig. 1, A and B): $InsP_5$ [3-OH] (IC_{50}: 56 nM) $\geq$ $InsP_6$ (IC_{50}: 58 nM) > $InsP_5$ [4-OH] (IC_{50}: 66 nM) > $InsP_5$ [2-OH] (IC_{50}: 146 nM) > $InsP_5$ [5-OH] (IC_{50}: 205 nM) > $InsP_5$ [6-OH] (IC_{50}: 363 nM) > $InsP_5$ [1-OH] (IC_{50}: 902 nM). The data suggest strong differences in the relative binding affinity of different $InsP_5$ isomers (including enantiomers) to the jasmonate receptor complex. For instance, the IC_{50} value of $InsP_5$ [1-OH] is 16-fold higher than that of $InsP_5$ [3-OH], suggesting a much higher affinity of the jasmonate receptor to $InsP_5$ [3-OH]. This is remarkable as both isomers are enantiomers that are chemically indistinguishable and for which a method to determine enantiomer identity has not yet been developed. Furthermore, the IC_{50} value for $InsP_5$ [2-OH], an isomer previously suggested to play a role in the activation of the jasmonate receptor (Mosblech et al., 2011), is 2.5-fold higher than that of $InsP_5$ [3-OH] and $InsP_6$, suggesting it is less effective in potentiating jasmonate receptor assembly (Fig. 1B).

COI1 LARGELY DETERMINES THE INOSITOL POLYPHOSPHATE BINDING SPECIFICITY

To investigate the contribution of the JAZ protein to the inositol polyphosphate binding specificity, we performed similar experiments as described above with JAZ2, JAZ4, and JAZ9 (Fig. 1, C–E) with $InsP_6$ and selected $InsP_5$ isomers at a fixed concentration of "cold" inositol polyphosphate. The effectiveness of $InsP_5$ isomers to compete with [^{3}H]$InsP_6$ binding largely recapitulated the observations from the experiment using the JAZ1 protein, showing binding affinities in the following order: $InsP_5$ [3-OH] $\geq$ $InsP_6$ > $InsP_5$ [2-OH]. Binding experiments with JAZ4 further indicate that, as in the case of JAZ1, $InsP_5$ [1-OH] has the weakest affinity, suggesting that the jasmonate receptor complex retains its ability to discriminate between the two enantiomers (1/3-OH) when using another JAZ protein. Altogether these data corroborate the idea that COI1, not the JAZ protein, determines inositol polyphosphate binding specificity.

The observation that $InsP_5$ [2-OH] has a weaker relative affinity than $InsP_6$ was surprising, as an increase of $InsP_5$ [2-OH] at the cost of $InsP_6$ in the Arabidopsis (*Arabidopsis thaliana*) *ipk1-1* mutant was previously proposed to activate COI1 function and to cause increased resistance to *Plutella xylostella* caterpillars (Mosblech et al., 2011).

INCREASE OF $INSP_5$ [2-OH] BY DEACTIVATION OF THE INOSITOL 1,3,4,5,6-PENTAKISPHOSPHATE 2-KINASE (IPK1) DOES NOT GLOBALLY ACTIVATE COI1 FUNCTIONS IN ARABIDOPSIS

To investigate whether findings by Mosblech et al. (2011) reflect a global role of $InsP_5$ [2-OH] in increasing COI1 functions, we analyzed the resistance of *ipk1-1* against *Alternaria brassicicola*, a fungal necrotroph that plants contain by COI1-dependent defenses (Leon-Reyes et al., 2010). In agreement with previous observations suggesting that $InsP_8$ (which is strongly reduced in *ipk1-1*) is critical for COI1 activation (Laha et al., 2015), the *ipk1-1* line showed a severe increase in susceptibility in this assay, similar to *coi1* mutant plants (Fig. 1F; Supplemental Fig. S1A). This is also in agreement with a previous report showing increased susceptibility of the *ipk1-1* line to *Botrytis cinerea*, another fungal necrotroph, in an assay where whole plants were sprayed with fungal spores and analyzed for plant survival (Murphy et al., 2008). We have repeated this assay with a complementary approach in which we spotted fungal spores onto the leaf surface and subsequently classified disease symptoms 72 h postinoculation. We again found increased susceptibility of the

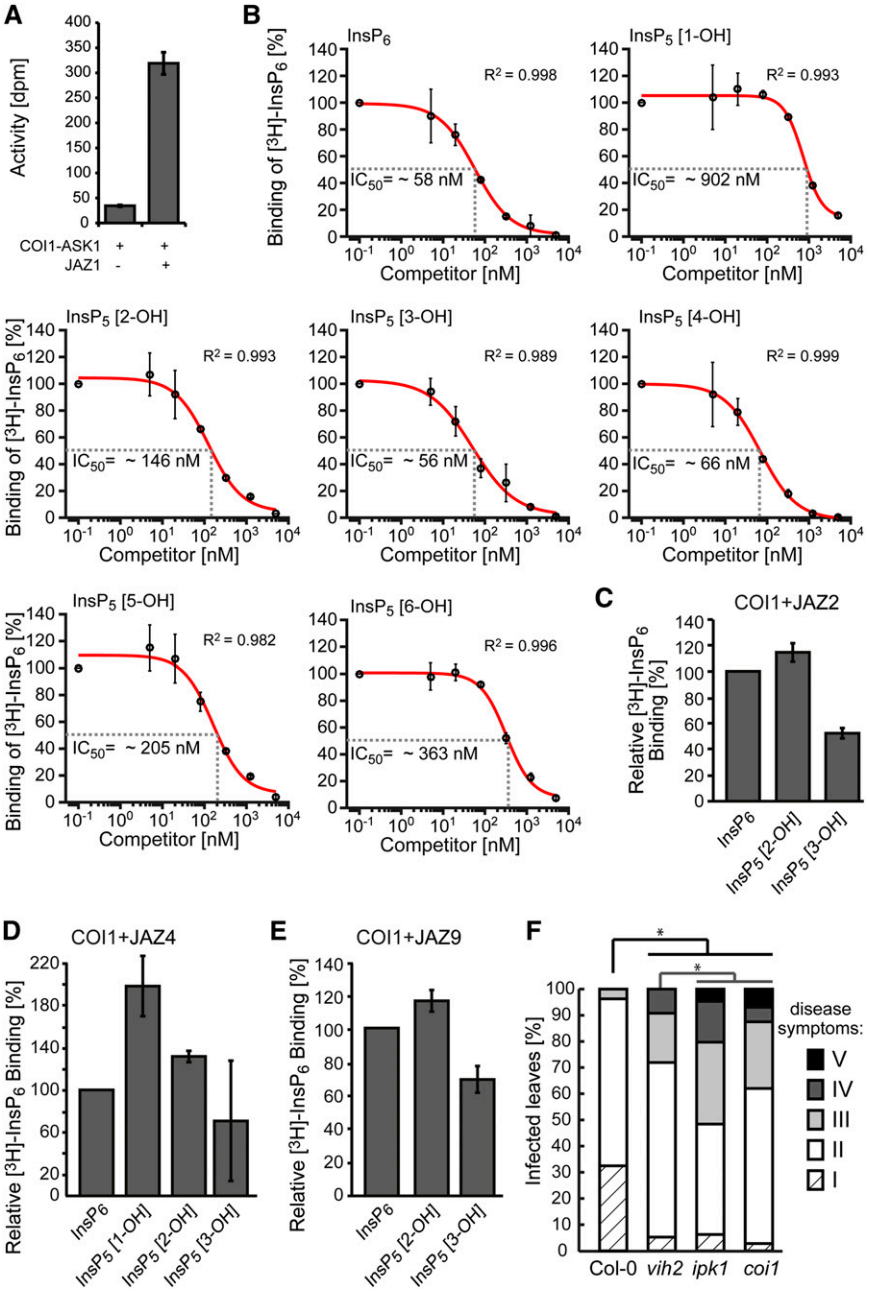

Figure 1. COI1 determines the inositol polyphosphate binding specificity of the jasmonate receptor complex. A, JAZ-dependent binding of [^{3}H]InsP$_6$ to ASK1-COI. Insect cell-purified ASK1-COI1 was incubated with recombinant His$_8$-MBP-JAZ1 and [^{3}H]InsP$_6$ in the presence of 1 μM coronatine. The complex was then purified by immobilized Ni^{2+} affinity chromatography (taking advantage of JAZ1's N-terminal His$_8$ tag), and the immobilized activity was determined by scintillation counting. A reaction in the absence of JAZ protein served as a negative control. Values show background-subtracted means ± SE. B, Competitive binding assays with [^{3}H]InsP$_6$ and unlabeled inositol polyphosphates as indicated. Results are presented as percentage of total binding. Nonlinear regression analysis was employed to fit data to a sigmoidal model, which allowed the determination of IC$_{50}$ values. R^2 values given in the plots provide estimations for goodness of fit. Error bars represent ±SE. C to E, Relative [^{3}H]InsP$_6$ binding to the ASK1-COI1 complex in the presence of 1 μM coronatine and different InsP$_5$ isomers and JAZ proteins as depicted. For the JAZ2 experiment, all competing InsP species were at 150 nM; for JAZ4, we used 80 nM of all InsP species; and for JAZ9, all competing InsP were at 50 nM. The average of [^{3}H]InsP$_6$ binding to the jasmonate receptor complex in the absence of unlabeled inositol polyphosphate was set to 100%. The experiment was repeated with similar results. Error bars denote ±SE. F, Compromised defenses of *vih2-4*, *ipk1-1*, and *coi1-t* against a necrotrophic fungus corroborates a role of higher inositol polyphosphates (≥InsP$_6$) in COI1-dependent responses. All genotypes were treated with 5 μL of an *A. brassicicola* spore suspension (1×10^6 spores/mL). Disease symptoms were scored in a double-blinded manner after 10 d of spore inoculation and categorized as different classes.

ipk1-1 line (Supplemental Fig. S1B) in complete agreement with Murphy et al. (2008). Collectively, these data question the idea that $InsP_5$ [2-OH] globally activates COI1 functions in vivo.

ANISOTROPIC COORDINATION OF THE COI1 SOLENOID BY INOSITOL POLYPHOSPHATE SUGGESTS ACTIVATION OF THE JASMONATE RECEPTOR BY AN ALLOSTERIC SWITCH

Our findings that the JAZ component of the jasmonate receptor has little, if any, effect on the relative inositol polyphosphate binding affinities (Fig. 1, B–E) suggest that COI1 largely determines the inositol polyphosphate binding specificity of the jasmonate receptor. This may be explained by in silico molecular docking experiments, which predicted the solenoid-fold of the F-box protein COI1 to provide an intricate network of electrostatic interactions engaging in inositol polyphosphate coordination (Laha et al., 2015). These docking experiments also predicted 1,5-$InsP_8$ to be a better ligand of the jasmonate receptor complex as compared with $InsP_5$ [3-OH], supporting a physiological role of $InsP_8$ jasmonate perception in agreement with defective defense gene expression and defective defenses against insect herbivores and necrotrophic fungi in plants compromised in $InsP_8$ synthesis (Laha et al., 2015). Unfortunately, the isomer identity of plant $InsP_8$ remains unknown. While our previous work indicates that VIH proteins convert 5-$InsP_7$ to 1,5-$InsP_8$ in yeast and thus have the ability to catalyze 1-PP bond formation (Laha et al., 2015), the isomer identity of VIH-dependent $InsP_8$ in plants remains elusive. This is mainly because the isomeric nature of plant $InsP_7$ is unknown. Since plant genomes do not encode Kcs1/IP6K enzymes (which are responsible for 5-$InsP_7$ production in nonplant eukaryotes) and since plant $InsP_7$ synthetases have not yet been identified, the structure identification of plant $InsP_7$ and $InsP_8$ remains a challenging task for future research. In addition, low amounts of these molecules in plant extracts complicate a thorough analysis. Assuming that VIH proteins retain their 1-PP synthetase activity independent of the $InsP_7$ substrate, we also performed in silico docking experiments with the remaining 1,*X*-$InsP_8$ isomers. All 1,*X*-$InsP_8$ isomers occupy largely overlapping sites of the presumptive inositol polyphosphate binding pocket (Fig. 2A; Supplemental Table S1). As we have previously seen for 1,5-$InsP_8$ and $InsP_5$ [3-OH], all inositol polyphosphates are coordinated by a single electrostatic interaction with the JAZ1 degron residue Arg-206 (Fig. 2, A and B; Supplemental Table S1). All 1,*X*-$InsP_8$ isomers are furthermore predicted to form extensive interactions with the highly basic concave surface of the COI1 solenoid. Interestingly, these interactions stabilize and hold together the two faces of the inner wall of the Leu-rich repeat (LRR) solenoid that are distal and proximal to the hormone binding pocket (Fig. 2, A and B). At the distal face, the following COI1 residues are predicted to coordinate 1,*X* $InsP_8$: Lys-79, Lys-81, His-118, Arg-120, and Arg-121. Additional residues at the distal face are Arg-85 (for 1,3-$InsP_8$; 1,4-$InsP_8$; 1,5-$InsP_8$), Lys-144 (for 1,3-$InsP_8$; 1,4-$InsP_8$; 1,6-$InsP_8$), and Lys-147 (for 1,2-$InsP_8$; 1,3-$InsP_8$; 1,4-$InsP_8$; 1,6-$InsP_8$). COI1 residues at the proximal face near the hormone binding site that are predicted to coordinate inositol polyphosphate are Arg-409, Arg-440, and additionally Arg-346 (for 1,2-$InsP_8$; 1,3-$InsP_8$; 1,5-$InsP_8$; 1,2-$InsP_8$) and Arg-492 (for 1,3-$InsP_8$; 1,4-$InsP_8$; 1,5-$InsP_8$; Fig. 2, A and B; Supplemental Table S1). The anisotropic nature of these interactions (which are partially compensated for by four single phosphate ions in the inositol polyphosphate-free crystal structure; PDB ID: 3OGM) is likely to have a strong effect on the elliptical shape of the LRR solenoid. Coronatine forms a salt bridge and hydrogen bond network with COI1 residues Arg-85, Arg-348, Arg-409, Tyr-444 and Arg-496. Two of these residues coordinate all (Arg-409) or most (Arg-85) inositol polyphosphate isomers and further stabilize the shape of the solenoid (Fig. 2, A and B). The elliptical shape in turn is likely critical for efficient recruitment of the JAZ1 degron to the top surface of the carboxy-terminal LRR domain: besides hydrophobic packing, a number of polar interactions stabilize the COI1-JAZ1 interface. For instance, strong interactions are mediated by a hydrogen bond formed between the backbone carbonyl of Ala-207 in JAZ1 and the backbone amide of COI1 residue Met-88, by the hydrogen bond interaction of Tyr-472 (COI1) with the backbone carbonyl of Leu-201 (JAZ1), a hydrogen bond donated by COI1 residue Arg-351 to the JAZ1 backbone carbonyl of Ile-203, a salt bridge formed between the side chain of JAZ1 residue Arg-205 and the carboxyl group of Glu-355 (COI1), a hydrogen bond donated by the same JAZ1 residue to the backbone carbonyl of Gly-352, a salt bridge formed between side chains of COI1 residue Glu-359 and Arg-216 in JAZ1, salt bridges formed between COI1 residues Glu-203/Asp-229 and JAZ1 residue Lys-215, hydrogen bonds between the COI1 backbone carbonyl of Met-203 and the side chain of JAZ residue Arg-211, as well as hydrogen bonds between the backbone carbonyl of Pro-202 in JAZ1 and the coronatine-interacting COI1 residue Arg-496 (Fig. 2C; Supplemental Fig. S2). The interaction is further stabilized by a hydrogen bond between the backbone

Figure 1. (*Continued.*)
Classes are defined as follows: Class I, light brown spots at the site of infection; Class II, dark brown spots on the site of infection; Class III, spreading necrosis; Class IV, leaf maceration; Class V, sporulation. The distribution of data were analyzed with a χ^2 test (no. of leaves, $n \geq 29$ classes contained at least 2.5% of total scorings per genotype), * $P < 0.05$. The experiments were repeated independently with similar results.

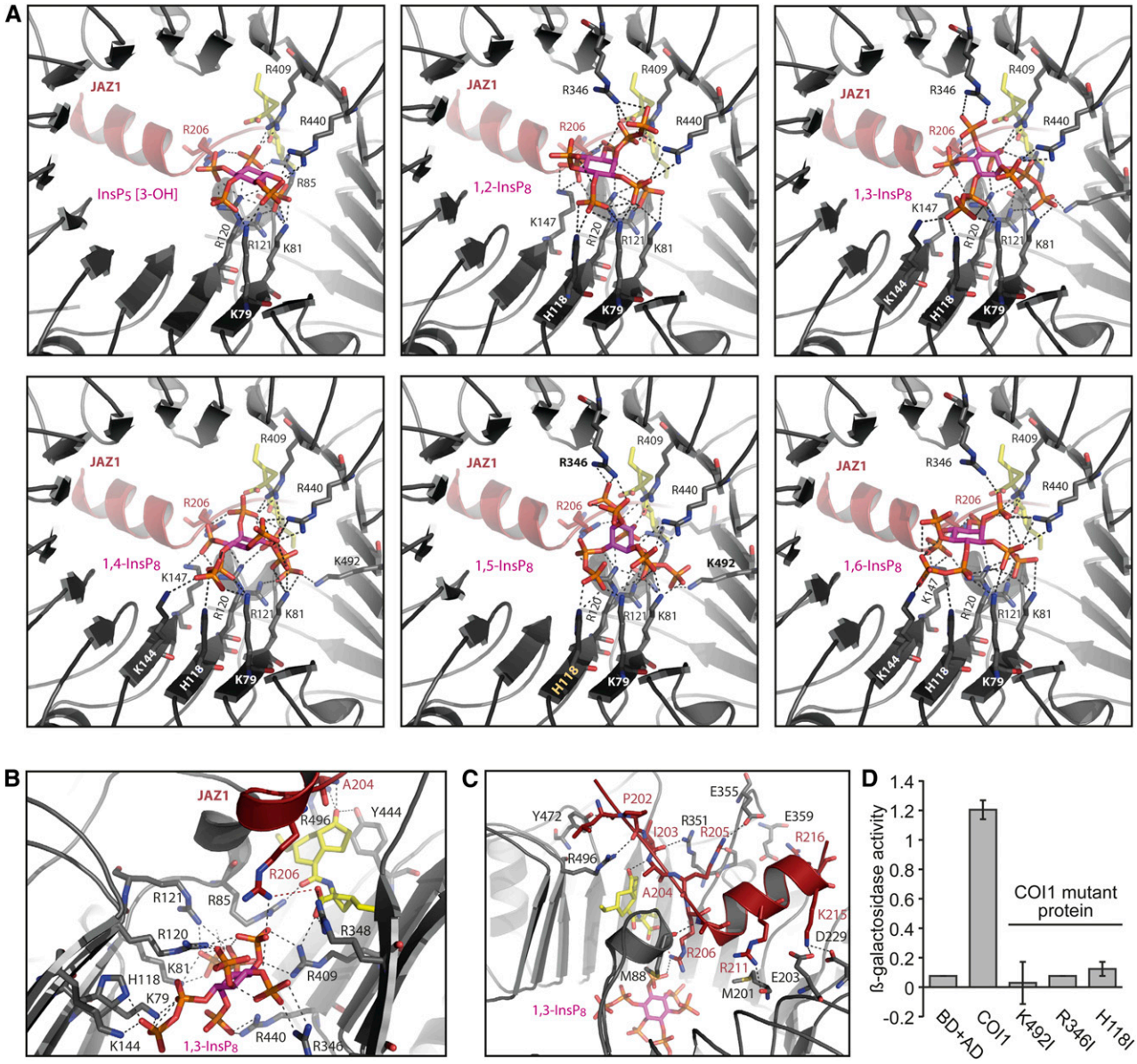

Figure 2. Anisotropic coordination of the COI1 solenoid by inositol polyphosphate suggests activation of the jasmonate receptor by an allosteric switch. A to C, Structural snapshots of the COI1-ASK1-JAZ1 degron complex bound to coronatine and different inositol polyphosphates (as indicated) generated from in silico docking experiments. COI1 (gray), JAZ1 degron (dark red), inositol polyphosphates (magenta stick), and coronatine (yellow stick) are presented. Residues employed for mutagenesis and yeast two-hybrid assays are depicted in bold (Arg-346, Lys-492) or orange (His-118) in the 1,5-$InsP_8$ structure. Bottom views (A) of $InsP_5$ [3-OH] and 1,X $InsP_8$ structures, as well as side view (B) and top view (C) of the presumed 1,3-$InsP_8$ and coronatine binding pockets, are shown. Dashed gray lines represent strong polar contacts; dashed firebrick lines mark a weak polar contact between the side chain of JAZ1 residue Arg-206 and the carboxy group of coronatine. D, JAZ12 interaction with wild-type or mutant COI1 in yeast was evaluated in the presence of 50 μM coronatine by coexpression of pGBKT7-COI1 (and mutated versions as indicated) with pGADT7-JAZ12 in yeast strain Y187 (Clontech) and subsequent quantification of β-galactosidase-mediated hydrolysis of *ortho*-nitrophenyl-β-D-galactopyranoside. Values represent means of two independent biological replicas ±SE. BD+AD, yeast strain harboring the empty vector controls pGBKT7 (expressing the Gal4 DNA-binding domain) and pGADT7 (expressing the Gal4 activation domain).

amide group of JAZ1 residue Ala-204 and the keto moiety of the hormone mimic coronatine, as well as by the interaction between JAZ1 residue Arg-206 and a phosphate group of the inositol polyphosphate ligand as mentioned above (Fig. 2C; Supplemental Fig. S2). Because of the involvement of several strong polar backbone interactions (eight in total), it seems likely that small changes in the elliptical shape of the COI1 solenoid will have a strong effect on JAZ recruitment because backbone interactions cannot adjust

easily compared with interactions mediated by amino acid side chains. We therefore propose that inositol polyphosphate might induce a conformational change or allosteric switch of the COI1 carboxy-terminal LRR solenoid that, with the help of coronatine/JA-Ile, allows docking of the JAZ degron.

To distinguish $InsP_5$- and $InsP_8$-dependent interaction of COI1-JAZ in the yeast system (in which, based on the catalytic activities of Kcs1/IP6K and Vip1/PPIP5K enzymes, the identity of $InsP_8$ is likely to represent 1,5-$InsP_8$; Wang et al., 2011; Draskovic et al., 2008), we have previously engineered single COI1 mutant proteins affected in residues His-118, Lys-492, and Arg-346. These residues were chosen since all three are predicted to interact with 1,5-$InsP_8$, but for geometrical reasons, not all three residues can interact simultaneously with an $InsP_5$ molecule (irrespective of $InsP_5$ isomer identity). The observation that all single mutant COI1 proteins failed to interact with JAZ1 in a yeast two-hybrid assay suggested that, at least in yeast, $InsP_5$ isomers are not critically involved in COI1-JAZ1 interaction (Laha et al., 2015). We have now extended these analyses to the interaction between COI1 and JAZ12. We have chosen JAZ12 because it is, together with JAZ11, most distantly related to JAZ1 (Cuéllar Pérez et al., 2014). While wild-type COI1 interacted robustly with JAZ12, all three single Ile substitutions of COI1 residues His-118, Lys-492, and Arg-346 strongly compromised COI1-JAZ interaction despite stable protein being made in all cases (Fig. 2D; Supplemental Fig. S3). These results suggest that for the interaction of COI1 with JAZ12, like JAZ1, in yeast, $InsP_5$ isomers are unlikely to play a major role, providing further evidence that COI1, not the JAZ partner, determines inositol polyphosphate binding specificity.

FUTURE TASKS

We envisage that the ability of the jasmonate receptor to discriminate between inositol polyphosphate enantiomers might be employed as a tool to reveal isomer identity of these molecules in biological samples, independent of their precise role in activating jasmonate perception. To address more directly the role of inositol pyrophosphates in triggering an allosteric switch of the COI1 carboxy-terminal LRR solenoid, we propose molecular dynamics simulations and/or crystallization of various ASK1-COI1 complexes in the presence and absence of ligands, as well as traditional biochemical measurements of affinity. The latter two approaches are currently complicated by the lack of commercially available $InsP_8$ isomers and, more importantly, because the isomer identity of plant $InsP_8$ remains unknown. It will be a major task for future research to develop technologies to determine the structure of inositol polyphosphates when present in only small amounts in biological extracts. Additionally, it will be important to identify the proteins that generate $InsP_7$ in plants so as to allow in vitro reactions to produce sufficient amounts of $InsP_7$ and $InsP_8$ for proper structure determination.

Accession Numbers

Sequence data from this article can be found in the Arabidopsis Genome Initiative or GenBank/EMBL databases under the following accession numbers: *VIH2* (At3g01310), *JAZ1* (At1g19180), *JAZ2* (At1g74950), *JAZ4* (At1g48500), *JAZ9* (At1g70700), *JAZ12* (At5g20900), *ASK1* (At1g75950), *COI1* (At2g39940), and *IPK1* (At5g42810). Accession numbers for T-DNA insertion lines are as follows: *vih2-4* (GK-080A07), *ipk1-1* (SALK_065337C), and *coi1-t* (SALK_035548).

Supplemental Data

The following supplemental materials are available.

Supplemental Figure S1. Increased susceptibility of the Arabidopsis *ipk1-1* mutant to fungal necrotrophs.

Supplemental Figure S2. Polar backbone interactions between JAZ1 and COI1 suggest strong influence of COI1 carboxy-terminal LRR solenoid shape on JAZ recruitment.

Supplemental Figure S3. Immunoblots of soluble lysates prepared from yeast transformants.

Supplemental Table S1. List of presumptive electrostatic interactions between inositol polyphosphate and the jasmonate receptor complex; script for plotting sigmoidal curves.

Supplemental Methods.

ACKNOWLEDGMENTS

We thank Birgit Kemmerling for providing spores of *A. brassicicola*, Elke Sauberzweig and Louis-Philippe Maier for their excellent help with plant work, Charles Brearley and Marília K.F. de Campos for helpful discussions, and Kristina E. Ile for critically reading the manuscript. No conflict of interest declared.

Received May 2, 2016; accepted June 7, 2016; published June 10, 2016.

LITERATURE CITED

Brearley CA, Hanke DE (1996) Inositol phosphates in barley (Hordeum vulgare L.) aleurone tissue are stereochemically similar to the products of breakdown of InsP6 in vitro by wheat-bran phytase. Biochem J **318:** 279–286

Calderón Villalobos LI, Lee S, De Oliveira C, Ivetac A, Brandt W, Armitage L, Sheard LB, Tan X, Parry G, Mao H, et al (2012) A combinatorial TIR1/AFB-Aux/IAA co-receptor system for differential sensing of auxin. Nat Chem Biol **8:** 477–485

Chini A, Fonseca S, Fernández G, Adie B, Chico JM, Lorenzo O, García-Casado G, López-Vidriero I, Lozano FM, Ponce MR, et al (2007) The JAZ family of repressors is the missing link in jasmonate signalling. Nature **448:** 666–671

Cuéllar Pérez A, Nagels Durand A, Vanden Bossche R, De Clercq R, Persiau G, Van Wees SC, Pieterse CM, Gevaert K, De Jaeger G, Goossens A, et al (2014) The non-JAZ TIFY protein TIFY8 from Arabidopsis thaliana is a transcriptional repressor. PLoS One **9:** e84891

Desai M, Rangarajan P, Donahue JL, Williams SP, Land ES, Mandal MK, Phillippy BQ, Perera IY, Raboy V, Gillaspy GE (2014) Two inositol hexakisphosphate kinases drive inositol pyrophosphate synthesis in plants. Plant J **80:** 642–653

Draskovic P, Saiardi A, Bhandari R, Burton A, Ilc G, Kovacevic M, Snyder SH, Podobnik M (2008) Inositol hexakisphosphate kinase products contain diphosphate and triphosphate groups. Chem Biol **15:** 274–286

Gillaspy GE (2013) The role of phosphoinositides and inositol phosphates in plant cell signaling. Adv Exp Med Biol **991:** 141–157

Hanke DE, Parmar PN, Caddick SEK, Green P, Brearley CA (2012) Synthesis of inositol phosphate ligands of plant hormone-receptor complexes: pathways of inositol hexakisphosphate turnover. Biochem J **444:** 601–609

Katsir L, Schilmiller AL, Staswick PE, He SY, Howe GA (2008) COI1 is a critical component of a receptor for jasmonate and the bacterial virulence factor coronatine. Proc Natl Acad Sci USA **105:** 7100–7105

Kuo HF, Chang TY, Chiang SF, Wang WD, Charng YY, Chiou TJ (2014) Arabidopsis inositol pentakisphosphate 2-kinase, AtIPK1, is required for growth and modulates phosphate homeostasis at the transcriptional level. Plant J **80:** 503–515

Laha D, Johnen P, Azevedo C, Dynowski M, Weiß M, Capolicchio S, Mao H, Iven T, Steenbergen M, Freyer M, et al (2015) VIH2 regulates the synthesis of inositol pyrophosphate $InsP_8$ and jasmonate-dependent defenses in Arabidopsis. Plant Cell **27:** 1082–1097

Lee HS, Lee DH, Cho HK, Kim SH, Auh JH, Pai HS (2015) $InsP_6$-sensitive variants of the Gle1 mRNA export factor rescue growth and fertility defects of the *ipk1* low-phytic-acid mutation in Arabidopsis. Plant Cell **27:** 417–431

Lemtiri-Chlieh F, MacRobbie EA, Brearley CA (2000) Inositol hexakisphosphate is a physiological signal regulating the K+-inward rectifying conductance in guard cells. Proc Natl Acad Sci USA **97:** 8687–8692

Leon-Reyes A, Van der Does D, De Lange ES, Delker C, Wasternack C, Van Wees SCM, Ritsema T, Pieterse CMJ (2010) Salicylate-mediated suppression of jasmonate-responsive gene expression in Arabidopsis is targeted downstream of the jasmonate biosynthesis pathway. Planta **232:** 1423–1432

Menniti FS, Miller RN, Putney JW Jr, Shears SB (1993) Turnover of inositol polyphosphate pyrophosphates in pancreatoma cells. J Biol Chem **268:** 3850–3856

Mosblech A, Thurow C, Gatz C, Feussner I, Heilmann I (2011) Jasmonic acid perception by COI1 involves inositol polyphosphates in Arabidopsis thaliana. Plant J **65:** 949–957

Mulugu S, Bai W, Fridy PC, Bastidas RJ, Otto JC, Dollins DE, Haystead TA, Ribeiro AA, York JD (2007) A conserved family of enzymes that phosphorylate inositol hexakisphosphate. Science **316:** 106–109

Munnik T, Nielsen E (2011) Green light for polyphosphoinositide signals in plants. Curr Opin Plant Biol **14:** 489–497

Munnik T, Vermeer JE (2010) Osmotic stress-induced phosphoinositide and inositol phosphate signalling in plants. Plant Cell Environ **33:** 655–669

Murphy AM, Otto B, Brearley CA, Carr JP, Hanke DE (2008) A role for inositol hexakisphosphate in the maintenance of basal resistance to plant pathogens. Plant J **56:** 638–652

Pauwels L, Goossens A (2011) The JAZ proteins: a crucial interface in the jasmonate signaling cascade. Plant Cell **23:** 3089–3100

Rao F, Cha J, Xu J, Xu R, Vandiver MS, Tyagi R, Tokhunts R, Koldobskiy MA, Fu C, Barrow R, et al (2014) Inositol pyrophosphates mediate the DNA-PK/ATM-p53 cell death pathway by regulating CK2 phosphorylation of Tti1/Tel2. Mol Cell **54:** 119–132

Sheard LB, Tan X, Mao H, Withers J, Ben-Nissan G, Hinds TR, Kobayashi Y, Hsu FF, Sharon M, Browse J, et al (2010) Jasmonate perception by inositol-phosphate-potentiated COI1-JAZ co-receptor. Nature **468:** 400–405

Shears SB, Ganapathi SB, Gokhale NA, Schenk TM, Wang H, Weaver JD, Zaremba A, Zhou Y (2012) Defining signal transduction by inositol phosphates. Subcell Biochem **59:** 389–412

Stephens L, Radenberg T, Thiel U, Vogel G, Khoo KH, Dell A, Jackson TR, Hawkins PT, Mayr GW (1993) The detection, purification, structural characterization, and metabolism of diphosphoinositol pentakisphosphate(s) and bisdiphosphoinositol tetrakisphosphate(s). J Biol Chem **268:** 4009–4015

Stevenson-Paulik J, Bastidas RJ, Chiou ST, Frye RA, York JD (2005) Generation of phytate-free seeds in Arabidopsis through disruption of inositol polyphosphate kinases. Proc Natl Acad Sci USA **102:** 12612–12617

Tan X, Calderon-Villalobos LI, Sharon M, Zheng C, Robinson CV, Estelle M, Zheng N (2007) Mechanism of auxin perception by the TIR1 ubiquitin ligase. Nature **446:** 640–645

Thines B, Katsir L, Melotto M, Niu Y, Mandaokar A, Liu G, Nomura K, He SY, Howe GA, Browse J (2007) JAZ repressor proteins are targets of the SCF(COI1) complex during jasmonate signalling. Nature **448:** 661–665

Thota SG, Bhandari R (2015) The emerging roles of inositol pyrophosphates in eukaryotic cell physiology. J Biosci **40:** 593–605

Tsui MM, York JD (2010) Roles of inositol phosphates and inositol pyrophosphates in development, cell signaling and nuclear processes. Adv Enzyme Regul **50:** 324–337

Wang H, Falck JR, Hall TM, Shears SB (2011) Structural basis for an inositol pyrophosphate kinase surmounting phosphate crowding. Nat Chem Biol **8:** 111–116

Wilson MSC, Livermore TM, Saiardi A (2013) Inositol pyrophosphates: between signalling and metabolism. Biochem J **452:** 369–379

9.3 Pries, Nöcker, Khan, Johnen, Hong et al., 2018

Target Identification and Mechanism of Action of Picolinamide and Benzamide Chemotypes with Antifungal Properties.

Pries, V.*, Nöcker, C.*, Khan, D.*, Johnen, P.*, Hong, Z.*, Tripathi, A., Keller, A. L., Fitz, M., Perruccio, F., Filipuzzi, I., Thavam, S., Aust, T., Riedl, R., Ziegler, S., Bono, F., Schaaf, G., Bankaitis, V. A., Waldmann, H. and Hoepfner, D.

*These authors contributed equally to this work.

Cell Chem Biol. 2018 Mar 15;25(3):279-290.e7. doi: 10.1016/j.chembiol.2017.12.007.

Cell Chemical Biology
Article

Target Identification and Mechanism of Action of Picolinamide and Benzamide Chemotypes with Antifungal Properties

Verena Pries,[1,5,9] Christina Nöcker,[2,7,9] Danish Khan,[3,8,9] Philipp Johnen,[4,5,9] Zebin Hong,[6,9] Ashutosh Tripathi,[3,8,9] Anna-Lena Keller,[4] Michael Fitz,[4] Francesca Perruccio,[1] Ireos Filipuzzi,[1] Sasikala Thavam,[2,7] Thomas Aust,[1] Ralph Riedl,[1] Slava Ziegler,[2,7] Fulvia Bono,[6] Gabriel Schaaf,[4,5] Vytas A. Bankaitis,[3,8] Herbert Waldmann,[2,7] and Dominic Hoepfner[1,10,*]
[1]Novartis Institutes for BioMedical Research, Novartis Pharma AG, Forum 1 Novartis Campus, 4056 Basel, Switzerland
[2]Max-Planck-Institute for Molecular Physiology, Otto-Hahn-Strasse 11, 44227 Dortmund, Germany
[3]Department of Biochemistry and Biophysics, Texas A & M University, College Station, TX 77843, USA
[4]Center for Plant Molecular Biology, Universität Tübingen, Auf der Morgenstelle 32, 72076 Tübingen, Germany
[5]Institute of Crop Science and Resource Conservation, Universität Bonn, Karlrobert-Kreiten-Strasse 13, 53113 Bonn, Germany
[6]Max Planck Institute for Developmental Biology, Spemannstrasse 35, 72076 Tübingen, Germany
[7]Technische Universität Dortmund, Fakultät für Chemie und Chemische Biologie, Otto-Hahn-Strasse 4a, 44227 Dortmund, Germany
[8]Department of Molecular and Cellular Medicine, Texas A & M University Health Science Center, College Station, TX 77843-1114, USA
[9]These authors contributed equally
[10]Lead Contact
*Correspondence: dominic.hoepfner@novartis.com
https://doi.org/10.1016/j.chembiol.2017.12.007

SUMMARY

Invasive fungal infections are accompanied by high mortality rates that range up to 90%. At present, only three different compound classes are available for use in the clinic, and these often suffer from low bioavailability, toxicity, and drug resistance. These issues emphasize an urgent need for novel antifungal agents. Herein, we report the identification of chemically versatile benzamide and picolinamide scaffolds with antifungal properties. Chemogenomic profiling and biochemical assays with purified protein identified Sec14p, the major phosphatidylinositol/phosphatidylcholine transfer protein in *Saccharomyces cerevisiae*, as the sole essential target for these compounds. A functional variomics screen identified resistance-conferring residues that localized to the lipid-binding pocket of Sec14p. Determination of the X-ray co-crystal structure of a Sec14p-compound complex confirmed binding in this cavity and rationalized both the resistance-conferring residues and the observed structure-activity relationships. Taken together, these findings open new avenues for rational compound optimization and development of novel antifungal agents.

INTRODUCTION

Invasive fungal infections (IFIs) are associated with high morbidity and mortality rates (Schmiedel and Zimmerli, 2016). Moreover, the incidence of fungal infections is rapidly escalating as the numbers of premature infants, patients receiving immunosuppressive therapy, and patients afflicted with AIDS, neoplastic disease, and advanced age increase (Pfaller et al., 2006). Although the incidence of IFIs is rising, the launch of initiatives aimed at antifungal drug discovery is lagging (Schmiedel and Zimmerli, 2016). Only three compound classes (i.e., azoles, polyenes, and echinocandins) are currently in therapeutic use (Prasad et al., 2016; Roemer and Krysan, 2014), and these act on the fungal plasma membrane, its biosynthetic pathways, and cell wall components, respectively. However, these drugs are only modestly effective in reducing the high mortality rates associated with IFIs because of: (1) restrictions in route of administration, (2) limited spectrum of activity, (3) poor bioavailability in target tissues, (4) significant toxicities that result from undesirable drug interactions, and (5) the emergence of drug-resistant pathogens (Brown et al., 2012). All of these factors highlight the acute demand for the discovery and development of novel classes of small-molecule inhibitors (SMIs) against a wider range of targets.

Genome-wide fitness profiling approaches using the surrogate model fungus *Saccharomyces cerevisiae* are proving themselves as powerful tools for identifying novel antifungal agents and developing hypotheses for their cellular target (Hoepfner et al., 2012; Richie et al., 2013). Haploinsufficiency profiling (HIP) identifies candidate pathways for direct inhibition by the compound as genes are identified in which one functional copy, compared with two, confers hypersensitivity to inhibition by that compound. In homozygous profiling (HOP), both gene copies are deleted so that information on synthetic lethal gene interactions and compensating pathways is accessed (Giaever et al., 1999; Hoon et al., 2008; Lee et al., 2014; Lum et al., 2004; Parsons et al., 2006; Roemer et al., 2011). Using the HIP-HOP approach, we identified compounds with benzamide and picolinamide scaffolds as inhibitors of Sec14p, the major phosphatidylinositol-transfer protein (PITP) in *S. cerevisiae*, whose activity is essential for cell viability (Bankaitis et al., 1989, 1990). A battery of genetic and biochemical assays

Table 1. Structures and IC_{50} Values for Active Compounds

Cpd	Structure	IC_{50} (μM) *S. cerevisiae* Wild-Type	Fold IC_{50} Shift *S. cerevisiae* Wild-Type/Wild-TypeΔ8	IC_{50} (μM) *S. cerevisiae* *SEC14/sec14*	IC_{50} (μM) HCT116	IC_{50} (μM) Lipid Transfer
1	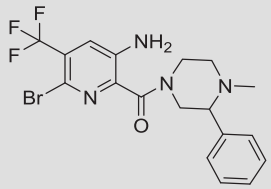	13.5	13.8×	5.9	30.4	ND
2	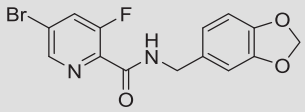	28.5	2.7×	9.4	>100	6.7
3	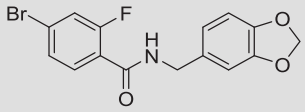	6.6	2.8×	1.7	>100	0.7
4	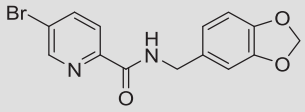	134.9	2.3×	99.4	>100	29.4
5	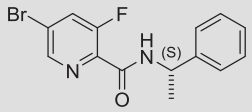	42.9	2.7×	32.6	>100	30.7
6	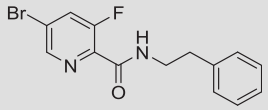	>200	ND	>200	>100	129

IC_{50} values were determined in a cell-based growth assay with the heterozygous *SEC14* deletion strain against a wild-type control, with a luminescent cell viability assay on HCT116 cells and in an *in vitro* lipid-transfer assay, as indicated. ND, not determined.

corroborated the target hypothesis. Finally, we report the first crystal structure for a Sec14p::SMI complex, - thus providing a detailed mechanism of inhibition. Taken together, these findings outline a path for rationale synthesis of the next generation of small-molecule Sec14p inhibitors with optimized antifungal properties.

RESULTS

Chemogenomic Profiling

Screening of the Novartis compound archive for SMIs with antifungal activity (Richie et al., 2013) identified the picolinamide-containing compound **1** (Table 1) as a novel inhibitor of *S. cerevisiae* growth with a half maximal inhibitory concentration (IC_{50}) value of 13.5 μM. Lack of potent cytotoxicity against mammalian HCT116 cells (Table 1) led us to initiate follow-up studies on this chemotype. To identify the target protein of compound **1**, HIP and HOP experiments were performed. For data analysis, the strain sensitivity was plotted against the *Z* score, which relates the sensitivity score of a strain in the compound profile to the variability in sensitivity of that strain across all the >3,000 compounds tested in the dataset (Hoepfner et al., 2014).

Execution of the HIP-HOP assay at a sub-lethal compound concentration (20 μM) identified a single strain to be significantly hypersensitive to compound **1**: the strain carrying a heterozygous deletion for *SEC14* (Figure 1A). *SEC14* encodes an essential phosphatidylinositol (PtdIns)/phosphatidylcholine (PtdCho) transfer protein (PITP) that plays a crucial role in protein transport from the *trans*-Golgi network (TGN) and endosomal system. As such, Sec14p function is essential for yeast cell viability (Bankaitis et al., 1990). HOP (Figure 1A) identified strains deleted for *ITR1*(Nikawa et al., 1991), encoding a *myo*-inositol transporter, *YPT31* (Benli et al., 1996), encoding a Rab GTPase essential for Golgi function, *ARL1* (Lee et al., 1997), and *ARL3* (Huang et al., 1999) encoding two ARF-like GTPases that are involved in TGN/endosomal membrane traffic and *SFH2*/*CSR1* (Li et al., 2000), a non-classical PITP, to be synthetic lethal. The significance of the HOP screen gene set was that it recapitulated independent screens that previously revealed genetic interactions between *SEC14* and *ARL1*, *ARL3*, *YPT31*, and *CSR1*/*SFH2* (Fairn et al., 2007; Mousley et al., 2008). Hypersensitivities of the strains identified in the genome-wide, pooled experiment, were validated by recording individual growth curves with the specific single strains picked from the HIP and HOP collection (Figure 1B). Taken together, the data from the genome-wide fitness profiling suggested that compound **1** exerts its antifungal action through Sec14p.

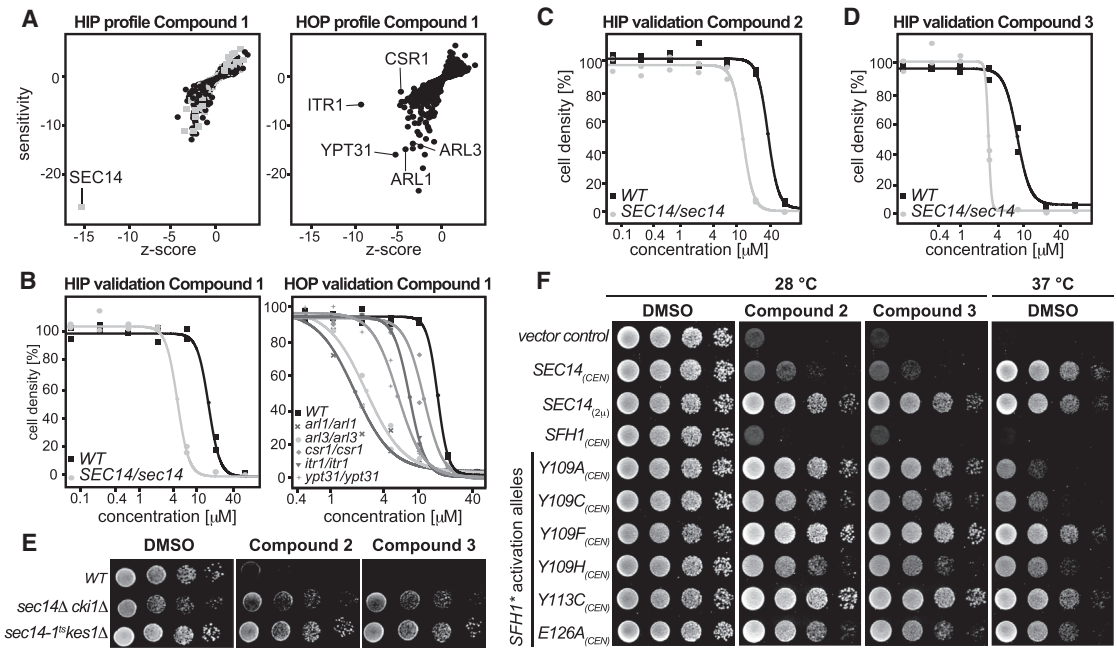

Figure 1. Chemogenomic Profiling and Hypersensitivity Validation

(A) Calculated profiles of the chemogenomic profiling experiment. HIP outlines hits directly affected by the test compound. HOP identifies synthetic interactions with the target. Essential genes are depicted by gray boxes, non-essential genes by black dots.

(B) Single-strain validation of hits from the chemogenomic profiling experiments as recorded in duplicates.

(C and D) Confirmation of hypersensitivity of the *Sec14/sec14* HIP strain against compounds **2** and **3** as recorded in duplicates.

(E) The wild-type and two bypass Sec14p strains were spotted on rich medium (YPD) supplemented with DMSO or 20 μM of compounds **2** and **3** and incubated at 30°C for 48 hr.

(F) Transformants of the temperature-sensitive *sec14-1^{ts}* yeast strain harboring centromeric (*CEN*) plasmids carrying either *SFH1* or the designated *SFH1* activation alleles (*SFH1**) were spotted on minimal medium supplemented with 120 μM of compound **2**, 30 μM of compound **3**, or DMSO, as indicated and incubated at permissive (left) or restrictive (right) temperature. Transformants harboring YCplac33 (empty vector), or *SEC14* expressed from a centromeric (*CEN*) or a multi-copy plasmid (*2μ*) served as controls.

Chemical Derivatization

Sec14p is an attractive antifungal target as it has been shown to be druggable (Filipuzzi et al., 2016; Nile et al., 2014), it executes essential functions in several pathogenic fungi and it is required for efficient secretion of pathogenicity factors (Chayakulkeeree et al., 2011). We therefore sought to delineate structure-activity relationships (SARs) by producing and testing a small compound collection generated by coupling different carboxylic acids and amines via established chemical synthesis methods (El-Faham and Albericio, 2010; El-Faham et al., 2009) (Figure 2; Data S1). All derivatives were tested for their activity against wild-type *S. cerevisiae* cells (Table S1). To ensure that the SMIs still acted at the level of Sec14p, hypersensitivity against the heterozygous *SEC14* deletion strain, as observed in the HIP assay for compound **1**, was verified. For compounds **2** and **3** (Figures 1C and 1D), and **4** and **5** (Table 1), decreased fitness of the *SEC14/sec14Δ* heterozygote was observed relative to the isogenic wild-type. Of this SMI series, the benzamide compound **3** was the most potent with an IC_{50} of 6.6 μM. These data indicated that the nitrogen of the picolinamide moiety was not essential for the Sec14p-targeted inhibition of these compounds. Compound **3**, however, had much reduced solubility in pure aqueous solutions at pH 7.4 (Table S2), thereby hampering subsequent testing by requiring careful handling when diluting into a variety of fungal and mammalian culture medium. Substituting the benzodioxole with benzene, biphenyl, fluorobenzene, pyridine, or pyrazine functional groups either reduced potency or ablated inhibitory activity entirely (Table S1). Similarly, exchange of bromine and fluorine on the benzamide/picolinamide moiety was also incompatible with inhibitor activity. One desirable property of the bioactive derivatives was that all active compounds of the collection showed reduced cytotoxicity for HCT116 cells compared with compound **1** (Table 1).

Validation of Sec14p as Cellular Target

Several independent approaches were taken to establish Sec14p as the direct target of the most bioactive benzamide (compound **3**) and picolinamides (compounds **1**, **2**, **4**, **5**, and **6**). First, we exploited the fact that the otherwise essential Sec14p activity is rendered dispensable in mutant cells deleted for structural genes of the cytidine diphosphate-choline pathway (e.g., *CKI1*; Cleves et al., 1991) or the structural gene for the oxysterol binding protein homolog Kes1p (Fang et al., 1996). In these "bypass Sec14p" mutants, a functional and Sec14p-independent balance of lipid metabolism and PtdIns-4-phosphate signaling for exocytic membrane trafficking from the yeast TGN/endosomal system is restored (Cleves et al., 1991; Fang et al., 1996; Li et al., 2002). It was previously shown that the growth-inhibitory activity of highly specific Sec14p-targeted SMIs is alleviated in genetic backgrounds carrying loss-of-function *cki1* or *kes1*

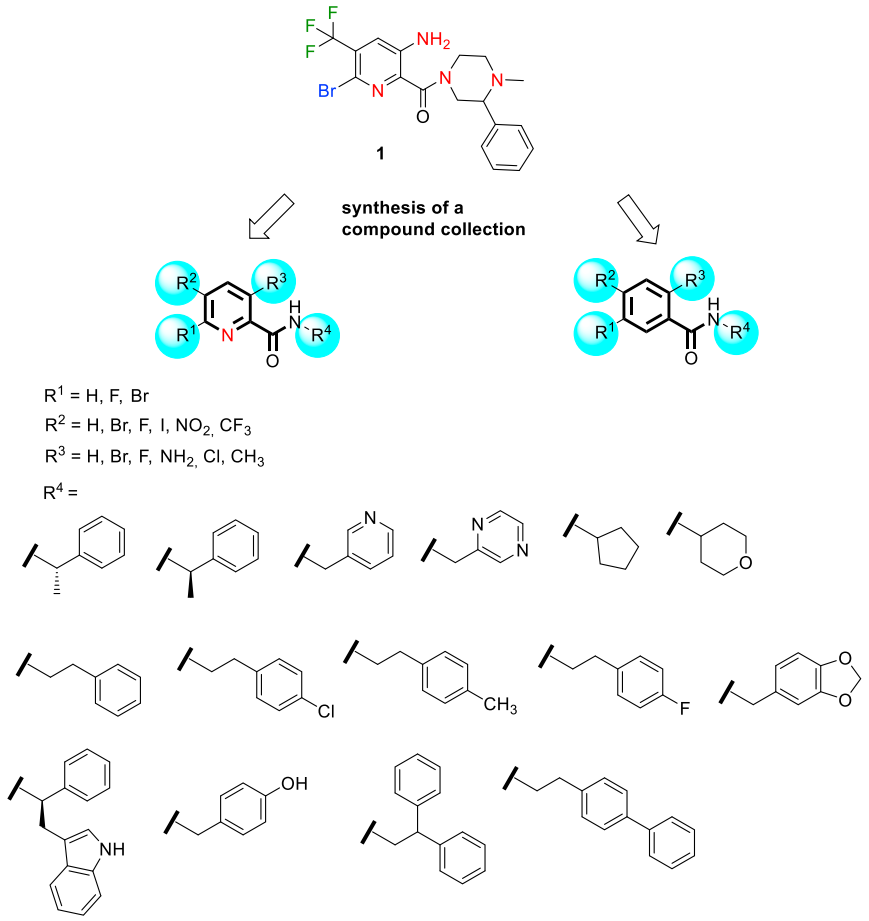

Figure 2. Synthesis of a Collection of Benz- and Picolinamides for Structure-Activity Relationship Studies

alleles (Nile et al., 2014). Thus, the *cki1* and *kes1* bypass Sec14p mutants were spotted on agar plates supplemented with compounds **2** and **3** to a final concentration of 20 μM (Figure 1E). Indeed, growth of the bypass Sec14p mutants was indifferent to challenge by these compounds.

To further investigate target specificity, we assessed the inhibitory effects of compounds **2** and **3** on Sfh1p, the closest Sec14p homolog (Schaaf et al., 2011) in *S. cerevisiae*. Sfh1p is a non-essential protein and therefore cannot be identified as a drug target by HIP profiling. In these experiments, we adopted the previously described strategy of assessing the inhibitory effects of compounds **2** and **3** on Sfh1p activation mutants that were identified by a directed evolution approach (Khan et al., 2016; Nile et al., 2014), and for which single-residue substitutions endow this pseudo-Sec14p with robust Sec14p-like PITP activities *in vivo* and *in vitro* (Schaaf et al., 2011). All *SFH1* activation alleles (*SFH1**) expressed from a single-copy plasmid endowed resistance to both compounds **2** and **3**, even when the SMI was used at concentrations sufficiently high (120 and 30 μM, respectively) that even an additional copy of wild-type *SEC14* failed to restore cell growth (Figure 1F). Rather, the *SFH1**-associated SMI-resistance phenotype resembled that of yeast expressing a multi-copy episomal *SEC14* expression plasmid or yeast carrying *cki1* or *kes1* "bypass Sec14p" mutations. Taken together, these results strongly suggest that Sec14p is the sole essential target for these compounds in the yeast cell.

SMIs Inhibit Sec14p Lipid-Transfer Activity *In Vitro*

Based on the knowledge gained from the cell-based growth inhibition tests, a subset of 15 compounds was chosen for direct analysis of their inhibitory effect on Sec14p-mediated phospholipid transfer in a purified *in vitro* system (Khan et al., 2016; Nile et al., 2014; Schaaf et al., 2008) (Figure 3A). To exclude the possibility that compound activity was due to non-specific membrane-active effects, the selected scaffolds were tested in parallel in phospholipid transfer assays reconstituted with the structurally unrelated mammalian PtdIns/PtdCho-transfer protein PITPα (Figure 3B). Recombinant Sec14p was pre-incubated with acceptor membranes and compounds for 30 min at 37°C, the assay was initiated by the addition of radiolabeled rat liver microsomes, and the reaction was terminated after incubation of the assay for 30 min at 37°C. The [^{3}H]PtdIns-transfer activities in the presence of test compounds were normalized to DMSO (mock) controls. Compounds **2**, **3**, **4**, **5**, and **6** showed clear inhibition of PtdIns transfer mediated by Sec14p, whereas no such inhibitory effects were observed when PtdIns transfer was catalyzed by the mammalian PITPα. Furthermore, IC_{50} values were determined for active compounds in subsequent titration experiments (Figure 3C; Table 1). In agreement with the growth inhibition data, compound **3** again scored as the most potent inhibitor of Sec14p PtdIns-transfer activity, with an IC_{50} of 0.7 μM (IC_{50} = 7 μM in *S. cerevisiae*). To assess if compounds **2** and **3** also inhibited the Sec14p of pathogenic species we recorded IC_{50} curves as described above on the purified proteins of *C. albicans* and *C. glabrata*. In this experiment both compounds scored similar activity on *S. cerevisiae* and *C. glabrata*, but did not inhibit PtdIns transfer by the *C. albicans* protein in the tested concentration range (Figure 3D). Activity on at least one other important fungal pathogen, and the absence of any measurable inhibition of PtdIns transfer by the mammalian PITPα, not only indicated that the Sec14p-directed inhibitory effect of compound **3** was fungal specific (and not the result of non-specific membrane-active effect), but it further emphasized the potential of this chemotype as antifungal lead.

Single-Amino Acid Substitutions Render Sec14p Resistant to Inhibition by Compounds 2 and 3

The genetic and biochemical data strongly supported Sec14p as the sole essential cellular target of this SMI series. To obtain additional resolution for how this chemotype engages its target,

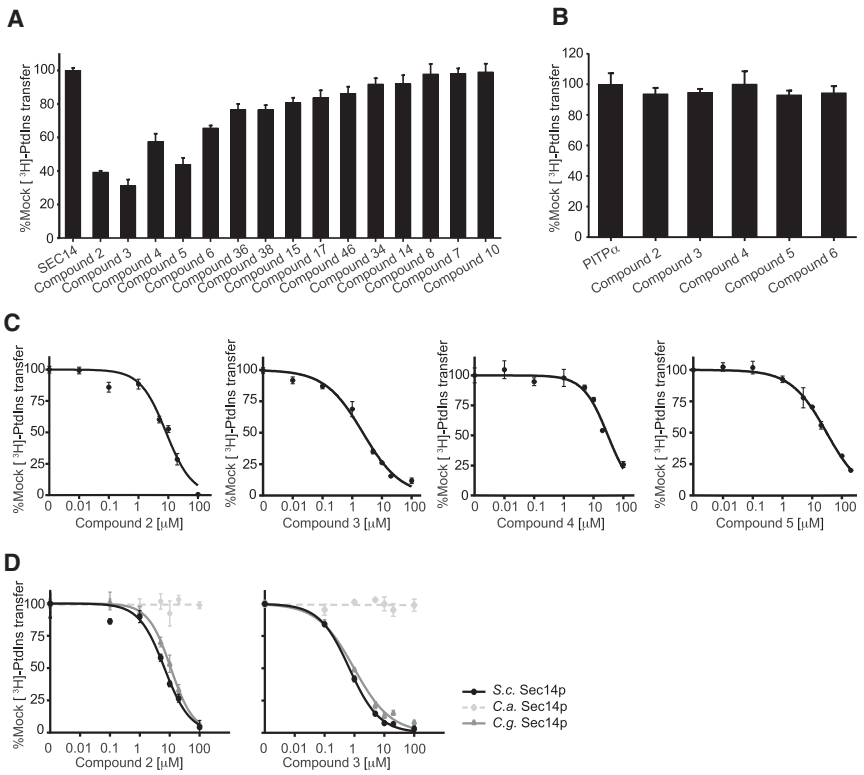

Figure 3. Analysis of Lipid-Transfer Inhibition with Recombinant Sec14p

(A) Fifteen compounds were tested for inhibition of Sec14p-mediated [^{3}H]PtdIns transfer at a fixed concentration of 20 μM SMI (see the STAR Methods). Values represent mean ± SEM of triplicate assay determinations from two independent experiments. Total radiolabel inputs per assay ranged from 8,356 to 9,604 cpm, backgrounds from 436 to 489 cpm, and the transfer efficiency from 14% to 16% of total input [^{3}H]PtdIns. Activities were normalized against the mock condition set at 100%.

(B) The five small molecules that inhibited Sec14p [^{3}H]PtdIns transfer by ≥30% in the endpoint assays in (A) were tested for inhibition of the structurally unrelated mammalian PITPα. [^{3}H]PtdIns input for these assays ranged from 10,703 to 11,202 cpm, assay background from 403 to 415 cpm, and [^{3}H]PtdIns-transfer efficiencies ranged from 10% to 11% of total input radiolabel. Values represent mean ± SEM of triplicate assay determinations from two independent experiments.

(C) IC_{50} values for Sec14p-active compounds. Small-molecule inhibitors of Sec14p were titrated into PtdIns-transfer assays to determine IC_{50} values. [^{3}H]PtdIns input into these assays varied from 9,649 to 11,034 cpm, backgrounds ranged from 243 to 648 cpm, and transfer efficiencies as functions of total [3H]PtdIns input ranged from 12% to 18%.

(D) IC_{50} curves for compounds **2** and **3** tested against Sec14p of *S. cerevisiae*, *C. albicans*, and *C. glabrata*. IC_{50} values represent a 95% confidence interval from two independent experiments, with triplicate determinations for each data point.

and to identify amino acids mediating interaction and selectivity for these compounds, a functional variomics screen was deployed (Huang et al., 2013; Pries et al., 2016). This assay exploited a library of plasmid-encoded *SEC14* genes mutagenized by error-prone PCR and screens for genetically dominant resistance of respective yeast transformants against the compound of interest. BY4743 wild-type cells (5×10^6) transformed with library DNA previously identified to be of a complexity above 2×10^5 (Huang et al., 2013) were plated onto 20 cm plates with synthetic defined media lacking uracil and containing growth-inhibitory concentrations of compound **2** (250 μM) or compound **3** (100 μM). Distinct colonies appeared after 72 hr, and 96 fast-growing colonies were selected from both SMI-resistance screens. The plasmid-encoded *SEC14* genes were then subjected to nucleotide sequence analysis and SNPs were identified. For both compounds, single-amino acid substitutions involving Tyr_{151}, Val_{154}, Val_{155}, and Ser_{201} were recovered. Among the 96 clones picked against each compound, the frequencies of mutations identified with unambiguous sequences were as follows: Tyr_{151} substitutions were identified 51 and 30 times in compounds **2** and **3** selections respectively, Val_{154} was recovered 1 and 3 times, Val_{155} 21 and 14 times, and Ser_{201} 6 and 25 times, respectively. Furthermore, the compound **2** resistance screen identified a missense substitution of Ser_{173} to Leu in four resistant clones (Figure 4A). Genotype-phenotype linkage of the most prominent SNPs, was verified by reintroduction of the plasmid-encoded mutant *SEC14* genes into the BY4743Δ8 *MATa/α* strain, which is deleted for eight genes involved in drug resistance. Resistance phenotypes were subsequently assessed by dose-response experiments (Figure 4B). Integration of an additional *SEC14* wild-type allele already yielded a 5-fold IC_{50} shift with compound **2** and a 3-fold IC_{50} shift with compound **3** compared with wild-type cells. However, with the sole exception of $SEC14^{V154G}$, all mutant alleles tested endowed naive yeast cells with significantly increased, or effectively complete, resistance to SMI challenge.

Next, these Sec14p variants were purified as recombinant proteins from *E. coli* and [^{3}H]PtdIns-transfer activities were measured for each in SMI titrations *in vitro*. All of these mutant Sec14ps exhibited substantially increased resistance to compounds **2**- and **3**-mediated inhibition of [^{3}H]PtdIns transfer relative to wild-type Sec14p. With regard to compound **2**, all mutant proteins exhibited IC_{50} values that were some 7- to 30-fold higher than that of wild-type Sec14p (Figure 4C; Table S3). Moreover, all mutant proteins but one were essentially indifferent to challenge with compound **3**. That exception, $Sec14p^{V155A}$, exhibited a more modest 17-fold increase in IC_{50} relative to wild-type Sec14p (Figure 4C; Table S3). In general, the IC_{50} values for each mutant protein were reflective of the levels of SMI resistance for the corresponding mutant yeast strains as measured by cell growth. These data unambiguously validate the identified resistance-conferring mutations by directly measuring PtdIns activities and demonstrating that the magnitude of intrinsic Sec14p resistance scaled proportionately to the SMI resistance of the corresponding yeast strain.

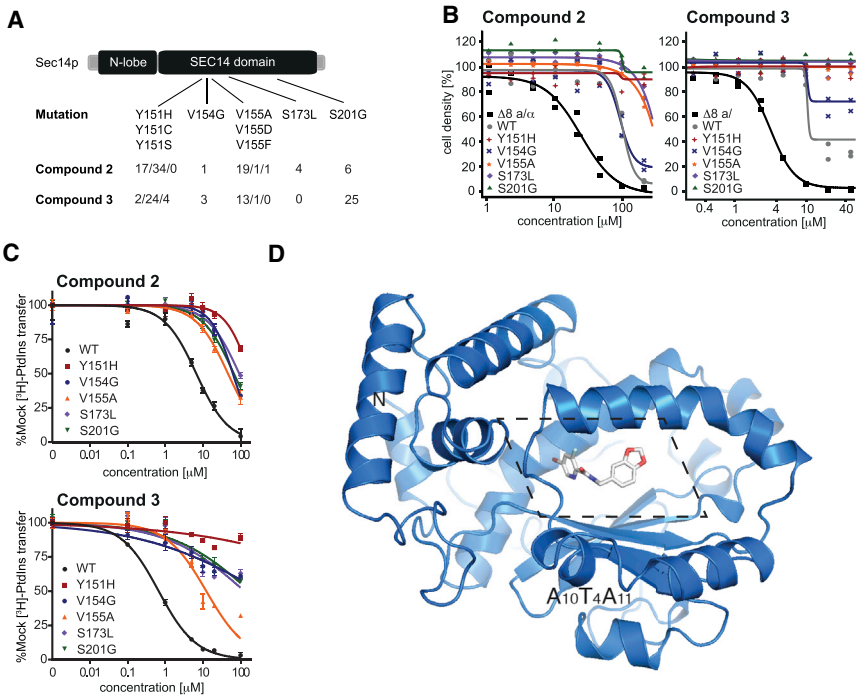

Figure 4. Structural and Functional Analysis of Sec14p-Compound Interactions

(A) SNPs and mutation frequency as identified by functional variomics for both tested compounds.

(B) Validation of identified mutations by integrative transformation of indicated *SEC14* allele into cells.

(C) Validation of identified mutations by *in vitro* testing on recombinant protein. Error bars in (B and C) indicate 1 SD.

(D) Overview of the structure of Sec14p (as cartoon, in marine) in complex with compound **2** (in sticks representation, in gray). The section displayed in detail in (E) is outlined by dotted lines.

(E) Detailed view (rotated 45° along the x axis for clarity) of the binding pocket of Sec14p bound to compound **2** as identified by co-crystallization at 2.6 Å resolution. Interacting residues and relevant secondary structure elements of Sec14p are labeled; side chains are colored in marine and shown as sticks. H- and halogen-bonding are visualized as solid lines in blue and green, respectively, while hydrophobic interactions are shown as gray dashed lines. π-π stackings are depicted as green dashed lines (light green for parallel stacking; smudge green for perpendicular stacking), with aromatic ring centers as gray spheres. Functional groups of compound **2** are indicated.

Mode of Ligand Binding

To identify the mechanism of inhibition, Sec14p was co-crystallized with picolinamide compound **2**, and the crystal structure of the complex was determined at 2.6 Å resolution. Compound **2** was prioritized for increased potency over compound **1** and better solubility than compound **3** (Table S2). The structure was solved by Molecular Replacement using Sec14p (PDB: 1aua; Sha et al., 1998) as input model in PHASER (Mccoy et al., 2007). The model was rebuilt and refined using PHENIX and COOT (Adams et al., 2010; Emsley and Cowtan, 2004). The final model exhibited an R_{factor} of 19.9% and an R_{free} of 22.5%, with good stereochemistry (Table S4). The asymmetric unit contained one molecule and Sec14p residues from 4 to 303 were identified in the final model. A discrete portion of the electron density in the 2mFo-DFc map (contoured at 1σ) revealed the presence of the ligand (Figure S1). As expected, the protein exhibited a typical Sec14p fold consisting of a globular structure with an N-terminal tripod motif and a C-terminal lobe that included a large hydrophobic pocket of sufficient volume to accommodate a single phospholipid molecule (Schaaf et al., 2008; Sha et al., 1998) (Figures 4D and S2). In the structure, Sec14p showed an open conformation, with the helical gate (helix $A_{10}T_4A_{11}$ [Bankaitis et al., 2010; Ryan et al., 2007; Schaaf et al., 2008]) displaced, as in the previously described detergent-bound Sec14p (Sha et al., 1998). Superposition with a known structure of Sec14p in the open conformation showed that the two structures were very similar overall, with a root-mean-square deviation of 0.336 Å over 1,917 atoms (PDB: 1aua; Sha et al., 1998) (Figure S2).

In the crystallized complex, compound **2** occupied the lipid-binding pocket of Sec14p, where it was deeply buried in the cavity away from the solvent-exposed Sec14p surface (Figures 4D and 4E). The buried surface area of the ligand was 440.32 $Å^2$. The bromo-pyridine group (H1) of the picolinamide moiety pointed toward the core of the cavity, while the 1,3-benzodioxole ring (H2) was oriented toward solvent. The bromine was in van der Waals contact with Val_{154} and Val_{155} (range from 3.7 to 4.2 Å) and interacted with the carboxyl group of Tyr_{151} (3.51 Å). The pyridine ring engaged in a π-π stacking interaction with Tyr_{151} on one side, and in a hydrogen-bond (H-bond) interaction between the amine and the carboxyl of Ser_{173} on the other. On

this side, the Arg_{208} side-chain and backbone atoms engaged in van der Waals interactions and further stabilized SMI binding. The fluorine atom interacted with Ser_{201} and Tyr_{151} and was in long-range interactions with Tyr_{205}. The linker (L) that connected rings H1 and H2 of compound **2** was stabilized by interactions with Ser_{201} and Tyr_{151} as well as with Met_{209} and Thr_{175}. The 1,3-benzodioxole ring was positioned for H-bond interaction with Ser_{201} and also engaged in van der Waals interactions with Phe_{212}, Thr_{175}, and Met_{177} on the other side. These structural data were fully consistent with the results of the functional variomics screen described above, which independently identified missense substitutions for Tyr_{151}, Val_{154}, Val_{155}, Ser_{201}, and Ser_{173} as incompatible with SMI binding.

SAR Analysis

SAR data assigned the relative importance of individual functional groups for the benz- and picolinamide analogs to their activities as Sec14p inhibitors. In that regard, an obligatory requirement for the *para*-Br on the phenyl ring (H1) and the H1 ring itself were notable, as demonstrated by compounds **2–6** showing inhibition of Sec14p PtdIns-transfer activity, while compounds **7–11** were ineffective inhibitors (Table S1). The crystal and *in silico* docking data rationalized these obligate requirements (Figures 4D, 4E, S3, and S4). The hydrophobic planar ring system (H1) was critical for inhibitor activity as it: (1) acted as a scaffold to properly position the hydrophobic *para*-Br group for a functionally essential interaction with $V_{154}V_{155}$ and the backbone carboxyl of Tyr_{151}, and (2) provided a planar ring system for stacking interactions within the hydrophobic sub-pocket composed of residues Y_{151}, V_{154}, V_{155}, and R_{208}. Those latter stacking interactions lent significant stability to scaffold binding. The fluorine on Group R3 at the *meta* position of planar ring H1 contributed additional hydrophobicity (compounds **2**, **3**, **5**, and **6**). Polar substitutions (compounds **29**, **34**, and **38**) and incorporation of larger moieties (e.g., CH3, Cl, and Br; see compounds **7**, **11**, and **36**) at that position were not well tolerated. Similarly, a halogen substitution on the R1 group (compounds **9**, **10**, and **11**) also failed to enhance the inhibitory activities of these compounds.

Nitrogen substitution in the hydrophobic planar ring H1 resulted in decreased activity, while inhibitory activity was enhanced when H1 was a hydrophobic phenyl ring system. The carboxyl oxygen (A) of the carboxamide group was required for the activity of the compounds as it favorably contributed to the polar amphipathic microenvironment of the PtdCho binding site. Similarly, the carboxamide amide nitrogen contributed to polarity of the molecule and engaged residue Thr_{175} in polar and/or H-bond interactions.

The methylene group linker (L), which connects the carboxamide group and planar ring H1 with the proximal hydrophobic planar ring system (H2), also contributed to the activity of the picolinamide analogs. The SAR indicated the methylene group was well tolerated and oriented the benzodioxole planar ring H2 in a conformation favorable for docking to the amphipathic region of the binding cavity. However, extending the linker region (L), or substitution of methyl or phenyl group on the linker, was incompatible with inhibition of Sec14p activity. Several modifications of the hydrophobic planar ring system H2 were investigated and affect the potencies of active picolinamides. Alterations in size of that ring system, or modification of the ring system with polar substitutions, was also predicted to compromise SMI incorporation into the Sec14p hydrophobic cleft with the result that inhibitory activity was ablated.

Structure-Based Optimization of the Benzamide/Picolinamide Series

Based on the Sec14p::compound **2** co-crystal structure, a medicinal chemistry transformation approach was applied to design novel chemical structures by structure-based transformation and optimization of existing ligands. van der Waals interaction maps of the Sec14p lipid-binding pocket were generated to identify steric incompatibility boundaries. For this purpose, we also generated an extended set of strains with mutations in the binding pocket (Figure S6). These analyses suggest the availability of space between the respective C-terminal section of β strand B_3 and the A_9 helix, which might be productively exploited in alternative derivatizations of the benzodioxole planar ring H2 in further compound optimizations. Electrostatic maps and contact preference statistics were also created/applied to identify preferred energetically favorable locations for: (1) hydrophobic entities, and (2) hydrogen-bond donors and acceptors for potential ligand substitutions (Figures 4E, S4, and S5). This model was used to screen fragment substitutions with filters based on drug-like properties and favorable pharmacophoric features for optimal binding (see the STAR Methods). Out of a total of ~41,000 fragments screened, 582 fragments were retrieved, and the top 15 were ranked and prioritized based on their estimated binding affinities (Figure S5). The novel designed compounds are devoid of chemically reactive groups, fulfill Lipinski's rule of five for bioavailable drug-likeness (Lipinski et al., 2001), and are predicted to exhibit higher Sec14p binding affinities relative to compound **2**. This strategy represents a prototypic approach comprising all structural and genetic data collected in this study for the design of second-generation, improved Sec14p SMIs as candidates for synthesis.

Importance of the VV Motif in SMI Sensitivity

Residues Val_{154} and Val_{155} constitute what is termed the VV motif, and it was previously recognized that: (1) this motif is a reliable predictor of sensitivity of fungal Sec14ps to NPPMs, and (2) that this motif is not conserved between the Sec14ps of *S. cerevisiae* and other pathogenic fungi (Khan et al., 2016) (Figure 5A). This observation took on added significance given that the Sec14ps of *S. cerevisiae* and *Candida glabrata* both naturally harbor a VV motif, and that the [^{3}H]PtdIns-transfer activities of both proteins were sensitive to inhibition by compounds **2** and **3** *in vitro* (IC_{50} values of 6.7 and 10.9 μM for compound **2**, and 0.7 versus 1.0 μM for compound **3**, respectively; Figure 3D). In contrast, the *Candida albicans* Sec14p, which is divergent at these positions was completely resistant to inhibition by both compounds **2** and **3** *in vitro*, even at concentrations that approached saturation in aqueous solution (IC_{50} > 100 μM for each compound). The co-crystal data obtained in this study confirmed the VV motif to be involved in interactions with bioactive picolinamides and benzamides. Thus, we tested whether reconstitution of the VV motif

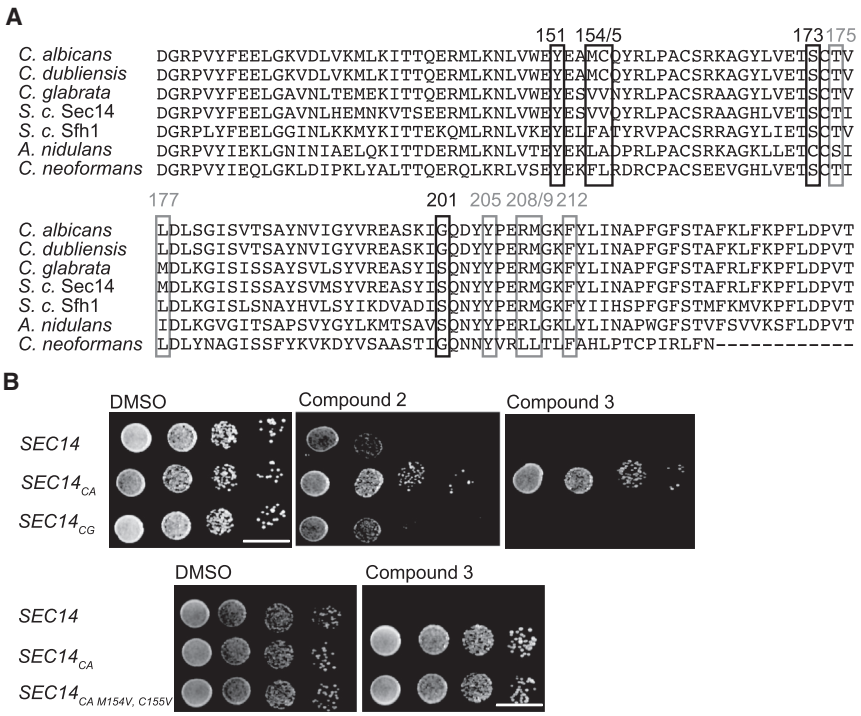

Figure 5. Sec14p Sequence Comparison and Investigations into the VV Motif

(A) Protein sequence alignment of *Saccharomyces cerevisiae* Sec14p and Sfh1p and Sec14p of the pathogenic fungi *C. albicans*, *Candida dubliniensis*, *C. glabrata*, *Aspergillus nidulans*, and *Cryptococcus neoformans*. Resistance-conferring amino acids identified by the functional variomics screen are marked with black boxes, sites predicted by co-crystal structure to be involved in compound interactions with gray boxes.

(B) A wild-type strain and isogenic derivatives expressing physiological levels of *C. albicans* and *C. glabrata* Sec14 PITPs were spotted on rich medium (YPD) agar medium supplemented with the indicated compounds and incubated at 30°C for 48 hr. Transplacement of the VV motif into $Sec14p_{CA}$ (the $M_{154}V$, $C_{155}V$ double mutant) did not render this PITP sensitive to compound **3** (lower panel). The scale bar represents 1 cm.

sensitized otherwise resistant Sec14ps to these SMI chemotypes. To that end, Sec14p-deficient *S. cerevisiae* were reconstituted with the Sec14p of *C. albicans* and *C. glabrata* by the previously described strategy (Khan et al., 2016), and those strains were spotted on rich medium (YPD) containing 20 μM inhibitor. Only the strain expressing *C. glabrata* Sec14p (naturally harboring the VV motif) was sensitive to SMI challenge, whereas the strain reconstituted with *C. albicans* Sec14p was resistant to SMI challenge (Figure 5B). To further investigate whether reconstitution of the VV motif in a Sec14p that naturally lacks it sensitized the protein to SMI treatment, the VV motif was transplaced into the *C. albicans* Sec14p. However, unlike the case with NPPMs (Khan et al., 2016), transplacement of the VV motif into $Sec14_{CA}$ ($M_{154}V$, $C_{155}V$ double mutant) was insufficient to render the strain sensitive to challenge with compound **3** (Figure 5B). Why this is so remains an important and outstanding conundrum.

Antifungal Activity

The initial aim of this study was to identify novel antifungal compounds. Identification of Sec14p as cellular target of the tested compounds by the methodologies described above motivated prioritization of the two optimized compounds, **2** and **3**, for further antifungal testing. As Sec14ps play an important role in pathogenicity and virulence of pathogenic fungi (Chayakulkeeree et al., 2011), it was of interest to determine whether compounds **2** and **3** exerted activity beyond the *S. cerevisiae* PITP. Thus, the inhibitory effects of compounds **2** and **3** were tested *in vitro* following the Clinical Laboratory Standards Institute guidelines against four diverse and clinically relevant pathogens (Wayne, 2008a, 2008b). These included two dimorphic fungi of the *Candida* genus (*C. albicans* and *C. glabrata*), one filamentous fungus (*Aspergillus brasiliensis*) and, as representative of the *Basidiomycota*, the yeast *Cryptococcus neoformans*. Posaconazole, a triazole compound, was used as positive control. For compound **2**, a minimal inhibitory concentration (MIC) of 100 μM was measured for *C. albicans* and *C. glabrata*, and an MIC of 50 μM for *A. brasiliensis*. Compound **3** inhibited growth of *C. glabrata* with an MIC of 50 μM, but residual growth was observed at higher concentrations (likely due to compound precipitation at higher dose, see Table S2). No growth inhibition was observed for *C. neoformans* (Table 2).

DISCUSSION

This report describes the identification of a series of picolinamide- and benzamide-containing compounds as a novel class of SMIs of the *S. cerevisiae* PtdIns/PtdCho-transfer protein Sec14p. Although there are two previous reports of Sec14 inhibitors (Filipuzzi et al., 2016; Nile et al., 2014), this study presents the first Sec14p::SMI co-crystal structure. This structure, rationalized by both the functional variomics and SAR results of more than 40 generated analogs, supports strong structural fungal selectivity over the mammalian homolog and represents a quantum leap for rational design of the next generation of improved Sec14p inhibitors. The picolinamides and benzamides share some similarity with related inhibitors reported previously by Nile et al. (2014). However, they also differ considerable from these by the substituent patterns and the heteroatom in the aromatic acid part and by different amine substituents than reported before, thus opening up the chemical landscape for the design of novel Sec14p SMIs.

Sec14p is the major PITP of the budding yeast *S. cerevisiae* and potentiates the efficient production of phosphoinositides, in particular PtdIns(4)P, whose signaling is specifically channeled to protein trafficking in the yeast TGN-endosomal system (Bankaitis et al., 1990) and for biogenesis of secretory vesicles from the TGN (Phillips et al., 2006). The sequence homology of

Table 2. Growth-Inhibitory Concentrations against Pathogenic Fungi

	Minimal Inhibitory Concentration (μM)					
	S. cerevisiae BY4743	*S. cerevisiae* BY4743Δ8	*Candida albicans* ATCC 10231	*Candida glabrata* ATCC 2001	*Cryptococcus neoformans* DSM 70219	*Aspergillus brasiliensis* ATCC 16404
Posaconazole	<0.3	<0.3	<0.3	3.125	<0.3	<0.3
Compound **2**	200	100	100	100	>200	50
Compound **3**	>200	50	>200	50	>200	>200

Minimal inhibitory concentrations on solid medium have been determined following the Clinical Laboratory Standards Institute reference in triplicates.

Sec14p from *S. cerevisiae* with that of pathogenic fungi ranges from 45% to 86%, but amino acids that line the lipid-binding cavity surface are highly conserved. Although the role of Sec14p in other fungal species is less well characterized, it is reported to be involved in yeast dimorphism, sporulation, and in sustaining mycelial growth, all prerequisites for the infectivity and pathogenicity of fungal pathogens (Chayakulkeeree et al., 2011; Lopez et al., 1994; Monteoliva et al., 1996; Phillips et al., 2006; Rudge et al., 2004). Compared with the *in vitro* potency measured on some fungal proteins, the recorded potencies on the tested pathogenic fungi were relatively low. But the used cell-based assay only recapitulated mitotic growth, but not any of the other functional aspects of Sec14p inhibition stated above. While the presented compounds need further evaluation to qualify as clinical candidates, the analytical platform and structural data identify a path for application of rational medicinal chemistry approaches.

The fact that, at least in *S. cerevisiae*, SMI sensitivity is overcome by loss of function in any one of one of seven different genes (bypass Sec14p mutations [Bankaitis et al., 1990; Cleves et al., 1989; Fang et al., 1996]), or by single-amino acid substitutions in Sec14p itself, would seem to reduce enthusiasm for Sec14p as an attractive antifungal target. However, bypass Sec14p mutations derange lipid metabolism and are accompanied by pleiotropic effects that generally reduce the fitness of the organism, particularly under stress conditions (Cleves et al., 1989; Mousley et al., 2012). Sec14p amino acid substitutions that result in SMI resistance influence key residues required for optimal protein function and therefore are also likely to be deleterious under conditions of high Sec14p demand as in pathogenic settings.

Specificity of target is always a primary issue in drug design. The presented benz- and picolinamides, while toxic to fungi, were not cytotoxic to mammalian cells and failed to inhibit the structurally unrelated mammalian PtdIns-transfer proteins *in vitro*. The benz- and picolinamides reported here target the PtdCho head group coordination substructure of the Sec14p lipid-binding pocket. As none of the mammalian SEC14L proteins exhibit this substructure, it is highly unlikely that these activities will be targeted. Thus, the benz- and picolinamide compounds described herein represent privileged scaffolds that exhibit exquisite specificity among fungal Sec14-like PtdIns/PtdCho-transfer proteins.

In summary, the structural and functional data gained by the experimental approach in this study, together with the experimental tools and data from previous studies (Filipuzzi et al., 2016; Khan et al., 2016; Nile et al., 2014), now provide the scientific community a robust roadmap to the design, synthesis, and validation of the next generation of Sec14p inhibitors aimed at treating severe fungal infections.

SIGNIFICANCE

Due to increasing numbers of elderly or immunocompromised patients, severe antifungal infections are on the rise, and the mortality numbers are unacceptably high. Existing treatments suffer from emerging drug resistance against established pathogens and lack of efficacy as the spectrum of pathogenic fungi identified in patients today is much broader than a few decades ago. Despite this, the current pharmaceutical drug discovery pipeline lists less than a handful of compounds in clinical phases that modulate novel targets. This report describes benz- and picolinamide compounds with versatile and robust chemistry, which exert antifungal activity against the model organism *Saccharomyces cerevisiae*, but also against pathogenic *Candida* and *Aspergillus* species. Using a combination of genetic methodologies, the fungal lipid-transfer protein Sec14 was identified as the target of these compounds. Importantly, the tested benz- and picolinamides, while toxic to fungi, were not cytotoxic to mammalian cells and failed to inhibit the structurally diverged mammalian lipid-transfer proteins *in vitro,* further emphasizing their antifungal potential. A potent compound of the series was successfully co-crystallized with Sec14p, yielding the first high-resolution structural dataset for a phosphatidylinositol-transfer protein in complex with an inhibitor. The compound-protein data obtained by the structural approach was in full agreement with a series of genetic point mutants and the structure-activity data derived from 48 compound derivatives. Combined, this dataset paves the way and provides the protocols for rational optimization of benz- and picolinamides as antifungal Sec14 inhibitors.

STAR★METHODS

Detailed methods are provided in the online version of this paper and include the following:

- KEY RESOURCES TABLE
- CONTACT FOR REAGENT AND RESOURCE SHARING
- EXPERIMENTAL MODEL AND SUBJECT DETAILS
  - Microbial Strain Description, Culture Conditions and Plasmids Construction
- METHOD DETAILS

- Compound Synthesis
- Compound Analysis by NMR
- Compound Analysis by LC-MS
- Chemogenomic Profiling (HIP-HOP)
- Growth Curves
- Expression and Purification of Recombinant Proteins
- Lipid Transfer Assays
- Functional Variomics
- Mutant Validation
- Protein Expression, Purification, and Crystallization
- Crystallography
- *In Silico* Docking
- Structure-based Design and MedChem Transformation
- Antifungal Testing

- QUANTIFICATION AND STATISTICAL ANALYSIS
- DATA AND SOFTWARE AVAILABILITY

SUPPLEMENTAL INFORMATION

Supplemental Information includes six figures, four tables, and one data file and can be found with this article online at https://doi.org/10.1016/j.chembiol.2017.12.007.

ACKNOWLEDGMENTS

We would like to thank Jürg Eichenberger and Nicole Hartmann for processing, and Sven Schuierer for analyzing, the HIP-HOP microarray data. Furthermore, we thank David Estoppey for performing the cell viability assay on HCT116 cells, Dr. Matthias Baumann for conducting compound solubility and permeability assays, and Eva M. Winklbauer for cloning support. We also thank the staff at the Swiss Light Source synchrotron for assistance during data collection, and the Laboratory for Molecular Simulation and High Performance Research Computing at Texas A&M University for providing software, support, and computer time. D.K., A.T., and V.B. were supported by grants GM44530 and BE-0017 to V.B. from the NIH and Robert A. Welch Foundation, respectively. P.J., A.L.K., M.F., and G.S. were supported by the Deutsche Forschungsgemeinschaft (Emmy Noether grant SCHA 1274/2-1, SFB 1101/TP A05 and research grant SCHA 1274/4-1 to G.S.), and P.J. also by the Studienstiftung des Deutschen Volkes. F.B. and Z.H. received support from the Max-Planck-Gesellschaft, the European Research Council under the European Union's Seventh Framework Program (FP7/2007–2013), ERC grant agreement no. 310957, and the Deutsche Forschungsgemeinschaft (BO3588/2-1 to F.B.). The authors with the affiliation Novartis Institutes for BioMedical research are employees of Novartis Pharma AG and may own stock in the company.

AUTHOR CONTRIBUTIONS

V.P., D.K., P.J., I.F., T.A., R.R., and S.Z. designed and performed the genetic experiments. C.N. and S.T. designed, synthesized, and analyzed the compounds. P.J., A.L.K., and M.F. conducted the crystallization experiments. Z.H. and F.B. determined and analyzed the structure. A.T. and F.P. generated docking poses. A.T. developed the SAR, conducted the MD simulations, structure-based design, and MedChem transformation of new analogs. D.K. purified Sec14p and the various mutant derivative proteins designed and performed the *in vitro* lipid-transfer experiments. V.P., F.B., G.S., V.B., H.W., and D.H. conceived the study, analyzed data, prepared figures and wrote the manuscript.

Received: September 5, 2017
Revised: October 18, 2017
Accepted: December 6, 2017
Published: January 4, 2018

REFERENCES

Adams, P.D., Afonine, P.V., Bunkoczi, G., Chen, V.B., Davis, I.W., Echols, N., Headd, J.J., Hung, L.W., Kapral, G.J., Grosse-Kunstleve, R.W., et al. (2010). PHENIX: a comprehensive Python-based system for macromolecular structure solution. Acta Crystallogr. D Biol. Crystallogr. *66*, 213–221.

Bankaitis, V.A., Aitken, J.R., Cleves, A.E., and Dowhan, W. (1990). An essential role for a phospholipid transfer protein in yeast Golgi function. Nature *347*, 561–562.

Bankaitis, V.A., Malehorn, D.E., Emr, S.D., and Greene, R. (1989). The *Saccharomyces cerevisiae* SEC14 gene encodes a cytosolic factor that is required for transport of secretory proteins from the yeast Golgi complex. J. Cell Biol. *108*, 1271–1281.

Bankaitis, V.A., Mousley, C.J., and Schaaf, G. (2010). The Sec14 superfamily and mechanisms for crosstalk between lipid metabolism and lipid signaling. Trends Biochem. Sci. *35*, 150–160.

Benli, M., Döring, F., Robinson, D.G., Yang, X., and Gallwitz, D. (1996). Two GTPase isoforms, Ypt31p and Ypt32p, are essential for Golgi function in yeast. EMBO J. *15*, 6460–6475.

Brown, G.D., Denning, D.W., Gow, N.A.R., Levitz, S.M., Netea, M.G., and White, T.C. (2012). Hidden killers: human fungal infections. Sci. Transl. Med. *4*, 165rv113.

Chayakulkeeree, M., Johnston, S.A., Oei, J.B., Lev, S., Williamson, P.R., Wilson, C.F., Zuo, X., Leal, A.L., Vainstein, M.H., Meyer, W., et al. (2011). SEC14 is a specific requirement for secretion of phospholipase B1 and pathogenicity of *Cryptococcus neoformans*. Mol. Microbiol. *80*, 1088–1101.

Cleves, A.E., McGee, T.P., Whitters, E.A., Champlon, K.M., Altken, J.R., Dowhan, W., Goebl, M., and Bankaitis, V.A. (1991). Mutations in the CDP-choline pathway for phospholipid biosynthesis bypass the requirement for an essential phospholipid transfer protein. Cell *64*, 789–800.

Cleves, A.E., Novick, P.J., and Bankaitis, V.A. (1989). Mutations in the SAC1 gene suppress defects in yeast Golgi and yeast actin function. J. Cell Biol. *109*, 2939–2950.

El-Faham, A., and Albericio, F. (2010). COMU: a third generation of uronium-type coupling reagents. J. Pept. Sci. *16*, 6–9.

El-Faham, A., Subiros Funosas, R., Prohens, R., and Albericio, F. (2009). COMU: a safer and more effective replacement for benzotriazole-based uronium coupling reagents. Chemistry *15*, 9404–9416.

Emsley, P., and Cowtan, K. (2004). Coot: model-building tools for molecular graphics. Acta Crystallogr. D Biol. Crystallogr. *60*, 2126–2132.

Fairn, G.D., Curwin, A.J., Stefan, C.J., and McMaster, C.R. (2007). The oxysterol binding protein Kes1p regulates Golgi apparatus phosphatidylinositol-4-phosphate function. Proc. Natl. Acad. Sci. USA *104*, 15352–15357.

Fang, M., Kearns, B.G., Gedvilaite, A., Kagiwada, S., Kearns, M., Fung, M.K., and Bankaitis, V.A. (1996). Kes1p shares homology with human oxysterol binding protein and participates in a novel regulatory pathway for yeast Golgi-derived transport vesicle biogenesis. EMBO J. *15*, 6447–6459.

Filipuzzi, I., Cotesta, S., Perruccio, F., Knapp, B., Fu, Y., Studer, C., Pries, V., Riedl, R., Helliwell, S.B., Petrovic, K.T., et al. (2016). High-resolution genetics identifies the lipid transfer protein Sec14p as target for antifungal ergolines. PLoS Genet. *12*, e1006374.

Giaever, G., Shoemaker, D.D., Jones, T.W., Liang, H., Winzeler, E.A., Astromoff, A., and Davis, R.W. (1999). Genomic profiling of drug sensitivities via induced haploinsufficiency. Nat. Genet. *21*, 278–283.

Hoepfner, D., Helliwell, S.B., Sadlish, H., Schuierer, S., Filipuzzi, I., Brachat, S., Bhullar, B., Plikat, U., Abraham, Y., Altorfer, M., et al. (2014). High-resolution chemical dissection of a model eukaryote reveals targets, pathways and gene functions. Microbiol. Res. *169*, 107–120.

Hoepfner, D., Karkare, S., Helliwell, S.B., Pfeifer, M., Trunzer, M., De Bonnechose, S., Zimmerlin, A., Tao, J., Richie, D., Hofmann, A., et al. (2012). An integrated approach for identification and target validation of antifungal compounds active against Erg11p. Antimicrob. Agents Chemother. *56*, 4233–4240.

Hoon, S., Smith, A.M., Wallace, I.M., Suresh, S., Miranda, M., Fung, E., Proctor, M., Shokat, K.M., Zhang, C., Davis, R.W., et al. (2008). An integrated platform of genomic assays reveals small-molecule bioactivities. Nat. Chem. Biol. *4*, 498–506.

Huang, C.-F., Buu, L.-M., Yu, W.-L., and Lee, F.-J.S. (1999). Characterization of a novel ADP-ribosylation factor-like protein (yARL3) in *Saccharomyces cerevisiae*. J. Biol. Chem. *274*, 3819–3827.

Huang, Z., Chen, K., Zhang, J., Li, Y., Wang, H., Cui, D., Tang, J., Liu, Y., Shi, X., Li, W., et al. (2013). A functional variomics tool for discovering drug-resistance genes and drug targets. Cell Rep. *3*, 577–585.

Kabsch, W. (1993). Automatic processing of rotation diffraction data from crystals of initially unknown symmetry and cell constants. J. Appl. Crystallogr. *26*, 795–800.

Khan, D., McGrath, K.R., Dorosheva, O., Bankaitis, V.A., and Tripathi, A. (2016). Structural elements that govern Sec14-like PITP sensitivities to potent small molecule inhibitors. J. Lipid Res. *57*, 650–662.

Lebedev, A.A., Young, P., Isupov, M.N., Moroz, O.V., Vagin, A.A., and Murshudov, G.N. (2012). JLigand: a graphical tool for the CCP4 template-restraint library. Acta Crystallogr. D Biol. Crystallogr. *68*, 431–440.

Lee, A.Y., St Onge, R.P., Proctor, M.J., Wallace, I.M., Nile, A.H., Spagnuolo, P.A., Jitkova, Y., Gronda, M., Wu, Y., Kim, M.K., et al. (2014). Mapping the cellular response to small molecules using chemogenomic fitness signatures. Science *344*, 208–211.

Lee, F.-J.S., Huang, C.-F., Yu, W.-L., Buu, L.-M., Lin, C.-Y., Huang, M.-C., Moss, J., and Vaughan, M. (1997). Characterization of an ADP-ribosylation factor-like 1 protein in *Saccharomyces cerevisiae*. J. Biol. Chem. *272*, 30998–31005.

Li, X., Rivas, M.P., Fang, M., Marchena, J., Mehrotra, B., Chaudhary, A., Feng, L., Prestwich, G.D., and Bankaitis, V.A. (2002). Analysis of oxysterol binding protein homologue Kes1p function in regulation of Sec14p-dependent protein transport from the yeast Golgi complex. J. Cell Biol. *157*, 63–78.

Li, X., Routt, S.M., Xie, Z., Cui, X., Fang, M., Kearns, M.A., Bard, M., Kirsch, D.R., and Bankaitis, V.A. (2000). Identification of a novel family of nonclassic yeast phosphatidylinositol transfer proteins whose function modulates phospholipase D activity and Sec14p-independent cell growth. Mol. Biol. Cell *11*, 1989–2005.

Lipinski, C.A., Lombardo, F., Dominy, B.W., and Feeney, P.J. (2001). Experimental and computational approaches to estimate solubility and permeability in drug discovery and development settings. Adv. Drug Deliv. Rev. *46*, 3–26.

Lopez, M.C., Nicaud, J.M., Skinner, H.B., Vergnolle, C., Kader, J.C., Bankaitis, V.A., and Gaillardin, C. (1994). A phosphatidylinositol/phosphatidylcholine transfer protein is required for differentiation of the dimorphic yeast *Yarrowia lipolytica* from the yeast to the mycelial form. J. Cell Biol. *125*, 113–127.

Lum, P.Y., Armour, C.D., Stepaniants, S.B., Cavet, G., Wolf, M.K., Butler, J.S., Hinshaw, J.C., Garnier, P., Prestwich, G.D., Leonardson, A., et al. (2004). Discovering modes of action for therapeutic compounds using a genome-wide screen of yeast heterozygotes. Cell *116*, 121–137.

Mccoy, A.J., Grosse-Kunstleve, R.W., Adams, P.D., Winn, M.D., Storoni, L.C., and Read, R.J. (2007). Phaser crystallographic software. J. Appl. Crystallogr. *40*, 658–674.

Monteoliva, L., Sánchez, M., Pla, J., Gil, C., and Nombela, C. (1996). Cloning of *Candida albicans* SEC14 gene homologue coding for a putative essential function. Yeast *12*, 1097–1105.

Mousley, C.J., Tyeryar, K., Ile, K.E., Schaaf, G., Brost, R.L., Boone, C., Guan, X., Wenk, M.R., and Bankaitis, V.A. (2008). *trans*-Golgi network and endosome dynamics connect ceramide homeostasis with regulation of the unfolded protein response and TOR signaling in yeast. Mol. Biol. Cell *19*, 4785–4803.

Mousley, C.J., Yuan, P., Gaur, N.A., Trettin, K.D., Nile, A.H., Deminoff, S.J., Dewar, B.J., Wolpert, M., Macdonald, J.M., Herman, P.K., et al. (2012). A sterol-binding protein integrates endosomal lipid metabolism with TOR signaling and nitrogen sensing. Cell *148*, 702–715.

Nikawa, J., Tsukagoshi, Y., and Yamashita, S. (1991). Isolation and characterization of two distinct myo-inositol transporter genes of *Saccharomyces cerevisiae*. J. Biol. Chem. *266*, 11184–11191.

Nile, A.H., Tripathi, A., Yuan, P., Mousley, C.J., Suresh, S., Wallace, I.M., Shah, S.D., Pohlhaus, D.T., Temple, B., Nislow, C., et al. (2014). PITPs as targets for selectively interfering with phosphoinositide signaling in cells. Nat. Chem. Biol. *10*, 76–84.

Parsons, A.B., Lopez, A., Givoni, I.E., Williams, D.E., Gray, C.A., Porter, J., Chua, G., Sopko, R., Brost, R.L., Ho, C.H., et al. (2006). Exploring the mode-of-action of bioactive compounds by chemical-genetic profiling in yeast. Cell *126*, 611–625.

Pfaller, M.A., Pappas, P.G., and Wingard, J.R. (2006). Invasive fungal pathogens: current epidemiological trends. Clin. Infect. Dis. *43*, S3–S14.

Phillips, S.E., Vincent, P., Rizzieri, K.E., Schaaf, G., Bankaitis, V.A., and Gaucher, E.A. (2006). The diverse biological functions of phosphatidylinositol transfer proteins in eukaryotes. Crit. Rev. Biochem. Mol. Biol. *41*, 21–49.

Pierce, S.E., Davis, R.W., Nislow, C., and Giaever, G. (2007). Genome-wide analysis of barcoded *Saccharomyces cerevisiae* gene-deletion mutants in pooled cultures. Nat. Protoc. *2*, 2958–2974.

Pierce, S.E., Fung, E.L., Jaramillo, D.F., Chu, A.M., Davis, R.W., Nislow, C., and Giaever, G. (2006). A unique and universal molecular barcode array. Nat. Methods *3*, 601–603.

Prasad, R., Shah, A.H., and Rawal, M.K. (2016). Antifungals: mechanism of action and drug resistance. In Yeast Membrane Transport, J. Ramos, H. Sychrová, and M. Kschischo, eds. (Springer International Publishing), pp. 327–349.

Pries, V., Cotesta, S., Riedl, R., Aust, T., Schuierer, S., Tao, J., Filipuzzi, I., and Hoepfner, D. (2016). Advantages and challenges of phenotypic screens: the identification of two novel antifungal geranylgeranyltransferase I inhibitors. J. Biomol. Screen. *21*, 306–315.

Richie, D.L., Thompson, K.V., Studer, C., Prindle, V.C., Aust, T., Riedl, R., Estoppey, D., Tao, J., Sexton, J.A., Zabawa, T., et al. (2013). Identification and evaluation of novel acetolactate synthase inhibitors as antifungal agents. Antimicrob. Agents Chemother. *57*, 2272–2280.

Roemer, T., and Krysan, D.J. (2014). Antifungal drug development: challenges, unmet clinical needs, and new approaches. Cold Spring Harb. Perspect. Med. https://doi.org/10.1101/cshperspect.a019703.

Roemer, T., Xu, D., Singh, S.B., Parish, C.A., Harris, G., Wang, H., Davies, J.E., and Bills, G.F. (2011). Confronting the challenges of natural product-based antifungal discovery. Chem. Biol. *18*, 148–164.

Rudge, S.A., Sciorra, V.A., Iwamoto, M., Zhou, C., Strahl, T., Morris, A.J., Thorner, J., and Engebrecht, J. (2004). Roles of phosphoinositides and of Spo14p (phospholipase D)-generated phosphatidic acid during yeast sporulation. Mol. Biol. Cell *15*, 207–218.

Ryan, M.M., Temple, B.R.S., Phillips, S.E., and Bankaitis, V.A. (2007). Conformational dynamics of the major yeast phosphatidylinositol transfer protein Sec14p: insight into the mechanisms of phospholipid exchange and diseases of Secl4p-like protein deficiencies. Mol. Biol. Cell *18*, 1928–1942.

Salentin, S., Schreiber, S., Haupt, V.J., Adasme, M.F., and Schroeder, M. (2015). PLIP: fully automated protein-ligand interaction profiler. Nucleic Acids Res. *43*, W443–W447.

Schaaf, G., Betts, L., Garrett, T.A., Raetz, C.R.H., and Bankaitis, V.A. (2006). Crystallization and preliminary X-ray diffraction analysis of phospholipid-bound Sfh1p, a member of the *Saccharomyces cerevisiae* Sec14p-like phosphatidylinositol transfer protein family. Acta Crystallogr. Sect. F Struct. Biol. Cryst. Commun. *62*, 1156–1160.

Schaaf, G., Dynowski, M., Mousley, C.J., Shah, S.D., Yuan, P., Winklbauer, E.M., de Campos, M.K.F., Trettin, K., Quinones, M.-C., Smirnova, T.I., et al. (2011). Resurrection of a functional phosphatidylinositol transfer protein from a pseudo-Sec14 scaffold by directed evolution. Mol. Biol. Cell *22*, 892–905.

Schaaf, G., Ortlund, E.A., Tyeryar, K.R., Mousley, C.J., Ile, K.E., Garrett, T.A., Ren, J., Woolls, M.J., Raetz, C.R.H., Redinbo, M.R., et al. (2008). Functional anatomy of phospholipid binding and regulation of phosphoinositide homeostasis by proteins of the Sec14 superfamily. Mol. Cell *29*, 191–206.

Schmiedel, Y., and Zimmerli, S. (2016). Common invasive fungal diseases: an overview of invasive candidiasis, aspergillosis, cryptococcosis, and *Pneumocystis pneumonia*. Swiss Med. Wkly. *146*, w14281.

Sha, B., Phillips, S.E., Bankaitis, V.A., and Luo, M. (1998). Crystal structure of the *Saccharomyces cerevisiae* phosphatidylinositol-transfer protein. Nature *391*, 506–510.

Wayne, P. (2008a). Reference Method for Broth Dilution Antifungal Susceptibility Testing of Filamentous Fungi; Approved Standard - Second Edition. CLSI Document MA38-A2 (Clinical and Laboratory Standards Institute).

Wayne, P. (2008b). Reference Method for Broth Dilution Antifungal Susceptibility Testing of Yeast; Approved Standard - Third Edition. CLSI Document M27-A3 (Clinical and Laboratory Standards Institute).

STAR★METHODS

KEY RESOURCES TABLE

REAGENT or RESOURCE	SOURCE	IDENTIFIER
Bacterial Strains		
E.c. BL21	New England BioLabs	Cat# C2527I
E.c. BL21-CodonPlus (DE3)-RIL	Agilent Technologies	#230245
Fungal Strains		
S.c. BY4743	OpenBiosystems	Cat# YSC1050
S.c. BY4743Δ8	Dominic Hoepfner's lab	*BY4743Δ8*
S.c heterozygous, genome-wide deletion collection	OpenBiosystems	Cat# YSC1055
S.c homozygous, genome-wide deletion collection	OpenBiosystems	Cat# YSC1056
S.c. CTY1-1A	Bankaitis' lab	CTY1-1A
S.c. CTY159	Bankaitis' lab	CTY159
S.c. CTY303	Bankaitis' lab	CTY303
C.albicans	American Type Culture Collection (ATCC)	Cat# 10231
C.glabrata	American Type Culture Collection (ATCC)	Cat# 2001
A.brasiliensis	American Type Culture Collection (ATCC)	Cat# 16404
C.neoformans	Royal Botanic Gardens, Kew	Cat# DSM70219
Mammalian Cell Lines		
Human colorectoral carcinoma cell line HCT116	American Type Culture Collection (ATCC)	Cat# CCL-247
Recombinant DNA		
Plasmid: $SEC14_{CG}$	Bankaitis' lab	pDK247
Plasmid: $SEC14_{CA}$	Bankaitis' lab	pDK9
Plasmid: $SEC14_{CA}^{M154V,\ C154V}$	Bankaitis' lab	pDK265
Plasmid: pDR195-*SEC14*	Bankaitis' lab	pDR195
Plasmid: YCplac33-*SFH1*	Schaaf's lab	N/A
Plasmid: YCplac33-*SFH1**	Schaaf's lab	N/A
Plasmid: YCplac33-*SEC14*	Schaaf's lab	N/A
Plasmid: BYInt	Hoepfner's lab	pBYInt_LEU
Chemicals and Recombinant Proteins		
Compounds 1-48	Waldman's lab	Compound number as listed in Table S1
His_8-Sec14	Schaaf's lab	N/A
His_8-$Sec14_{Y151H}$	Bankaitis' lab	N/A
His_8-$Sec14_{V154G}$	Bankaitis' lab	N/A
His_8-$Sec14_{V155A}$	Bankaitis' lab	N/A
His_8-$Sec14_{S173L}$	Bankaitis' lab	N/A
His_8-$Sec14_{S201G}$	Bankaitis' lab	N/A
Software and Algorithms		
Tibco Spotfire	TIBCO Software Inc.	http://www.spotfire.tibco.com
GOLD Suite	The Cambridge Crystallographic Data Centre (CCDC)	https://www.ccdc.cam.ac.uk
Pymol	Schrödigner	https://pymol.org
XDS	Kabsch et al., Max-Plack Institute, Heidelberg	http://xds.mpimf-heidelberg.mpg.de
Phaser	McCoy et al., University of Cambridge	http://www.ccp4.ac.uk/html/phaser.html

(*Continued on next page*)

Continued

REAGENT or RESOURCE	SOURCE	IDENTIFIER
Coot	Emsley et al., University of Cambridge	https://www2.mrc-lmb.cam.ac.uk/personal/pemsley/coot/
MOE	Chemical Computing Group	https://www.chemcomp.com/
Critical Commercial Assays		
CellTiter-Glo Luminescent Cell Viability Assay	Promega	Cat# G7573
Deposited Data		
S.c. Sec14::compound **2** co-crystal structure	Protein databank	PDB 6F0E (http://www.rcsb.org/pdb/explore/explore.do?structureId=6F0E)

CONTACT FOR REAGENT AND RESOURCE SHARING

Further information and requests for resources and reagents can be directed to and will be fulfilled by the Lead Contact, Dominic Hoepfner (dominic.hoepfner@novartis.com). For simplicity, if compounds are requested they can also directly be requested from the Waldmann lab (Herbert.Waldmann@mpi-dortmund.mpg.de) or genetic reagents listed in the Key Resources Table can be requested from the indicated labs (Bankaitis lab: vytas@medicine.tamhsc.edu, Schaaf lab: gabriel.schaaf@uni-bonn.de).

Signing of a material transfer agreement (MTA) will be required for reagents originating from Novartis. The MTA will restrict use of provided materials to research purposes in pre-clinical context and will exclude any administration to humans. Special conditions may apply if reagents are requested for experiments on human embryonic stem cells or for in vivo experiments.

EXPERIMENTAL MODEL AND SUBJECT DETAILS

Microbial Strain Description, Culture Conditions and Plasmids Construction

Strains BY4743 (*MATa/α his3Δ1/his3Δ1 leu2Δ0 /leu2Δ0 LYS2/lys2Δ0 met15Δ0/MET15 ura3Δ0/ura3Δ0*), BY4743Δ8 (as above but with *snq2Δ::KanMX4/snq2Δ::KanMX4, pdr3Δ::KanMX4/pdr3Δ::KanMX4, pdr5Δ::KanMX4/pdr5Δ::KanMX4, pdr1Δ::NatMX4/pdr1Δ::NatMX4, yap1Δ::NatMX4/yap1Δ::NatMX4, pdr2Δ /pdr2Δ, yrm1Δ /yrm1Δ, yor1Δ /yor1Δ),* CTY182 (*MATa ura3-52 lys2-801 his3Δ-200*) and its isogenic derivatives CTY1-1A (*MATa ura3-52 lys2-801 his3Δ-200 sec14-1^{ts}*), CTY159 (*MATa ura3-52 lys2-801 Δhis3-200 sec14-1^{ts} kes1 Δ*), and CTY303 (*MATa ura3-52 lys2-801 his3Δ-200 sec14Δ cki1Δ::HIS3*)(Cleves et al., 1991; Fang et al., 1996; Li et al., 2002). Gene replacement constructs were used to integrate $SEC14_{CG}$, $SEC14_{CA}$ and $SEC14_{CA}^{M154V,\ C154V}$ expression cassettes into the *LEU2* locus as described by Khan et. al.(Khan et al., 2016). Yeast strains were grown on YPD (yeast extract 1%, peptone 2%, dextrose 2%) plates or in liquid medium. If plasmid selection was necessary, the strains were grown on synthetic complete medium lacking uracil. Compound **1** was obtained from the Novartis compound store. All other reagents, chemicals, and buffer salts were purchased from Sigma-Aldrich Chemicals (St. Louis, MO), Fluka (Buchs, Switzerland), Alfa Aesar (Karlsruhe, Germany) and Acros Organics (Geel, Belgium). Centromeric YCplac33(*URA3*) plasmids carrying *SEC14*, *SFH1* and *sfh1* activation alleles under control of a *SEC14* promoter fragment (Schaaf et al., 2011) as well as episomal high-copy (*2μ)* plasmid pDR195-*SEC14* in which the *SEC14* ORF (without its intron) is expressed under control of a strong plasma membrane ATPase (*PMA1*) promoter fragment (Schaaf et al., 2008) were described previously. Individual mutations were introduced in YCplac33-*SEC14* by site-directed mutagenesis (QuickChangeTM, Stratagene).

METHOD DETAILS

Compound Synthesis

Unless otherwise noted, all commercially available compounds were used as provided without further purifications. Chemicals and solvents were purchased from the companies Sigma Aldrich, Alfa Aesar and Acros Organics. Dry solvents (e.g. dimethylformamide (DMF)) were used as commercially available. Solvents for preparative HPLC (acetonitrile HPLC grade) were used as commercially available. Analytical thin-layer chromatography (TLC) was performed on *Merck silica gel aluminum plates* with F-254 indicator. Compounds were visualized by irradiation with UV light or potassium permanganate staining. Solvent mixtures are understood as volume/volume. Extended information on compound synthesis and analytical methods can be found in Data S1.

Compound Analysis by NMR

^{1}H-NMR and ^{13}C-NMR were recorded on a Mercury VX400 (Varian) (400 MHz), Bruker DRX400 (400 MHz), Bruker DRX500 (500 MHz), INOVA500 (500 MHz) and INOVA600 (600 MHz) using $CDCl_3$, MeOD, CD_2Cl_2, DMSO as solvent. Data are reported in the following order: chemical shift (δ) values are reported in ppm with the solvent resonance as internal standard ($CDCl_3$: δ = 7.26 ppm for ^{1}H, δ = 77.16 ppm for ^{13}C, MeOD: δ = 3.34 ppm for ^{1}H, δ = 49.86 ppm for ^{13}C; CD_2Cl_2: δ = 5.32 ppm for ^{1}H, δ = 54.00 ppm for ^{13}C

DMSO: δ = 2.54 ppm for ^{1}H, δ = 40.45 ppm for ^{13}C); multiplicities are indicated br s (broad singlet), s (singlet), d (doublet), dd (double doublet), t (triplet), q (quartet) m (multiplet); coupling constants (*J*) are given in Hertz (Hz). Extended information on compound synthesis and analytical methods can be found in Data S1.

Compound Analysis by LC-MS

LC-MS measurements were performed on a LCQ Advantage ESI from Agilent 1100 series. As precolumn, a VP 50/21 Nucleodur C18 Gravity 5 μm was used and as main column a 125/4 Nucleodur C18 Gravity 3 μm. The flow rate was 1 mL per min. Eluent A: H_2O + 0.1% HCOOH; Eluent B: Acetonitril + 0.1% HCOOH. The parameters used for the different methods (named A, B, C, D) are listed below:

Method A

Used Gradient: 0-1 min: 90% A / 10% B; 1-10 min: 0% A / 100% B; 10-12 min: 0% A/ 100% B; 12-12.1 min: 90% A / 10% B; 12.1-15 min: 90% A / 10% B. Furthermore, LC-MS measurements were performed on a LCQ Fleet from Thermo Ultimate 3000 series. As precolumn a VP 50/21 Nucleodur C18 Gravity 5 μm was used and as main column a 50/2 Nucleodur C18 Gravity 1.8 μm. The flow rate was 0.4 mL per min. Eluent A: H_2O + 0.1% HCOOH; Eluent B: Acetonitril + 0.1% HCOOH.

Method B

Used Gradient: 0-0.5 min: 90% A / 10% B; 0.5-7.5 min: 5% A / 95% B; 7.5-9.0 min: 5% A/ 95% B; 9.0-11 min: 90 % A / 10% B. High resolution mass spectra were recorded on a LTQ Orbitrap mass spectrometer coupled to an Accela HPLC-System (HPLC column: Hypersyl GOLD, 50 mm x 1 mm, particle size 1.9 μm, ionization method: electron spray ionization). GC-MS measurements were done on an Agilent Technologies 7890A GC System. It was used a 5975C inert XI MSD with Triple-Axis Detector.

Method C

DB_100_S: flow rate: 20 ml per min, 1 min hold at 100°C, during 10 min increase to 300°C, at 11 min 300°C for 5 min.

The preparative HPLC purifications were carried out on an Agilent HPLC (1100 series) with LC/MSD VL (ESI-MS) mass detector with parallel UV-detection. A reversed-phase C18 column (Nucleodur C18, diameter 10 mm, Macherey & Nagel) was used.

Method D

Flow rate 6.0 mL/ min, (A = acetonitrile + 0.1 % trifluoroacetic acid (TFA), B = water + 0.1 % TFA). Gradient: 1-25 min: 10 % A, 90 % B; 26-28 min: 100 % A, 0 % B; 28.10-30 min: 10 % A, 90 % B. Optical activities were measured with a Schmidt + Haensch Polartronic HH8 polarimeter. Chemical yields refer to pure isolated substances. Melting points were measured on the apparature B-450 instrument from Büchi. Up open capillaries were used.

The amine (1.0 eq) was dissolved in dimethylformamide (DMF) (1 mL) at room temperature. In a separate flask, the carboxylic acid (1.0 eq) was dissolved in DMF (1 mL) and 1-cyano-2-ethoxy-2-oxoethylidenaminooxy)dimethylamino-morpholino-carbenium hexafluorophosphate (COMU) (1.5 eq.), ethyl (hydroxyimino)-cyanoacetate (Oxyma) (1.5 eq) were added. After addition of N,N-diisopropylethylamine (DIPEA) (4.5 eq.) to the mixture, the flask was shaken for 30-60 s and the mixture was added dropwise to the solution of the amine and stirred at room temperature for 18 h. The reaction mixture was diluted with 1 M HCl (50 mL) and extracted with ethylacetate (3 x 50 mL). The combined organic phases were washed with sat. $NaHCO_3$ (1 x 50 mL), with sat. NaCl (1 x 50 ml), dried with magnesium sulfate and concentrated in vacuo. The crude residue was purified by preparative HPLC (method D). Aqueous solubility of compounds was determined by spectrophotometrical measurement of the kinetic solubility of a 500 μM compound solution in aqueous buffer at pH 7.4 compared to a solution in the organic solvent acetonitrile after 90 minutes of vigorous shaking at room temperature. Permeability through artificial membranes (PAMPA) was performed at an initial concentration of 500 μM of the compound in the donor compartment. After an incubation period of 20 hours, absorption of the receiver wells was measured by spectrophotometry and permeation was calculated by normalization of the compound flux across a blank filter. Extended information on chemical synthesis, analytical data and NMR spectra are collected in Data S1.

Chemogenomic Profiling (HIP-HOP)

Potency Determination

The growth-inhibitory potency of compounds was determined using wildtype *S. cerevisiae* BY4743 as described by Pierce et al.(Pierce et al., 2007). OD_{600} values of exponentially growing cultures in rich medium were recorded with a robotic system. Twelve-point serial dilutions of the tested compounds were assayed in 96-well plates with a reaction volume of 150 μl, start OD_{600} was 0.05. Solutions containing dimethyl sulfoxide (DMSO) were normalized to 2%. IC_{50} values were calculated using logistic regression curve fits generated by TIBCO Spotfire v.6.5.3 (TIBCO Software Inc.).

HIP Assay Execution

The HIP assay was performed in 24 well plates (Greiner 662102), with 1600 μl /well YPD. Experimental compounds were tested at n=2 within the same plate at or close to their IC_{30} concentration. Each plate contained two no drug controls, one positive control (Benomyl, CMB991), 10 experimental compounds in duplicates and one contamination control that received no cells. A standard experiment was 4 plates / 40 experimental compounds processed robotically on a BiomekFX (Beckman Coulter) without human intervention. YPD / compound filled wells were inoculated with ~250 yeast cells/strain (100 μl of a 1.5 OD_{600}/ml culture) from an overnight log phase pre-culture to start the experiment. The plates were pipetted with a standard 96 pipettor head by providing tip boxes pre-configured with a special tip pattern. Plates were incubated for 16 hours in a robotic shaking incubator at 30°C/550 RPM allowing for ~5 doublings. ~250 yeast cells/strain (120 μl of a 1.2 OD_{600}/ml culture) were subsequently transferred into a pre-configured 24 well plate that was stored in a robotic plate reservoir at 4°C until 30 minutes prior to its use where it was pre-warmed to 30°C. Once

inoculated the new plate was incubated at 30°C/550 RPM to allow the next 5 yeast generations (generation 6-10) and the plate containing the first 5 doubling cultures was stored at 4°C. This procedure was repeated 2x more until the final plate containing the yeast with ~20 generations were stored at 4°C. Detailed information about the robotic setup have been published previously (Hoepfner et al., 2014).

HOP Assay Execution

The HOP assay was performed similar to the HIP experiment but the duration was reduced to ~5 doublings and no dilutions were necessary. Before the experiment, aliquots of the HOP pool were thawed and recovered for 3 hours in YPD. The robotic system inoculated the wells prefilled with YPD and compound at the onset of the experiment with ~320 yeast cells/strain (110 μl of a 1.5 OD_{600}/ml culture) from an overnight log phase pre-culture. Plates were incubated for 16 hours in a robotic shaking incubator at 30°C/550RPM allowing for ~5 doublings and where then stored at 4°C.

.HIP, HOP, and microarray analysis was performed as described previously(Hoepfner et al., 2014; Pierce et al., 2007). Sensitivity was computed as the median absolute deviation logarithmic *(MADL)* score for each compound/concentration combination. Z-scores are based on a robust parametric estimation of gene variability from >3000 different profiles and were computed as described in detail in Hoepfner *et al.* (Hoepfner et al., 2014).

gDNA Extraction, TAG Amplification, and Hybridization

An aliquot of 5 OD_{600} units of yeast/well from the HIP and HOP experiments were arrayed in 96 well plates, spun and the supernatant discarded. gDNA extraction was performed using the ChargeSwitch kit (Invitrogen #18000) in a partially automated process. 150 ul/well of Zymolyase buffer (2 U Zymolyase, 50 ng RNase A, in 20 mM DTT and 20 mM Tris pH 7.5) were added and the cells were incubated at 37°C /700 RPM for 45 minutes. 300 μl/well lysis buffer (L18, Invitrogen) was added and the plate incubated at 56°C/ 700 RPM for 30 minutes. 200 μl/well ice cold precipitation buffer (N2, Invitrogen) was added and the precipitate pelleted by centrifugation at 4°C. The supernatant was saved to a new deep well plate (AB-0932, Abgene) suitable to lock on the Invitrogen MagnaRack magnet and 40 μl/well of pre-dispersed ChargeSwitch magnetic beads were added. The plate was incubated at room temperature for 5 minutes followed by incubation on the MagnaRack for 5 minutes to pellet the beads. All supernatant was carefully aspirated. The deep well plate was removed from the MagnaRack and 500 ul/well wash buffer (W12, Invitrogen) were added and mixed to disperse the beads. The washing was repeated three times and the wash buffer completely removed. Finally, 70 μl of elution buffer (E6, Invitrogen) were added. The beads were resuspended by mixing and the plate incubated for 10 min at RT. The beads were pelleted for one last time by incubation on the magnet for 5 minutes and the supernatant (containing the gDNA) was transferred to a new plate. The TAG PCR amplification and GenFlex Tag16K v2 hybridization protocol was used as described (Pierce et al., 2006).

Processing of TAG16K v2 Data

The raw probe intensity values of the CEL are summarized and normalized to tag intensities as described (Pierce et al., 2006). Tags with low intensity values in control samples are removed by computing an intensity value threshold based on the comparison of the correlation between the logarithmic intensity ratios for uptags and downtags across different intensity ranges. The tag intensities are then averaged to obtain a strain intensity value. In order to measure the relative abundance of each strain with respect to the averages of the control samples we compute *MAD logarithmic* (*MADL*) scores for each compound/concentration combination. If we denote the logarithm of the ratio of the average intensity of the compound samples over the average intensity of the control samples as r_L, then the MADL score is given as $(r_L - \mathrm{med}(r_L))/\mathrm{MAD}(r_L)$ where the median and MAD are computed over all strains in one sample. MADL scores can be viewed as robustly computed experiment-wise z-scores. We also compute the t-test p-value, *p,* between the two replicates for a compound and the four to eight control replicates as a measure of the variability of the compound and control sample intensities across the experiment and. The final (adjusted) score a_L is decreased for highly variable strains and computed as:

$$a_L = \min(0.05/p, 1) \cdot s_L$$

Then, we compute gene-wise z-scores (across all experiments) which are based on a robust parametric estimation of gene variability allowing for up to 15% outliers. To do this we consider the adjusted MADL scores (a_1, ..., a_n) of a strain over n experiments. Usually, the z-score transformation of score a_i is defined as $z_i = (a_i - \bar{a}) / \sigma$ where $\bar{a}$ is the mean and σ the standard deviation of the values a_i. However, due to the special nature of the HIP-HOP data it is advantageous to introduce a number of changes to the computation of the adjusted MADL z-score transformation. Since an (adjusted) MADL score of zero indicates a relative growth rate of a strain in the compound treated sample that is equal to the relative growth rate of the strain in the untreated control, we set $\bar{a} = 0$, for all strains. What remains is to estimate σ as a measure of the variability of the strain which is described in the following.

In order to avoid biasing the computation of the standard deviation of a strain profile we allow at most five entries of the same compound/concentration combination in the data set. The samples of the sixth or greater occurance are discarded. We normalize the positive and negative scores separately; that is, we treat the positive and the negative scores as the halves of two separate distributions (artificially creating two perfectly symmetric distributions in this way). In the following we only consider the negative scores. Let the profile of the negative scores of a gene be (s_1, ..., s_n) where we assume that the scores are sorted in ascending order. We assume that the scores follow a normal distribution $N(\mu,\sigma)$. Note that since the distribution is perfectly symmetric around 0, $\mu = 0$; moreover, for each *i,* the expectation of the score s_i is the $i/(2n+1)$-quantile q_i of the standard normal distribution $N(0,1)$ times σ. In other words, s_i / q_i is an estimator $\hat{\sigma}_i$ for σ, for each i. These estimators are computed only for the indices i in the interval $[0.15n, 0.85n]$, that is, we consider only the middle 70% of the data to estimate σ . We assume that the scores s_i are drawn for a normal distribution only if the standard deviation of the $\hat{\sigma}_i$ is at most 0.05 times the mean $\bar{\sigma}$ of $\hat{\sigma}_i$; in this case, the estimators $\hat{\sigma}_i$ are considered to

be consistent and $\overline{\sigma}$ a good estimate of σ. If the standard deviation is larger, we abandon the parametric approach and just set $\overline{\sigma}$ to be the standard deviation of sample (s_1, ..., s_n, $-s_1$, ..., $-s_n$). The estimate $\overline{\sigma}$ of σ obtained from the single-array data is used to compute the normalized z-score transformation ($a_1/\overline{\sigma}$, ..., $a_n/\overline{\sigma}$) of the adjusted MADL scores (a_1, ..., a_n).

Growth Curves

HIP-HOP profiles were validated by picking the individual strains from the HIP or HOP collections (OpenBiosystems, Cat # YSC1056 and YSC1055) and testing log-phase cultures in 96-well microtiter plates in YPD medium with serial dilutions of the compound. The assay volume was 150 μl/well, start OD_{600} was 0.05, DMSO was normalized to 2%. Curves were calculated by taking the 13-14 h OD_{600} measurements and applying a logistic regression curve fit in TIBCO Spotfire v6.5.3. Strain *HO/YDL228C* was used as the wild-type reference.

For determination of cell viability in HCT116 cells 1500 cells/well were seeded in a 384 well plate and incubated for 72 hours with serial dilutions of the compound. The readout was done with CellTiter-Glo Luminescent Cell Viability Assay (Promega).

Expression and Purification of Recombinant Proteins

Recombinant *S. cerevisiae, C. glabrata* and *C. albicans* Sec14 proteins were purified as previously described (Khan et al., 2016; Schaaf et al., 2008). The murine PITPα structural gene was subcloned into pET28b(+) as an *Nco1-SacI* PCR fragment encoding an N-terminal octa-histidine epitope tag appended to the PITPα open reading frame. The construct was transformed in *E. coli* BL21 (DE3) cells and cultured in LB plus antibiotics at 37°C until an OD_{600} of 0.6 was reached. Protein production was induced by adding IPTG to a final concentration of 60μM at which time the culture was shifted to 16°C and incubated overnight with shaking. Cells were pelleted, resuspended in buffer A (50 mM NaH_2PO_4 300 mM NaCl pH 7.8) supplemented with PMSF and 2-mercaptoethanol (1 mM each, final concentration). Cells were disrupted by two successive passages through a French Press (10,000 p.s.i.), and crude lysates clarified by two successive rounds of centrifugation at 2800 *g* and 27,000 *g* for 30 minutes each. Clarified lysates were incubated with Co-TALON metal affinity beads for 3 hours at 4°C followed by exhaustive washing with buffer A. Bound proteins were eluted in a 20-200 mM imidazole gradient incremented in 1 ml steps of 20, 40, 60, 80, 100, 150, and 200 mM imidazole in buffer A and evaluated by SDS-PAGE using BSA mass standards to estimate PITPα yield.

Lipid Transfer Assays

Compounds of interest were maintained as 20 mM stock solutions in DMSO and stored at room temperature in the dark. *In vitro* sensitivities of Sec14p to the compounds was investigated as described by Nile et al.(Nile et al., 2014). Briefly, protein was incubated with DMSO/compound, as applicable, in the presence of liposomes. Compound concentrations were fixed at 20 μM throughout the experiments. Total [^{3}H]-PtdIns input per assay ranged from 8356-9604 c.p.m., background transfer from 436-489 c.p.m., and transfer efficiencies from 14-16%. Protein concentrations were clamped at 287 nM (~10 μg per assay).

For IC_{50} determinations, % [^{3}H]PtdIns transfer (normalized to mock) was plotted as a function of $\log_{10}$ of the compound concentration. The IC_{50} was determined using GraphPad Prism Version 6 software. IC_{50} values are determined at 95% confidence level from at least two independent experiments, each done in triplicate. [^{3}H]-PtdIns input for Sec14, its mutant proteins, $Sec14_{CA}$ and $Sec14_{CG}$, ranged from 7111-11517 c.p.m. per assay; background ranged between 212-510 c.p.m. per assay. The transfer efficiencies are as follows: Sec14 (25-30%), $Sec14_{CA}$ (39-43%), $Sec14_{CG}$ (30-34%), $Sec14^{Y151H}$ (32-35%), $Sec14^{V154G}$ (15-18%), $Sec14^{V155A}$ (26-31%), $Sec14^{S201G}$ (40-43%) and $Sec14^{S173L}$ (25-27%). Protein was clamped at 10 μg per assay throughout these experiments.

Functional Variomics

A functional variomics screen to isolate SMI-resistant Sec14p variants was performed (Huang et al., 2013; Pries et al., 2016). 6 x 10^7 BY4743 yeast transformants harboring the *SEC14* variomic library (the *SEC14* ORF amplified by error-prone PCR and cloned under control of the endogenous promoter into a low-copy expression plasmid, at a pre-determined complexity above 2 x 10^5 primary alleles, (Huang et al., 2013)) were plated onto a 15 cm petridish containing uracil-free synthetic complete agar supplemented with either 250 μM of compound **2** or 100 μM of compound **3**. The plates were incubated for four days at 30°C. Ninety-six resistant colonies were picked for each condition, the plasmids purified using the Wizard SV 96 plasmid DNA purification system (A2250, Promega,). The inserts were amplified by PCR Platinum Hot Start PCR Master Mix (13000012, Invitrogen) using the oligonucleotides 5'CTGTTGGGAAGGGCGATC3' and 5'CCAGGCTTTACACTTTATGCT3' respectively and performing the reaction as specified in Invitrogen's manual. Single nucleotide polymorphisms (SNPs) were then idenetified by Sanger sequencing.

Mutant Validation

To confirm the SNPs identified with the functional variomics screen, the isolated plasmids were cut with *Sac*I and *BamH*I, ligated with a pBYInt-URA plasmid and transformed into BY4743Δ8 MATa/α strain, that is deleted for eight genes involved in drug resistance (efflux pumps *SNQ2, PDR5, YOR1*; transcription factors *PDR1, PDR2, PDR3, YAP1, YRM1,* detailed genotype is described in the Fungal Strains section above). This sensitized strain was chosen to open up the observable resistance window in the dose-response validation as testing of high compound concentrations were limited by solubility (Table S2). Growth curves were recorded over 24 hours as described in the growth curve section described above. In vitro validation with recombinant protein was performed as described above.

Protein Expression, Purification, and Crystallization

Octahistidine-tagged Sec14p was purified from BL21-CodonPlus (DE3)-RIL cells (Agilent Technolgies) as described for Sfh1(Schaaf et al., 2006) with minor modifications. Protein expression was induced with 60 μM isopropyl-β-D-thiogalactoside at 16°C for 20 h, prior to harvesting cells and extracting protein in a modified lysis buffer (300 mM NaCl, 25 mM sodium phosphate pH 7.5 and 5 mM β-mercaptoethanol). After purification with a Ni-NTA affinity resin (Macherey-Nagel), the protein was subjected to size exclusion chromatography (Superdex 75 16/600 column, GE Healthcare) at a flow rate of 1 mL/min in modified lysis buffer. Fractions of the second peak were pooled and concentrated to 5 mg ml^{-1}. Initial crystallization screens were carried out manually by sampling an array of circa 1500 conditions that represent variations on crystallization conditions established for the Sec14 homolog Sfh1 (Schaaf et al., 2006, 2008). In this initial screen, His_8-Sec14p was supplemented with 1 volume % compound 2 (30 mM in DMSO), and a sitting-drop geometry was employed in which drops consisted of 1 μL protein/compound solution and 1 μl well solution. After an incubation time of ca. 1 week at room temperature, crystals appeared in one condition where the solution consisted of 129,5 mM sodium acetate, 64,8 mM TRIS, 4,6 % (w/v) PEG 4000, and 11.9 % (v/v) glycerol adjusted to pH 7.0 (by acetic acid).

Crystallography

For data collection, crystals were transferred to a cryo solution (129.5 mM sodium acetate, 64.8 mM TRIS, 10 % (w/v) PEG 4000, 20 % (v/v) glycerol, pH 7.0) and flash frozen in liquid nitrogen. Diffraction data were collected at the Beamline PXII of the Swiss Light Source. Data scaling and processing was performed with XDS (Kabsch, 1993). The structure was solved by Molecular Replacement with PHASER(Mccoy et al., 2007) using the structure of Sec14p prior to removal of the detergent coordinates (pdb id.: 1aua (Sha et al., 1998)). Cycles of model building and restrained refinement were carried out in COOT and PHENIX (Adams et al., 2010; Emsley and Cowtan, 2004). Ligand restraints were generated with Jligand (Lebedev et al., 2012). Protein-ligand interaction was analysed with PLIP(Salentin et al., 2015). Protein structure figures were generated using PyMOL (http://www.pymol.org). The coordinates and structure factors have been deposited in the RSCB PDB database with ID code 6F0E.

In Silico Docking

Computational docking was carried out using the genetic algorithm-based ligand docking program GOLD 5.2.1 that exhaustively explores ligand conformations and provides limited flexibility of protein side chains with hydroxyl groups by reorienting hydrogen bond donor and acceptor groups. For computational docking, the Sec14p::compound **2** crystal structure was used. The binding site was defined by taking cognate ligand in the crystal structure as reference center and defining a 10 Å boundary around it using the GOLD cavity detection algorithm. GOLD docking was carried out without constraint to explore all possible solutions. To explore all possible binding modes, docking was carried out with early termination turned off. All other parameters were as the defaults. Compounds of interest were docked and scored using CHEMPLP scoring function within GOLD as it gives the highest success rates for pose prediction and virtual screening experiments against diverse validation test sets.

Structure-based Design and MedChem Transformation

Structure-based optimization and MedChem Transformation of the picolinamide series was carried out using MOE software (https://www.chemcomp.com/). The Sec14p::compound **2** crystal structure was used as starting structure for optimization. Binding pocket within the Sec14p Lipid Binding Domain was mapped in an area 6Å around the co-crystallized ligand. Compound **2** was used as lead template for transformation and optimization. Van der Waals interaction surface were generated near the lead template to determine accessible space for R group substitutions. Ligand R-vectors were generated on the lead template to show positions at which the heavy atom could be substituted without introducing > 2 kcal/mol of Van der Waals clash energy.

To ascertain biochemically favorable regions for substitutions, Electrostatic Feature Maps were generated that predict the electrostatically preferred locations of hydrophobic, H-bond acceptor and H-bond donor sites. Similarly, probabilistic receptor preference maps were calculated to predict non-bonded contact preferences - i.e. the preferred locations of hydrophobic and hydrophilic ligand atoms. A fragment screen was generated and drug-like filters were used such that total molecular weight of compound does not exceed 500 daltons, total polar surface area (TPSA) descriptor between 40 and 140 with no reactive group substitutions. These parameters were imposed on an MOE fragment and linkers database screen for R-group substitutions. Considering the amphipathic nature of the sub-pocket, a pharmacophoric feature was included in the query that would position the fragment for interaction with Glu_{124}. Binding poses of compounds retrieved from the screen were refined by energy minimization within the pocket, and their binding affinities estimated using the GBVI/WSA dG scoring function.

Antifungal Testing

Fungal strains used for testing were as follows: *Candida albicans* (ATCC 10231), *Candida glabrata* (ATCC 2001), *Cryptococcus neoformans* (DSM 70219) *Aspergillus brasiliensis* (ATCC 16404). Antifungal susceptibility testing was performed in triplicates according to the Clinical and Laboratory Standards Institute (CLSI) guidelines for broth microdilution M27-A3 and M38-A2 (Wayne, 2008a, 2008b). By performing 1:2 serial dilutions, 10 concentrations in a range between 200 and 0.3 μM were tested for growth inhibitory activity on solid medium in 8 cm petridishes prepared with 15 ml Mueller-Hinton agar medium (2.0 g7/l beef extract, 17.5 g/l casein hydrolysate, 1.5 g/l starch, 17 g/l agar), with pH adjusted to pH 7.2, in triplicates. 1 μl spore inoculi were spotted manually onto the plates and absence of growth was scored visually after 72 hours incubation at 30°C to determine the minimal inhibitory concentration.

QUANTIFICATION AND STATISTICAL ANALYSIS

Chemogenomic profiles were acquired as independent duplicates and then averaged and computed against 8 no drug controls as outlined in the corresponding section above. The statistical analysis performed in described in detail in the chemogenomic profiling section. Fungal growth curves were acquired as duplicates, biochemical inhibition assays were conducted in triplicates, cytotoxicity assays were conducted in triplicates. Curves were calculated using the logistic regression curve fit function of TIBCO Spotfire (TIBCO Software Inc.) or Prism (GraphPad Inc.). MIC experiments were determined in triplicates and lack of colony formation scored visually.

DATA AND SOFTWARE AVAILABILITY

Used software packages are listed in the corresponding experimental sections and the Key Resources Table. The co-crystal structures have been uploaded to RCSB protein data bank and can be found and retrieved under the code 6F0E or the following link: http://www.rcsb.org/pdb/explore/explore.do?structureId=6F0E.

9.4 Johnen et al., in preparation

Al-tolerance mediated by SEC14-type lipid transfer proteins reveals that membrane charge is both a primary target of Al-toxicity and a tool to increase Al-tolerance in yeast and plants

This manuscript was written by Philipp Johnen;
ZMBP; Plant Physiology; University of Tübingen, Germany.

The work presented in this manuscript is a team effort. All contributions are denoted in the section “Author contributions” at the end of this manuscript.

Abstract

Aluminum (Al) toxicity represents a major factor for limitations in crop production worldwide. However, how Al acts on the cellular level is poorly understood. Based on an Arabidopsis cDNA screen in *Saccharomyces cerevisiae*, we show that *2μ* expression of two ScSec14 homologs, *AtSFH5* and *ScSFH1*, mediate Al tolerance in yeast. Observed tolerance phenotypes were not linked to overall Al content and were specific for Al among several tested metals. Through a genome wide screen in yeast, we identify a functional cell wall integrity (CWI) pathway as essential for ScSfh1-mediated Al tolerance and show that Al treatment triggered CWI signaling. Further, we report a negative synthetic interaction between ScSfh1 and ScPkc1, and that *ScSFH1* (*2μ*) expression altered localization of mCherry-Rho1 and ScPkc1-GFP, both representing major players in CWI signaling. Additionally, we show that *ScSFH1* acts as multi-copy suppressor of different $mss4^{ts}$ alleles. Interestingly, our data provide evidence that partial bypass of the ScMss4 requirement is independent of global phosphatidyl inositol-4,5-bisphosphate (PtdIns(4,5)P_2) levels. The ability of ScSfh1 to bind to phosphatidyl choline (PtdCho), but not to PtdIns, is essential for observed Al tolerance and partial $mss4^{ts}$ rescue, suggesting that lipids are involved in reported phenotypes. Indeed, we observed that *2μ* expression of *ScSFH1/AtSFH5* increased plasma membrane (PM) localization of the PtdIns(4)P fluorescent lipid-associated reporter (FLARE) GFP-2xPH^{ScOsh2}, but not of other FLAREs binding to PtdSer, PtdIns(3)P or PtdIns(4,5)P_2. Interestingly, global PtdIns(4)P levels appeared not to be changed. Our results indicate that *ScSFH1* (*2μ*) expression changes phosphatidyl ethanolamine (PtdEtn) and PtdCho biosynthesis rates. Based on these findings, we provide first hints that ScSfh1 might drive a PtdEtn/PtdCho transfer *in vivo* and that PtdEtn abundance at the PM might influence PtdIns(4)P accessibility or specific PtdIns(4)P pools. Furthermore, employing a genetically encoded charge sensor suggested that *ScSFH1* (*2μ*) expression increased overall negative charge of the PM. Subsequent genetic manipulation of negatively charged phospholipids in yeast and Arabidopsis showed a strong correlation of Al tolerance with the abundance of negatively charged lipid species. Using different FLAREs, charge sensors and endogenously PM-targeted proteins, we show that Al treatment disrupts proper PM recruitment in yeast and plants. Together these findings suggest negative charge of the PM as a primary target for Al. Based on our findings, we propose that binding of Al to the inner leaflet of the PM competes with endogenous membrane-targeted proteins, providing a model how Al can affect cellular integrity.

Introduction

Aluminum (Al) is the most abundant metal in the earth crust (2). In acid soils with a pH below 5.0, Al-oxides become soluble and Al^{3+} is taken by plants leading to root growth inhibition (3). Around 50 % of the arable land is considered acidic with a pH below 5.0 (4, 5). Thus, toxic effects of Al on root development and subsequent plant growth represent one of the biggest abiotic limitations to crop production worldwide.

Plants developed two main strategies to cope with Al toxicity: i) exclusion of Al from the root by the exudation of organic acids into the rhizosphere and subsequent chelation of Al and ii) sequestration of Al in the vacuole (3). Since Al is mainly accumulating in the root apoplasm (6) but it is also quickly taken up by the root (7) there is an ongoing debate whether Al toxicity originate from apoplastic or symplastic effects. A variety of direct molecular targets of Al were proposed to underlie observed phenotypes at toxic Al conditions: cell wall (8), plasma membrane (PM,(9)), cytoskeleton (10), distinct enzymes (11), cation-/metal binding proteins (12, 13) and chromatin (10). Most of the suggested direct targets of Al are based on observation of Al-accumulation within the cell, global changes in cell morphology or *in vitro* experiments. With the many proposed targets it remains unclear which (if any) of them represents the target that is compromised first by increasing Al-concentrations and hence represents the limiting factor for plant growth in acid soils.

Due to high accumulation of Al in the apoplast, cell wall components represent an attractive putative target of Al. Al strongly interacts with the cell wall and leads to its rigidification (14, 15). Furthermore, the cell wall composition changes upon Al treatment (16, 17). Overexpression of *ARABIDOPSIS THALIAN WALL ASSOCIATED KINASE 1* (*AtWAK1*), which binds to pectin (18) and was suggested to represent a cell wall sensor (19), leads to Al tolerance (20). Whereas in plants insights in cell wall integrity (CWI) sensing is just emerging (21), in yeast the CWI signaling pathway is more extensively studied (22). In *Saccharomyces cerevisiae,* cell wall stress is sensed by a family of cell surface sensors, proposed as mechano-sensors (23), which consist of ScWsc1-3, Mid2 and Mtl1 (22). ScWsc1 and Mid2 represent the predominant sensor or for cell wall stress (22). Together with phosphatidylinositol-4,5-bisphophate ($PtdIns(4,5)P_2$)-recruited ScRom1/2 GTP exchange factors (GEFs) the cell wall sensors activate CWI master regulator ScRho1 (22). Furthermore, ScPkh1/2 protein kinases and the ScTus1 GEF regulate ScRho1 activity. In its active GTP-bound state, ScRho1 triggers a MAPK signaling cascade containing ScPkc1 (MAP4K), ScBck1 (MAP3K), ScMkk1/2 (MAP2K) and Mpk1 (MAPK) (22). The MAPK signaling cascade alters activity of different

transcription factors which regulate genes involved in cell wall homeostasis (22). Furthermore, active ScRho1 directly affects several proteins involved in the regulation of cell wall composition, cytoskeleton organization and membrane trafficking (22). Mutant strains of CWI signaling compartments are more sensitive to Al treatment (24, 25) suggesting that also in yeast the cell wall composition is linked to Al toxicity.

Besides the cell wall, in plants, the PM is extensively discussed as a target of Al toxicity (2, 9). Among the variety of cellular membranes, the PM has been shown to be the most negatively charged membrane in yeast, mammalian and plant cells (26, 27) likely representing the membrane with the highest Al affinity. The negative charge of the PM is considered a hallmark of this membrane-type and is e.g. important for protein recruitment to the PM, which is mediated by simple basic hydrophobic (BH) motifs allowing a charge-dependent PM localization (26-28). Additionally, membrane recruitment is also mediated by lipid binding domains, which bind stereospecific to distinct lipid ligands (e.g. via C1, PH, FYVE, PX, and ENTH domains) (29). Thus, the composition and distribution of phospholipids (PLs) in a membrane determines protein recruitment and is therefore an essential feature of a living organism (29). The PM PL composition is a result of an interplay between the biosynthesis, degradation, membrane trafficking and transfer of PLs. In yeast, the starting point for PL biosynthesis is phosphatidic acid (PtdOH) (30), which is produced from glycerol-3-phosphate or dihydroxyacetone phosphate after fatty acyl coenzyme A (CoA)-dependent reactions that are catalyzed by the glycerol-3-phosphate acyltransferases, ScSct1 and ScGpt2 (31-33), and by the lysophospholipid acyltransferases, ScSlc1 and ScSlc4 (34, 35). From PtdOH cytidine diphosphate diacylglycerol (CDP-DAG) is produced by the CDP-DAG synthase ScCds1 (36). From CDP-DAG either phosphatidylinositol (PtdIns) by ScPis1 (37, 38), phosphatidylglycerol (PtdGly) by ScPgs1/ScGep4 (39, 40) or phosphatidylserine (PtdSer) by ScCho1 is produced (41). Decarboxylcation of PtdSer by ScPsd1 or ScPsd2 leads to phosphatidylethanolamine (PtdEtn) production (42, 43). PtdEtn is triple methylated by ScCho2 and ScOpi3 resulting in phosphatidylcholine (PtdCho) production (44). PtdEtn and PtdCho can also be synthesized from exogenously supplied ethanolamine (Etn) or choline (Cho), respectively (45). In addition to described PLs, phosphoinositides (PIPs) represent another class of PLs, which have PtdIns as a building block and which are involved in a variety of cellular processes (46). The main PIP species found at the yeast PM are phosphatidylinositol 4-phosphate (PtdIns(4)P) and phosphatidylinositol 4,5-bisphosphate (PtdIns(4,5)P_2) (47). PtdIns(4)P is produced by phosphorylation of PtdIns at the D-4 position

through ScPik1 or ScStt4 (48, 49). PtdIns(4,5)P_2 is produced by ScMss4 through phosphorylation of PtdIns at the D-5 position (50).

In plants, the *AtPI4Kα* and *AtPI4Kβ* families show PtdIns 4-kinase activity (51-53) and the *AtPIP5K* family PtdIns(4)P 5-kinase activity (53-55). PtdOH and PtdGly synthesis is similar to the yeast biosynthesis (56). The main biosynthetic pathways for PtdSer, PtdEtn and PtdCho production differ from the ones described in yeast. PtdEtn and PtdCho are synthesized by attaching phosphocholine or phosphoethanolamine to the DAG backbone, catalyzed by AtAAPT1 or AtAAPT2 (56, 57). In contrast to yeast, the biosynthesis of PtdSer is solely mediated by AtPSS1 (58, 59). Because the distribution of PLs is not determined by the location of synthesis alone, the interplay between biosynthesis, membrane trafficking and degradation influences membrane composition. Furthermore, PL transfer proteins are essential for proper lipid distribution in the cell (60, 61). PL transfer proteins are proteins, which are able to transfer PLs from one bilayer to another. One prominent member of the PL transfer proteins is *Saccharomyces cerevisiae* Secretory 14 (ScSec14). ScSec14 facilitates PtdIns and PtdCho transfer between membrane bilayers *in vitro* and regulates PtdCho and PtdIns(4)P homeostasis at the *trans*-Golgi network (TGN) *in vivo*, which is essential for viability (62, 63). However, the underlying molecular mechanism of ScSec14 *in vivo* is still under debate. Two attractive models are proposed: i) ScSec14 transfers PtdIns from its place of synthesis, the ER, to the TGN, delivering the substrate for the Golgi-resident Pik1, thereby increasing the PtdIns(4)P synthesis at the TGN (46, 64) and ii) ScSec14 presents PtdIns, which in a bilayer is a poor substrate, to Pik1 through a heterotypic exchange with PtdCho (Schaaf 2008). Sec14-type proteins are highly conserved and found in all eukaryotic organisms (65). Interestingly, in plants, the majority of Sec14-type proteins adopt a multi-domain structure linking ScSec14 activity to complementary functions (66). As in yeast, also in plants ScSec14 function was linked to PL homeostasis (67).

For Al two ideas arose how it might act on the PM: i) by interaction with the PM Al decreases overall surface charge on the apoplastic leaflet altering for e.g. cation uptake of the root (68, 69) and ii) binding of Al affects the cytosolic leaflet of the PM thereby influencing the activity of different PM-localized enzymes (70, 71). However, underlying data for presented ideas were either based on *in vitro* experiments using artificial membranes or were concluded from indirect observations. Thus, it remains elusive whether Al has a direct influence on the PM.

Based on a screen with an *Arabidopsis thaliana* cDNA library in the model organism yeast, here we show that (*2μ*) expression of *ARABIDOPSIS THALIANA SEC FOURTEEN*

HOMOLOG 5 (*AtSFH5*) and *SACCHAROMYCES CERIVISIAE SEC FOURTEEN HOMOLOG 1* (*ScSFH1*) confers Al tolerance in yeast. Observed tolerance is not correlating with overall cellular Al content and is independent of classical *Saccharomyces cerevisiae* ScSec14 function. Through a genome wide screen, using a yeast knock out collection, we show that an intact cell wall integrity (CWI) pathway is essential for mediation of Al tolerance by ScSfh1. Furthermore, we provide evidence that *ScSFH1* (*2μ*) expression increases PM localization of the CWI components, ScPkc1 and ScRho1. Additionally, we show that *ScSFH1* is a multi-copy suppressor of $mss4^{ts}$ related defects without affecting PtdIns(4,5)P_2 levels. A combination of analytical and cell biological methods indicate that *ScSFH1* (*2μ*) expression increase overall negative charge of the inner PM leaflet representing an explanation for observed phenotypes. Using different fluorescent lipid-associated reporters (FLAREs) we show that *ScSFH1* (*2μ*) expression increased the PtdIns(4)P FLARE GFP-2xPH^{Osh2} localization at the PM, while localization of other FLAREs were hardly affected. Phospholipodom analyses suggested that *ScSFH1* (*2μ*) expression mainly changes PtdEtn and PtdCho synthesis *in vivo*. In the same line, we show that ScSfh1 is able to transfer PtdEtn and PtdCho *in vitro*. Yeast mutant strains with defects in PtdEtn, as well as PtdCho, showed different localization of GFP-2xPH^{Osh2} suggesting that PtdEtn and PtdCho affect PtdIns(4)P distribution or accessibility *in vivo*. Further we provide evidence that overall negative charge of the PM strongly correlates with Al tolerance in yeast and *in planta* and that an increase of the biosynthesis of negatively charged PLs increased Al tolerance in yeast and plants. Moreover, we show that yeast and *in planta* efficient stereospecific and charge-dependent PM recruitment of FLAREs and endogenous proteins is impaired by Al treatment. Taken together, our data led us to a model in which Al binds to the cytosolic leaflet of the PM thereby decreasing overall charge, which disturbs protein recruitment to the PM. Thus, we propose PM charge as a possible primary cellular target for Al toxicity.

Results

Ectopic (*2μ*) expression of genes encoding certain Sec14-type proteins increases Al tolerance in *Saccharomyces cerevisiae*

To identify plant genes involved in Al tolerance mechanisms we heterologously expressed a cDNA library from *Arabidopsis thaliana* (72) in the model organism *Saccharomyces cerevisiae* (BY4741) and grew transformants on toxic Al conditions. We identified 10 genes, which overcame toxic Al levels when expressed in yeast (Table S1). As most robust hit, we identified the gene At1g75370, *ARABIDOPSIS THALIANA SEC FOURTEEN HOMOLOG 5* (*AtSFH5*), encoding a homolog of the ScSec14 protein family known to be involved in regulation of phospholipid (PL) homeostasis in yeast (66). AtSFH5 is a multi domain Sec14-type protein with an N-terminal SEC14 domain (Sec14D) and C-terminal Nlj16 domain. For further analysis, we expressed full length *AtSFH5* and the *AtSFH5 Sec14D* from a high-copy *2μ* vector driven by the strong Plasma membrane P2-TYPE H^+-ATPase (ScPMA1) promoter. As shown in Fig 1A, expression of full length *AtSFH5* (*2μ*) mediates Al tolerance as well as expression of *AtSFH5 Sec14D* (*2μ*) was sufficient to increase Al tolerance in yeast. To address if increasing Al tolerance is a common characteristic of proteins with ScSec14 activity and if it is based on classical ScSec14 functions we tested whether different ScSec14 homologs from yeast, mammals and plants and other PL transfer proteins with ScSec14-like activity are able to mediate Al tolerance and compared it with the ability to rescue defects of the *sec14-1^{ts}* strain. Interestingly, expression of *ScSEC14* (*2μ*) rescued *sec14-1^{ts}* defects but did not increase Al tolerance in yeast (Fig 1B). For AtSFH5 we found that expression of *AtSFH5 Sec14D* (*2μ*) increased Al tolerance and rescued *sec14-1^{ts}* defects (Fig S1A). Expression of *SEC FOURTEEN HOMOLOG 1* (*ScSFH1*) (*2μ*), the closest related ScSec14 homolog in *S. cerevisiae*, caused Al tolerance, but in accordance to previous reports (73, 74) did not rescue *sec14-1^{ts}*-releated growth defects. Also for other thirteen tested Sec14 homologs and PL transfer proteins, we could not find a correlation between mediation of Al tolerance and rescue of *sec14-1^{ts}* defects (Fig 1A, 1B, S1A and S1B) indicating that the observed Al tolerance phenotype is not enabled by classical ScSec14 functions. Among tested ScSec14-type proteins besides *AtSFH5* only expression of *ScSFH1* (*2μ*), robustly increased Al tolerance in yeast (Fig 1B, S1A and S1B). To further investigate the independence of ScSec14 function and mediation of Al tolerance, we tested if the *ScSFH1** activation allele *ScSFH1^{Y113C}*, which endows the pseudo ScSec14 protein, ScSfh1, with robust ScSec14-like activities in *in vitro* and *in vivo* (74), influenced ScSfh1-mediated Al tolerance. In agreement

with described Al tolerance phenotype being independent of ScSec14 activity, we observed that expression of the *ScSFH1** (*2μ*) activation allele led to an increase in Al tolerance comparable to *ScSFH1* (*2μ*) (Fig S1C).

PtdCho binding but not PtdIns binding of ScSfh1 is required for Al tolerance phenoytpe

For ScSec14-function two properties were shown to be essential *in vivo*: i) the ability to transfer PtdCho and PtdIns between different bilayers *in vitro* (75) and ii) in *cis* binding capability to phosphatidylinositol (PtdIns) and phosphatidylcholine (PtdCho) (75). To test if lipid binding is required for mediation of Al tolerance, we tested mutants of ScSfh1 and ScSfh1* activation mutant defective in binding PtdIns and/or PtdCho, which were generated based on available structural data (75), checked for stability (Fig S1D and (74)) and confirmed in PL transfer assays (Fig 6 and (74)). Analysis of ScSfh1^{L179W,I196W} and ScSfh1*^{L179W,I196W} globally impaired in PL binding showed that PL binding in general is crucial for the increase of Al tolerance (Fig 1C and S1C). ScSfh1^{S175I,T177I} and ScSfh1*^{S175I,T177I} mutants defective in PtdCho binding were compromised in mediating Al-tolerance. In contrast, expressing the PtdIns binding mutants *ScSFH1*^{T238D} and *ScSFH1**^{T238D} indicated that PtdIns binding was not relevant for the ScSfh1-mediated Al tolerance (Fig 1C and S1C). The samepattern was observed in an independent yeast wild type strain (Fig S1E).

Among other tested metals *AtSFH5* (*2μ*) and *ScSFH1* (*2μ*) expression only increased tolerance to Al

Testing the growth behavior of yeast expressing *AtSFH5*, *AtSFH5 Sec14D*, *ScSFH1* and *ScSec14* on solid media supplement with Cu^{2+}, Fe^{2+}, Mn^{2+}, Ni^{2+} or Zn^{2+}), we did not find a global increase of tolerance by *AtSFH5*, *AtSFH5 Sec14D*, *ScSFH1* (*2μ*) expressoin (Fig S2A). This finding indicated that the ScSFH1/AtSFH5-mediated tolerance was specific for Al.

In liquid culture Al tolerance did not correlate with intracellular Al contents

Because matrix components of agar-based solid growth medium strongly bind (and hence inactivate Al), for solid media assays, high Al concentrations have to be employed. However, using a liquid culture, low nutrient and low pH yeast medium, we observed yeast growth

defects at concentrations (Fig S2B) in range with free Al^{3+} concentrations reported to impair root growth in natural soils (76). In accordance to results on solid media, also in liquid media expression of *ScSFH1* (*2μ*) increased Al tolerance of yeast in between 0-100 μM (Fig S2B). Underlying mechanisms of higher tolerance to Al may originate from i) a decreased uptake or an increased export of Al resulting in lower intracellular Al concentration, ii) a detoxification of Al in the vacuole leading to a hyper-accumulation of Al due to the vacuole acting as sink for Al or iii) a change in Al-toxicity independent of changes in subcellular Al-concentrations. The comparison between the intracellular Al levels of Al-sensitive yeast harboring *empty vector* (*ev*) or pDR195-*ScSEC14* with Al-tolerant yeast harboring pDR195-*AtSFH5* or pDR195-*ScSFH1-V5*, showed no consistent correlation between intracellular Al concentration and Al tolerance (Fig 1D). This indicates that AtSFH5/Sfh1-induced Al-tolerance is unlikely the result of altered uptake or sequestration. A tolerance mechanism, in which either the molecular target of Al is altered or in which detrimental effects of Al-induced cell injury are attenuated appears therefore likely. Furthermore, we measured a variety of other metals and nutrients to see if *AtSFH5* (*2μ*) or *ScSFH1* (*2μ*) expression had an effect on their homeostasis and found no correlation between their amounts and growth behavior on Al containing media (Fig S2C).

Taken together, we found that ectopic expression of certain Sec14-type proteins increase yeast tolerance to Al. Observed tolerance is not related to canonical ScSec14 functions and might be caused by a change of cellular targets of Al.

The cell wall integrity pathway is essential for the ScSfh1-mediated Al tolerance in yeast

To identify signaling and biosynthetic pathways that are important for AtSFH5- or ScSfh1-mediated Al tolerance we performed a genome wide screen using the MAT*a* Library of the Saccharomyces Genome Deletion Project out collection (for details see the Methods section) containing around 5200 viable yeast knock out strains. We screened for strains, in which *ScSFH1* (*2μ*) expression did not increase Al tolerance any more with the incentive to identify pathways essential for Sfh1/AtSFH5-mediated Al tolerance, as illustrated in the cartoon in Fig 2A. For two practical reasons we focused on ScSfh1: i) ScSfh1 is a single domain protein and ii) ScSfh1 high-resolution structures in complex with different phospholipids (PLs) are available (74, 75). After two rounds of verification, we identified 67 knock out strains in which Sfh1-mediated increase in Al-tolerance was severely compromised (Table S2). We identified genes encoding proteins involved in lipid homeostasis, membrane trafficking,

membrane sorting, cell wall integrity (CWI), cell cycle, gene expression, amino acid metabolism, chaperon function, spermidine/spermine biosynthesis and mitochondrial fusion (Table S2). Strikingly for the CWI pathway, except of essential proteins or proteins with functional redundant homologs, we identified most components previously linked to proper CWI signaling (Table S2). We identified the two cell-surface sensors ScWsc1 and ScMid2, described as main sensors for the CWI pathway (22), to be essential for ScSfh1-mediated Al tolerance (Fig 2B). Further, we found that GTP exchange factors (GEFs) ScRom2 and ScTus1 (Fig 2C) and two mitogen-activated kinases (MAPKs) ScBck1 and ScMpk1 (Fig 2D), both essential for the CWI signaling (22), were required for ScSfh1-mediated Al tolerance. This data suggested that ScSfh1 might be involved in the regulation of CWI signaling. Interestingly, the *sfh1Δ* knock out strain showed a slightly reduced growth on Al containing medium. This growth reduction was complemented introducing a single copy plasmid that allows expression of *ScSFH1* under its native promoter (Fig 2E). To corroborate an influence of ScSfh1 in CWI signaling, we investigated a possible synthetic interaction with ScPkc1 a key player in CWI signaling (22). Employing a synthetic genetic array (SGA, (77)) we identified a negative synthetic interaction between *sfh1Δ* and *pkc1-3^{ts}* in presence of the cell wall antagonist Calcofluor white (Fig 2F). Taken together, these results suggest an endogenous role of ScSfh1 in CWI signaling. The CWI pathway was previously linked to Al in yeast by the observation, that mutant strains of CWI components showed a decreased growth when treated with Al (24, 25). However, so far it was not elucidated if Al treatment influences CWI signaling directly. In collaboration with the Molina Lab (Madrid, Spain), we used ScMpk1 phosphorylation as a readout for CWI pathway activity and observed in a time course experiment that already after 30 min of Al treatment, the CWI pathway reached maximum activation which, was maintained at least for 8 h suggesting a direct stimulation of CWI signaling by Al (Fig 2G). Interestingly, expression of *ScSFH1* (*2μ*) did not increase ScMpk1 phosphorylation. Given that a proper localization of CWI pathway components are crucial for efficient CWI signaling (22, 78, 79), we further investigated the effect of *ScSFH1* (*2μ*) expression on the localization of the central CWI components ScRho1 and ScPkc1 (22). Indeed, *ScSFH1* (*2μ*) expression led to an increased plasma membrane (PM) localization of mCherry-ScRho1, as quantified by the PM localization relative to intracellular signal (relative PM localization, Fig 2H and 2I). For Pkc1-GFP, *ScSFH1* (*2μ*) expression led to a significantly change in localization as well, as quantified by counting cells with diffuse, PM, bud tip and septum localization (Fig. 2J and 2K). Post hoc followed by planned comparison analysis (80) showed that *ScSFH1* (*2μ*) expression led to significantly increased membrane

and bud localization and significantly decreased septum localization (Bonferoni corrected p = 0.00625) of ScPkc1-GFP. Taken together, our data show that Al induces CWI signaling, that an intact CWI pathway is essential for ScSfh1-mediated Al tolerance and that ectopic expression of *ScSFH1* alters the localization of the key CWI signaling components ScRho1 and ScPkc1.

ScSFH1 is a multi-copy suppressor of *mss4^{ts}* at semi-restrictive temperatures

One important regulatory layer of the CWI pathway is the modulation of PIPs, particular by PtdIns(4,5)P_2-dependent PM of ScRho1 (81, 82) or its GEF ScRom2 (83). Since ScSec14 was described to be involved in the modulation of PIP homeostasis in yeast (62, 75, 84), we aimed to test the effect of *ScSFH1* (*2μ*) expression on growth behavior of yeast with defects in PIP levels (*pik1^{ts}*, *stt4^{ts}* and *mss4^{ts}*). Interestingly, we identified *ScSFH1* as a multi-copy suppressor of *mss4^{ts}* at semi-restrictive temperatures (Fig 3A). In *pik1^{ts}* and *stt4^{ts}* strains expression of *ScSFH1* (*2μ*) had a negative on growth performance (Fig 3A). Also in an independent *ts*-allele, *mss4-5^{ts}, ScSFH1* (*2μ*) expression increased growth at semi-restrictive temperature (Fig S3A). Interestingly, we observed a rescue of *mss4^{ts}* at semi-restrictive temperatures for the *ScSFH1* and *ScSFH1^{T238D}* but not for *ScSFH1$^{S175I,\ S177I}$* (Fig 3B) resembling the pattern of ScSfh1-mediated Al tolerance (Fig 1C and S1E). In order to see if ScSfh1 is able stimulate ScMss4 activity by presenting its substrate phosphatidylinositol 4-phosphate (PtdIns(4)P) in similar fashion as proposed previously for ScSec14 and ScPik1 (75), we tested if recombinant ScSfh1, ScSfh1 lipid binding mutants or ScSec14 (Fig S3B) can stimulate ScMss4 in an *in vitro* kinase assay (based on (50), Fig 3C). Indeed ScSfh1 caused a protein concentration-dependent stimulation of PtdIns(4,5)P_2 production (Fig 3D). As control we used PtdIns(4,5)P_2 as substrate and could not detect any ScMss4 activity (Fig S3C). Surprisingly, ScSfh1^{T238D}, impaired in PtdIns binding, showed a wild typic stimulation of PtdIns(4,5)P_2 production (Fig 3D) suggesting that an ScSfh1 mutant defective in PtdIns binding is still able to bind and present PtdIns(4)P. In contrast, Sec14 had only a minor effect on MSS4-dependent PtdIns(4)P phosphorylation (Fig S3D). Unexpectedly, ScSfh1$^{S175I,\ T177I}$ stimulated ScMss4 kinase activity comparable to ScSfh1 (Fig 3E). Since PtdCho binding is essential for Sfh1 multi-copy suppression of *mss4^{ts}* defects and for the induction of Al tolerance, these findings question the physiological relevance of this *in vitro* assay. Because our experimental set up did not differentiate between protein-bound and membrane-resident PtdIns(4,5)P_2, we wondered whether protein-bound PtdIns(4)P might be efficiently

phosphorylated *in situ*, but may not be released into the membrane from the ScSfh1$^{S175I, T177I}$ protein in contrast to Sfh1, where such a release might take place by a heterotypic lipid exchange with PtdCho. For this reason we performed a PtdIns(4,5)P_2 *in vitro* release assay (Figure 3D) and tested for differences between ScSfh1 and ScSfh1$^{S175I, T177I}$ (Fig S3E). We were able to detect *in situ* phosphorylation of PtdIns(4)P for Sfh1 (Fig S3F). However, no differences in the ability to release PtdIns(4,5)P_2 into liposomes were observed when comparing Sfh1 and ScSfh1$^{S175I, T177I}$ independent of whether light PtdCho liposomes or heavy sucrose-loaded PtdCho liposomes were employed (Fig 3G and Fig S3G). Together with the observation that ScSfh1-mediated stimulation of PtdIns(4,5)P_2 synthesis is very inefficient, these results indicate that a Sfh1-mediated presentation of PtdIns(4)P to ScMss4 appears not to be of physiological relevance and is unlikely responsible for the rescue of *mss4^{ts}* growth at semi-restrictive temperatures or for the Al tolerance phenotype. In agreement with that multi-copy *ScSFH1* expression did not increase PtdIns(4,5)P_2 levels as revealed by SAX-HPLC analyses of deacetylated PIPs extracted from [^{3}H]-*myo*-inositol-labeled *mss4^{ts}* transformants (Fig 3H). Also other PIPs appear unaffected by *ScSFH1* expression with the exception of a weak increase in PtdIns(4)P (Fig 3H). To investigate if *ScSFH1* (*2μ*) expression affected ScMss4 localization and may thereby facilitate suppression of *mss4^{ts}* defects, we localized ScMss4-GFP but could not find differences caused by Sfh1 (*2μ*) expression (Fig S3H).

In summary, *ScSFH1* (*2μ*) expression suppressed growth of *mss4^{ts}* at semi-restrictive temperatures. PtdCho binding but not PtdIns is essential for the suppression of *mss4ts* growth defects resembling the activity pattern for ScSfh1-mediated Al tolerance. Surprisingly, our data indicate that the partial rescue of *mss4^{ts}* was not caused by ScMss4 stimulation or relocalization of ScMss4 suggesting that *ScSFH1* (*2μ*) expression partially by-passes ScMss4 requirement.

ScSFH1 and *AtSFH5* (*2μ*) expression chang PtdIns(4)P accessibility at the PM

Localization of CWI signaling components has not only been linked to PIPs but also to other PLs (82, 85). To analyze if *ScSFH1* (*2μ*) expression might affect levels of not yet tested PLs, we performed thin layer chromatography (TLCs) with extracts of ^{32}P-labeled yeast transformants. Notably, *ScSFH1* (*2μ*) expression had no major effect on steady state PL levels (Fig 4A). To investigate whether *ScSFH1* (*2μ*) expression influences cellular PL distribution or accessibility without affecting total PL levels, we tested the influence of *ScSFH1* (*2μ*)

355 expression on FLAREs for PtdSer, PtdIns(3)P, PtdIns(4)P and PtdIns(4,5)P_2. Distribution of
356 PtdSer, PtdIns(3)P and PtdIns(4,5)P_2 FLAREs (GFP-LactC2, GFP-FYVE^{EEA1} and GFP-
357 2xPH$^{HsPlc\delta1}$) appeared to be unaltered or only mildly altered by *ScSFH1* (*2μ*) expression (Fig
358 S4A, S4B, S4C, S4D and S4E). In contrast, the relative PM localization for the PtdIns(4)P
359 reporter GFP-2xPH^{ScOsh2} was increased significantly when *ScSFH1* was overexpressed (Fig
360 4B and 4C) reflecting increased FLARE abundance at the PM. To further investigate whether
361 the ScSfh1-mediated change of PtdIns(4)P FLARE relate to Sfh1's ability to increase Al
362 tolerance and suppress *mss4^{ts}*-associated growth defects, we analyzed whether Sfh1-
363 dependent change in GFP-2xPH^{ScOsh2} localization is lipid dependent. Interestingly, increase in
364 PM localization of GFP-2xPH^{ScOsh2} correlated with the activity pattern for Al tolerance and
365 *mss4^{ts}* rescue in transformants expressing Sfh1 and the designated lipid binding mutants (Fig
366 4B and 4C). Notably, we also observed a significant increase of PM-localized PtdIns(4)P
367 sensor with *AtSFH5* and *AtSFH5 Sec14D* (*2μ*) expression (Fig 4D and 4E). To further
368 investigate a possible connection between an increased PtdIns(4)P sensor at the PM and the
369 mediation of Al tolerance in yeast we performed an unbiased directed evaluation approach
370 similar to (74) to endow the, in terms of Al tolerance, inactive ScSec14 (Fig 1B) with ScSfh1-
371 like activities to mediate Al tolerance. To this end we introduced random mutations into the
372 *ScSEC14* gene by error-prone PCR, reconstituted *2μ*-plasmids with mutagenized *ScSEC14* by
373 *in vivo* gap repair and screened transformants on selective media containing toxic Al
374 concentrations. From estimated 2 x 10^5 Ura^+ transformants we found 396 transformants with
375 increased Al tolerance. For 50 transformants plasmids were isolated and for 27 we obtained
376 qualitative sequencing results (Fig S5A). Interestingly, six of 27 constructs contained a
377 S173P substitution (Fig S5A) representing the most frequent substitution. In contrast to (*2μ*)
378 expression of wild typic *ScSEC14*, expression *ScSEC14^{S173P}* (*2μ*) increased Al tolerance to a
379 level comparable to *ScSFH1* (*2μ*) expression (Fig 4F). Interestingly, based on structural data
380 of ScSfh1 in complex with PtdCho and biochemical evidence, the S173 residue is involved in
381 PtdCho head group coordination (75). Notably, under restrictive temperatures, *SEC14^{S173P}*
382 (*2μ*) expression rescued *sec14-1^{ts}* growth defects comparable to expression of wild typic
383 *ScSEC14* (*2μ*) (Fig 5B) showing that the S173P substitution did not affect classical ScSec14
384 function and suggesting that S173P did not abolish PtdCho binding. Strikingly, while cells
385 expressing ScSec14 (*2μ*) displayed a pattern with internal patches of GFP-2xPH^{ScOsh2} similar
386 to control transformants, *ScSEC14^{S173P}* (*2μ*) expression caused a strong increase in PtdIns(4)P
387 FLARE PM localization, indistinguishable from *ScSFH1* (*2μ*) expressing cells (Fig 4G and
388 4H). Taken together, these results show a clear correlation between increased PM localization

of the PtdIns(4)P FLARE GFP-2xPH^{ScOsh2}, Al tolerance and *mss4^{ts}* rescue suggesting an increase of PtdIns(4)P accessibility or abundance as reason for observed effects. Even though *in vitro*, the GFP-2xPH^{ScOsh2} FLARE was described to not only bind to PtdIns(4)P but also other PIPs (86, 87) in combination with results that *ScSFH1* (*2μ*) expression did not change GFP-FYVE^{EEA1}, GFP-2xPH^{HsPlcδ1} localization (Fig S4B and S4C) and did not change PtdIns(3)P, PtdIns(3,5)P2 or PtdIns(4,5)P_2 levels *in vivo* (Fig 3H) our findings suggest that *ScSFH1/AtSFH5* (*2μ*) expression either affects accessibility or levels of PtdIns(4)P. Further, our findings that *ScSFH1* (*2μ*) expression did not dramatically alter PtdIns(4)P levels in Wt yeast (Fig 4A) or *mss4^{ts}* at semi-restrictive temperatures suggest that ScSfh1 might rather affect specific pools than affecting global PtdIns(4)P abundance at the PM.

Preliminary data provide hints that ScSfh1 has no PtdIns(4)P transfer activity *in vitro*

Lipid binding characteristics of ScSfh1 affect its ability to increase Al tolerance, to partially rescue *mss4^{ts}*-related defects and correlates with a change in PtdIns(4)P FLARE GFP-2xPH^{ScOsh2} distribution. Thus, we wondered whether Sfh1 might affect PtdIns(4)P FLARE localization by a direct PtdIns(4)P transfer. To address this possibility, in a collaboration with Chris Stefan and Taki Nishimura (MRC London), we performed PtdIns(4)P transfer assays (Fig 5A) based on (88). As expected and previously shown, we detected robust PtdIns(4)P transfer activity for ScOsh6 Δ69 serving as a positive control for the assay (Fig 5B and (88)). In contrast, ScSfh1 did not display PtdIns(4)P transfer activity in this assay (Fig 5B) suggesting that direct PtdIns(4)P transfer may not be responsible for relocalization of GFP-2xPH^{ScOsh2} localization in *ScSFH1*(*2μ*) expressing cells. It needs to be mentioned that for two reasons these results need to be considered as preliminary: i) the experiment was only performed once and ii) recombinant proteins where shipped from Germany to England and we cannot be sure if they were still active. This experiment needs to be repeated and a positive control (e.g. PtdIns *in vitro* transfer activity) needs to be included.

ScSFH1 (*2μ*) expression affects PtdEtn and PtdCho homeostasis

To address if *ScSFH1* (*2μ*) expression altered PL fluxes *in vivo,* we performed pulse experiments with ^{32}P-labeled orthophosphate to detect even small changes in PL metabolism as a potential consequence of Sfh1-dependent *in vivo* lipid transfer. After a 60 min pulse of ^{32}P-orthophosphate, we did not observe differences in PtdIns(4)P abundance after expression of *ScSFH1* (*2μ*). However, we observed an increase of PtdCho and, to a lesser degree, an

increase of PtdEtn when *ScSFH1* was overexpressed (Fig 5C) indicating that ScSfh1 influences PtdCho and/ or PtdEtn biosynthesis rates. This activity was strongly compromised in transformants expressing the PtdCho binding mutant (ScSfh1$^{S175I, T177I}$, Fig 5C, 5D, 5E and 5F). In contrast, transformants expressing the PtdIns binding mutant (ScSfh1^{T238D}) displayed a strong increase in biosynthesis rates of the aminophospholipids PtdEtn and PtdCho (Fig 5C, 5D, 5E and 5F). Thus, the ability to increase PtdEtn and PtdCho biosynthesis rate of ScSfh1 and the respective PL binding mutants correlated with the ability to mediate Al tolerance, to partially rescue *mss4^{ts}*-related defects and to alter PtdIns(4)P FLARE PM localization.

Mutants yeast strains impaired in PtdEtn and PtdCho biosynthesis exhibit altered PtdIns(4)P FLARE distribution

To investigate whether PtdIns(4)P FLARE localization is regulated by aminophospholipid levels independent of *ScSFH1* (*2μ*) expression, we employed mutants of the major biosynthesis route of PtdEtn and PtdCho, *psd1Δ psd2Δ* and *cho2Δ opi3Δ* (Fig 5G, for PL profiles see Fig S6A). Additionally, we tested the effect of bypassing the ScPsd1/2-, ScCho2-, ScOpi3-dependent methylation pathway by the addition of ethanolamine (Etn) and choline (Cho) or only Cho to growth media enabling PtdEtn or PtdCho biosynthesis via the Kennedy pathway (Fig 5G). Interestingly, in wild type cells, addition of 1 mM Cho increased PM localization of GFP-2xPH^{ScOsh2} significantly whereas simultaneous addition of 1 mM Etn and 1 mM Cho led to a weak but significant decrease of PM localization (Fig S6B, S6C, S6D and S6E). Furthermore, in absence of Etn or Cho, for *psd1Δ psd2Δ* and *cho2Δ opi3Δ*, we observed a significant decrease of PM localization of GFP-2xPH^{ScOsh2} (Fig S6B, S6C, S6D and S6E). Since the presence of Etn and/or Cho in the growth media had effects on of GFP-2xPH^{ScOsh2} in wild type yeast, we normalized the relative PM localization obtained in the mutant strains to wild type ratio in respective media (Fig 5H and 5I). Microscopic images along with not normalized data are shown in Fig S6B, S6C, S6D and S6E, respectively. Interestingly, for *psd1Δ psd2Δ*, addition of Cho alone did significantly increase PM localization of GFP-2xPH^{ScOsh2}, however not to wild typic levels of PM localization (Fig 5H). In contrast, PM localization was fully rescued by addition of Etn and Cho (Fig 5H). For *cho2Δ opi3Δ*, addition of Cho was sufficient to rescue PM localization of GFP-2xPH^{ScOsh2} (Fig 5I). The data presented under this headline have to be considered preliminary and need independent repetitions. Taken together, our preliminary findings suggest that yeast strains impaired in PtdEtn and PtdCho biosynthesis exhibit an altered GFP-2xPH^{ScOsh2} localization suggesting an influence of PtdEtn and PtdCho on PtdIns(4)P abundance or accessibility.

A change in PtdEtn abundance by *PSD2* (*2μ*) expression affected Al tolerance, *mss4*^{ts} growth performance and PtdIns(4)P FLARE distribution

To investigate whether changes in PtdEtn abundance alone increased Al tolerance, we overexpressed *ScPSD1* or *ScPSD2* and tested Al tolerance. Interestingly, in contrast to mitochondrial localized *ScPSD1* (Zinser et al., 1991), *ScPSD2* (*2μ*) expression, robustly increased Al tolerance (Fig 5J). Additionally, *ScPSD2* (*2μ*) expression partially rescued *mss4*^{ts} defects (Fig 5K) and preliminary data suggested a significant increase in GFP-2xPH^{ScOsh2} PM localization (Fig 5L and S6F). Interestingly, TLC-based PL analysis indicated that *ScPSD2* (*2μ*) expression mainly increased PtdEtn levels at the expense of PtdSer, but did not affect PtdCho levels (Fig S6A). To investigate whether expression of *ScSFH1* (*2μ*) increased PtdEtn at the PM we used the drug Duramycin, which has been reported to bind to PtdEtn at the PM leading to a transbilayer movement of lipids resulting in cell death (89-91). Expression of *ScPSD2* (*2μ*) led to hypersensitivity to Duramycin (Fig 5M) showing that overall increase of PtdEtn affected the Duramycin sensitivity. Interestingly, expression of *ScSFH1* (*2μ*) increased Duramycin sensitivity as well (Fig 5N). In agreement with a stronger efficiency of *SFH1* (*2μ*) to increase Al-tolerance and rescue *mss4*^{ts} associated defects, growth inhibition was stronger than that observed for *ScPSD*2 (*2μ*) expressing transformants. In line with our previous finding, *ScSFH1*^{S175I,T177I} did not alter Duramycin sensitivity (Fig N). Taken together, these findings suggest that an increase of PtdEtn increases Al tolerance and counteracts *mss4*^{ts} -related defects at semi-restrictive temperatures. Further, based on the Duramycin assays our data provide first hints that ScSfh1 changes PtdEtn abundance at the PM.

A coupled transfer of PtdCho and PtdEtn mediated by ScSfh1.

ScSfh1 and the ScSfh1* activation mutant catalyzes the energy-independent transfer of PtdCho between membrane bilayers *in vitro* (74). Additionally, ScSfh1 purified from *E.coli* accommodated almost exclusively bacterial PtdEtn as determined by mass spec analyses (92) and crystallized with PtdEtn in the lipid binding pocket (75). These findings raise two questions: i) Do ScSfh1 and respective lipid binding mutants transfer PtdEtn *in vitro* and ii) is PtdCho transfer coupled with PtdEtn transefer? To address these questions we established an *in vitro* PL transfer assay with defined big sucrose-loaded donor liposomes (L_D: PtdCho:PtdSer in a ratio of 1:10 supplemented with ^{14}C-PtdCho or ^{14}C-PtdEtn:) and defined light acceptor liposomes (L_A, PtdSer or PtdEtn:PtdSer in a ratio of 1:10), which are separable

by centrifugation (Fig 6A). We observed a robust transfer of ^{14}C-PtdCho by ScSfh1 and the PtdIns-binding mutant ScSfh1^{T238D} (Fig 6B). As expected, ^{14}C-PtdCho transfer was absent for the PtdCho-binding mutant ScSfh1^{S175,S177I}. Interestingly, increasing PtdCho levels in L_A from 0 to 10 mol% increased ^{14}C-PtdCho transfer activity for ScSfh1 and for ScSfh1^{T238D}. For ScSfh1 we also observed an increase of ^{14}C-PtdCho transfer by increasing PtdIns level in L_A from 0 to 10 mol% (Fig 6B). This increase was absent for ScSfh1^{T238D} (Fig 6B). These results were in accordance to literature (75) and confirm that the *in vitro* PL transfer protocol employed represents a valuable new tool for studying effects of PL composition on lipid transfer. Substituting ^{14}C-PtdCho with radiolabeled ^{14}C-PtdEtn showed that ScSfh1 was able to transfer PtdEtn *in vitro* as well (Fig 6C). Surprisingly, despite of similar binding modes of PtdEtn and PtdCho, ^{14}C-PtdEtn transfer was only slightly reduced in ScSfh1^{S175,S177I} (Fig 6C). ScSfh1^{T238D} showed ^{14}C-PtdEtn transfer activities comparable to ScSfh1 wild type (Fig 6C). To address if PtdCho and PtdEtn are coupled, we tested ^{14}C-PtdCho transfer into L_A supplemented with 10 mol% PtdEtn. Interestingly, the presence of PtdEtn led to a ~ 40 % increase of ^{14}C-PtdCho transfer (Fig 6D). However, increase of ^{14}C-PtdCho transfer was 4 times higher when PtdCho levels were increased from 0 to 10 mol% in L_A suggesting PtdCho as superior counter substrate. Taken together our results show that ScSfh1 is able to transfer PtdCho and PtdEtn between unilammelar liposomes *in vitro*. Furthermore, supplementation of L_A with PtdEtn stimulated PtdCho transfer. Interestingly, the PtdCho lipid binding mutant, ScSfh1^{S175I,S177I}, still displayed robust PtdEtn transfer *in vitro*. Together with the result that expression of *ScSFH1^{S175,S177I}* (*2μ*) did not increase Duramycin sensitivity, this suggests a coupling of PtdCho and PtdEtn transfer *in vivo*.

A translational eGFP-AtSFH5 fusion localizing to PM and a specific pool of lipid droplets (LDs) robustly increased Al tolerance

To address the question, which membranes might be involved in such a PtdEtn/PtdCho transfer we looked at the localization of ScSfh1-GFP and of eGFP-AtSFH5. The latter contains a Nlj16 domain, which was shown to be involved in membrane targeting (67). Both the expression of ScSFH1-GFP (*CEN, pPMA1*) fusion and the *EGFP-AtSFH5* (*2μ*) fusion were functional as shown by increase in Al (Fig S6G and 7A). As previously shown (93), ScSfh1-GFP showed a diffuse localization in the cytosol and the nucleus (Fig S6H). To address the question whether ScSfh1-mediated Al tolerance is based on a cytosolic and/or nuclear activity of ScSfh1, we tested the ability of ScSFH1-GFP fused to a nuclear localization signal (NLS) or a nuclear export signal (NES, Fig S6H) to mediate Al tolerance.

519 Interestingly, expression of *ScSFH1-GFP-NLS* (*CEN, pPMA1*) only slightly increased Al
520 tolerance, which was to a lesser extent than expression of *ScSFH1-GFP* (*CEN, pPMA1*) and
521 *ScSfh1-GFP-NLS* (*CEN, pPMA1*). Furthermore, expression ScSFH1-GFP-NES (*CEN,*
522 *pPMA1*) slightly increased Al tolerance when compared to ScSFH1-GFP (*CEN, pPMA1*)
523 expression. Together, these findings suggest that the ability to mediated Al tolerance is based
524 on a cytosolic activity of ScSfh1. However, the diffuse cytosolic localization did not allow us
525 to draw any conclusions on the involvement of certain membrane. Therefore, we looked at the
526 localization of eGFP-AtSFH5. Interestingly, eGFP-AtSFH5 localized to punctate structures,
527 which were observed in close proximity to the PM (Fig 7B). Additionally, by using the
528 PtdIns(4,5)P_2 mCherry-Nlj16^{AtSFH1} FLARE as PM membrane marker (67), we observed that
529 eGFP-AtSFH5 partially localized to the PM in a patchy pattern. To identify the origin of
530 observed localization pattern we performed correlative light and electron microscopy. The
531 punctate fluorescent signal always coincided with round structures framed by lipid
532 monolayers corresponding to lipid droplets (LDs, Fig 7C). Interestingly, the PM signal of
533 eGFP-AtSFH5 coincided with cortical endoplasmic reticulum (ER, Fig 7C) suggesting
534 localization at ER-PM contact sites. However, localization of Cerulan-AtSFH5 in a *tetherΔ*
535 yeast strain with dramatically reduced number of ER-PM contact sites showed that in contrast
536 to the ER-PM contact site marker, ScTcb3-GFP, Cerulan-AtSFH5 localization was
537 comparable to its localization in wild type yeast (Fig S6I) suggesting that AtSFH5 PM
538 recruitment was independent of ER-PM contact sites. Using confocal microscopy, we
539 observed that eGFP-AtSFH5 localized at the LD surface (Fig 7D). Interestingly, eGFP-
540 AtSFH5 localization was enriched at the site facing the PM. Co-localization analysis with the
541 PtdIns(4,5)P_2 FLARE mCherry-Nlj16^{AtSFH1} showed that, in contrast to PM-localized eGFP-
542 AtSFH5, LD-localized eGFP-AtSFH5 never showed co-localization (Fig 7D and 7E).
543 Interestingly, at sites where the fluorescent signal of LD-localized eGFP-AtSFH5 was
544 enriched towards the PM, we hardly detected any mCherry-Nlj16^{AtSFH1} fluorescence (Fig 7D
545 and 7E). Furthermore, the surface co-localization of eGFP-AtSFH5 and mCherry-Nlj16^{AtSFH1}
546 revealed that at sites of LD-localized eGFP-AtSFH5, mCherry-Nlj16^{AtSFH1} fluorescence was
547 absent suggesting that the presence of LDs, closely localized to the PM, affected either the
548 presence of PtdIns(4,5)P_2 or its accessibility for mCherry-Nlj16^{AtSFH1} (Fig 7F and 7G). This
549 observation might suggest the existence of so far not yet described LD-PM contact sites.
550 Taken together, localization of eGFP/Cerulan-AtSFH5 to the LD surface of a subpool of LDs
551 (only those in close proximity to the PM) suggests that AtSFH5 might mediate transfer of

PtdCho and PtdEtn between LDs and the PM or between different pools at the PM itself thereby enriching PtdEtn at the PM at the expense of PtdCho.

Al treatment decreases FLARE recruitment to the PM

PtdEtn was suggested to change protonation state and hence negativity of phosphatidic acid (PtdOH) through inter-lipid H bonds (94, 95). If a potential ScSfh1-mediated increase of PtdEtn at the PM was able to affect the protonation status of PtdIns(4)P (and other lipids) as well, one would expect an overall increase of negative charge at the PM. To test this hypothesis we used the amphipathic motif of ScSpo20 fused to GFP (ScSpo20-GCC-GFP) described to be sensitive to membrane charge (96). In agreement with an overall increase in PM charge, *ScSFH1* (*2μ*) expression increased PM localization of the ScSpo20-GCC-GFP bioprobe (Fig 8A and S7A). Endomembrane localization of ScSpo20-GCC-GFP was severely reduced by *ScSFH1* (*2μ*) expression (Fig S7A). Interestingly, expression of $ScSFH1^{T238D}$ (*2μ*), but not $ScSFH1^{S175I,S177I}$, did resemble expression of wild type *ScSFH1* (*2μ*) in accordance to activity patterns of ScSfh1 and its lipid binding mutants in regard to Al tolerance, $mss4^{ts}$ partial rescue and GFP-2xPH^{ScOsh2} sensor redistribution. These results raised the question if mediation of Al tolerance by ScSfh1/AtSFH5 is based on alteration of negative membrane charge, in particular of the PM as membrane with highest negative charge (26) and if the PM might represents a direct target of Al *in vivo*. To this end we tested if Al treatment at subtoxic levels (150 μM, Fig S7B) affected PM localization of the ScSpo20-GCC-GFP bioprobe and of several FLAREs. In accordance with the idea that Al directly binds to the PM thereby changing its physico-chemical properties, we observed a decrease of PM/intracellular ratio of fluorescent signals for all tested sensors (Fig 8B and Fig S7C). This finding suggests that Al binds to the PM *in vivo* thereby affecting localization of PM binding proteins. To corroborate this idea, we tested if an overall decrease of negatively charged lipids would render yeast more sensitive to Al treatment. Indeed, yeast mutant defective in PtdSer, PtdIns(4)P and PtdIns(4,5)P_2 (*cho1Δ, $pik1^{ts}$, $stt4^{ts}$ and $mss4^{ts}$*) were more sensitive to Al treatment (Fig 8C). Vice versa, we tested if an overall increase of negatively charged PLs would increase Al tolerance. Indeed, as previously shown, expression of the wheat PtdSer synthase *TaPSS1* (*2μ*) increased Al tolerance (Fig S7D, (97)). Additionally, expression of *ScMSS4* (*2μ*) increased Al tolerance, as well (Fig 8D). As shown in Fig 2H and 2I, *ScSFH1* (*2μ*) expression increased PM localization of mCherry-ScRho1. Interestingly, ScRho1 was shown to be targeted to the membrane by the negatively charged lipids PtdIns(4,5)P_2 and PtdSer (81, 82). Since *ScSFH1* (*2μ*) did not increase PM localization of the PtdSer FLARE GFP-LactC2 (Fig S4D and S4E) we performed an *in silico* analysis using the basic hydrophobic (BH)-search algorithm (98,

586 99) to identify polybasic sequences possibly enabling charge dependent rather than
587 stereospecific PM recruitment. The analysis of the ScRho1 primary amino acid sequence
588 revealed a C-terminal polybasic sequence, with a BH-score higher than the threshold of 0.6
589 (Fig 8E). Interestingly, this motif was reported to be crucial for correct PM targeting *in vivo*
590 (81). Further testing of the ScSfh1 PtdCho and PtdIns binding mutants revealed that increased
591 PM localization of mCherry-ScRho1 was only mediated by wild type ScSfh1 and ScSfh1^{T238D}
592 (Fig 8F and 8G). In contrast, ScSfh1$^{S175I,\ T177I}$ only poorly affected mCherry-ScRho1 PM
593 localization. These results suggest that ScRho1 is recruited to the PM by charge dependent
594 mechanism. Since the ScRho family was linked to the rescue of *mss4–2^{ts}* (50) defects, we
595 tested if ScRho1 and the close homolog ScRho2 increased Al tolerance. Unfortunately,
596 expression of *ScRHO1* (*2μ*) severely impaired yeast growth on mock media (Fig S7E),
597 making an interpretation of Al tolerance difficult. Interestingly, the expression of the partial
598 redundant ScRho1 homolog (22), *ScRHO2* (*2μ*), described as suppressor of *mss4–2^{ts}*
599 increased Al tolerance as well (Fig S7F). Taken together, these results suggest that ScSfh1-
600 mediated changes in PM charge affect Al tolerance and growth of *mss4^{ts}* at semi-restrictive
601 temperature by increasing charge dependent PM recruitment of proteins, e.g. involved in CWI
602 signaling. Further these data suggest that overall PM charge is a primary toxicity target of Al.

603 ## Negative charge of the PM affected Al tolerance in plants

604 To investigate whether negative charge of the PM influences Al tolerance in plants as well,
605 we analyzed primary root growth of mutants defective in the biosynthesis of negatively
606 charged PLs on solid media containing subtoxic Al concentration (12-15 μM, media was
607 developed by (100, 101)). Interestingly, *atpss1-3* (59) defective in PtdSer biosynthesis,
608 *atpi4kβ1 atpi4kβ2* defective in PtdIns(4)P biosynthesis (102, 103), *atpip5k1* and *atpip5k1*
609 *atpip5k2* (55) impaired in PtdIns(4,5)P_2 biosynthesis exhibited all a significantly reduced
610 relative primary root growth when treated with Al (Fig 9A-9D). Vice versa using a line
611 expressing *AtPIP5K3* under the control of an estradiol inducible promoter shown to display
612 increased overall PtdIns(4,5)P_2 level in presence of estradiol (104), significantly increased
613 relative root growth after Al treatment (Fig 9E). Together these data resembled growth
614 phenotypes on Al containing media of yeast mutants with changes in the biosynthesis of
615 negatively charged PLs (Fig 8C and 8D) suggesting that also in plants, Al might affect the
616 negative charge of the PM directly and might alter proper PM recruitment of PM binding
617 proteins. To address this further, we investigated localization of cYFP-KA1^{HsMARK1} described
618 as charge sensor (27, 28) and FLAREs for PtdSer (cYFP-LactC2), PtdIns(4)P (cYFP-P4M)
619 and PtdIns(4,5)P_2 cYFP-2xPH$^{HsPlc\delta1}$ (27, 105) after Al treatment. As observed in yeast (Fig

620 8B), also in plants the PM/intracellular ratio significantly decreased after Al treatment for
621 cYFP-KA1^{HsMARK1}, cYFP-LactC2 and cYFP-P4M (Fig 9F and 9G). Interestingly only after
622 Al treatment, cYFP-KA1^{HsMARK1} and cYFP-P4M sensors decorated endomembrane structures
623 (Fig 9F), suggesting charge reduction primarily of the PM. For cYFP-2xPH$^{HsPlc\delta1}$ FLARE,
624 localization in mock conditions differed substantially from plant to plant. Therefore, time
625 course experiments were performed selecting plants with cYFP-2xPH$^{HsPlc\delta1}$ exclusively
626 localized to the PM. Also for PtdIns(4,5)P_2 FLARE 2xPH$^{HsPlc\delta1}$ the PM/intracellular ratio
627 significantly decreased after Al treatment (Fig 9H). These results were in accordance to
628 results observed in yeast (Fig 8B) and indicate a general mode of Al toxicity. To test if PM
629 recruitment of endogenous plant proteins would be affected by Al treatment, we tested the
630 localization of the AGC3 kinase ARABIDOPSIS THALIAN PINOID (AtPID), which was
631 shown to localize to the PM charge dependently (27). In accordance with Al affecting
632 negative charge of the PM, also the PM/intracellular ratios for AtPID-YFP and YFP-AtPID
633 were significantly reduced by Al treatment (Fig 9I, 9J, S8A and S8B). AtPID was described
634 to influence localization of the ARABIDOPSIS THALIANA PIN FORMED (AtPIN) protein
635 family (106). Effects of loss of PID function on PIN localization in roots were so far only
636 described for AtPIN2 in the *pid-9* loss-of-function allele resulting in an accumulation of
637 AtPIN2 endomembrane structures (107). Interestingly, also Al treatment led to an
638 accumulation of AtPIN2-GFP in endomembrane structures (Fig 9K) in accordance with
639 reduced PID activity. Furthermore, the fluorescent signal of AtPIN2-GFP increased at the PM
640 indicating a more general influence of Al on AtPIN2 cycling, as already described by (108).
641 Additionally, we observed a wavy phenotype for primary roots grown on Al-containing media
642 (Fig 9L), which resembled phenotypes described for mutant lines of the AGC3 kinase family
643 (109). Taken together our results indicate the Al is influencing the negative charge of the PM
644 *in vivo* in plants and yeast thereby changing recruitment of membrane targeted proteins
645 indicating the charge of PM as primary toxicity target of Al.
646

Discussion

Al is toxic for microbes, mammals and plants. It is discussed to be involved in several important processes such as the growth and composition of bacterial communities in soil (110), neurodegenerative diseases (111, 112) and it was shown to decrease root growth representing one of the biggest abiotic limitations for crop production worldwide (4, 5). In spite of intensive research efforts, direct targets of Al on a cellular level remain elusive. Here we report an unbiased approach to unravel cellular targets of Al toxicity using yeast genetics. Together our data provide evidence that negative PM charge is a primary toxicity target for Al in yeast and plants.

ScSFH1 (*2μ*) expression increases overall PM charge along increased PM localization of PtdIns(4)P FLARE probably by establishing a different PtdIns(4)P pool at the PM

Expression of *ScSFH1* (*2μ*) led to a robust increase of Al tolerance alongside an increase of PM targeting of membrane sensors and endogenously PM recruited proteins (Fig 2, 4, 8 and S5). Notably, steady state PL levels were not changed through *ScSFH1* (*2μ*) expression (Fig 4A). Localization studies with different FLAREs showed that PtdIns(4)P FLARE exhibited increased PM localization after *ScSFH1* (*2μ*) expression (Fig 4B and 4C). In contrast, PM localization of FLAREs for PtdSer, PtdIns(3)P, PtdIns(4,5)P_2 was not increased (Fig S5). While a ScSfh1 PtdIns binding mutant was behaving like wild type ScSfh1, a PtdCho binding mutant failed to induce an increase in PM recruitment of the PtdIns(4)P FLARE GFP-2xPH^{ScOsh2} (Fig 4B and 4C). This observation correlated with the observed Al tolerance phenotypes. Further, Al tolerance mediated by AtSFH5 and the *ScSEC14* Al tolerance activation allele *ScSEC14*^{S173P} induced PtdIns(4)P FLARE PM association as well. Analysis of the charge sensor GCC-GFP indicated that *ScSFH1* (*2μ*) expression increased overall negative charge at the PM. This correlated with an increase of PM recruitment of ScRho1-mCherry and ScPkc1-GFP. Based on these findings, two models for cellular ScSfh1 function arose: i) ScSfh1 increases PtdIns(4)P at the PM by direct *in vivo* transfer of PtdIns(4)P from endomembranes with PM localized PtdCho as counter lipid (Fig 10A) or ii) ScSfh1 indirectly changes lipid accessibility at the PM resulting in a changed PM recruitment of the tested PtdIns(4)P FLARE, charge sensors and endogenous proteins (Fig 10B). To address the first model of direct PtdIns(4)P/PtdCho *in vivo* transfer, we exploited an *in vitro* transfer system for PtdIns(4)P (113). Notably, in our preliminary results, ScSfh1 did not exhibit PtdIns(4)P

679 transfer activity (Fig 5B) questioning this model. Furthermore, our TLC- and HPLC-based
680 analysis of PtdIns(4)P levels *in vivo* (Fig 3H, 4A and 5C) revealed that *ScSFH1*(*2μ*) did not
681 affect PtdIns(4)P levels dramatically. Even though these results question that ScSfh1 transfer
682 PtdIns(4)P *in vivo*, we cannot exclude that PtdIns(4)P abundance in certain pools is altered
683 through *ScSFH1* (*2μ*) expression and that for *in vitro* transfer ScSfh1 needs unknown co-
684 factors.
685 Interestingly, pulse experiments with ^{32}P-labeled orthophosphate revealed that *ScSFH1* (*2μ*)
686 expression changed the biosynthesis rate of PtdEtn and PtdCho (Fig 5C - 5F). Furthermore,
687 tested ScSfh1 lipid binding mutants exhibited the same activity pattern as for Al tolerance.
688 These findings suggest that Sfh1-dependent binding or transfer of PtdEtn/PtdCho might be
689 involved in the observed phenotype. In accordance, in our genome wide screen we identified
690 ScCho2 as essential for ScSfh1-mediated Al tolerance (Table S2), we observed that an
691 increase in PtdEtn levels mediated by *ScPSD2* (*2μ*) expression increased Al tolerance and that
692 *ScSFH1* (*2μ*) expression increased sensitivity to Duramycin sensitivity, reflecting a higher
693 PtdEtn availability at the PM (Fig 5N). In agreement with the reported phenotypes, the
694 ScSfh1 PtdCho binding mutant did not alter the sensitivity to this compound (Fig 5N). These
695 findings suggest that ScSfh1 is increasing PtdEtn at the PM. ^{14}C-PtdCho and ^{14}C-PtdEtn *in*
696 *vitro* transfer assays showed that ScSfh1 robustly transferred PtdEtn and PtdCho and that
697 PtdCho transfer can be stimulated by presence of PtdEtn in acceptor membranes (Fig 6).
698 Thus, based on these findings we propose that ScSfh1 might increase PM PtdEtn levels by a
699 PtdEtn transport to the PM that is potentially energized by an Sfh1-dependent back transport
700 of PtdCho. This model is supported by the finding that even though the ScSfh1 PtdCho
701 binding mutant robustly transfers PtdEtn *in vitro* (Fig 6C) we did not observe an increased
702 Duramycin sensitivity or a change of the PtdCho/PtdEtn biosynthesis rate (Fig 5C-F).
703 But how can PtdEtn abundance at the PM might alter PM charge and PM recruitment of a
704 PtdIns(4)P FLARE? In 2005, Kooijman and colleagues (94) proposed that PtdEtn can change
705 the protonation status of PtdOH through interlipid contacts, resulting in higher negative
706 charge of PtdOH. Since lipid binding or membrane binding domains are coordinated by
707 positively charged amino acid residues, a change in the protonation state might subsequently
708 change the accessibility of PtdOH. If a similar mechanism took place for PtdIns(4)P one
709 would expect that mutants impaired in the PtdEtn biosynthesis would have an altered
710 PtdIns(4)P distribution. Interestingly, preliminary data suggested that PtdIns(4)P FLARE PM
711 localization was decreased in a *psd1Δ psd2Δ* (Fig 5H), suggesting that PtdEtn abundance
712 indeed affects PtdIns(4)P accessibility or distribution. In the same line we preliminarily

observed that *ScPSD2* (*2μ*) expression increased PM recruitment of the tested PtdIns(4)P FLARE (Fig 5L). Furthermore, if the proposed PtdEtn/PtdCho heterotypic transfer model operates *in vivo*, one would expect the same phenotypes for PtdIns(4)P FLARE distribution in mutants with impaired PtdCho synthesis. Notably, indeed we preliminarily observed a decrease in PM recruitment of the tested PtdIns(4)P FLARE in the *cho2Δ opi3Δ*, a strain devoid of PtdCho biosynthesis (Fig 5I). Together our data provide first evidence that PtdEtn abundance might change accessibility of PtdIns(4)P - potentially by an altered the protonation state of PtdIns(4)P - thereby changing overall PM charge, protein recruitment to the PM and possibly defining different PM PtdIns(4)P pools (Figure 10). In future, it will be important to investigate whether PtdEtn indeed can change the protonation state of lipids other than PtdOH. Further, it will be crucial to determine if PtdEtn is able to influence the affinity of different lipid binding domains (e.g. for PtdIns(4)P) and how PtdEtn, which is reported to be highly abundant at the inner leaflet of the PM (114), might be enriched through PtdCho transfer activity.

Do PL affinities determine ScSec14/ScSfh1-mediated lipid transfer *in vivo*?

Our transfer experiments with defined acceptor membranes reveal that composition of membranes influences the transfer rate of PLs by ScSfh1. A prerequisite for classical ScSec14 function is to bind PtdIns and PtdCho (75). Strikingly, the PtdIns binding mutant is still able to increase Al tolerance (Fig 1C and S1E), to partially rescue *mss4*^{ts}-related growth defects and PtdIns(4)P FLARE redistribution similar to wild type ScSfh1 (3B, 4C, 5C and 8G). This is in accordance with phenotypes being independent of classical ScSec14 function (Fig 1B, S1A, S1B and S1C). The directed evolution screen presented here revealed a S173P substitution as sufficient to activate ScSec14 in terms of mediation of Al tolerance and increasing PtdIns(4)P accessibility (Fig 4F, 4G, 4H and S5). Interestingly, S173 is involved in the coordination of PtdCho (75). Notably, the ScSec14^{S173P} rescued *sec14-1*^{ts} related growth defects comparable to wild typic ScSec14 (Fig S5B) indicating that PtdCho binding is not impaired. This leads to the question how the S173P substitution in ScSec14 renders ScSec14 active in terms of mediating Al tolerance and PtdIns(4)P FLARE redistribution. One possible explanation might be that the amino acid substitution influences overall PL binding affinities to different PL species thereby influencing *in vivo* lipid transfer. Following this idea, a model arises in which lipid binding affinity is a determinant for lipid transfer into certain membranes, pools or domains and define cellular functions and activities of different structurally close related ScSec14-type proteins with comparable *in vitro* transfer activities. Interestingly, ScSfh1 was recently proposed to transfer PtdSer between the ER and

endosomes when only non-fermentable carbon sources are available thereby indirectly changing ScPsd1-dependent PtdEtn levels at the mitochondria (115). In the line that PL transfer mediated by ScSfh1 might depend on the lipid binding properties, ScSfh1 lipid transfer might also be affected by the lipid composition of membranes. Interestingly, the lipid composition significantly changes when different carbon sources are used (116). Thus, in future it will be interesting to address if lipid transfer routes of LTPs, such as ScSfh1, are affected by the composition of donor or acceptor membranes. Therefore, it will be interesting to exploit the presented *in vitro* PL transfer assay. With this synthetic system it will be possible to address whether a change in the composition of L_A can influence the transfer rates of different ScSec14 homologs. In the same line it will be interesting to compare PtdEtn, PtdCho and PtdIns transfer rates of ScSec14^{S173P} with the rates of wild type ScSec14, ScSfh1 and the ScSec14 activation allele ScSfh1^{Y113C} (74).

Which membranes are involved in ScSfh1/AtSfh5-mediated lipid transfer?

To address which membranes might be involved in the proposed the ScSfh1-mediated PtdEtn/PtdCho transfer we also investigated AtSFH5, which phenocopies ScSfh1. We localized a functional eGFP-AtSFH5 protein fusion in yeast. Nlj16 domains were shown to bind PtdIns(4,5)P_2 and to be involved in membrane recruitment *in vivo* (67). Interestingly, in contrast to the single AtSFH5^{Nlj16} domain, which recruits a fluorophore fusion to nucleus-like structures (67), we found that eGFP-AtSFH5 localizes to the PM and the LD surface to a specific sub pool of LD closely localized to the PM. This finding indicates that not only the Nlj16 domain but also the ScSec14 domain of AtSFH5 determines cellular localization. Strikingly eGFP-AtSFH5 localization is enriched at the PM-oriented site of the LD subpool. Furthermore occurrence of eGFP-AtSFH5 LD signal close to the PM seems to repel the PtdIns(4,5)P_2 binding mCherry-AtSFH1^{Nlj16} protein fusion (Fig 7D-G). This finding suggests the existence of, not yet described, LD-PM contact sites. In future it will be interesting to see if the eGFP-AtSFH5 decorated LD pool are naturally occurring LDs or if AtSFH5 drives production of these LDs by a ScSfh1-like activity. Since AtSFH5 phenocopies ScSfh1 in regard to Al tolerance and PtdIns(4)P accessibility, it is an interesting idea that the dual localization of AtSFH5 to the PM and LD provide a hint that PtdEtn/PtdCho transfer might occur between the PM and LD. Indeed it was shown that PtdCho and PtdEtn are highly abundant in LD monolayers (117). Thus, it will be interesting to address if ScSfh1/AtSFH5 can still increase Al tolerance and change lipid accessibility in mutants lacking LDs (118) and if these mutants show a change in overall PM charge. Furthermore, ScSlc1, involved in PA biosynthesis, was identified in the LD proteome (119) and it was reported that *slc1Δ* mutant

781 yeast have altered LD contents (120). Interestingly, we identified *slc1Δ* in our genome wide
782 screen, suggesting that ScSlc1 function is essential for ScSfh1-mediated Al tolerance. Notably
783 ScSlc1 was reported to be redundant to ScSlc4 in terms of overall PA synthesis (121). A
784 specialized function for ScSlc1 at LD monolayers, maybe driving PtdEtn synthesis, might
785 explain why ScSlc1 alone is essential for ScSfh1 to mediate Al tolerance. Even though lipid
786 transfer between LDs and the PM is an attractive hypothesis it needs to be stated that ScSfh1
787 localizes to the cytoplasm and the nucleus (Fig S6H), and that, even though majority of the
788 signal is located to the PM and LDs, eGFP-AtSFH5 also localizes to the cytosol. Thus, future
789 experiments will have to address membranes involved in ScSfh1 lipid transfer. To address
790 this, it will be interesting to generate ScSfh1 fusions, with different lipid binding domains
791 facilitating the recruitment to different membrane pools and observe stimulation of Al
792 tolerance.

793 ## CWI and Al

794 In plants, Al treatment leads to a substantial cell wall thickening, to remodeling of cell wall
795 composition and to a decreased mechanical extensibility of the cell wall (16, 17). In the model
796 organism *S. cerevisiae* two independent genetic screens identified yeast impaired in CWI
797 signaling as more sensitive to Al treatment (24, 25) suggesting that remodeling of cell wall
798 composition is involved in yeast tolerance to Al. Here, we show that Al treatment triggers
799 CWI signaling as evident by increased ScMpk1 phosphorylation (Fig 2G). ScMpk1
800 phosphorylation occurs rapidly after 30 min of Al treatment and endures at least 8 h (Fig 2G).
801 Together with the findings that knock out of genes involved in CWI signaling are more
802 sensitive to Al (Fig 2B - 2D), this suggests that yeast are able to perceive Al-induced cell wall
803 stress. In contrast to mutants lacking one of the three other proposed mechano-sensors
804 (*wsc2Δ, wsc3Δ* and *mtl1Δ*), only *wsc1Δ* and *mid2Δ* are more sensitive to Al (Fig 2B)
805 corroborating that these two genes encode for the main CWI sensors and suggesting that these
806 two sensors are involved in the perception of Al induced cell wall stress in yeast (22).
807 Interestingly, even though both ScWsc1 and ScMid2 were shown to interact with ScRom2
808 (122), in the single mutants strains, *wsc1Δ* and *mid2Δ*, *ScSFH1* expression fails to induce Al
809 tolerance suggesting that ScWsc1 and ScMid2 act together. As it was proposed that cell wall
810 receptors concentration and nanoclustering influence intensity of damage signals (123-125)
811 this might play a role for ScSfh1-mediated Al tolerance, as well. Thus it would be important
812 to analyze nanoclustering of ScWsc1 and ScMid2 after Al treatment and *ScSFH1* (*2μ*)
813 expression. Furthermore, it would be interesting to analyze the cluster formation in mutants

impaired in PtdSer and PIP homeostasis to investigate whether stereospecific or charge-dependent protein-lipid interaction have an influence on ScWsc1 and ScMid2 nanoclustering. Moreover, components of the CWI pathway further downstream of ScWsc1 and ScMid2 are essential for increased Al tolerance mediated by *ScSFH1* (*2μ*) expression (Fig 2B – 2D). Further, we show that *sfh1Δ* yeast mutants are slightly more sensitive to Al (Fig 2E) and identified negative synthetic interaction of ScSfh1 with ScPkc1 (Fig 2F). This indicates an influence of ScSfh1 on CWI signaling. Surprisingly, ScSfh1 did not influence the degree of ScMpk1 phosphorylation after Al treatment (Fig 2G). However, *ScSFH1* (*2μ*) expression increase PM localization of ScRho1-mCherry and increased PM and bud tip recruitment of Pkc1-GFP. These results combined with the findings that *ScSFH1* (*2μ*) expression increased overall PM charge (Fig 8A) and that Al treatment impaired charge and stereospecific protein recruitment to the PM (Fig 8B), provide the following possible explanation for ScSfh1-mediated Al tolerance. The ScSfh1-mediated increase in PM negativity is able to counteract the Al induced decrease of PM protein recruitment, e.g. of ScRho1 and ScPkc1, thereby maintaining a functional CWI pathway longer under subtoxic Al conditions (Fig 10A and 10B). This is in accordance with the findings that proper ScRho1 localization is essential for CWI signaling (81) and that Pkc1-GFP localization is altered after cell wall stress (78, 79). To test this hypothesis, it will be interesting to analyze the localization of different CWI components after the combination of Al treatment and *ScSFH1* (*2μ*) expression.

Furthermore, our result suggest that PtdIns(4)P and/or PM charge is involved in CWI signaling. To this end it will be interesting to compare CWI signaling efficiency in a *cho1Δ* mutant with the signaling efficiency in a *sac1Δ* mutant. In a *cho1Δ* mutant strain, PtdSer, which was suggested as a main driving force for overall negative charge of the PM in yeast (26), is absent and PtdIns(4)P levels and PtdIns(4)P FLARE localization to the PM are increased (126, 127). In contrast, in a *sac1Δ* mutant PtdIns(4)P levels and PtdIns(4)P FLARE localization to PM are increased and PtdSer levels and PtdSer FLARE PM localization are decreased (63, 128). Interestingly, whereas in a *cho1Δ* mutant strain, after heat treatment Mpk1 phosphorylation is impaired (129), in a *sac1Δ* mutant Mpk1 phosphorylation is strongly activated (130). These results combined suggest that both PtdIns(4)P and PtdSer are involved in modulating CWI signaling. To explain observed results, a possible scenario might be that recruitment of ScRho1 is dependent on PtdIns(4)P or on charge of the PM and subsequent ScPkc1 activation is dependent on PtdSer as shown by (129). Along with this it is interesting to note, that we identified *sac1Δ* as a hit in our genome wide screen showing that *ScSFH1* (*2μ*) expression did not increase Al tolerance in the mutant (Table S2). This might be

explained by high PtdIns(4)P levels at the PM superposing effects of *ScSFH1* (*2μ*) expression. Furthermore, we found that an increase of the charge sensitive ScSpo20-GCC-GFP bioprobe correlated with increased PtdIns(4)P FLARE localization and did not correlate with PtdInsSer FLARE PM localization suggesting that both PtdIns(4)P and PtdSer contribute to overall charge of the PM. This is in contrast to observation that the localization of different KA1 domains, which bind to negatively charged PLs, were not altered in the *stt4*^{ts} *pik1*^{ts} double mutant at restrictive temperatures (28). Thus in future it will be interesting to investigate to what extend PtdIns(4)P and maybe PtdIns(4,5)P_2 contribute to overall PM charge. To address this question it will be necessary to compare different charge probes in temperature sensitive alleles impaired in PtdSer, PtdIns(4)P and/or PtdIns(4,5)P_2 after short term PL depletion. Furthermore, exploiting transient systems to deplete specific PLs at different membranes by PL phosphatases, e.g. using a system established by the Hammond lab (131), will be useful a tool to analyze the importance of the different negatively charged PLs on overall membrane negativity. Further it will be interesting to investigate if ScRho1 and ScPkc1 localization is charge dependent or dependent on stereospecific lipid interaction. To this end it will be interesting to mutate domains of ScRho1/ScPkc1 responsible for PM recruitment and replace them with different charge or PL binding domains and analyze the chimeric proteins in regard of CWI activity.

Our findings indicate that modulation of CWI signaling influences Al tolerance in yeast. In contrast to the well-studied CWI pathway in yeast first insights in the CWI pathway in plants are just emerging (21, 132). As possible candidates in mechano-sensing modules members of the *Catharanthus roseus* receptor-like kinase like (CrRLKL) family were suggested (21) with AtFER as most promising candidate (133). Also the phytohormone brassinosteroid (BR) along with its sensor AtBRI1, its co-receptor AtBAK1 and RLP44 were suggested to be involved in mechano-stress sensing (134). In future, it will be interesting to evaluate if Al tolerance can be increased by modulating CWI signaling and to clarify whether PL homeostasis is involved in CWI in plants as well.

PtdIns(4,5)P_2 independent rescue of *mss4*^{ts} at semi-restrictive temperatures

Expression of *ScSFH1* (*2μ*) partially suppressed *mss4*^{ts} related growth defects at semi-restrictive temperatures. In the same line also *ScPSD2* (*2μ*) expression led to a partial rescue, albeit to a lesser extent. PtdIns(4,5)P_2 analysis through SAX-HPLC of deacetylated PIPs and with the GFP-2xPH$^{HsPlc\delta1}$ FLARE specific for PtdIns(4,5)P_2 revealed that there was no influence of *ScSFH1* (*2μ*) expression on PtdIns(4,5)P_2 levels or accessibility (Fig 3H, S4B and S4C). Interestingly, the ScSfh1 PtdIns but not the PtdCho binding mutant were able to

partially rescue *mss4^{ts},* resembling the pattern observed for mediation of Al tolerance, change in PtdIns(4)P accessibility and increase in PM charge (Fig 4, 8A and S7A). These finding suggest that ScMss4 requirement can be partially bypassed by increased accessibility of PtdIns(4)P alongside an increase of overall PM charge. It is interesting to note that (82) described that under hyperosmotic shock ScRho1 recruitment to the PM, which was proposed to be mediated by increased PtdIns(4,5)P_2 levels (81), can be also medaited by PtdSer. Along with our results that suggest that ScRho1 recruitment might be charge dependent (independent of stereospecific interactions, Fig 8F and 8G) and that expression of *ScRHO2* (*2μ*), a the closest ScRho1 homolog with partially overlapping function (22), was able to partially bypass ScMss4 requirement (50) this provides a possible explanation for the observed partial rescue of *mss4^{ts}* mediated by ScSfh1. Future experiments will have to address if ScSfh1-mediated partial ScMss4 bypass is dependent on ScRho1 recruitment and to what extend PtdIns(4,5)P_2 is involved in charge dependent protein recruitment to the PM.

Plasma membrane charge influences Al tolerance and sensitivity in yeast and in plants

As barrier of the cell the PM was intensely discussed to be one early target for Al toxicity. It has been demonstrated that Al treatment is affecting overall lipid composition (135, 136) and various studies showed that Al binds to artificial liposomes and is present in microsomal fractions of different plant species (69, 137, 138). The affinity of Al to membranes increases with overall membrane charge (68) and the zeta-potential (expressing the membrane surface charge) of microsomal-based liposomes increases upon Al treatment reflecting a decrease of overall negative charge of a lipid bilayer. Based on these results, different concepts were postulated how Al might act on the PM: i) it was proposed that Al binds to the outer leaflet thereby reducing its surface charge and affecting e.g. uptake of other cations (69) and ii) it was suggested that after entering the cells Al binds to the inner, cytosolic leaflet thereby affecting activity of e.g. PM H^+-ATPase activity (71) and phospholipase C (70). However, these results are based on experiments with artificial or microsomal membranes raising the question of the influence of Al on the PM *in vivo*. Based on an unbiased yeast screen we show that increased accessibility or increased levels of negatively charged PLs increase Al tolerance in yeast and *in planta* (Fig 8C and 9D). Genetic modification of lipid biosynthesis in yeast and plants show that independent of the lipid species a reduction in negatively charged PLs (PtdSer, PtdIns(4)P or PtdIns(4,5)P_2) resulted in higher sensitivity to Al (Fig 8A, 8C, 8D and 9A-D). In contrast, increased levels of PtdSer, PtdIns(4,5)P_2 or an increase of PtdIns(4)P

FLARE recruitment along with an increase in overall PM charge also increased Al tolerance in yeast (Fig 8D and S7D). Likewise, increased PtdIns(4,5)P_2 levels resulted in higher Al tolerance *in planta* (Fig 9E). Along with these results, we show that *in vivo* lipid accessibility is changed after Al treatment. PM recruitment of charge sensors, different FLAREs and charge-dependent PM recruitment of endogenous proteins is reduced by Al treatment (Fig 8B, 8F, 8G, S7C, 9F and 9H). These results lead to a model in which Al is competing with proteins for membrane binding of the cytosolic leaflet resulting in a disruption of proper membrane targeting of proteins (Fig 11A and 11B). Our genetic data and microscopic data in yeast and plants support the idea that increasing the negative PM charge counteracts this effect and renders organisms more tolerant to Al treatment.

Physiological influence of changed PM charge *in planta*

Inhibition of root growth induced by Al treatment is caused by a combination of a reduction in cell elongation and cell division (9). Both cell elongation and cell division are complex processes and heavily dependent on extensive membrane trafficking events (139, 140). Membrane trafficking itself is facilitated by the actin cytoskeleton (141). Interestingly, both membrane trafficking and actin organization are disrupted by Al treatment (142, 143). One common regulatory component for membrane trafficking and the actin cytoskeleton are negatively charged PLs (144). Interestingly, in the presented genome wide screen besides hits representing components of CWI pathway and lipid homeostasis, various genes involved in the cell cycle, in the regulation of the cytoskeleton and in membrane trafficking were identified to be essential for ScSfh1-mediated Al tolerance (Table S2). Based on these findings the question arises if i) ScSfh1 mediates Al tolerance on several levels thereby influencing CWI, membrane trafficking and actin cytoskeleton formation, ii) does the ScSfh1-mediated increase in PM charge reflect a common feature influencing different processes or iii) does CWI signaling influence membrane trafficking and actin cytoskeleton formation directly. To address this, a combination of genetic (e.g. generation of higher order mutant strains) and microscopic (localization of components involved) approaches will be interesting to perform.

We confirmed the observation that AtPIN2-GFP trafficking is misregulated by Al treatment (Fig 9I and (108)). As shown by (108), after Al treatment we observed an increased AtPIN2-GFP signal at the PM in accordance with PM lipids involved in endocytosis of AtPIN2 (55, 103) and higher sensitivity of plant lines defective in PIP homeostasis (Fig 9B – 9D). For AtPIN2-GFP, we also observe dotted intracellular structures after Al treatment (Fig 9K), indicating that PM recycling of AtPIN2 is influenced by Al treatment as well. Interestingly,

we observed that localization of the AGC3 kinase AtPID was misregulated by Al treatment. AtPID is essential for proper PIN2 cycling in the root and *pid*-loss of function resulted AtPIN2 accumulation in dotted cytosolic structures (107), similar to intracellular AtPIN2 structures observed after Al treatment (Fig 9K). Taken together these results suggest that Al influences PIN cycling by affecting membrane trafficking and by mislocalization of AtPID. Al-induced changes on cellular processes are manifold (9). For the future, it will be interesting to dissect phenotypes caused by Al treatment, which are linked to changes in lipid accessibility/membrane charge or phenotypes independent of lipid homeostasis and accessibility. To address this, it will be interesting to generate AtPID variants, which are charge independently recruited to PM and investigate the Al tolerance of plants expressing these proteins.

PM charge: an adaptation to Al toxicity.

Interestingly, PL analysis of two dominant woody species that grow in tropical acid sulfate soils (*Melastoma malabathricum* L. and *Melaleuca cajuputi* Powell), described as more Al tolerant than rice (*Oryza sativa* L. (145)), revealed that the Al tolerant species had a substantial lower ratio between PLs and galactolipids than rice (146). In the same line, in near-isogenic Al tolerant (ET8) and Al sensitive (ES8) wheat (*Triticum aestivum*) lines, the PM membrane charge (measured by the zeta-potential of microsomal liposomes) was significantly higher for the Al sensitive line (147). These results suggest that an increase in PM charge renders plants more sensitive to Al. On the first sight, these findings seem contradictory to the results presented in this study. However, for ES8 and ET8 lines mainly the zeta potential of right-side-out (apoplastic side out) microsomal liposomes were analyzed. Further the findings of (146) raises the question if acidic soils with high concentrations of soluble Al lead to a selective pressure for plants concerning overall PL content and PM charge. In future, it will be interesting to investigate how cytosolic charge of Al adapted plant species differs from Al sensitive plants. In this regard it will be interesting to see if PM targeting mechanisms of proteins adapt to lower PM charge by increasing charge affinity, pronounced stereospecific PM recruitment or by membrane interaction modules that are largely charge independent (such as lipid or isoprenoid anchors that interact with membrane largely by Van der Waals interactions). Combining low charge of the apoplastic leaflet, to decrease Al binding thereby reducing toxic apoplastic effects and potentially the Al uptake, with a high charge of the cytosolic leaflet of the PM might describe a promising strategy to increase overall Al tolerance in plants.

Material and Methods

Reagents

Standard reagents were purchased from Sigma-Aldrich, (St. Louis, MO, USA) or Roth (Karslruhe, BW; Germany). Unlabeled lipids were purchased from Avanti Polar Lipids, Inc. (Alabaster, AL, USA). Radiolabeled lipids were purchased from Biotrend (Cologne, NRW, Germany). Other radiolabeled reagents were purchased from HARTMANN ANALYTIC GmbH (Braunschweig, NDS, Germany). Monoclonal Anti-V5 antibodies were obtained from Invitrogen, Carlsbad.

Cloning

Individual mutations were introduced in pDR195-*ScSFH1-V5*, pDR195-*ScSEC14-V5* or pET28-*ScSFH1* by site-directed mutagenesis (QuickChangeTM, Stratagene). The resulting constructs were subcloned into pDR195 or pET28 respectively.

To generate pDR195*(LEU2)*, pDR195*(LEU2)-ScSFH1-V5*, pDR195*(LEU2)-ScSFH1*^{T238D}*-V5* and pDR195*(LEU2)-ScSFH1*^{S175I,T177I}*-V5* yeast *in vivo* recombination was exploited using the following *ScLEU2* PCR fragment obtained from a PCR on yeast (BY4741) gDNA with following primers 5´-ATACATGCATTTACTTATAATACAGTTTTTTAAGCAAGGATTTTCTTAACTTCTTCG- 3’ and 5´-AAAACATGCAGGAAACGAAGATAAATCATGTCTGCCCCTAAGAAGATC - 3’ and the respective pDR195 plasmids.

For pDR195-*ScPSD1*, *ScPSD1* was amplified from yeast (BY4741) gDNA with following primers 5´- GCGCGCAATTACTTATCACTATGAATATCTTTAAATTATTGTT - 3’ and 5´- GCGCGCAGAATTTATTTAAAATGTGGACAATTAGTTTCTAAA - 3’. The resulting fragment was subcloned into pJET1.2/blunt (CloneJET PCR Cloning Kit) and cloned into pDR195 using *XhoI* and *SacII* for opening *pDR195* and SalI and SacII for *pJET* digestion.

For pDR195-*ScPSD2*, *ScPSD2* was amplified from yeast (BY4741) gDNA with following primers 5´- gagactcgagATGAGGATTATTAAGGGCAGAAAGCGAG - 3’ and 5´-AGTccgcggccgcTCATAGCCCAGCAAAATCTTTATTC - 3’. The resulting fragment was subcloned into pJET1.2/blunt (CloneJET PCR Cloning Kit) and cloned into *pDR195* using *XhoI* and *SacII* for opening *pDR195* and SalI and SacII for *pJET* digestion.

For pDR195-*TaPSS1*, *TaPSS1* was amplified from *pTaPSS1* (97) using 5´-ATACCCCAGCCTCGAGATGTCGAAGCGAGCCAC- 3’ and 5´-

GTCCAAAGCTGGATCCCTAAGGCTTGGGTATGCGG - 3'. The resulting fragment was subcloned into pJET1.2/blunt (CloneJET PCR Cloning Kit) and cloned into *pDR195* via *BamHI* and *XhoI*.

For of pDR195-*ScMSS4prom(short):MSS4* and pDR195-*ScMSS4prom(long):MSS4* fragments were amplified from yeast (BY4741) gDNA using either 5´-gagactcgaggatccATGAAGAAGATGAGACAATCTTTGCTG- 3' and 5´-gagactcgagccgcggtTCAGTCTTTATAATTTTTCTGGTTAG - 3' or using 5´-gagactcgaggatccATGTCAGTCTTGCGATCACAACCTC - 3' and 5´-gagactcgagccgcggtTCAGTCTTTATAATTTTTCTGGTTAG - 3'. The resulting fragments were subcloned into pJET1.2/blunt (CloneJET PCR Cloning Kit) and cloned into *pDR195* via *XhoI* and *SacII*.

For pDR195-*ScSFH3*, *ScSFH3* was amplified from yeast (BY4741) gDNA using following primers 5´- TTTGCGGCCGCTATGTTCAAGAGATTTAGCAAAAAGAAGGA- 3' and 5´-TTTGGATCCTTTACACGGTACTGCTTTCCG - 3'. The resulting fragment was subcloned into pJET1.2/blunt (CloneJET PCR Cloning Kit) and cloned into *pDR195* using XhoI and SacII for opening pDR195 and *SalI* and *SacII* for *pJET* digestion.

For pDR195-*ScRHO1:RHO1*, *pRHO1:ScRHO1* was amplified from yeast (BY4741) gDNA using 5´- CACCAAGCTTTTCCCTCATTTCCAATAACATTGTC- 3' and 5´-CTATAACAAGACACACTTCTTCTTCTTTTC- 3'.

For generation of pAG414GPD-*eGFP-AtSFH5* and pAG425GPD-*Cerulean-AtSFH5*, *AtSFH5* was amplified from Col-0 cDNA using following primers 5´-CACCATGTCAGGCTCTCTTGATCGATT- 3' and 5´- TCACCAGCACACCTTCTTTTTC - 3'. The resulting fragment was subcloned into *pENTR-D-TOPO* using *pENTR™/D-TOPO™* Cloning Kit and swapped into pAG414GPD-*eGFP-ccdB* or pAG425GPD-*Cerulean-ccdB* using Gateway™ LR Clonase™ II Enzyme mix.

Yeast growth conditions

If not mentioned differently, yeast cells were grown at 28°C. For yeast growth without selection, YPD (148) was used. For auxotrophy selection, YNB media (149) was used and supplemented with CSM amino acids mixes (MP Biomedicals, Santa Ana, CA, USA). For Al treatments, a modified MY media (150) was changed as follows and called MY* media: 3 % Glucose (w/v) and 0.2 $MgSO_4$. Al gradient plates were prepared with MY* as described in

(151). For liquid culture assays yeast transformants were diluted to same starting OD600 and grown at 28°C in indicated media.

Plant Material and growth conditions

All lines used in this study are in the Col-0 ecotype. Seeds used in this study: *atpss1-3* (59), *atpss1-4* (59), *atpi4kβ1 atpi4kβ2* (102), *atpip5k1-1* (SALK_146728C from Nottingham Arabidopsis Seed Stock Center (NASC)), *atpip5k1-1 atpip5k2-1* were obtained by crossing of *atpip5k1-1* with *atpip5k2-1*. ER8-GFP and ER8-PIP5K3 (104). All lipid sensor lines (27). PID:PID:YFP (152), PIN2:PIN2-GFP (153) and PID:YFP:PID (154) .

For each experimental setup, seeds, including Col-0, were grown in parallel under identetical conditions on soil (16 h light and 8 h dark, day/ night temperature 22/18°C and 120 $mmol^{-1}$ m^{-2} light intensity) and the respective progenies were used. Before using the seeds, they were sterilized in 70% (v/v) ethanol and 0.05% (v/v) Triton X-100 for 30 min and washed twice in 90% (v/v) ethanol. Al treatments were performed as described in (100) except of pre-germination for 5 days on 0.5 MS, 1% sucrose, 0.7 % phytagel before transfer of seedlings to Al containing media. Seedlings were grown on plates at 16 h light and 8 h dark, day/ night temperature 22/18°C and 120 $mmol^{-1}$ m^{-2} light intensity, 50 % humidity.

Al yeast screen

The initial screen was performed as described in (155) using YNB media supplemented with toxic Al concentration of 2500 µM $AlCl_3$.

ICP-OES for Al content analysis

Yeast transformants grown to mid log phase in MY* 4% glucose supplemented with mock or 400 µM $AlCl_3$ were incubated for 4-6 h and cooled on ice for at least 1 h. For each sample 32 ODs were harvested using a Hoefer Ten-Place Filtration Manifold. Samples were washed with 1 mM sodium citrate buffer pH 7 and vacuum filterd and freeze dried. Samples were extracted via high pressure method with 2,5 mL supra pure HNO_3 65% using an ultraCLAVE III Microwave Digestor (MLS GmbH, Leutkirch, Germany), diluted to 10 mL with MQ water and analyzed for Al, Ca, Cu, K, Mg, Mo, P and Zn on an ICP-MS ELAN 6000 (PerkinElmer, Waltham, USA) using a Mira Mist nebulizer and a flow rate of 0.8 mL min^{-1} or an ICP-OES VISTA-PRO (Varian, Palo Alto, USA) using a Meinhard nebulizer and a flow rate of 1.0 mL min^{-1}. NIST-Standard 1575a was used for calibration.

Genome wide screen

The *MATa* Library of the Saccharomyces Genome Deletion Project (http://www-sequence.stanford.edu/group/yeast_deletion_project/deletions3.html) obtained from Open Biosystems was transformed with the empty vector (*pDR195*) and *pDR195-SFH1-V5* in a 96-well format. The yeast knockout collection was inoculated from YPD plates using a pin replicator (Boekel, # Model 140500) and grown overnight in 96-well plates (Carl Roth GmbH + Co. KG) each well containing 100 µl YPD. In the morning, 4 µl yeast culture was added to 22.6 µl transformation mix containing 10.32 µg denatured salmon sperm DNA, 40% (w/v) PEG (Serva 4000), 100 mM lithium acetate, 1 x TE buffer pH 7.5 and ca. 600 ng of the DNA construct using a "Liquidator96" (Steinbrenner Laborsysteme GmbH). After an incubation of 4 h at 28°C the transformation reaction was heat shocked for 20 min at 42°C and afterwards 20 µl were spotted on square plates containing selective YNB media using "Liquidator96". Plates were incubated at 28°C for 2 d. Transformants were inoculated using a pin replicator and cultured for 24 h in 96-well plates (Carl Roth GmbH + Co. KG) containing 100 µl selective YNB media. Drops of yeast culture were spotted on plates containing MY* media with and without Al. *pDR195* and *pDR195-SFH1-V5* transformants were plated on the same square plate by positioning the 96-well pin replicator about 2-3 mm apart for the second transformation set (so that the two transformations of the same yeast strain were spotted directly next to each other for better comparison). The range of Al concentrations used was from 0.8 mM to 1.5 mM Al. Yeast strains which did not show an increased Al tolerance by *2µ* expression of *ScSFH1* in comparison to the empty vector control were picked from control plates and were verified by an additional growth assay. For this, yeast was resuspended in water, diluted to OD 1 and spotted in 8- or ten- fold serial dilutions on selective media containing different concentrations of $AlCl_3$ or on control media. To confirm the resulting candidate genes, the positive yeast strains were independently transformed with *pDR195* and *pDR195-SFH1-V5* and yeast growth assays were performed using Al gradient plates using an OD of 0.005.

Synthetic genetic array screen

The synthetic genetic array (SGA) screen was modified from (156). In short, single colonies from yeast strain grown on YPDA (1% (w/v) yeast extract, 2 % (w/v) peptone, 20 % (w/v), 15 µg/L adenine, glucose 2 % (w/v) and for solid media 2 % (w/v) agar) or for strains harboring *KanR* supplemented on YPDA supplemented with 200 mg/L G418 were inoculated in either liquid YPDA with or without G418 and grown over night at 28°C. Liquid cultures were

streaked onto YPDA or YPDA + G418 and grown for 2 days at 28°C. For mating, query gene deletion strains were streaked onto YPDA and array gene deletion strains were streaked on top of the respective query strains. After a 1-day incubation at 22.5°C, yeast were streaked on YPDA supplemented with G418 and clonNAT (100 mg/L) and grown for 2 days at 28°C. Yeast were streaked onto a plate with enriched sporulation medium (1 % (w/v) potassium acetate, 0.1 % (w/v) yeast extract 0.05 % (w/v) glucose, 12.5 mg/L L-histidine, 62.5 mg/L L-leucine, 12.5mg/L L-lysine, 12.5 mg/L L-uracil and 50 mg/L G418) and incubated at 22.5°C. After 5 days, yeast were resuspended in 1 ml MQ and for no genotype selection 20 µL, of cell suspension was plated onto SD/AS medium (1.7 g/L yeast nitrogen base, 5 g ammonium sulfate, 362.5 mg/L L-leucine, 72.5 mg/L L-methionin, 72.5 mg/L L-uracil, 50 mg/L canavanine, 50 mg/L thialysine, 2% (w/v) glucose, 20 µg/mL calcofluor-white (CCW) and 2% (w/v) Oxoid Agar). For selection of G418 resistant single knockouts, 40 µl cell suspension was plated onto onto SD/MSG (1.7 g/L yeast nitrogen base, 5 g ammonium sulfate, 181.3 mg/L L-leucine, 72.5 mg/L L-methionin, 72.5 mg/L L-uracil, 50 mg/L canavanine, 50 mg/L thialysine, 2% (w/v) glucose, 500 µg/mL CCW and 2% (w/v) Oxoid Agar) supplemented with 200 mg/L G418. For selection of clonNAT resistant single knock outs, 40 µl were plated onto SD/MSG supplemented with 100 mg/L clonNAT and for selection of double knock outs 80 µL cell suspension was plated onto SD/MSG plates supplemented with 200 mg/L G418 and 100 mg/L clonNAT. Plates were incubated for 2 days at 28°C recorded with a digital camera. Colony size was determined using OpenCFU 3.9.0. (Geissmann, 2013) setting thresholds to regular, 5; minimum size: 4.

ScMpk1 phosphorylation assay

Detection of ScMpk1 phosphorylation was performed as described in (157) using MY* medium as growth media in presence or absence of 300 µM $AlCl_3$.

Generation of Liposomes

All lipids were purchased from Avanti Polar Lipids, Inc., Alabaster, AL, USA. Lipids, dissolved in $CHCl_3$, were mixed (if necessary) and dried out under a N_2 gas stream. Lipid films were resuspended in water or respective buffer by vortexing for 2 min. Then lipids were either sonicated for 30 s (SONOPULS HD 2070, BANDELIN electronic GmbH & Co. KG, Berlin, Germany; 20 % power) or generated by extrusion. For extrusion, the Mini Extruder (Avanti Polar Lipids, Inc., Alabaster, AL, USA) was used as recommended by manufacturer

using polycarbonate membranes with a pore size of 1 µm. Before use of sonicated liposomes, they were centrifuged at 20 000 x g only supernatant was used for further experiments.

ScMss4 kinase stimulation assays

ScMss4 was purified as described in (50), with the minor change for washing steps as no detergent was used in the buffers. ScMss4 kinase stimulation assay was based on (50). In short, sonicated liposomes consisting of soy PtdCho (Avanti #840054) and brain, porcine PtdIns(4)P (Avanti #840045) or brain, porcine PtdIns(4,5)P_2 (Avanti #840046) in a molar ratio 300µM:100µM PtdCho:PtdIns(4)P/PtdIns(4,5)P_2 prepared in ScMss4 kinase buffer (25 mM HEPES, pH7.4, 2 mM MgCl, 0.2 mM EDTA, 1 mM EGTA, 5mM *β*-glycerophosphate, 1 mM dithiothreitol, and 120 mM NaCl). GST-ScMss4 bound to gluthatione beads was mixed with liposome solution in a ratio of 1:10. 50 µL of Liposome-GST-ScMss4 suspension was distributed to individual reaction vials while constantly mixing using a magnetic stirrer. To 50 µL liposome-GST-ScMss4 suspension, if not mentioned differently, 5 µL lysis buffer or ScSec14-type protein (1 µg μL^{-1}) was added resulting in a 30 x excess of substrate to ScSec14-type protein. ScMss4 kinase reaction was started by addition of 15 µl of ScMss4 kinase buffer containing 5 µCi [γ-^{32}P]ATP (SRP-301, Hartmann Analytics, Braunschweig, Germany) and 43 µM ATP, and was incubated for 30 min at RT on a spinning wheel. PtdIns(4,5)P_2 was extracted as described in (158), mixed with scintillation cocktail (Perkin-Elmer; ULTIMA-FLO AP) and analyzed by scintillation counting.

PtdIns(4,5)P_2 *in vitro* release assay

50 µg brain, porcine PtdIns(4)P (Avanti #840045) was dried under a N_2 gas stream, resuspended in 1 mL MQ water and sonicated for 2 min (SONOPULS HD 2070, BANDELIN electronic GmbH & Co. KG, Berlin, German; 20 % power). The PtdIns(4)P suspension was divided into two tubes and mixed with lysis buffer (300 mM NaCl, 50 mM NaH_2PO_4, pH 7.5, 5 mM β-mercaptoethanol) 1:2. To 1,5 mL lipid suspension 50 µL lysis buffer or 50 µL ScSec14-type protein (1 µg μL^{-1}) was added and incubated over night at room temperature. Then ScSec14-type proteins were bound to 30 µl Ni-NTA beads (bed volume, Thermo Fisher R90115), washed 3 x with lysis buffer and 2 x washed with ScMss4 kinase buffer (25 mM HEPES, pH7.4, 2 mM MgCl, 0.2 mM EDTA, 1 mM EGTA, 5 mM *β*-glycerophosphate, 1 mM dithiothreitol, and 120 mM NaCl). ScSec14-type protein was eluted using two times 50 µL of ScMss4 kinase buffer with 250 mM imidazol. 100 µL control/protein solution were then dialyzed two times for 30 min with 500 mL ScMss4 kinase buffer to decrease the imidazol concentration. 65 µL suspension of GST-ScMss4 bound to glutathione beads were

added to each sample and the kinase reaction was started by addition of 15 µl of ScMss4 kinase buffer containing 5 µCi [γ-^{32}P]ATP and 43 µM ATP. Samples were incubated for 30 min at room temperature on a spinning wheel. Then GST-Mss4 beads were pelleted for 5 min at 700 x g and the supernatant was recovered. 10 µL of the supernatant were taken, lipids were extracted as described in (158) as normalization control and were mixed with scintillation cocktail (Perkin-Elmer; ULTIMA-FLO AP) and analyzed by scintillation counting.

For PtdIns(4,5)P_2 release in light acceptor liposomes, 100 µL of sonicated soy PtdCho liposomes in ScMss4 kinase buffer with a concentration of 500 µM PtdCho, was added to samples and incubated for 60 min at room temperature. Then ScSec14-type protein with 30 µL Ni-NTA beads (bed volume) and incubated for 60 min. After incubation, the supernatant was recovered and lipids were extracted as described in (158), mixed with scintillation cocktail (Perkin-Elmer; ULTIMA-FLO AP) and analyzed by scintillation counting. The Ni-NTA bead pellet was washed 5 times with ScMss4 kinase buffer and beads were directly mixed with scintillation cocktail (Perkin-Elmer; ULTIMA-FLO AP) and analyzed by scintillation counting.

For PtdIns(4,5)P2 release in heavy sucrose-loaded acceptor liposomes 100 µL of extruded soy PtdCho liposomes in ScMss4 kinase buffer containing 10% (w/v) sucrose with a concentration of 500 µM of PtdCho, were added to samples and incubated for 60 min at room temperature. The ScSec14-type/liposome mix was centrifuged at 20 000 x g for 10 min at room temperature. 50 µL was separated as supernatant sample. Subsequently, the rest of the sample, including the pelleted lipids, were extracted as described in (158) mixed with scintillation cocktail (Perkin-Elmer; ULTIMA-FLO AP) and analyzed by scintillation counting.

Extraction and HPLC analysis of PIPs

Yeast cells were grown over night in MY* media containing supplemented with 35 µCi [^{3}H]-myo-inositol and 200 mM glycine (pH 3.0) at 26°C. Thereafter yeast was subcultured in this MY* media (supplemented with 200 mM glycine (pH 3.0) and 30 µCi [^{3}H]-*myo*-inositol) for 3 h hours and then shifted to 34,5°C for 2 h. To kill cells trichloricacetic acid (TCA) was added to a final volume of 5 % (w/v). Cells were pelleted with 2800 x g and pellets were washed two times with ice cold water and resuspended in 500 µl 4.5 % (w/v) perchloric acid. Cells were disrupted by bead beating using glass beads (0.25 - 0.45 mm) for 5 min at 4 °C. The homogenate was pelleted at 20 000 x g for 10 min at 4 °C. Pellets were washed with 100 mM EDTA and resuspended in 700 µl deacylation reagent that was generated as follows: To a

in 12.3 mL consisting of 6.2 mL methanol, 4.6 mL water and 1.5 mL 1-butanol gaseous methylamine was added to a final volume of 20 mL. Deacylation was performed at 53 °C for 60 min while shaking at 600 rpm followed by drying samples in a speed vacuum centrifuge at 60°C over night. Pellets were resuspended in 300 µl MQ-H_2O and 300 µL extraction reagent (16 % (v/v) petrol ether, 4 % (v/v) ethyl formate in 1-butanol), vortexed for 30 s and pelleted at 20.800 x g for 10 min. The aqueous phase was washed two times with extraction reagent, filtered with a 0.2 µm filter and stored at – 80°C. Phosphinositide profiles were resolved by strong anion exchange chromatography (SAX) HPLC (using the PartiSphere SAX 4.6 x 250 mm column, Whatman) at a flow rate of 0.5 mL min^{-1} with the gradient of buffer A (1 mM EDTA) and B [1 mM EDTA and 1.25 M (NH4)2HPO4, pH 3.8, adjusted with H3PO4] with follwing gradient: 0 min, 0 % buffer B; 5 min, 10 % buffer B; 70 min, 28 % buffer B; 85 min, 60 % buffer B, 95 min, 100 % buffer B, 106 min, 0 % buffer B. Fractions were collected each minute, mixed with scintillation cocktail (Perkin-Elmer; ULTIMA-FLO AP), and analyzed by scintillation counting.

Directed evolution screen

The directed evolution screen was carried out as described earlier (74) and was performed as follows. For the induction of mutations polymerase chain reactions were carried out with Taq DNA polymerase in the presence of 120 µM $MnCl_2$, a decreased concentration of dATP or dGFP (0.3 x) and 35 PCR cycles using pET28-ScSec14 (75) as template with following oligonucleotides (*ScSEC14 pDR199 Pst*I F and *pDR199 Pst*I F, see Table S4). PCR-products were precipitated with 3 M NaAc (pH 5,2, 1/10 vol) and EtOH (2.56 vol), washed and resuspended in 1x TE buffer (pH7.5) buffer. For *in vivo* recombination and to screen for *ScSEC14* alleles able to mediate Al tolerance in yeast, wild type yeast (BY4741) was transformed with with PCR product and with linearized *pDR199* (74). For linearization of *pDR199 Eco*RI and *BamH*I were used. Transformants were plated on MY* medium supplemented with 1.25 mM $AlCl_3$. Al tolerance mediating plasmids were retransformed into naïve BY4741 to confirm the phenotype or directly subjected to DNA sequencing analysis.

Thin layer chromatography (TLC)

Yeast transformants were grown in YNB-based selective media for 1 day at 28 °C for steady state experiments in the presence of 7 µCi ^{32}P orthophosphate (PRB1, HARTMANN ANALYTIC GmbH, Braunschweig, NDS, Germany). For pulse experiments, yeast cells were washed 3x with MY* low-phosphate medium (containing 7 mM phosphate) and cultured to mid-log phase. Afterwards [^{32}P] orthophosphate (PRB1, HARTMANN ANALYTIC GmbH,

Braunschweig, NDS, Germany) was added to a final concentration of 80 µCi/mL and incubated for 1 h. For steady state and pulse experiments, yeast cells were killed by addition of trichloricacetic acid (TCA) to a final volume of 5 % (w/v). Cells were centrifuged at 1700 x g and washed twice with ice-cold MQ water and resuspended in 4.5 % (w/v) perchloric acid. Cells were disrupted by bead beating using glass beads (0.5 mm), the suspension was transferred to a new tube and membranes were pelleted by centrifugation at 20 000 x g for 10 min at 4°C. Pellets were twice with 100 mM EDTA (pH 7.4). Lipids were extracted as described in (158) and solvent was dried out using a speed vacuum centrifuge. Lipid pellets were solved in 30 µL $CHCl_3$ and 3 µL were mixed with scintillation cocktail (Perkin-Elmer; ULTIMA-FLO AP) and analyzed by scintillation counting for normalizing TLC loading). TLC was performed as described in (159). Densiometric was performed using ImageJ.

PtdIns(4)P transfer assay

NBD-PH^{FAPP} proteins were prepared as follows. $PH_{FAPP\ T13C\ C37S\ C94S}$/pGEX6P-1 was prepared by introducing point mutations for NBD labeling. *E.coli* strain BL21(DE3) was used as a host cell line. Expression of GST-$PH_{FAPP\ T13C\ C37S\ C94S}$ recombinant protein was induced with 0.01 mM IPTG at 22°C. The cell pellets were collected and resuspended in ice-cold homogenization buffer (50 mM Tris-HCl pH 6.8, 300 mM NaCl, 1 mM dithiothreitol (DTT, Thermo Fisher Scientific, R0861), 0.1 mM AEBSF (Thermo Fisher Scientific, 78431), and complete EDTA-free protease inhibitor (Thermo Fisher Scientific, A32955). Cells were then disrupted by sonication in ice-cold homogenization buffer. The homogenized cells were centrifuged at 20,800 × g for 30 min to remove cell debris. GST-tagged recombinant proteins were purified with glutathione-Sepharose (GE Healthcare, 17-0756-01) and cleaved from GST by using 0.1 U/µL PreScission protease (GE Healthcare, 270843). After cleavage of GST tag, untagged $PH_{FAPP\ T13C\ C37S\ C94S}$ was dialyzed in TBS (50 mM Tris-HCl pH 6.8, and 150 mM NaCl) three times to remove DTT, and then labeled with a 10-fold excess of IANBD-amide (Invitrogen, D2004). After overnight incubation at 4°C, the reaction was stopped with 4 mM cysteine and residual IANBD-amide was removed by dialysis (50 mM Tris-HCl pH 6.8, 150 mM NaCl, and 1 mM DTT). NBD-labeled proteins were mixed with equal volume of glycerol and stored at -80°C before analysis.

Liposomes werer prepared as follows. Lipids were mixed at the desired molar ratio and the organic solvent was removed in a rotary evaporator. The lipid films were hydrated in buffer A (50 mM Na-phosphate pH7.5, 300 mM NaCl, 5 mM β-ME) or buffer B (25 mM Na-phosphate pH 7.5, 300 mM NaCl, 5 mM β-ME) for 30 min at room temperature. The suspensions were sonicated in a bath sonicator. Liposomes were used within 1 day.

PI4P transfer assay was carried out in buffer A (for ScSec14) or buffer B (for ScSfh1) and measured with a Fluoromax spectrometer (HORIBA Scientific). Briefly, the sample (150 µL) containing liposomes (400 µM total lipids, L_D: 4 mol% PtdIns(4)P, 2 mol% Rhod-PE and 94 mol% PtdCho; L_A; 100 mol% PtdCho) were mixed with NBD- PH_{FAPP} (final conc. 400 nM) in a 200 µL quartz cell. After 5 min, the indicated amount of ScSec14 or ScSfh1 was added. NBD fluorescence (ex/em 468 nm/530 nm) was recorded every second. The excitation and emission slits were set at 5 nm bandwidths. We calculated an increase in signal of NBD fluorescence ($\Delta Em_{530,\ raw\ data}$) from that measured before ScSec14 or ScSfh1 addition. To subtract the contribution of liposomes alone, a signal change of NBD fluorescence ($\Delta Em_{530,\ BG}$) was measured with the NBD-PH_{FAPP} after the addition of only buffer. Finally, a NBD signal increase dependently of ScSec14 or ScSfh1 was calculated by using this equation: $\Delta Em_{530} = \Delta Em_{530,\ raw\ data} - \Delta Em_{530,\ BG}$. Data were analyzed by using RStudio and Graphpad Prsim 6 software.

Microscopy

Yeast imaging was performed with an Epi-fluorescence microscope Zeiss Imager M2 equipped with a Hamamatsu ORCA-flash 4.0 V.2 CMOS camera or Confocal Zeiss LSM 880 Airyscan (fast), inverted. For plant imaging, Confocal Leica TCS SP8 AOBS-FLIM-FCS equipped with resonant scanner and HyD detector, was used.

Quantitative analysis of PM/intracellular ratio

Analysis of the PM/intracellular ratio from yeast or plants was performed using the herein developed software PixelAnalysis. PixelAnalysis was developed in MATLAB 2016a (The MathWorks Inc., Natick, MA, USA). Webinstaller, source code and additional information are provided here https://github.com/sbitters/PixelAnalysis. Additionally, detailed description and the source code of the PixelAnalysis are provided in supplement data (SData 1). Calculation of relative PM was as follows: (PM_{max}/intracellular signal-1), PM_{max} = average(2xPM_{maxima}, from cross section of yeast cell), $PM_{max,plants}$ = integral(1x$PM_{maximum}$, between cells) and cytosolic signal = average(intracellular signal).

Sfh1 *in vitro* PL-transfer assays

For generation of heavy sucrose-loaded donor liposomes, soy PtdSer, PtdCho (16:1, Δ9-cis) and C14-PtdCho (ARC 0376) or C14-PtdEtn (ARC 3078) were used. PtdSer (100 µM final), PtdCho (10 µM final) and 4 µL of ^{14}C-PtdCho or ^{14}C-PtdEtn were mixed and liposomes were generated in 10 % (w/v) sucrose by extrusion. For generation of light acceptor liposomes, soy

PtdSer and PtdCho (16:1, Δ9-cis) or soy PtdIns were used. PtdSer (100 µM final) and PtdCho (10 µM final) were mixed and liposomes were generated by sonication in MQ water. Donor liposomes, acceptor liposomes and transfer buffer (300 mM NaCl, 50 mM Na_2HPO_4, 1 mM EDTA) was mixed 1:1:1 (end volume 900). After mixing by pipetting, 200 µL were taken from each sample as pre-centrifugation control. Then either protein elution buffer or ScSec14-type protein was added to a concentration of 300 µM and incubated for 30 min at 37°C. Heavy donor and light acceptor liposomes were separated by centrifugation at 20 000 x g for 1 h. Then 350 µL supernatant was taken, mixed with scintillation cocktail (Perkin-Elmer; ULTIMA-FLO AP) and analyzed by scintillation counting. ^{14}C-PtdCho and ^{14}C-PtdEtn transfer activity were calculated by protein-related increase of ^{14}C in supernatant and normalized to pre-centrifugation control.

Correlative light and electron microscopy

For correlative light and electron microscopy (CLEM), yeast cells were fixed with 4% formaldehyde (1 h; Merck) followed by 8% formaldehyde (1 h) in microtubule-stabilizing buffer MTSB (50 mM Pipes, 5 mM EGTA and 5 mM $MgSO_4$, pH 7), embedded in 10% gelatine (Merck), infiltrated with a mixture of 1.8 M sucrose (Merck) and 20% polyvinylpyrrolidone (PVP-10; Sigma-Aldrich, Steinheim, Germany) (160). Thereafter gelatine blocks were mounted on stubs and frozen in liquid nitrogen. GFP-labelling of thawed cryosections failed, therefore a correlative approach was chosen. 300 nm thick cryosections were cut at -90°C (Leica cryoultramicrotome EM UC7/FC7), mounted on Celllocate microgrid coverslips (square size 55 µm) with an etched surface pattern (Eppendorf-Netheler-Hinz, Hamburg, Germany) and viewed in a Zeiss Imager M2 (equipped with differential interference contrast (DIC); Zeiss, Germany) with an Orca-flash 4.0 sCMOS black/white (Hamamatsu, Japan) camera. After obtaining fluorescence and DIC images, sections mounted on coverslips were postfixed with 2.5% glutaraldehyde, 1% osmiumtetroxide (Science Services, München, Germany), and 1% aqueous uranyl acetate (Science Services, München, Germany). After dehydration in a graded series of ethanol, sections were infiltrated with Epon (Roth, Karlsruhe, Germany) and polymerized at 60°C (48 h). The glass coverslip was removed by plunching into liquid nitrogen. The glass derived surface pattern on the Epon block surface was used for targeted ultramicrotomy. The first four sections of the resin block containing the 300 nm cryosection of interest were stained with 1% aqueous uranyl acetate and lead citrate. Sections were viewed in a JEM-1400plus (120 kV) TEM (Jeol, Japan) equipped with a 4k CMOS TemCam-F416 camera (TVIPS, Gauting, Germany). Fluorescence

images, DIC images, and TEM images were aligned with Adobe Photoshop CS5 (Puppet Warp function).

Acknowledgements

We thank Jörn Breuer for performing the ICP-MS and ICP-OES analyses. We also thank T. Aoyama, Y. Jaillais, J. Friml, C. Schwechheimer for kindly providing seeds. We thank V. Bankaitis for kindly providing the *sec14-1*^{ts} and *mss4-5*^{ts} yeast strains and the anti-ScKes1 antibody. We thank S. Emr for providing us the pik1ts, stt4ts and mss4ts yeast strains. We thank Mesut Bilgin for providing us the *psd1Δ psd1Δ* and *cho2Δ opi3Δ* yeast strains. We thank M. Kf de Campos for providing us the pDR199-*mRFP-AtSFH1-Nlj16* plasmid. We want to thank the Deutsche Forschungsgemeinschaft (Emmy Noether grant SCHA 1274/2-1, SFB 1101/TP A05 and research grant SCHA 1274/4-1), the Landesgraduiertenförderung and the Studienstiftung des deutschen Volkes for their support.

Author contributions

Following authors contributed to the presented manuscript.

Johnen, P.[1], Winklbauer, E. M.[2], Herrmann, D.[2] , Pankalla, S.[2], Fitz, M.[2], Hagenberg, J.[2], Enderle, B.[3], Martín, H.[4], González, G.[4], Nishimura, T.[5], Ile, K.E.[1], Krieger, N.[1], Bitters, S.T.[2], Ackermann, F.[2], Richter, S.[2], Stierhof, Y.D.[2], von Wirén, N.[6], Stefan, C.J[5]., Molina, M.[4], and Schaaf, G.[1*]

1 Institute of Crop Science and Resource Conservation, Universität Bonn, 53113 Bonn, Germany

2 Center for Plant Molecular Biology, University of Tuebingen, 72076 Tuebingen, Germany.

3 Institute of Biology II, Faculty of Biology, University of Freiburg, 79104 Freiburg Germany

4 Departamento de Microbiología y Parasitología, Facultad de Farmacia. Universidad Complutense de Madrid e Instituto Ramón y Cajal de Investigaciones Sanitarias (IRYCIS), Spain

5 Medical Research Council Laboratory for Molecular Cell Biology, University College London, London WC1E 6BT, United Kingdom.

6 Molecular Plant Nutrition, Leibniz Institute of Plant Genetics and Crop Plant Research (IPK), Corrensstrasse 3, 06466, Gatersleben, Germany.

[*] corresponding author: gabriel.schaaf@uni-bonn.de

The manuscript was written by P. Johnen and revised by G. Schaaf. Experiments were designed by G. Schaaf, P. Johnen and E.M. Winklbauer.

Yeast growth assays and cartoons shown in Figure 1A, 1C, 2A, 2E, 3A, 3B, 4F, 5J, 5K-M, 7A, 8C, 8D, S1E, S2A, S3A, S5B, S7B and S7F performed and drawn by P. Johnen. Yeast growth assay shown in Figure 1B were performed by F. Ackermann and P. Johnen (data also partially shown in Bachelor thesis of F. Ackermann, 2017). Microscopy and subsequent analysis shown in Figure 2H, 2I, 4B-E, 4G, 4H, 5H, 5I, 5L, 7B, 8A, 8B, 8F, 8G, 9F-K, S3H, S4A-S4E, S6B-E, S6H, S7A, S7C, S8A and S8B were performed by P. Johnen. ScMss4 *in vitro* kinase assays, PtdIns(4,5)P_2 release assays and PL transfer assays with respective analysis of protein stability and respective cartoons shown in Figure 3C, 3D, 3F, 3G, 5A, 6A-D and S3C-G were performed or drawn by P. Johnen . SAX-HPLC-based PIP analysis shown in 3H was performed by P. Johnen using lipid extracts generated by D. Herrmann. TLC-based

PL analysis and PL biosynthesis scheme shown in Figure 4A, 5C-G and S6A was performed or drawn by P. Johnen. *In silico* BH-Score analysis shown in Figure 8E was performed by P. Johnen. Plant growth assays shown in Figure 9A-E and 9L were performed by P.Johnen, S. Pankalla, F. Ackermann and R. Witty (data also partially shown in Master thesis of S. Pankalla, 2016). Models shown in Figure 10A, 10B, 11A and 11B were drawn by P. Johnen. Analytics shown in Figure 1D and S2C were performed by J. Breuer and analyzed by P. Johnen and E.M. Winklbauer (data also shown in Dissertation of E.M. Winklbauer, 2016). Yeast growth assays shown in Figure 2B-D, S1A, S1B and S7D were performed by D. Hermann (data also partially shown in the Dissertation of D. Hermann, 2016). ScMss4 kinase stimulation assays with respective protein stability assays shown in Figure 3E ans S3B were performed by D. Hermann (data also shown in Dissertation of D. Hermann, 2016). SGA Screen shown in Figure 2F were performed by Jonas Hagenberg (data also shown in Bachelor thesis of Jonas Hagenberg, 2015). ScMpk1 phosphorylation assay and microscopy shown Figure 2G, 2J and 2K were designed and performed by, G. González, H. Martín and M. Molina. *In vitro* PtdIns(4)P transfer assays shown in Figure 5B were designed and performed by T. Nishimura and. C.J. Stefan (proteins were generated by P. Johnen). Sample preparation for microscopy shown in Figure 7C was performed by Y. Stierhof. Microscopy and subsequent analysis shown in Figure 7D-G and S6I was performed by Y. Stierhof, S. Richter and P. Johnen. Yeast growth assays and protein stability assays were shown in Figure S1C, S1B, S2B and S6G were performed by E.M. Winklbauer (data also shown in Dissertation of E.M. Winklbauer, 2016). Directed evolution screen shown in S5A were performed by E.M. Winklbauer, N. Krieger and M. Fitz (data also partially shown in Bachelor thesis of N. Krieger, 2012). Yeast growth assays shown in Figure 7G was performed by B. Enderle (data also shown in Master thesis of B. Enderle, 2012). Al screen shown in Table S1 was peformed by G. Schaaf. Genome wide screen shown in Table S2 was peformed by G. Schaaf, E.M. Winklbauer and B. Enderle (data also shown in Dissertation of E.M. Winklbauer, 2016 and Master thesis of B. Enderle). If not indicated otherwise, plasmids used in this study were generated by E.M. Winklbauer, D. Herrmann, B. Enderle, G. Schaaf, M. Fitz or N. Krieger (plasmids also partially used in the Dissertations of E.M. Winklbauer, D. Hermann, in the Master thesis of B. Enderle and the Bachelor thesis of N. Krieger). Respective parts of the material and methods section were written by the persons performing the respective experiment (see above). If experiments were already published elsewhere, sections will be similar to respective publication (see above).

References

1. Jiang C, Liu L, Li X, Han R, Wei Y, Yu Y. Insights into aluminum-tolerance pathways in Stylosanthes as revealed by RNA-Seq analysis. Sci Rep. 2018.
2. Panda SK, Baluska F, Matsumoto H. Aluminum stress signaling in plants. Plant Signal Behav. 2009;4(7):592-7.
3. Kochian LV, Pineros MA, Liu J, Magalhaes JV. Plant Adaptation to Acid Soils: The Molecular Basis for Crop Aluminum Resistance. Annu Rev Plant Biol. 2015;66:571-98.
4. Vonuexkull HR, Mutert E. Global Extent, Development and Economic-Impact of Acid Soils. Plant Soil. 1995;171(1):1-15.
5. Wood S, Sebastian K, Scherr SJ. Agroecosystems pilot analysis of global ecosystems. Washington, DC: World Resources Institute; 2000. XII, 110 S. p.
6. Liu Q, Yang JL, He LS, Li YY, Zheng SJ. Effect of aluminum on cell wall, plasma membrane, antioxidants and root elongation in triticale. Biol Plantarum. 2008;52(1):87-92.
7. Lazof DB, Goldsmith JG, Rufty TW, Linton RW. Rapid Uptake of Aluminum into Cells of Intact Soybean Root-Tips - a Microanalytical Study Using Secondary-Ion Mass-Spectrometry. Plant physiology. 1994;106(3):1107-14.
8. Horst WJ, Wang Y, Eticha D. The role of the root apoplast in aluminium-induced inhibition of root elongation and in aluminium resistance of plants: a review. Annals of botany. 2010;106(1):185-97.
9. Kopittke PM, Menzies NW, Wang P, Blamey FP. Kinetics and nature of aluminium rhizotoxic effects: a review. J Exp Bot. 2016;67(15):4451-67.
10. Zheng SJ, Yang JL. Target sites of aluminum phytotoxicity. Biol Plantarum. 2005;49(3):321-31.
11. Kochian LV. Cellular Mechanisms of Aluminum Toxicity and Resistance in Plants. Annu Rev Plant Phys. 1995;46:237-60.
12. Ezaki B, Sasaki K, Matsumoto H, Nakashima S. Functions of two genes in aluminium (Al) stress resistance: repression of oxidative damage by the AtBCB gene and promotion of efflux of Al ions by the NtGDI1gene. J Exp Bot. 2005;56(420):2661-71.
13. Rengel Z. Role of Calcium in Aluminum Toxicity. New Phytol. 1992;121(4):499-513.
14. Jones DL, Blancaflor EB, Kochian LV, Gilroy S. Spatial coordination of aluminium uptake, production of reactive oxygen species, callose production and wall rigidification in maize roots. Plant, cell & environment. 2006;29(7):1309-18.
15. Kopittke PM, Moore KL, Lombi E, Gianoncelli A, Ferguson BJ, Blamey FPC, et al. Identification of the Primary Lesion of Toxic Aluminum in Plant Roots. Plant physiology. 2015;167(4):1402-11.
16. Levan H, Kuraishi S, Sakurai N. Aluminum-Induced Rapid Root Inhibition and Changes in Cell-Wall Components of Squash Seedlings. Plant physiology. 1994;106(3):971-6.
17. Tabuchi A, Matsumoto H. Changes in cell-wall properties of wheat (Triticum aestivum) roots during aluminum-induced growth inhibition. Physiol Plant. 2001;112(3):353-8.
18. Decreux A, Messiaen J. Wall-associated kinase WAK1 interacts with cell wall pectins in a calcium-induced conformation. Plant Cell Physiol. 2005;46(2):268-78.
19. Kohorn BD, Kohorn SL. The cell wall-associated kinases,WAKs, as pectin receptors. Frontiers in Plant Science. 2012;3.
20. Sivaguru M, Ezaki B, He ZH, Tong H, Osawa H, Baluska F, et al. Aluminum-induced gene expression and protein localization of a cell wall-associated receptor kinase in Arabidopsis. Plant physiology. 2003;132(4):2256-66.
21. Voxeur A, Hofte H. Cell wall integrity signaling in plants: "To grow or not to grow that's the question". Glycobiology. 2016;26(9):950-60.

22. Levin DE. Regulation of cell wall biogenesis in Saccharomyces cerevisiae: the cell wall integrity signaling pathway. Genetics. 2011;189(4):1145-75.
23. Kock C, Dufrene YF, Heinisch JJ. Up against the Wall: Is Yeast Cell Wall Integrity Ensured by Mechanosensing in Plasma Membrane Microdomains? Appl Environ Microb. 2015;81(3):806-11.
24. Schott EJ, Gardner RC. Aluminum-sensitive mutants of Saccharomyces cerevisiae. Molecular & general genetics : MGG. 1997;254(1):63-72.
25. Kakimoto M, Kobayashi A, Fukuda R, Ono Y, Ohta A, Yoshimura E. Genome-wide screening of aluminum tolerance in Saccharomyces cerevisiae. Biometals. 2005;18(5):467-74.
26. Yeung T, Gilbert GE, Shi J, Silvius J, Kapus A, Grinstein S. Membrane phosphatidylserine regulates surface charge and protein localization. Science. 2008;319(5860):210-3.
27. Simon MLA, Platre MP, Marques-Bueno MM, Armengot L, Stanislas T, Bayle V, et al. A PtdIns(4)P-driven electrostatic field controls cell membrane identity and signalling in plants. Nat Plants. 2016;2(7).
28. Moravcevic K, Mendrola JM, Schmitz KR, Wang YH, Slochower D, Janmey PA, et al. Kinase associated-1 domains drive MARK/PAR1 kinases to membrane targets by binding acidic phospholipids. Cell. 2010;143(6):966-77.
29. Lemmon MA. Membrane recognition by phospholipid-binding domains. Nat Rev Mol Cell Biol. 2008;9(2):99-111.
30. Carman GM, Han GS. Regulation of Phospholipid Synthesis in the Yeast Saccharomyces cerevisiae. Annu Rev Biochem. 2011;80:859-83.
31. Athenstaedt K, Daum G. Biosynthesis of phosphatidic acid in lipid particles and endoplasmic reticulum of Saccharomyces cerevisiae. J Bacteriol. 1997;179(24):7611-6.
32. Athenstaedt K, Weys S, Paltauf F, Daum G. Redundant systems of phosphatidic acid biosynthesis via acylation of glycerol-3-phosphate or dihydroxyacetone phosphate in the yeast Saccharomyces cerevisiae. J Bacteriol. 1999;181(5):1458-63.
33. Zheng ZF, Zou JT. The initial step of the glycerolipid pathway - Identification of glycerol 3-phosphate/dihydroxyacetone phosphate dual substrate acyltransferases in Saccharomyces cerevisiae. J Biol Chem. 2001;276(45):41710-6.
34. Nagiec MM, Wells GB, Lester RL, Dickson RC. A Suppressor Gene That Enables Saccharomyces-Cerevisiae to Grow without Making Sphingolipids Encodes a Protein That Resembles an Escherichia-Coli Fatty Acyltransferase. J Biol Chem. 1993;268(29):22156-63.
35. Riekhof WR, Wu J, Jones JL, Voelker DR. Identification and characterization of the major lysophosphatidylethanolamine acyltransferase in Saccharomyces cerevisiae. J Biol Chem. 2007;282(39):28344-52.
36. Shen HF, Heacock PN, Clancey CJ, Dowhan W. The CDS1 gene encoding CDP-diacylglycerol synthase in Saccharomyces cerevisiae is essential for cell growth. J Biol Chem. 1996;271(2):789-95.
37. Nikawa J, Kodaki T, Yamashita S. Primary Structure and Disruption of the Phosphatidylinositol Synthase Gene of Saccharomyces-Cerevisiae. J Biol Chem. 1987;262(10):4876-81.
38. Nikawa J, Yamashita S. Molecular cloning of the gene encoding CDPdiacylglycerol-inositol 3-phosphatidyl transferase in Saccharomyces cerevisiae. Eur J Biochem. 1984;143(2):251-6.
39. Chang SC, Heacock PN, Clancey CJ, Dowhan W. The PEL1 gene (renamed PGS1) encodes the phosphatidylglycerophosphate synthase of Saccharomyces cerevisiae. J Biol Chem. 1998;273(16):9829-36.
40. Osman C, Haag M, Wieland FT, Brugger B, Langer T. A mitochondrial phosphatase required for cardiolipin biosynthesis: the PGP phosphatase Gep4. Embo J. 2010;29(12):1976-87.

41. Letts VA, Klig LS, Baelee M, Carman GM, Henry SA. Isolation of the Yeast Structural Gene for the Membrane-Associated Enzyme Phosphatidylserine Synthase. P Natl Acad Sci-Biol. 1983;80(23):7279-83.
42. Trotter PJ, Pedretti J, Voelker DR. Phosphatidylserine Decarboxylase from Saccharomyces-Cerevisiae - Isolation of Mutants, Cloning of the Gene, and Creation of a Null Allele. J Biol Chem. 1993;268(28):21416-24.
43. Trotter PJ, Pedretti J, Yates R, Voelker DR. Phosphatidylserine decarboxylase 2 of Saccharomyces cerevisiae. Cloning and mapping of the gene, heterologous expression, and creation of the null allele. J Biol Chem. 1995;270(11):6071-80.
44. Kodaki T, Yamashita S. Yeast phosphatidylethanolamine methylation pathway. Cloning and characterization of two distinct methyltransferase genes. J Biol Chem. 1987;262(32):15428-35.
45. Gibellini F, Smith TK. The Kennedy Pathway-De Novo Synthesis of Phosphatidylethanolamine and Phosphatidylcholine. Iubmb Life. 2010;62(6):414-28.
46. Strahl T, Thorner J. Synthesis and function of membrane phosphoinositides in budding yeast, Saccharomyces cerevisiae. Bba-Mol Cell Biol L. 2007;1771(3):353-404.
47. De Craene JO, Bertazzi DL, Bar S, Friant S. Phosphoinositides, Major Actors in Membrane Trafficking and Lipid Signaling Pathways. Int J Mol Sci. 2017;18(3).
48. Garciabustos JF, Marini F, Stevenson I, Frei C, Hall MN. Pik1, an Essential Phosphatidylinositol 4-Kinase Associated with the Yeast Nucleus. Embo J. 1994;13(10):2352-61.
49. Yoshida S, Ohya Y, Goebl M, Nakano A, Anraku Y. A novel gene, STT4, encodes a phosphatidylinositol 4-kinase in the PKC1 protein kinase pathway of Saccharomyces cerevisiae. J Biol Chem. 1994;269(2):1166-72.
50. Desrivieres S, Cooke FT, Parker PJ, Hall MN. MSS4, a phosphatidylinositol-4-phosphate 5-kinase required for organization of the actin cytoskeleton in Saccharomyces cerevisiae. J Biol Chem. 1998;273(25):15787-93.
51. Stevenson JM, Perera IY, Boss WF. A phosphatidylinositol 4-kinase pleckstrin homology domain that binds phosphatidylinositol 4-monophosphate. J Biol Chem. 1998;273(35):22761-7.
52. Xue HW, Pical C, Brearley C, Elge S, Muller-Rober B. A plant 126-kDa phosphatidylinositol 4-kinase with a novel repeat structure. Cloning and functional expression in baculovirus-infected insect cells. J Biol Chem. 1999;274(9):5738-45.
53. Mueller-Roeber B, Pical C. Inositol phospholipid metabolism in Arabidopsis. Characterized and putative isoforms of inositol phospholipid kinase and phosphoinositide-specific phospholipase C. Plant physiology. 2002;130(1):22-46.
54. Westergren T, Dove SK, Sommarin M, Pical C. AtPIP5K1, an Arabidopsis thaliana phosphatidylinositol phosphate kinase, synthesizes PtdIns(3,4)P-2 and PtdIns(4,5)P-2 in vitro and is inhibited by phosphorylation. Biochem J. 2001;359:583-9.
55. Ischebeck T, Werner S, Krishnamoorthy P, Lerche J, Meijon M, Stenzel I, et al. Phosphatidylinositol 4,5-bisphosphate influences PIN polarization by controlling clathrin-mediated membrane trafficking in Arabidopsis. The Plant cell. 2013;25(12):4894-911.
56. Nakamura Y. Plant Phospholipid Diversity: Emerging Functions in Metabolism and Protein-Lipid Interactions. Trends in Plant Science. 2017;22(12):1027-40.
57. Liu Y, Wang G, Wang X. Role of aminoalcoholphosphotransferases 1 and 2 in phospholipid homeostasis in Arabidopsis. The Plant cell. 2015;27(5):1512-28.
58. Yamaoka Y, Yu YB, Mizoi J, Fujiki Y, Saito K, Nishijima M, et al. PHOSPHATIDYLSERINE SYNTHASE1 is required for microspore development in Arabidopsis thaliana. Plant Journal. 2011;67(4):648-61.

59. Platre MP, Noack LC, Doumane M, Bayle V, Simon MLA, Maneta-Peyret L, et al. A Combinatorial Lipid Code Shapes the Electrostatic Landscape of Plant Endomembranes. Dev Cell. 2018;45(4):465-80 e11.
60. Bankaitis VA, Mousley CJ, Schaaf G. The Sec14 superfamily and mechanisms for crosstalk between lipid metabolism and lipid signaling. Trends Biochem Sci. 2010;35(3):150-60.
61. Stefan CJ, Trimble WS, Grinstein S, Drin G, Reinisch K, De Camilli P, et al. Membrane dynamics and organelle biogenesis-lipid pipelines and vesicular carriers. Bmc Biol. 2017;15.
62. Cleves AE, McGee TP, Whitters EA, Champion KM, Aitken JR, Dowhan W, et al. Mutations in the CDP-choline pathway for phospholipid biosynthesis bypass the requirement for an essential phospholipid transfer protein. Cell. 1991;64(4):789-800.
63. Rivas MP, Kearns BG, Xie ZG, Guo SL, Sekar MC, Hosaka K, et al. Pleiotropic alterations in lipid metabolism in yeast sac1 mutants: Relationship to "bypass sec14p" and inositol auxotrophy. Mol Biol Cell. 1999;10(7):2235-50.
64. Cleves A, McGee T, Bankaitis V. Phospholipid transfer proteins: a biological debut. Trends Cell Biol. 1991;1(1):30-4.
65. Phillips SE, Vincent P, Rizzieri KE, Schaaf G, Bankaitis VA, Gaucher EA. The diverse biological functions of phosphatidylinositol transfer proteins in eukaryotes. Critical reviews in biochemistry and molecular biology. 2006;41(1):21-49.
66. Kf de Campos M, Schaaf G. The regulation of cell polarity by lipid transfer proteins of the SEC14 family. Current opinion in plant biology. 2017;40:158-68.
67. Ghosh R, de Campos MK, Huang J, Huh SK, Orlowski A, Yang Y, et al. Sec14-nodulin proteins and the patterning of phosphoinositide landmarks for developmental control of membrane morphogenesis. Mol Biol Cell. 2015;26(9):1764-81.
68. Jones DL, Kochian LV. Aluminum interaction with plasma membrane lipids and enzyme metal binding sites and its potential role in Al cytotoxicity. Febs Lett. 1997;400(1):51-7.
69. Kinraide TB, Ryan PR, Kochian LV. Interactive effects of Al, h, and other cations on root elongation considered in terms of cell-surface electrical potential. Plant physiology. 1992;99(4):1461-8.
70. Jones DL, Kochian LV. Aluminum Inhibition of the Inositol 1,4,5-Trisphosphate Signal Transduction Pathway in Wheat Roots: A Role in Aluminum Toxicity? The Plant cell. 1995;7(11):1913-22.
71. Ahn SJ, Sivaguru M, Osawa H, Chung GC, Matsumoto H. Aluminum inhibits the H(+)-ATPase activity by permanently altering the plasma membrane surface potentials in squash roots. Plant physiology. 2001;126(4):1381-90.
72. Minet M, Dufour ME, Lacroute F. Complementation of Saccharomyces cerevisiae auxotrophic mutants by Arabidopsis thaliana cDNAs. The Plant journal : for cell and molecular biology. 1992;2(3):417-22.
73. Li X, Xie Z, Bankaitis VA. Phosphatidylinositol/phosphatidylcholine transfer proteins in yeast. Biochimica et biophysica acta. 2000;1486(1):55-71.
74. Schaaf G, Dynowski M, Mousley CJ, Shah SD, Yuan PH, Winklbauer EM, et al. Resurrection of a functional phosphatidylinositol transfer protein from a pseudo-Sec14 scaffold by directed evolution. Mol Biol Cell. 2011;22(6):892-905.
75. Schaaf G, Ortlund EA, Tyeryar KR, Mousley CJ, Ile KE, Garrett TA, et al. Functional anatomy of phospholipid binding and regulation of phosphoinositide homeostasis by proteins of the sec14 superfamily. Mol Cell. 2008;29(2):191-206.
76. Kopittke PM, Blamey FPC. Theoretical and experimental assessment of nutrient solution composition in short-term studies of aluminium rhizotoxicity. Plant Soil. 2016;406(1-2):311-26.

77. Costanzo M, Baryshnikova A, Bellay J, Kim Y, Spear ED, Sevier CS, et al. The genetic landscape of a cell. Science. 2010;327(5964):425-31.
78. Delarue M, Poterewicz G, Hoxha O, Choi J, Yoo W, Kayser J, et al. SCWISh network is essential for survival under mechanical pressure. Proceedings of the National Academy of Sciences of the United States of America. 2017;114(51):13465-70.
79. Mishra R, van Drogen F, Dechant R, Oh S, Jeon NL, Lee SS, et al. Protein kinase C and calcineurin cooperatively mediate cell survival under compressive mechanical stress. Proceedings of the National Academy of Sciences of the United States of America. 2017;114(51):13471-6.
80. Beasley TM, Schumacker RE. Multiple regression approach to analyzing contingency tables: Post hoc and planned comparison procedures. J Exp Educ. 1995;64(1):79-93.
81. Yoshida S, Bartolini S, Pellman D. Mechanisms for concentrating Rho1 during cytokinesis. Genes Dev. 2009;23(7):810-23.
82. Hatakeyama R, Kono K, Yoshida S. Ypk1 and Ypk2 kinases maintain Rho1 at the plasma membrane by flippase-dependent lipid remodeling after membrane stresses. J Cell Sci. 2017;130(6):1169-78.
83. Audhya A, Emr SD. Stt4 PI 4-kinase localizes to the plasma membrane and functions in the Pkc1-mediated MAP kinase cascade. Dev Cell. 2002;2(5):593-605.
84. Fang M, Kearns BG, Gedvilaite A, Kagiwada S, Kearns M, Fung MK, et al. Kes1p shares homology with human oxysterol binding protein and participates in a novel regulatory pathway for yeast Golgi-derived transport vesicle biogenesis. Embo J. 1996;15(23):6447-59.
85. Nunez LR, Jesch SA, Gaspar ML, Almaguer C, Villa-Garcia M, Ruiz-Noriega M, et al. Cell Wall Integrity MAPK Pathway Is Essential for Lipid Homeostasis. J Biol Chem. 2008;283(49):34204-17.
86. Roy A, Levine TP. Multiple pools of phosphatidylinositol 4-phosphate detected using the pleckstrin homology domain of Osh2p. J Biol Chem. 2004;279(43):44683-9.
87. Hammond GR, Fischer MJ, Anderson KE, Holdich J, Koteci A, Balla T, et al. PI4P and PI(4,5)P2 are essential but independent lipid determinants of membrane identity. Science. 2012;337(6095):727-30.
88. von Filseck JM, Vanni S, Mesmin B, Antonny B, Drin G. A phosphatidylinositol-4-phosphate powered exchange mechanism to create a lipid gradient between membranes. Nat Commun. 2015;6.
89. Makino A, Baba T, Fujimoto K, Iwamoto K, Yano Y, Terada N, et al. Cinnamycin (Ro 09-0198) promotes cell binding and toxicity by inducing transbilayer lipid movement. J Biol Chem. 2003;278(5):3204-9.
90. Iwamoto K, Hayakawa T, Murate M, Makino A, Ito K, Fujisawa T, et al. Curvature-dependent recognition of ethanolamine phospholipids by duramycin and cinnamycin. Biophysical journal. 2007;93(5):1608-19.
91. Sartorel E, Barrey E, Lau RK, Thorner J. Plasma membrane aminoglycerolipid flippase function is required for signaling competence in the yeast mating pheromone response pathway. Mol Biol Cell. 2015;26(1):134-50.
92. Schaaf G, Betts L, Garrett TA, Raetz CR, Bankaitis VA. Crystallization and preliminary X-ray diffraction analysis of phospholipid-bound Sfh1p, a member of the Saccharomyces cerevisiae Sec14p-like phosphatidylinositol transfer protein family. Acta Crystallogr Sect F Struct Biol Cryst Commun. 2006;62(Pt 11):1156-60.
93. Schnabl M, Oskolkova OV, Holic R, Brezna B, Pichler H, Zagorsek M, et al. Subcellular localization of yeast Sec14 homologues and their involvement in regulation of phospholipid turnover. Eur J Biochem. 2003;270(15):3133-45.
94. Kooijman EE, Carter KM, van Laar EG, Chupin V, Burger KNJ, de Kruijff B. What makes the bioactive lipids phosphatidic acid and lysophosphatidic acid so special? Biochemistry-Us. 2005;44(51):17007-15.

95. Shin JJH, Loewen CJR. Putting the pH into phosphatidic acid signaling. Bmc Biol. 2011;9.
96. Horchani H, de Saint-Jean M, Barelli H, Antonny B. Interaction of the Spo20 Membrane-Sensor Motif with Phosphatidic Acid and Other Anionic Lipids, and Influence of the Membrane Environment. Plos One. 2014;9(11).
97. Delhaize E, Hebb DM, Richards KD, Lin JM, Ryan PR, Gardner RC. Cloning and expression of a wheat (Triticum aestivum L.) phosphatidylserine synthase cDNA. Overexpression in plants alters the composition of phospholipids. J Biol Chem. 1999;274(11):7082-8.
98. Brzeska H, Guag J, Remmert K, Chacko S, Korn ED. An experimentally based computer search identifies unstructured membrane-binding sites in proteins: application to class I myosins, PAKS, and CARMIL. J Biol Chem. 2010;285(8):5738-47.
99. Bailey MJ, Prehoda KE. Establishment of Par-Polarized Cortical Domains via Phosphoregulated Membrane Motifs. Dev Cell. 2015;35(2):199-210.
100. Hoekenga OA, Vision TJ, Shaff JE, Monforte AJ, Lee GP, Howell SH, et al. Identification and characterization of aluminum tolerance loci in Arabidopsis (Landsberg erecta x Columbia) by quantitative trait locus mapping. A physiologically simple but genetically complex trait. Plant physiology. 2003;132(2):936-48.
101. Hoekenga OA, Maron LG, Pineros MA, Cancado GMA, Shaff J, Kobayashi Y, et al. AtALMT1, which encodes a malate transporter, is identified as one of several genes critical for aluminum tolerance in Arabidopsis. Proceedings of the National Academy of Sciences of the United States of America. 2006;103(25):9738-43.
102. Antignani V, Klocko AL, Bak G, Chandrasekaran SD, Dunivin T, Nielsen E. Recruitment of PLANT U-BOX13 and the PI4Kbeta1/beta2 phosphatidylinositol-4 kinases by the small GTPase RabA4B plays important roles during salicylic acid-mediated plant defense signaling in Arabidopsis. The Plant cell. 2015;27(1):243-61.
103. Lin F, Krishnamoorthy P, Schubert V, Hause G, Heilmann M, Heilmann I. A dual role for cell plate-associated PI4Kbeta in endocytosis and phragmoplast dynamics during plant somatic cytokinesis. Embo J. 2019.
104. Kusano H, Testerink C, Vermeer JEM, Tsuge T, Shimada H, Oka A, et al. The Arabidopsis phosphatidylinositol phosphate 5-kinase PIP5K3 is a key regulator of root hair tip growth. The Plant cell. 2008;20(2):367-80.
105. Simon ML, Platre MP, Assil S, van Wijk R, Chen WY, Chory J, et al. A multi-colour/multi-affinity marker set to visualize phosphoinositide dynamics in Arabidopsis. The Plant journal : for cell and molecular biology. 2014;77(2):322-37.
106. Friml J, Yang X, Michniewicz M, Weijers D, Quint A, Tietz O, et al. A PINOID-dependent binary switch in apical-basal PIN polar targeting directs auxin efflux. Science. 2004;306(5697):862-5.
107. Sukumar P, Edwards KS, Rahman A, DeLong A, Muday GK. PINOID Kinase Regulates Root Gravitropism through Modulation of PIN2-Dependent Basipetal Auxin Transport in Arabidopsis. Plant physiology. 2009;150(2):722-35.
108. Hong S, Hou NY, Schlicht M, Wan YL, Mancuso S, Baluska F. Aluminium toxicity targets PIN2 in Arabidopsis root apices: Effects on PIN2 endocytosis, vesicular recycling, and polar auxin transport. Chinese Sci Bull. 2008;53(16):2480-7.
109. Dhonukshe P, Huang F, Galvan-Ampudia CS, Mahonen AP, Kleine-Vehn J, Xu J, et al. Plasma membrane-bound AGC3 kinases phosphorylate PIN auxin carriers at TPRXS(N/S) motifs to direct apical PIN recycling (vol 137, pg 3245, 2010). Development. 2015;142(13):2386-7.
110. Pina RG, Cervantes C. Microbial interactions with aluminium. Biometals. 1996;9(3):311-6.

111. Kawahara M, Kato-Negishi M. Link between Aluminum and the Pathogenesis of Alzheimer's Disease: The Integration of the Aluminum and Amyloid Cascade Hypotheses. Int J Alzheimers Dis. 2011;2011:276393.
112. Maya S, Prakash T, Madhu KD, Goli D. Multifaceted effects of aluminium in neurodegenerative diseases: A review. Biomed Pharmacother. 2016;83:746-54.
113. von Filseck JM, Copic A, Delfosse V, Vanni S, Jackson CL, Bourguet W, et al. Phosphatidylserine transport by ORP/Osh proteins is driven by phosphatidylinositol 4-phosphate. Science. 2015;349(6246):432-6.
114. Fadeel B, Xue D. The ins and outs of phospholipid asymmetry in the plasma membrane: roles in health and disease. Critical reviews in biochemistry and molecular biology. 2009;44(5):264-77.
115. Mizuike A, Kobayashi S, Rikukawa T, Ohta A, Horiuchi H, Fukuda R. Suppression of respiratory growth defect of mitochondrial phosphatidylserine decarboxylase deficient mutant by overproduction of Sfh1, a Sec14 homolog, in yeast. Plos One. 2019;14(4):e0215009.
116. Tuller G, Nemec T, Hrastnik C, Daum G. Lipid composition of subcellular membranes of an FY1679-derived haploid yeast wild-type strain grown on different carbon sources. Yeast. 1999;15(14):1555-64.
117. Ren J, Pei-Chen Lin C, Pathak MC, Temple BR, Nile AH, Mousley CJ, et al. A phosphatidylinositol transfer protein integrates phosphoinositide signaling with lipid droplet metabolism to regulate a developmental program of nutrient stress-induced membrane biogenesis. Mol Biol Cell. 2014;25(5):712-27.
118. Sorger D, Athenstaedt K, Hrastnik C, Daum G. A yeast strain lacking lipid particles bears a defect in ergosterol formation. J Biol Chem. 2004;279(30):31190-6.
119. Currie E, Guo X, Christiano R, Chitraju C, Kory N, Harrison K, et al. High confidence proteomic analysis of yeast LDs identifies additional droplet proteins and reveals connections to dolichol synthesis and sterol acetylation. Journal of lipid research. 2014;55(7):1465-77.
120. Bozaquel-Morais BL, Madeira JB, Maya-Monteiro CM, Masuda CA, Montero-Lomeli M. A new fluorescence-based method identifies protein phosphatases regulating lipid droplet metabolism. Plos One. 2010;5(10):e13692.
121. Benghezal M, Roubaty C, Veepuri V, Knudsen J, Conzelmann A. SLC1 and SLC4 encode partially redundant acyl-coenzyme A 1-acylglycerol-3-phosphate O-acyltransferases of budding yeast. J Biol Chem. 2007;282(42):30845-55.
122. Philip B, Levin DE. Wsc1 and Mid2 are cell surface sensors for cell wall integrity signaling that act through Rom2, a guanine nucleotide exchange factor for Rho1. Molecular and cellular biology. 2001;21(1):271-80.
123. Dupres V, Alsteens D, Wilk S, Hansen B, Heinisch JJ, Dufrene YF. The yeast Wsc1 cell surface sensor behaves like a nanospring in vivo. Nat Chem Biol. 2009;5(11):857-62.
124. Heinisch JJ, Dupres V, Wilk S, Jendretzki A, Dufrene YF. Single-Molecule Atomic Force Microscopy Reveals Clustering of the Yeast Plasma-Membrane Sensor Wsc1. Plos One. 2010;5(6).
125. Jin CY, Parshin AV, Daly I, Strich R, Cooper KF. The Cell Wall Sensors Mtl1, Wsc1, and Mid2 Are Required for Stress-Induced Nuclear to Cytoplasmic Translocation of Cyclin C and Programmed Cell Death in Yeast. Oxid Med Cell Longev. 2013.
126. Zhong S, Hsu F, Stefan CJ, Wu X, Patel A, Cosgrove MS, et al. Allosteric activation of the phosphoinositide phosphatase Sac1 by anionic phospholipids. Biochemistry-Us. 2012;51(15):3170-7.
127. Meca J, Massoni-Laporte A, Martinez D, Sartorel E, Loquet A, Habenstein B, et al. Avidity-driven polarity establishment via multivalent lipid-GTPase module interactions. Embo J. 2019;38(3).

128. Tani M, Kuge O. Involvement of Sac1 phosphoinositide phosphatase in the metabolism of phosphatidylserine in the yeast Saccharomyces cerevisiae. Yeast. 2014;31(4):145-58.
129. Nomura W, Ito Y, Inoue Y. Role of phosphatidylserine in the activation of Rho1-related Pkc1 signaling in Saccharomyces cerevisiae. Cell Signal. 2017;31:146-53.
130. Omnus DJ, Manford AG, Bader JM, Emr SD, Stefan CJ. Phosphoinositide kinase signaling controls ER-PM cross-talk. Mol Biol Cell. 2016;27(7):1170-80.
131. Zewe JP, Wills RC, Sangappa S, Goulden BD, Hammond GR. SAC1 degrades its lipid substrate PtdIns4P in the endoplasmic reticulum to maintain a steep chemical gradient with donor membranes. Elife. 2018;7.
132. Wolf S. Plant cell wall signalling and receptor-like kinases. Biochem J. 2017;474:471-92.
133. Shih HW, Miller ND, Dai C, Spalding EP, Monshausen GB. The Receptor-like Kinase FERONIA Is Required for Mechanical Signal Transduction in Arabidopsis Seedlings. Current Biology. 2014;24(16):1887-92.
134. Wolf S, van der Does D, Ladwig F, Sticht C, Kolbeck A, Schurholz AK, et al. A receptor-like protein mediates the response to pectin modification by activating brassinosteroid signaling. Proceedings of the National Academy of Sciences of the United States of America. 2014;111(42):15261-6.
135. Zhang GC, Slaski JJ, Archambault DJ, Taylor GJ. Alteration of plasma membrane lipids in aluminum-resistant and aluminum-sensitive wheat genotypes in response to aluminum stress. Physiol Plantarum. 1997;99(2):302-8.
136. Chaffai R, Marzouk B, El Ferjani E. Aluminum mediates compositional alterations of polar lipid classes in maize seedlings. Phytochemistry. 2005;66(16):1903-12.
137. Akeson MA, Munns DN, Burau RG. Adsorption of Al3+ to phosphatidylcholine vesicles. Biochimica et biophysica acta. 1989;986(1):33-40.
138. Matsumoto H, Yamamoto Y, Kasai M. Changes of some properties of the plasma membrane-enriched fraction of barley roots
related to aluminum stress: Membrane-associated
ATPase, aluminum and calcium. Soil Science and Plant Nutrition. 1992.
139. Ebine K, Ueda T. Roles of membrane trafficking in plant cell wall dynamics. Front Plant Sci. 2015;6:878.
140. Albertson R, Riggs B, Sullivan W. Membrane traffic: a driving force in cytokinesis. Trends Cell Biol. 2005;15(2):92-101.
141. Wang PW, Hussey PJ. Interactions between plant endomembrane systems and the actin cytoskeleton. Frontiers in Plant Science. 2015;6.
142. Krtkova J, Havelkova L, Krepelova A, Fiser R, Vosolsobe S, Novotna Z, et al. Loss of membrane fluidity and endocytosis inhibition are involved in rapid aluminum-induced root growth cessation in Arabidopsis thaliana. Plant Physiol Biochem. 2012;60:88-97.
143. Amenos M, Corrales I, Poschenrieder C, Illes P, Baluka F, Barcelo J. Different Effects of Aluminum on the Actin Cytoskeleton and Brefeldin A-Sensitive Vesicle Recycling in Root Apex Cells of Two Maize Varieties Differing in Root Elongation Rate and Aluminum Tolerance. Plant Cell Physiol. 2009;50(3):528-40.
144. Pleskot R, Pejchar P, Staiger CJ, Potocky M. When fat is not bad: the regulation of actin dynamics by phospholipid signaling molecules. Frontiers in Plant Science. 2014;5.
145. Osaki M, Watanabe T, Tadano T. Beneficial effect of aluminum on growth of plants adapted to low pH soils. Soil Science and Plant Nutrition. 1997;43(3):551-63.
146. Maejima E, Watanabe T. Proportion of phospholipids in the plasma membrane is an important factor in Al tolerance. Plant Signal Behav. 2014;9(7):e29277.

147. Ahn SJ, Rengel Z, Matsumoto H. Aluminum-induced plasma membrane surface potential and H+-ATPase activity in near-isogenic wheat lines differing in tolerance to aluminum. New Phytol. 2004;162(1):71-9.
148. Sherman F. Getting started with yeast. Methods Enzymol. 1991;194:3-21.
149. Wickerham LJ. A critical evaluation of the nitrogen assimilation tests as commonly used in the classification of the yeasts. J Bacteriol. 1946;51:567.
150. Zonneveld BJM. Cheap and Simple Yeast Media. J Microbiol Meth. 1986;4(5-6):287-91.
151. Watanabe A, Ito H, Chiba M, Ito A, Shimizu H, Fuji S, et al. Isolation of novel types of Arabidopsis mutants with altered reactions to cadmium: cadmium-gradient agar plates are an effective screen for the heavy metal-related mutants. Planta. 2010;232(4):825-36.
152. Michniewicz M, Zago MK, Abas L, Weijers D, Schweighofer A, Meskiene I, et al. Antagonistic regulation of PIN phosphorylation by PP2A and PINOID directs auxin flux. Cell. 2007;130(6):1044-56.
153. Xu J, Scheres B. Dissection of Arabidopsis ADP-RIBOSYLATION FACTOR 1 function in epidermal cell polarity. The Plant cell. 2005;17(2):525-36.
154. Weller B, Zourelidou M, Frank L, Barbosa ICR, Fastner A, Richter S, et al. Dynamic PIN-FORMED auxin efflux carrier phosphorylation at the plasma membrane controls auxin efflux-dependent growth. Proceedings of the National Academy of Sciences of the United States of America. 2017;114(5):E887-E96.
155. Schaaf G, Catoni E, Fitz M, Schwacke R, Schneider A, von Wiren N, et al. A putative role for the vacuolar calcium/manganese proton antiporter AtCAX2 in heavy metal detoxification. Plant Biology. 2002;4(5):612-8.
156. Tong AH, Boone C. Synthetic genetic array analysis in Saccharomyces cerevisiae. Methods Mol Biol. 2006;313:171-92.
157. Fernandez-Acero T, Rodriguez-Escudero I, Molina M, Cid VJ. The yeast cell wall integrity pathway signals from recycling endosomes upon elimination of phosphatidylinositol (4,5)-bisphosphate by mammalian phosphatidylinositol 3-kinase. Cell Signal. 2015;27(11):2272-84.
158. Downing GJ, Kim S, Nakanishi S, Catt KJ, Balla T. Characterization of a soluble adrenal phosphatidylinositol 4-kinase reveals wortmannin sensitivity of type III phosphatidylinositol kinases. Biochemistry-Us. 1996;35(11):3587-94.
159. Munnik T, Zarza X. Analyzing plant signaling phospholipids through 32Pi-labeling and TLC. Methods Mol Biol. 2013;1009:3-15.
160. Tokuyasu KT. Use of Poly(Vinylpyrrolidone) and Polyvinyl-Alcohol) for Cryoultramicrotomy. Histochem J. 1989;21(3):163-71.

Figure captions

Fig 1. 2µ expression of *AtSFH5* and *ScSFH1* mediates Al tolerance in yeast. (A) Al growth assay with AtSFH5. Wild type yeast (BY4741) was transformed with episomal pDR195(*URA3*) empty vector as control or plasmids carrying *AtSFH5* full length coding sequence (CDS) or *AtSFH5 Sec14D* and were spotted in 8-fold serial dilutions onto solid MY* media in presence or absence of Al and incubated for 4 d at 28°C. **(B)** Al and *sec14-1^{ts}* growth assay with yeast ScSec14 homologs. Wild type yeast (BY4741) or *sec14-1^{ts}* was transformed with episomal pDR195(*URA3*) empty vector as control or plasmids carrying the CDS for designated ScSec14 homologs and were spotted in 8-fold serial dilutions onto solid MY* media for Al treatment or on YNB based media for *sec14-1^{ts}* in presence or absence of Al and incubated for 2-4 d at 28°C or at indicated temperatures. **(C)** Al tolerance spotting with ScSfh1 lipid binding mutants. Wild type yeast transformed with pDR195(*URA3*) empty vector as control or plasmids carrying *SFH1* or designated *sfh1* lipid binding mutants were spotted in 8-fold serial dilutions onto solid MY* media in presence or absence of Al and incubated for 4 d at 28°C. **(D)** Determination of Al content. Wild type yeast (BY4741) transformed with pDR195(*URA3*) carrying *AtSFH5*, *ScSFH1* and *ScSEC14* were grown to mid-log phase in MY* media in presence (400 µM) or absence of Al. Al content was determined using ICP-MS. Averages of four biological replicates ± SEM are shown. Statistical significant differences are indicated by letters (Students *t*-test, * $p < 0.05$).

Fig 2. CWI pathway is essential for ScSfh1-mediated Al tolerance. (A) Schematic overview of genome wide screen for the identification of pathways essential for Sfh1-mediated Al tolerance. **(B)** to **(D)** Al growth assay with CWI related yeast strains. Wild type yeast (BY4741) or yeast knock out strains related to CWI pathway transformed with pDR195(*URA3*) empty vector as control or carrying *ScSFH1* were spotted in 8-fold serial dilutions onto solid MY* media in presence or absence of Al and incubated for 4 d at 28°C. **(E)** Al growth assay with *sfh1Δ*. Wild type yeast (SEY6210) or yeast knock out strain transformed with YCplac33(*CEN*) as control or carrying *pSFH1:ScSFH1* (*CEN*) were spotted in 8-fold serial dilutions onto solid MY* media in presence or absence of Al and incubated for 5 d at 28°C. (**F)** Synthetic genetic array (SGA) of *Δsfh1* and *pkc1-3^{ts}* on MY* media containing calcofluor white (CCW). The fitness (average colony size relative to the average colony size of respective wild type strain) of single knock outs and double knock outs emerged from matings between *Δsfh1* (MATa) *pkc1-3^{ts}* (MATα) and *Δsfh1* (MATα) / *pkc1-3^{ts}* (MATa) is shown. Averages ± SEM of at least 243 independent colonies are shown.

Statistical significant differences are indicated by letters (Students *t*-test, $p < 0.05$). **(G)** Effect of Al treatment and *ScSFH1* (*2μ*) expression in an Al time course experiment on ScMpk1 phosphorylation in yeast. After indicated time points of Al treatment, a western blot with protein extracts of BY4741 transformants carrying indicated plasmids was performed. Immunodetection was performed with anti-phospho-p42/44, anti-Slt2 and - as loading control - anti-G6PDH antibodies. **(H)** Effect of *ScSFH1* (*2μ*) expression on mCherry-Rho1 localization. Wild type yeast (SEY6210) transformants carrying YCpLAC11-*mCherry-RHO1* and designated pDR195*(URA3*) plasmids were grown to mid-log phase and imaged. Shown are representative pictures. Scale bar, 5 μm. **(I)** Quantification of PM localization of mCherry-Rho1. Shown are averages ± SEM ($n \geq 100$) of the mCherry-ScRho1 PM localization relative to intracellular signal [(PM_{max}/intracellular signal)-1], for details see material and methods. Statistical significant differences are indicated by stars (Students *t*-test, *** $p < 0.0001$). Similar results were observed in an independent experiment. **(J)** Effect of *ScSFH1* (*2μ*) expression on ScPkc1-GFP localization. PKC1-GFP expressing cells (MML550 strain) carrying indicated pDR195(*URA3*) plasmids were grown to mid-log phase treated for 3 h with mock or 300 μM Al at 28°C and imaged. Shown are representative pictures. **(K)** Quantification of PM localization of mCherry-Rho1 by classification of diffuse localization, PM localization, septum localization and bud tip localization combining three biological replicates (n=3). Statistically significant differences are indicated by letters (Pearson χ^2 analysis, $p < 0.05$).

Fig 3. *ScSFH1* (*2μ*) expression partially rescues *mss4ts* defects at semi-restrictive temperatures. (A) and **(B)** Yeast growth assay with strain defective in PIP homeostasis. Wild type (SEY6210), $pik1^{ts}$, $stt4^{ts}$ and $mss4^{ts}$ transformed with pDR195(*URA3*) empty vector as control and for (A) pDR195(*URA3*) carrying *ScSFH1* or for (B) *ScSFH1,* $ScSFH1^{S175I,T175I}$ and *ScSFH1,* $ScSFH1^{T238D}$ were spotted in 8-fold serial dilutions and incubated for 2-3 d at indicated temperatures. **(C)** Schematic overview of *in vitro* ScMss4 kinase stimulation assay. **(D)** ScMss4 kinase stimulation assay. ScSfh1 was assayed in 5-fold concentration increases (8 nM, 40 nM 200 nM, 1000 nM) in reactions containing GST-ScMss4, PtdIns:PtdCho liposomes, and [γ^{32}P]-ATP. Average values ± STD (n=2) are plotted as percentage of available PtdIns(4)P. **(E)** ScMss4 kinase stimulation assay. Indicated proteins were assayed in a concentration of 3 μM in reactions containing GST-ScMss4, PtdIns(4)P:PtdCho liposomes, and [γ^{32}P]-ATP. Average values ± STD (n=2) are plotted as percentage of available PtdIns(4)P. **(F)** Schematic overview of PtdIns(4,5)P_2 *in vitro* release assay **(G)** PtdIns(4,5)P_2 *in vitro* release assay. PtdIns(4,5)P_2 release from indicated proteins into PC liposomes are

plotted. Separation of PC liposomes and ScSec14-type protein-PtdIns(4,5)P_2 complex via bead purification. For detailed description of procedure, see Methods section. **(H)** PIP analysis. *mss4^{ts}* strain (SEY6210 background) carrying indicated pDR195(*URA3*) or pDR195-*ScSFH1-V5* were grown over night, then subcultured to mid-log phase at 26°C and then shifted to 34,5°C for 2 h always in the presence of [^{3}H]-*myo*-inositol. Deacylated PIPs were resolved using Partisphere SAX HPLC. Data were normalized to total activity. Shown are averages ± SEM of changes *ScSFH1* to *ev* (n=3 biological replicates) relative to PtdIns. Statistical significant differences are indicated by letters (Students *t*-test, *** $p < 0.05$).

Fig 4. *ScSFH1/AtSFH5* (*2μ*) expression leads to relocalization of PtdIns(4)P FLARE to PM. (A) Steady state PL analysis via TLC. Wild type yeast (BY4741) carrying indicated pDR195(*URA3*) plasmids were grown for 1d and subcultured to mid-log phase always in the presence of [^{32}P] orthophosphate. Lipids were extracted and separated by TLC. Autoradiograph of TLC is shown. PL species are indicated based on analysis of yeast strains impaired in specific PL biosynthesis pathways (Fig S7A). **(B)**, **(D)** and **(G)** Localization of GFP-2xPH^{Osh2} PtdIns(4)P FLARE. Wild type yeast (SEY6210) carrying pRS424-*GFP-2xPH^{Osh2}* and indicated pDR195(*URA3*) plasmids were grown to mid-log phase at 28°C and imaged. Shown are three representative pictures. Scale bar, 5 μm. **(C)**, **(E)** and **(H)** Quantification of PM-localized PtdIns(4)P FLARE GFP-2xPH^{Osh2}. Shown are averages ± SEM ($n \geq 278$) of the FLARE PM localization relative to intracellular signal [(PM_{max}/intracellular signal)-1], for details see material and methods. Statistical significant differences are indicated by letters (One-way ANOVA with post hoc Tukey HSD, $p < 0.05$). Same results were observed in at least one independent experiment. **(F)** Al tolerance growth assay with Sec14* activation mutant. Wild type yeast (BY4741) transformants carrying indicated pDR195(*URA3*) plasmids were spotted in 8-fold serial dilutions onto solid MY* media in presence or absence of Al and incubated for 4 d at 28°C.

Fig 5. *ScSFH1* (*2μ*) expression changes PtdEtn and PtdCho biosynthesis rates. (A) Cartoon of PtdIns(4)P transfer assay. **(B)** PtdIns(4)P transfer assay using NBD-PH_{FAPP1} and two pools of sonicated liposomes. ScSfh1, ScSec14 and Osh6 Δ69 as control were tested for ability to transfer PtdIns(4)P from donor liposomes (L_D) to acceptor liposomes (L_A) resulting in retargeting of NBD-PH_{FAPP1} to L_A accompanied by increased NBD fluorescence due to absence of Rho-PE quencher in L_A. **(C)** Pulse PL analysis via TLC. Wild type yeast (BY4741) transformants carrying indicated pDR195(*URA3*) plasmids were grown for 1d in YNB-based media, subcultured in MY* low phosphate media in presence of presence of [^{32}P] orthophosphate and incubated for 1h. Lipids were extracted and separated by TLC.

Autoradiograph of TLC is shown. **(D)**, **(E)** and **(F)** Densiometric quantification of PtdEtn and PtdCho normalized to total PL is presented in (C). **(G)** Schematic overview of PtdCho biosynthetic pathways. **(H)** and **(I)** Normalized data for comparison of GFP-2xPH^{Osh2} PM localization in Wt, *psd1Δ psd2Δ* and *cho2Δ opi3Δ* mutant yeast (non-normalized data are presented in S6C and S6E). Wild type yeast (BY4741), *psd1Δ psd2Δ* and *cho2Δ opi3Δ* carrying pRS424-GFP-2xPH^{Osh2} were grown overnight in selective media in the presence of 1 mM Etn and Cho. After 3 washing steps with selective media without Etn and Cho, yeast cells were subcultured for 5 h in selective media in indicated presence or absence of Etn and/or Cho. Shown are the averages ± SEM ($n \geq 99$) of the PM/intracellular ratio [PM_{max}/intracellular intensity], for details see material and methods, normalized to PM/intracellular ratio [PM_{max}/intracellular intensity] of Wild type yeast in respective growth condition. Statistical significant differences are indicated by letters (One-way ANOVA with post hoc Tukey HSD, $p < 0.05$). **(J)** Effect of *ScPSD2* (*2μ*) expression on Al tolerance. Wild type yeast (BY4741) carrying indicated pDR195(*URA3*) plasmids were spotted in 8-fold serial dilutions onto solid MY* media in presence or absence of Al and incubated for 4 d at 28°C. **(K)** Effect of *ScPSD2* (*2μ*) expression on growth performance of *mss4^{ts}*. Wild type yeast (SEY6210) or *mss4^{ts}* carrying indicated pDR195(*URA3*) plasmids were spotted in 8-fold serial dilutions and incubated for 2-3 d at indicated temperatures. Shown results were repeated independently. **(L)** Effect of *ScPSD2* (*2μ*) expression on PM localization of GFP-2xPH^{Osh2}. Wild type yeast (SEY6210) carrying pRS424-GFP-2xPH^{Osh2} and indicated pDR195(*URA3*) plasmids were grown to mid-log phase at 28°C and imaged. Shown are averages ± SEM ($n \geq 222$) of the FLARE PM localization relative to intracellular signal [(PM_{max}/intracellular signal)-1], for details see material and methods.. Statistical significant differences are indicated by letters (Students *t*-test, $p < 0.001$). **(M)** and **(N)** Equivalent numbers of wild type yeast (SEY6210) cells carrying indicated pDR195(*URA3*) plasmids were each plated as a lawn on Agar plates with selective media. Paper disks with 10 µl of a Duramycin solution (8 mM) were immediately placed onto lawn and plates were incubated for 2 d at 28°C. Shown results were repeated independently.

Fig 6. ScSfh1 transfers PtdCho and PtdEtn. (A) Cartoon of transfer assay with ^{14}C-labeled PtdCho using big sucrose-loaded donor liposomes (L_D) and small light acceptor liposomes (L_A) with defined lipid compositions. **(B)** ^{14}C-PtdCho transfer assay with wild type ScSfh1 and lipid binding mutants. ^{14}C-PtdCho transfer activity of indicated ScSfh1 proteins from big sucrose-loaded L_D consisting of PtdSer:PtdCho:^{14}C-PtdCho (100µM:10µM:10µM) into respective small light L_A consisting of PtdSer only, PtdSer:PtdCho or PtdSer:PtdIns

(100µM:10µM) was assayed. Shown are averages ± STD (n = 2 technical replicates). The experiment was repeated independently with similar results. **(C)** ^{14}C-PtdEtn transfer assay with ScSfh1. ^{14}C-PtdEtn transfer activity of ScSfh1 from big sucrose-loaded L_D consisting of PtdSer:PtdCho:^{14}C-PtdEtn (100µM:10µM:10µM) into small light L_A consisting of PtdSer was assayed. Shown are the averages ± STD (n = 2 technical replicates). **(D)** ^{14}C-PtdCho transfer assay with wild type ScSfh1 into PtdEtn containing acceptor liposomes. ^{14}C-PtdCho transfer activity of indicated ScSfh1 proteins from big sucrose-loaded L_D consisting of PtdSer:PtdCho:^{14}C-PtdCho (100µM:10µM:10µM) into respective small light L_A consisting of PtdSer only, PtdSer:PtdEtn or PtdSer:PtdCho (100µM:10µM) was assayed. Shown is the relative stimulation of ScSfh1 ^{14}C-PtdCho transfer activity into indicated L_A (average ± STD, n = 2 technical replicates). The experiment was repeated independently with similar results. For detailed information see Material and Methods.

Fig 7. GFP-AtSFH5 localizes to LDs and the PM. (A) Al growth assay with GFP-AtSFH5. Wild type yeast (SEY6210) carrying indicated YCplac22(*TRP1*) as *ev* control or pAG414-eGFP-AtSFH5(*TRP1*) was spotted in 8-fold serial dilutions onto solid MY* media in presence or absence of Al and incubated for 4 d at 28°C. **(B)** Localization of eGFP-AtSFH5 in yeast. Wild type yeast (SEY6210) carrying pAG414-eGFP-AtSFH5 and mCherry-Nlj16^{AtSFH1} as PM marker were grown to mid-log phase at 28°C and imaged. Shown are representative pictures. Scale bar, 5 µm. Arrowheads indicate PM localization of eGFP-AtSFH5. **(C)** Correlative light and electron microscopy with GFP-AtSFH5.Wild type yeast (SEY6210) carrying pAG414-eGFP-AtSFH5 were grown to mid-log phase at 28°C and processed and imaged as described in Material and Methods. First panel shows fluorescent signal, second panel shows TEM images and third panel shows the overlay. Asterisks indicate LD with monolayer membrane. Arrowheads indicate PM free of ER contact site. The plus symbol indicates an ER-PM contact site. **(D)** and **(F)** Confocal microscopic images of eGFP-AtSFH5 and mCherry-Nlj16^{AtSFH1} localization. (D) represents a mid-section and (F) a surface view of yeast. Wild type yeast (SEY6210) carrying pAG414-eGFP-AtSFH5 and pDR199- mCherry-Nlj16^{AtSFH1} as PM marker were grown to mid-log phase at 28°C and imaged. Shown are representative pictures. Scale bar, 5 µm. Arrowheads indicate ring-shaped LD localization of eGFP-AtSFH5. **(E)** and **(G)** Analysis of colocalization shown in (D) using fluorescence intensity plots. **(F)** Surface view of pAG414-eGFP-AtSFH5 and pDR199- mCherry-Nlj16^{AtSFH1} localization.

Fig 8. Negative charge of PM correlates with Al tolerance in yeast. (A) Effect of *ScSFH1* (*2µ*) expression on charge sensor localization in yeast. Wild type yeast (SEY6210) carrying ScSpo20-GCC-GFP and indicated pDR195(*URA3*) plasmids were grown to mid-log phase at

28°C and imaged. Shown are averages ± SEM (n ≥ 303) of the FLARE PM localization relative to intracellular signal [(PM_{max}/intracellular signal)-1], for details see material and methods. Statistically significant differences are indicated by letters (One-way ANOVA with post hoc Tukey HSD) $p < 0.05$). Similar results were observed in at least one independent experiment. (**B)** Effect of Al on charge sensor and different FLAREs. Wild type yeast (SEY6210) carrying indicated sensors were grown to mid-log phase and incubated for 5 h at subtoxic Al concentrations (150 µM) and imaged. Shown are averages ± SEM (n ≥ 203) of the FLARE PM localization PM/intracellular ratio [PM_{max}/intracellular intensity], for deteals see material and methods, relative to mock. Statistically significant differences are indicated by letters (One-way ANOVA with post hoc Tukey HSD) $p < 0.05$). **(C)** Al growth assay with yeast mutant strains defective in the biosynthesis of negatively charged PLs. Corresponding wild type yeast and indicated strains carrying indicated pDR195(*URA3*) plasmids were spotted in 8-fold serial dilutions onto solid MY* media in presence or absence of Al at the indicated temperatures and incubated for 2-4 d at the indicated temperatures. **(D)** Effect of *ScMSS4* (*2µ*) expression on yeast growth on Al media. Two different *MSS4* versions were expressed under a native *MSS4* promoter fragment, the shorter encoding a truncated protein lacking a N-terminal autoinhibitory domain. Wild type yeast (BY4741) cells carrying indicated pDR195(*URA3*) plasmids were spotted onto solid MY* media in presence or absence of Al at 28 °C and incubated for 4 d. **(E)** BH-score of ScRho1 (amino acid 180-end). Score was calculated using the BH-Search web application. **(F)** Effect of *ScSFH1* (*2µ*) expression on mCherry-Rho1 localization. Wild type yeast (SEY6210) carrying YCpLAC11-*mCherry-RHO1* and indicated pDR195(*URA3*) plasmids were grown to mid-log phase at 28°C and imaged. Shown are three representative pictures. Scale bar, 5 µm. **(G)** Quantification of PM localization of mCherry-Rho1. Shown are averages ± SEM (n ≥ 278) of the increase of mCherry-Rho1 PM localization relative to intracellular signal [(PM_{max}/intracellular signal)-1], for details see material and methods, normalized to the ev PM localization. Statistical significant differences are indicated by letters (Mann-Whitney-U-test, $p < 0.05$).

Fig 9. Alteration in of the biosynthesis of negatively charged PLs correlates with Al tolerance in plants and Al treatment influenced PM localization of FLAREs, a charge sensor and an of AtPID-YFP. (A) to **(D)** Al root growth of Wt (Col-0) and indicated mutant lines compromised in PL synthesis. After 3 d stratification, seeds of indicated plant lines were germinated on Al-free solid media and transferred to mock or Al solid media 5 d after germination. Presented are the averages ± SEM (n ≥ 81) of primary root length after 2 d for

(A), (B) and (D) and 5 d for (C) relative to mock grown seedlings in %. Statistically significant differences are indicated by letters or stars (Students *t*-test, for letters $p < 0.05$, for stars * $p < 0.05$, ** $p < 0.01$, *** $p < 0.001$). Similar results were obtained in two additional experiments using seedlings from an independent seed stock. **(E)** Effect of *AtPIP5K3* overexpression on primary root growth on Al containing media. After 3 d stratification seeds of control line ER8-GFP and ER8-PIP5K3 line were germinated on Al and β-estradiol-free solid media and transferred to mock or Al solid media containing 10 µM β-estradiol 5 d after germination. Presented are the averages ± SEM ($n \geq 90$) of primary root length 5 d relative to mock grown seedlings in %. Statistically significant differences are indicated by letters (Students *t*-test, $p < 0.05$). Similar results were obtained in two additional experiments using seedlings from an independent seed stock. **(F and G)** Effect of Al treatment on charge sensor and FLAREs *in planta*. After 3 d stratification, seeds of indicated plant lines were germinated on Al free solid media. 5 d-old seedlings were transferred to solid mock or Al media and imaged after 5 h incubation. Shown are representative pictures in (F) and in (G) averages ± SEM ($n \geq 167$ cells) of the FLARE PM localization relative to mock PM/intracellular ratio [$PM_{max,plants}$/intracellular signal], for details see material and methods, are shown. Presented decreases of PM/intracellular ratios are all statistical significant (Students *t*-test, $p < 0.001$). Similar results were observed in independent experiments. **(H)** Effect of Al on PtdIns(4,5)P_2 FLARE *in planta*. 5 d-old seedlings were transferred to object slides containing liquid mock or Al media (50 µM). Roots were imaged for 21 min. Shown are averages ± SEM of the FLARE PM localization relative to mock PM/intracellular ratio [$PM_{max,plants}$/intracellular signal], for details see material and methods, (n=6 cells, Students *t*-test, $p < 0.05$). **(I)** Effect of Al treatment on AtPID:YFP PM association. After 3 d stratification, seeds of the *AtpPID:AtPID-YFP* line was germinated on Al free solid media. 5 d-old seedlings were transferred to solid mock or Al media and imaged after 5 h incubation. Shown are representative pictures and in **(J)** averages ± SEM ($n \geq 173$ cells) of the FLARE PM/intracellular ratio [$PM_{max,plants}$/intracellular signal], for details see material and methods, are shown. Presented decreases of PM/intracellular ratios are all statistical significant (Students *t*-test, $p < 0.001$). **(K)** Effect of Al treatment on PIN2-GFP localization. 5 d-old seedlings were transferred to solid mock or Al media and imaged after 5 h incubation. Shown are representative pictures seen in two independent experiments. **(L)** Root morphology of 5 d-old seedlings treated with or without Al. Seedlings were geminated on solid mock or Al media. Shown are representative pictures seen in three independent experiments.

Fig 10. Models of ScSfh1-mediated lipid transfer in yeast. (A) Model for PtdIns(4)P/PtdCho counter transfer. PtdIns(4)P is transferred by *in vivo* lipid transfer mediated by ScSfh1 from endomembranes to the PM with the counter substrate PtdCho, which is transferred in the opposite direction. Also a transfer between different pools of PtdIns(4)P might be possible. **(B)** Model for PtdEtn/PtdCho counter transfer. PtdEtn is transferred by *in vivo* lipid transfer mediated by ScSfh1from endomembrane structures (e.g. LDs) to the PM with PtdCho as counter substrate. Also here a transfer between different pools might be possible. PtdEtn increase might change the protonation state of PtdIns(4)P by interlipid H-bonding and subsequently increase accessibility of PtdIns(4)P, similar to the proposed influence of PtdEtn on PtdOH (94).

Fig 11. Model for mode of action of Al at cellular level. (A) Al is absent: Undisturbed PM recruitment of proteins targeted by charge or stereospecific interaction takes place facilitating proper downstream signaling. **(B)** After Al treatment: Al competes with proteins targeted to the PM via charge or stereospecific interaction followed by a decrease of overall PM charge and proper protein recruitment leading to a disruption of downstream signaling.

Fig S1. Activities of Sec14-type proteins, mammalian PITPs and ScSfh1 lipid transfer mutants. (A) and **(B)** Al and *sec14-1*^{ts} growth assay with plant and mammalian ScSec14 homologs and non-squence related mammalian PITPs. Wild type yeast (BY4741) carrying indicated pDR195(*URA3*) plasmids were spotted in 8-fold serial dilutions onto solid MY* media in presence or absence of Al and incubated for 4 d at 28°C or at 37°C as indicated. **(C)** Al growth assay with ScSfh1* activation mutant and ScSfh1* lipid binding mutants. Wild type yeast carrying indicated pDR195(*URA3*) plasmids were spotted in 8-folg serial dilutions onto solid MY* media in presence or absence of Al and incubated for 4 d at 28°C. **(D)** Protein stability of ScSfh1 lipid binding mutants. Wild type (BY4741) yeast carrying indicated pDR195(*URA3*) plasmids were grown to saturation. Proteins were extracted and ScSfh1-V5 proteins were detected by western blot, using an anti-V5 monoclonal antibody (Thermo Fischer Scientific). As loading control endogenous ScKes1 was detected using an anti-ScKes1 antibody. **(E)** Al growth assay with SEY6210. Wild type yeast (SEY6210) carrying indicated pDR195(*URA3*) plasmids were spotted in 8-fold serial dilutions onto solid MY* media in presence or absence of Al and incubated for 4 d at 28°C.

Fig S2. Specificity of AtSFH5/ScSfh1-mediated metal tolerance and element composition changes induced by *AtSFH5/ScSFH1* (*2μ*) expression. (A) Specificity of AtSFH5/ScSfh1-mediated metal tolerance. Wild type yeast (BY4741) carrying indicated pDR195(*URA3*) plasmids were spotted in 8-fold serial dilutions onto solid MY*/YNB supplemented with

indicated metals and incubated for 4 d at 28°C. **(B)** Yeast Al growth assay in liquid culture. Saturated cultures of wild type yeast (BY4741) carrying indicated pDR195(*URA3*) plasmids were adjusted to the same optical density and grown for indicated time. Shown are averages ± SEM (n=2) of OD600 measurements at indicated time points. **(C)** Effect of *AtSFH5/ScSFH1* (*2μ*) expression on metal/nutrient contents. Wild type yeast (BY4741) carrying indicated pDR195(*URA3*) plasmids were treated as described in material and methods. Shown are averages ± SEM (n=4) of ICP-MS/OES measurements. Statistical significant differences are indicated by letters (Students *t*-test, $p < 0.05$)

Fig S3. Effect of ScSfh1 on ScMss4 kinase stimulation and localization. (A) *ScSFH1* (*2μ*) expression in *mss4-5^{ts}*. Indicated strains carrying indicated pDR195(*URA3*) plasmids were spotted in 8-fold serial dilutions onto solid YPD and incubated for 2-3 d at indicated temperatures. **(B)** Determination of protein concentration of ScSfh1/Sec14 wild type and mutant proteins. After protein extraction from *E.coli* and purification (for details see methods section) 1µL of protein was separated by SDS-PAGE and Coomassie stained. **(C)** and **(D)** ScMss4 kinase stimulation assay. Indicated proteins were assayed in a concentration of 3 µM in reactions containing GST-ScMss4, PtdIns(4)P:PtdCho or PtdIns(4,5)P_2 liposomes, and [γ^{32}P]-ATP. Average values ± STD (n=2) are plotted as percentage of available PtdIns(4)P or PtdIns(4,5)P_2. **(E)** Protein concentration of ScSfh1 wild type and mutant protein. After protein extraction from *E.coli* and purification (for details see methods section) 1 µL, 0,5 µL and 0,25 µL of protein was separated by SDS-PAGE and Coomassie stained. Shown is scanned picture of gel. **(F)** *in situ* phosphorylation of ScSfh1. ScSfh1 was pre-loaded with sonicated PtdIns(4)P. After Ni-NTA purification of ScSfh1 and thoroughly washing, an *in vitro* ScMss4 kinase assay was performed as described for (C) and (D). **(G)** PtdIns(4,5)P_2 *in vitro* release assay. PtdIns(4,5)P_2 release from indicated proteins into PC liposomes are plotted. Separation of PC liposomes and ScSec14-type protein-PtdIns(4,5)P_2 complex via sedimentation of big sucrose-loaded liposomes. For detailed description of procedure, see material and methods. **(H)** Effect of *ScSFH1* (*2μ*) expression on ScMss4-GFP localization. Wild type yeast (BY4741) carrying pRS416_MSS4prom_MSS4-GFP (pCS321) were grown to mid log phase and imaged. Shown are representative pictures.

Fig S4. Effect of *ScSFH1* (*2μ*) expression on different FLAREs. (A), **(B)** and **(D)** FLARE localization. Wild type yeast (SEY6210) carrying indicated plasmids were grown to mid-log phase at 28°C and imaged. Shown are three representative pictures. Scale bar, 5 µm. **(C)** and **(E)** Quantification of indicated PM-localized FLARE. Shown are the averages ± SEM ($n \geq 202$) of the FLARE PM localization relative to intracellular signal [(PM_{max}/intracellular

intensity)-1]. Statisticallly significant differences are indicated by letters (One-way ANOVA with post hoc Tukey HSD, $p < 0.05$. Similar results were observed in at least one independent experiment.

Fig S5. Directed evolution screen to endow ScSec14 with ScSfh1-like to Al-tolterance inducing activities. (A) ScSec14* activation variants. Protein alignment of 27 *ScSEC14** activation mutants obtained in the directed evolution screen. For comparison the wild typic sequence of ScSec14 is presented on top. Red boxes indicate amino acid different from wild type sequence. Green box highlights position S173. Grey boxes mark area of unclear sequencing results. **(B)** *sec14-1^{ts}* growth assay**.** *sec14-1^{ts}* transformed with episomal pDR195(*URA3*) empty vector as control or indicated plasmids were spotted in 8-fold serial dilutions onto YNB based media and incubated for 2-4 d at indicated temperatures.

Fig S6. Effect of *ScSFH1* (*2μ*) expression on PL biosynthesis. (A) PL analysis by TLC after [^{32}P] orthophosphate pulse. Wild type yeast (BY4741) or indicated yeast knock out strains carrying pDR195(*URA3*) *ev* were grown for 1d in YNB-based media, subcultured in MY* low phosphate media in presence or absence of 1 mM Etn or Cho, supplemented with [^{32}P] orthophosphate and incubated for 1h. Lipids were extracted and separated by TLC. Autoradiograph of TLC is shown. All bands shown were run on the same TLC plate. Please note that *ev* control shown here is identical with Fig 5C. **(B)** and **(D)** Localization of GFP-2xPH^{Osh2} in Wt, *psd1Δ psd2Δ* and *cho2Δ opi3Δ* mutant yeast. Wild type yeast (BY4741), *psd1Δ psd2Δ* and *cho2Δ opi3Δ* carrying pRS424-GFP-2xPH^{Osh2} were grown overnight in selective media in the presence of 1 mM Etn and Cho. After 3 washing steps with selective media without Etn and Cho, yeast were subcultured for 5 h in selective media in indicated presence or absence of Etn and/or Cho. Shown are three representative pictures. Scale bar, 5 µm. **(C)** and **(E)** Quantification of PM localized PtdIns(4)P FLARE GFP-2xPH^{Osh2} in wild type yeast (BY4741), *psd1Δ psd2Δ* and *cho2Δ opi3Δ*. Shown are averages ± SEM ($n \geq 99$) of the FLARE PM localization relative to intracellular signal [(PM_{max}/ intracellular intensity)-1]. Statistical significant differences are indicated by letters (One-way ANOVA with post hoc Tukey HSD, $p < 0.05$). **(F)** Localization GFP-2xPH^{Osh2} with *ScPSD2* (*2μ*) expression. Shown are representative pictures. **(G)** Confocal microscopy of Cerulan-AtSFH5 in SEY6210.1 and *tetherΔ*. Shown are representative pictures of *Cerulan-AtSFH5* and *ScTCB3-GFP* in wild type (SEY6210.1) and *tetherΔ*. Wild type yeast (SEY6210.1) or *tetherΔ* carrying pAG425GPD-*Cerulean-AtSFH5* or pRS415-*TCB3-GFP* (pAM43, encoding as ER-PM contact site marker) were grown to mid-log phase at 28°C and imaged. Shown are representative pictures. Scale bar, 5 µm.

Fig S7. Influence of membrane charge on Al tolerance and effect of *ScSFH1* (*2μ*) expression on PM charge. (A) *ScSFH1* (*2μ*) expression changed localization of ScSpo20-GCC-GFP charge sensor. Wild type yeast (SEY6210) carrying ScSpo2-GCC-GFP and indicated pDR195(*URA3*) plasmids were grown to mid-log phase at 28°C and imaged. Shown are three representative pictures. Scale bar, 5 μm. **(B)** Yeast Al growth assay in liquid culture. Saturated cultures of wild type yeast (SEY6210) carrying indicated pDR195(*URA3*) plasmids were adjusted to the same optical density and grown for indicated time. Shown are averages ± SEM (n=2) of OD600 measurements at indicated time points. **(C)** Localization of FLAREs after Al treatment. Wild type yeast (SEY6210) in mid-log phase carrying indicated FLAREs were grown in liquid MY* media in the presence or absence of 150 μM Al for 5 h at 28°C and imaged. Shown are three representative pictures. Scale bar, 5 μm **(D)** Effect of *TaPSS1* (*2μ*) expression on Al tolerance in yeast. Wild type yeast (BY4741) carrying indicated pDR195(*URA3*) plasmids were spotted onto solid MY* media in presence or absence of Al at 28 °C and incubated for 4 d. Two independent *TaPSS1* transformants are shown. **(E)** Effect of *ScRHO1* (*2μ*) expression on yeast growth. Wild type yeast (BY4741) carrying indicated pDR195(*URA3*) were spotted onto solid MY* media incubated at 28°C for 4 d. **(F)** Effect of *ScRHO2* (*2μ*) expression on yeast Al tolerance. Wild type yeast (BY4741) carrying indicated pDR195(*URA3*) as ev or *pScRHO2:ScRHO2* (pC-186, *2μ*, *URA3*) were spotted onto solid MY* media incubated at 28°C for 4 d.

Fig S8. Effect of Al treatment on YFP-AtPID localization. (A) Effect of Al treatment on YFP-PID PM association. After 3 d stratification seeds of the *pAtPID:YFP-AtPID* line were germinated on Al-free solid media. 5 d-old seedlings were transferred to solid mock or Al media and imaged after 5 h incubation. Shown are representative pictures. **(B)** Quantification of YFP-PID PM association after Al treatment. Shown are averages ± SEM ($n \geq 72$ cells) of the FLARE PM localization relative to mock PM/intracellular ratio [PM_{max}/intracellular intensity]. Presented decreases of PM/intracellular ratios are all statistical significant (Students *t*-test, ***$p < 0.001$).

Figure 1

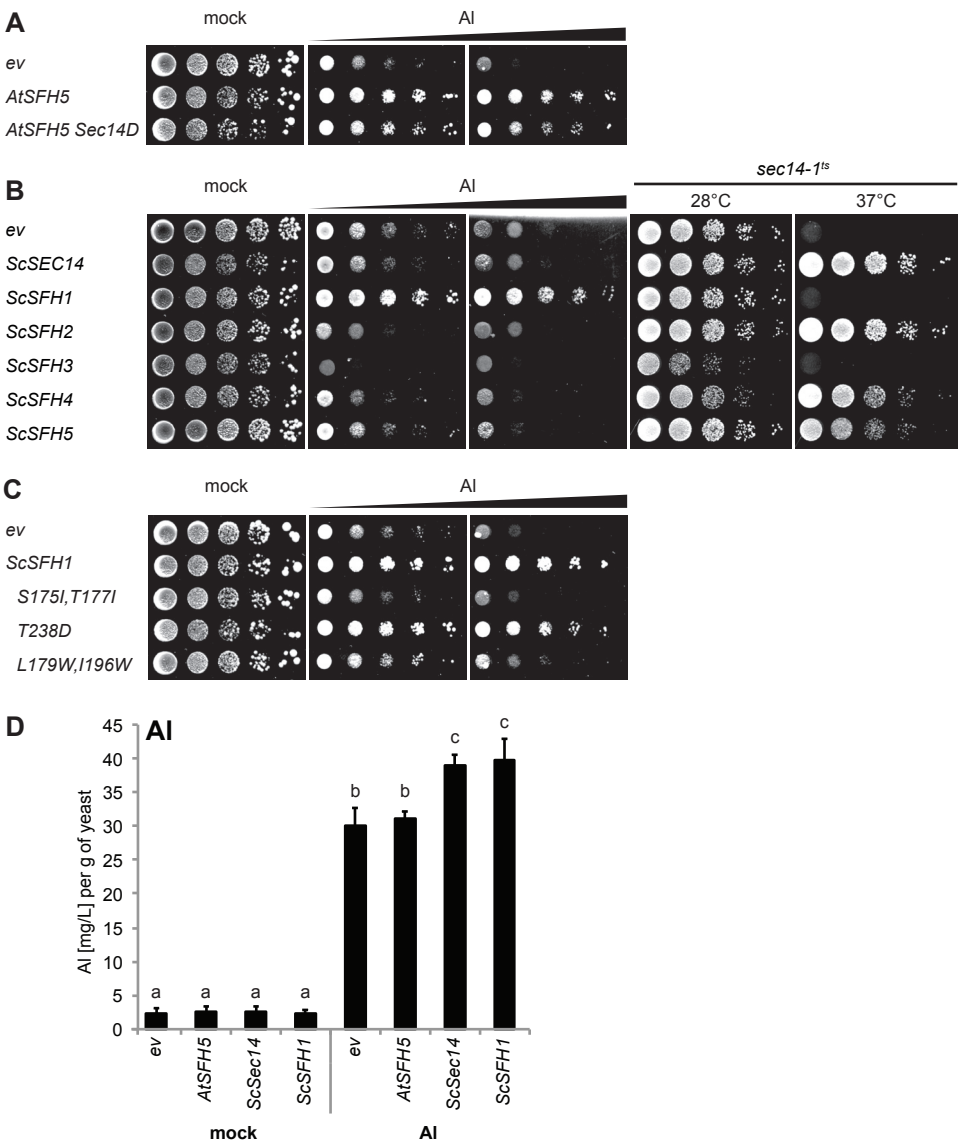
A
mock
Al
ev
AtSFH5
AtSFH5 Sec14D
B
mock
Al
sec14-1ts
28°C
37°C
ev
ScSEC14
ScSFH1
ScSFH2
ScSFH3
ScSFH4
ScSFH5
C
mock
Al
ev
ScSFH1
S175I,T177I
T238D
L179W,I196W
D
Al
Al [mg/L] per g of yeast
45
40
35
30
25
20
15
10
5
0
a
a
a
a
b
b
c
c
ev
AtSFH5
ScSec14
ScSFH1
ev
AtSFH5
ScSec14
ScSFH1
mock
Al

Figure 2

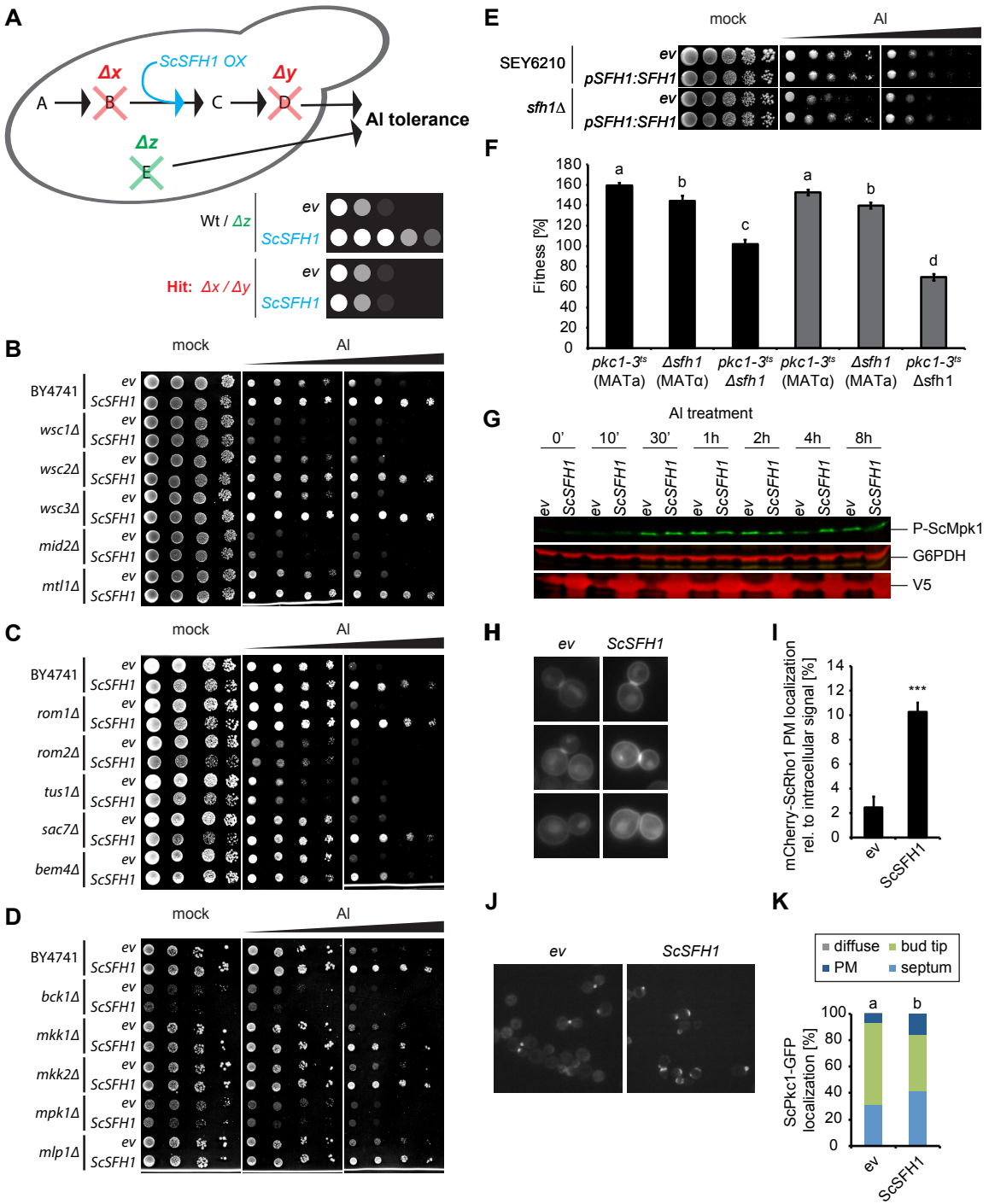
A
ScSFH1 OX
Δx
Δy
Δz
A
B
C
D
E
AI tolerance
Wt / Δz
Hit: Δx / Δy
ev
ScSFH1
B
mock
AI
BY4741
wsc1Δ
wsc2Δ
wsc3Δ
mid2Δ
mtl1Δ
C
rom1Δ
rom2Δ
tus1Δ
sac7Δ
bem4Δ
D
bck1Δ
mkk1Δ
mkk2Δ
mpk1Δ
mlp1Δ
E
SEY6210
sfh1Δ
pSFH1:SFH1
F
Fitness [%]
pkc1-3ts (MATa)
Δsfh1 (MATα)
pkc1-3ts Δsfh1
pkc1-3ts (MATα)
Δsfh1 (MATa)
pkc1-3ts Δsfh1
G
AI treatment
0'
10'
30'
1h
2h
4h
8h
P-ScMpk1
G6PDH
V5
H
I
mCherry-ScRho1 PM localization rel. to intracellular signal [%]
***
J
K
diffuse
bud tip
PM
septum
ScPkc1-GFP localization [%]

Figure 3

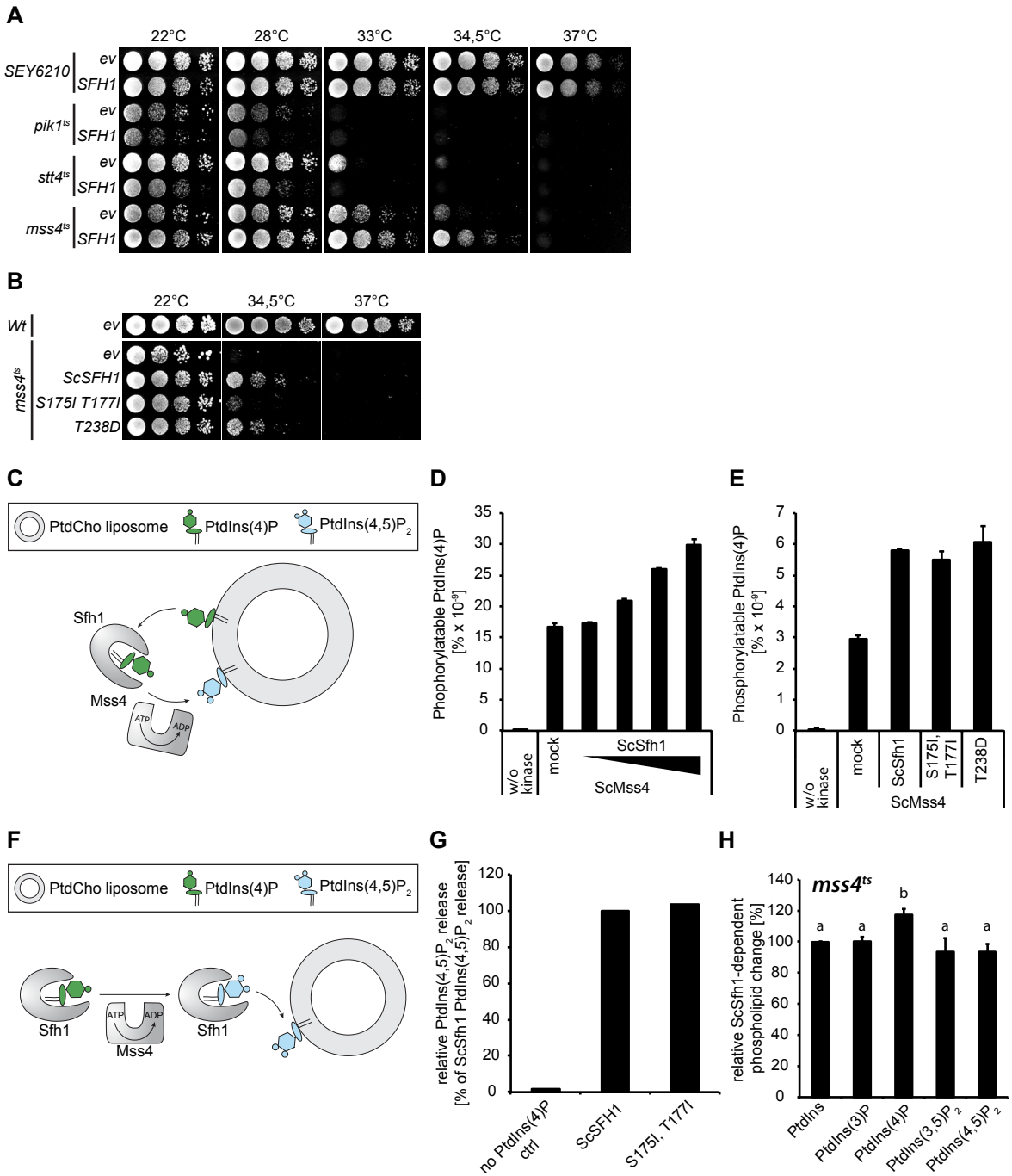
A
22°C
28°C
33°C
34,5°C
37°C
SEY6210
ev
SFH1
pik1ts
stt4ts
mss4ts
B
Wt
ScSFH1
S175I T177I
T238D
C
PtdCho liposome
PtdIns(4)P
PtdIns(4,5)P2
Sfh1
Mss4
ATP
ADP
D
Phophorylatable PtdIns(4)P [% x 10-9]
w/o kinase
mock
ScSfh1
ScMss4
E
Phosphorylatable PtdIns(4)P [% x 10-9]
S175I, T177I
T238D
F
G
relative PtdIns(4,5)P2 release [% of ScSfh1 PtdIns(4,5)P2 release]
no PtdIns(4)P ctrl
ScSFH1
S175I, T177I
H
mss4ts
relative ScSfh1-dependent phospholipid change [%]
PtdIns
PtdIns(3)P
PtdIns(4)P
PtdIns(3,5)P2
PtdIns(4,5)P2

Figure 4

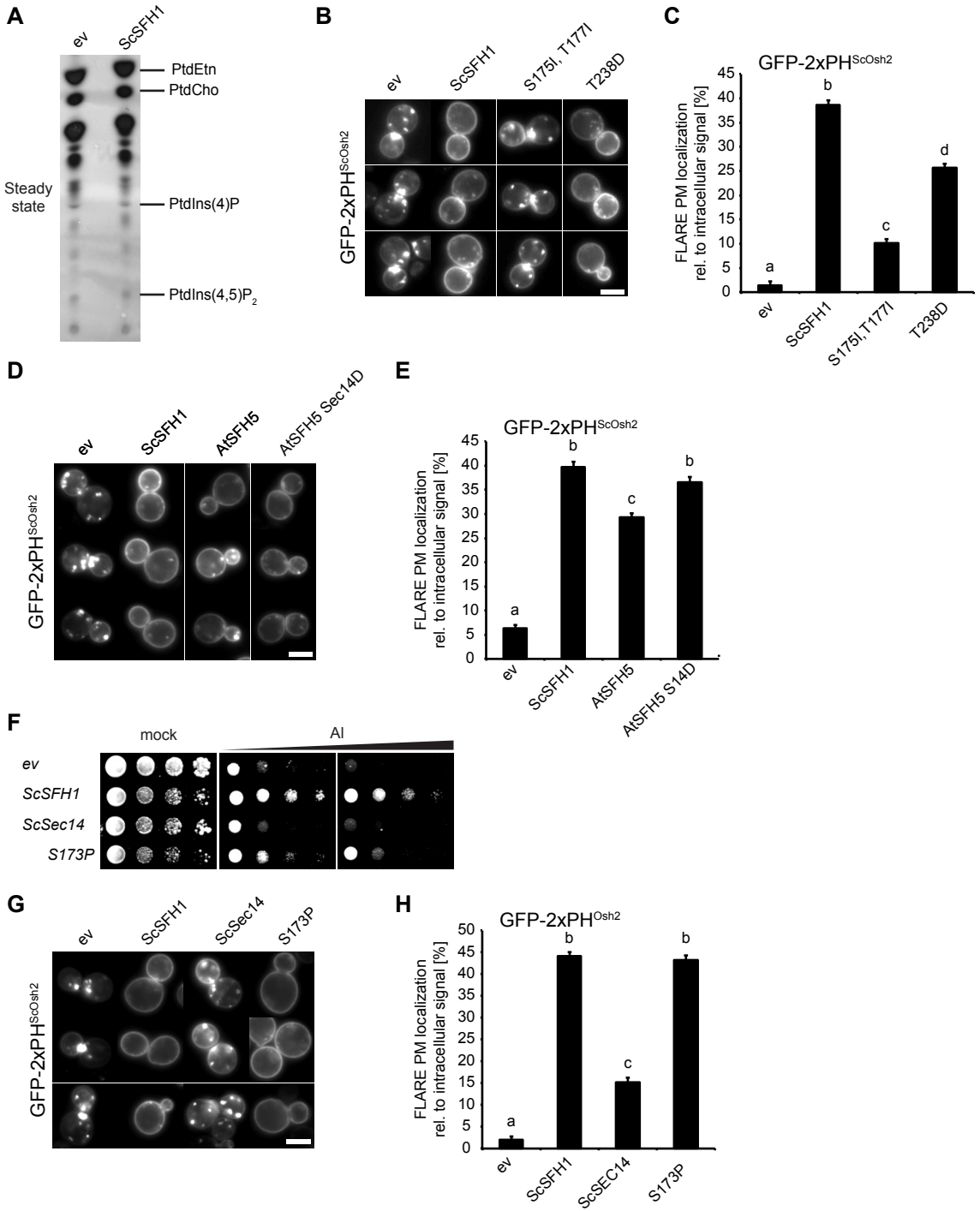
A
ev
ScSFH1
PtdEtn
PtdCho
Steady state
PtdIns(4)P
PtdIns(4,5)P2
B
ev
ScSFH1
S175I, T177I
T238D
GFP-2xPHScOsh2
C
GFP-2xPHScOsh2
FLARE PM localization rel. to intracellular signal [%]
a
b
c
d
ev
ScSFH1
S175I,T177I
T238D
D
ev
ScSFH1
AtSFH5
AtSFH5 Sec14D
GFP-2xPHScOsh2
E
GFP-2xPHScOsh2
FLARE PM localization rel. to intracellular signal [%]
a
b
c
b
ev
ScSFH1
AtSFH5
AtSFH5 S14D
F
mock
Al
ev
ScSFH1
ScSec14
S173P
G
ev
ScSFH1
ScSec14
S173P
GFP-2xPHScOsh2
H
GFP-2xPHOsh2
FLARE PM localization rel. to intracellular signal [%]
a
b
c
b
ev
ScSFH1
ScSEC14
S173P

Figure 5

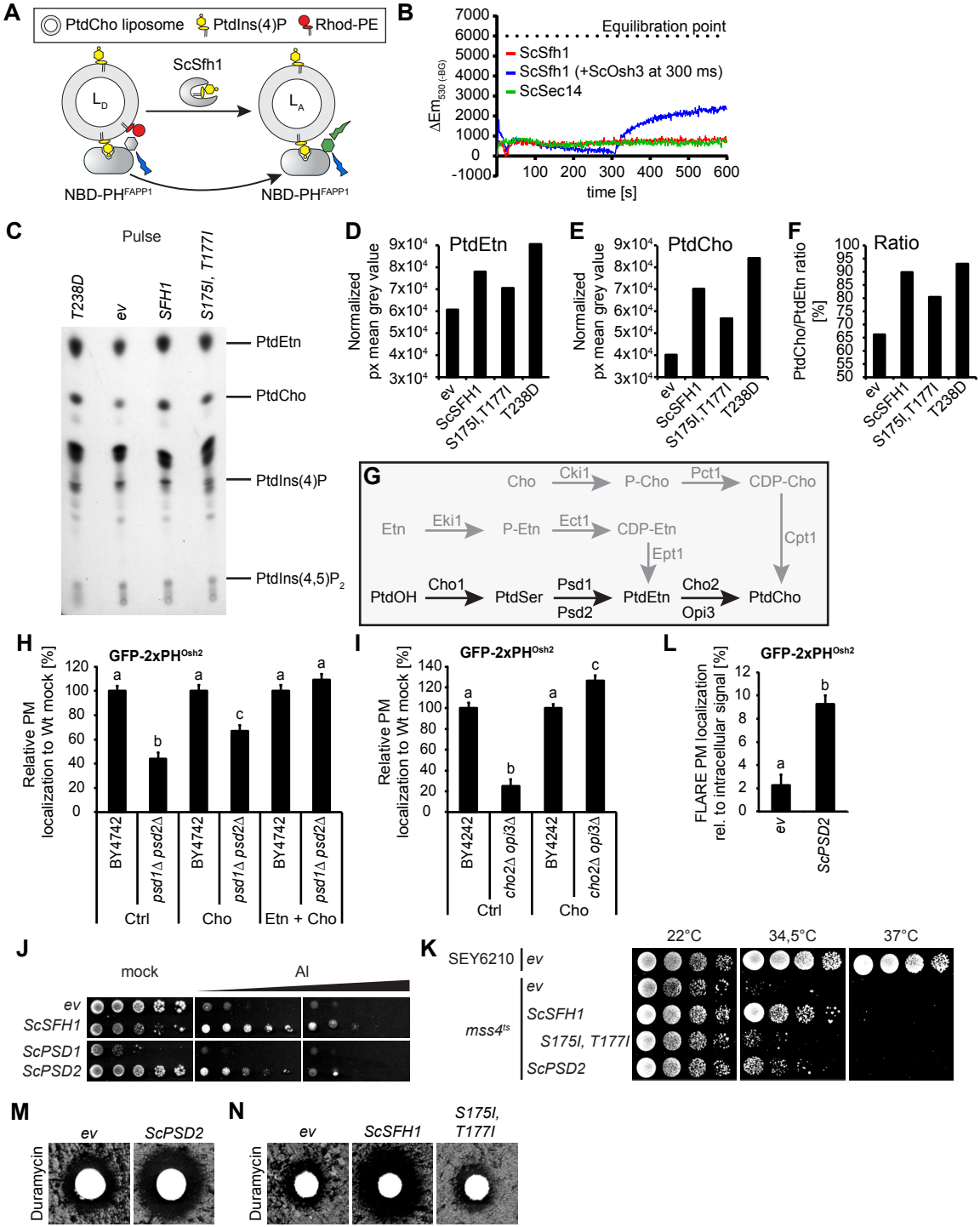
A
PtdCho liposome
PtdIns(4)P
Rhod-PE
ScSfh1
L_D
L_A
NBD-PH^FAPP1
NBD-PH^FAPP1
B
Equilibration point
ScSfh1
ScSfh1 (+ScOsh3 at 300 ms)
ScSec14
ΔEm530 (-BG)
time [s]
C
Pulse
T238D
ev
SFH1
S175I, T177I
PtdEtn
PtdCho
PtdIns(4)P
PtdIns(4,5)P2
D
PtdEtn
Normalized px mean grey value
ev
ScSFH1
S175I,T177I
T238D
E
PtdCho
Normalized px mean grey value
F
Ratio
PtdCho/PtdEtn ratio [%]
G
Cho
Cki1
P-Cho
Pct1
CDP-Cho
Etn
Eki1
P-Etn
Ect1
CDP-Etn
Cpt1
Ept1
PtdOH
Cho1
PtdSer
Psd1
Psd2
PtdEtn
Cho2
Opi3
PtdCho
H
GFP-2xPH^Osh2
Relative PM localization to Wt mock [%]
BY4742
psd1Δ psd2Δ
Ctrl
Cho
Etn + Cho
I
GFP-2xPH^Osh2
Relative PM localization to Wt mock [%]
BY4242
cho2Δ opi3Δ
Ctrl
Cho
L
GFP-2xPH^Osh2
FLARE PM localization rel. to intracellular signal [%]
ev
ScPSD2
J
mock
Al
ev
ScSFH1
ScPSD1
ScPSD2
K
22°C
34,5°C
37°C
SEY6210
ev
mss4ts
ev
ScSFH1
S175I, T177I
ScPSD2
M
ev
ScPSD2
Duramycin
N
ev
ScSFH1
S175I, T177I
Duramycin

Figure 6

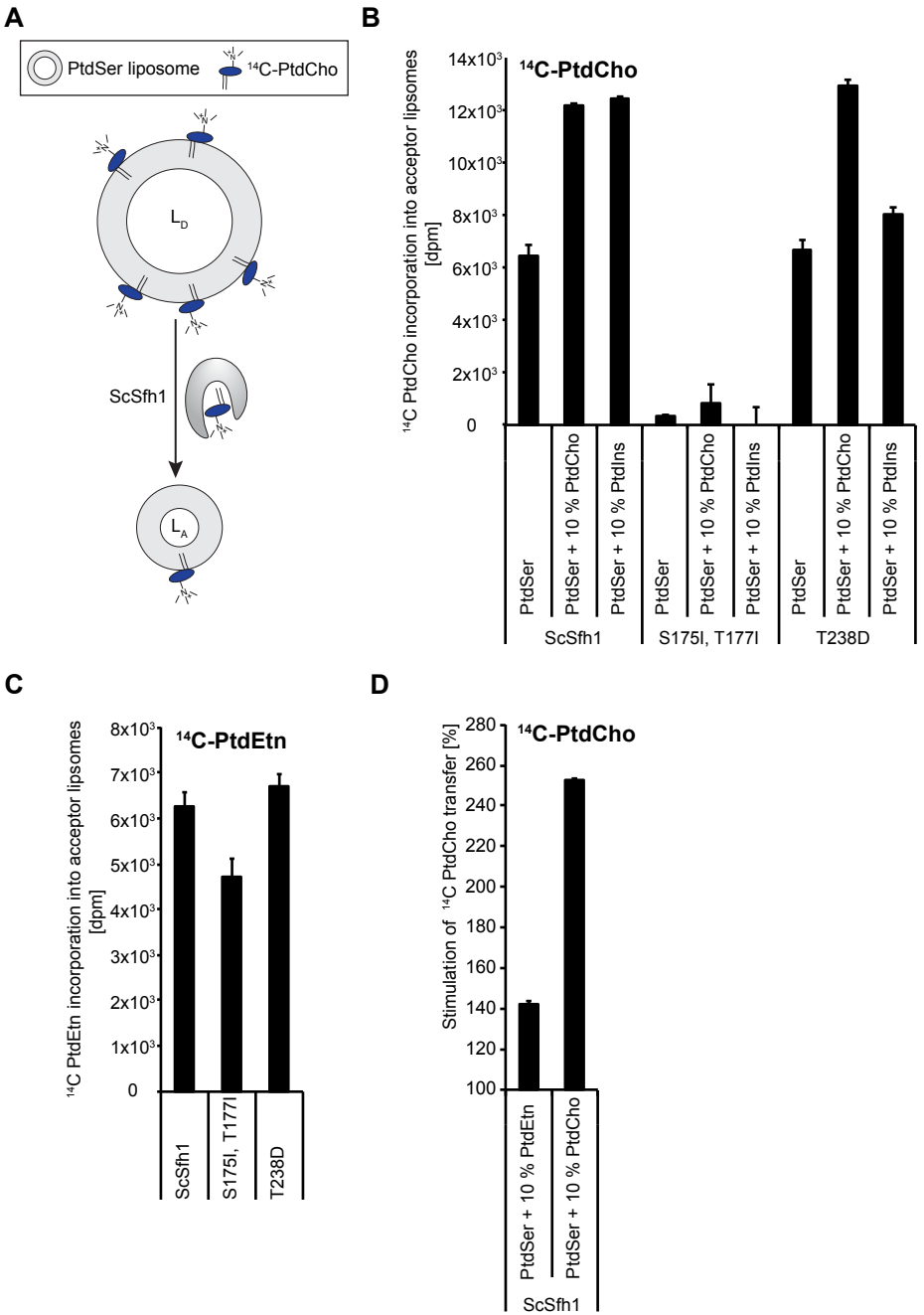
A
PtdSer liposome
14C-PtdCho
LD
ScSfh1
LA
B
14C-PtdCho
14C PtdCho incorporation into acceptor lipsomes [dpm]
14x10³
12x10³
10x10³
8x10³
6x10³
4x10³
2x10³
0
PtdSer
PtdSer + 10 % PtdCho
PtdSer + 10 % PtdIns
PtdSer
PtdSer + 10 % PtdCho
PtdSer + 10 % PtdIns
PtdSer
PtdSer + 10 % PtdCho
PtdSer + 10 % PtdIns
ScSfh1
S175I, T177I
T238D
C
14C-PtdEtn
14C PtdEtn incorporation into acceptor lipsomes [dpm]
8x10³
7x10³
6x10³
5x10³
4x10³
3x10³
2x10³
1x10³
0
ScSfh1
S175I, T177I
T238D
D
14C-PtdCho
Stimulation of 14C PtdCho transfer [%]
280
260
240
220
200
180
160
140
120
100
PtdSer + 10 % PtdEtn
PtdSer + 10 % PtdCho
ScSfh1

Figure 7

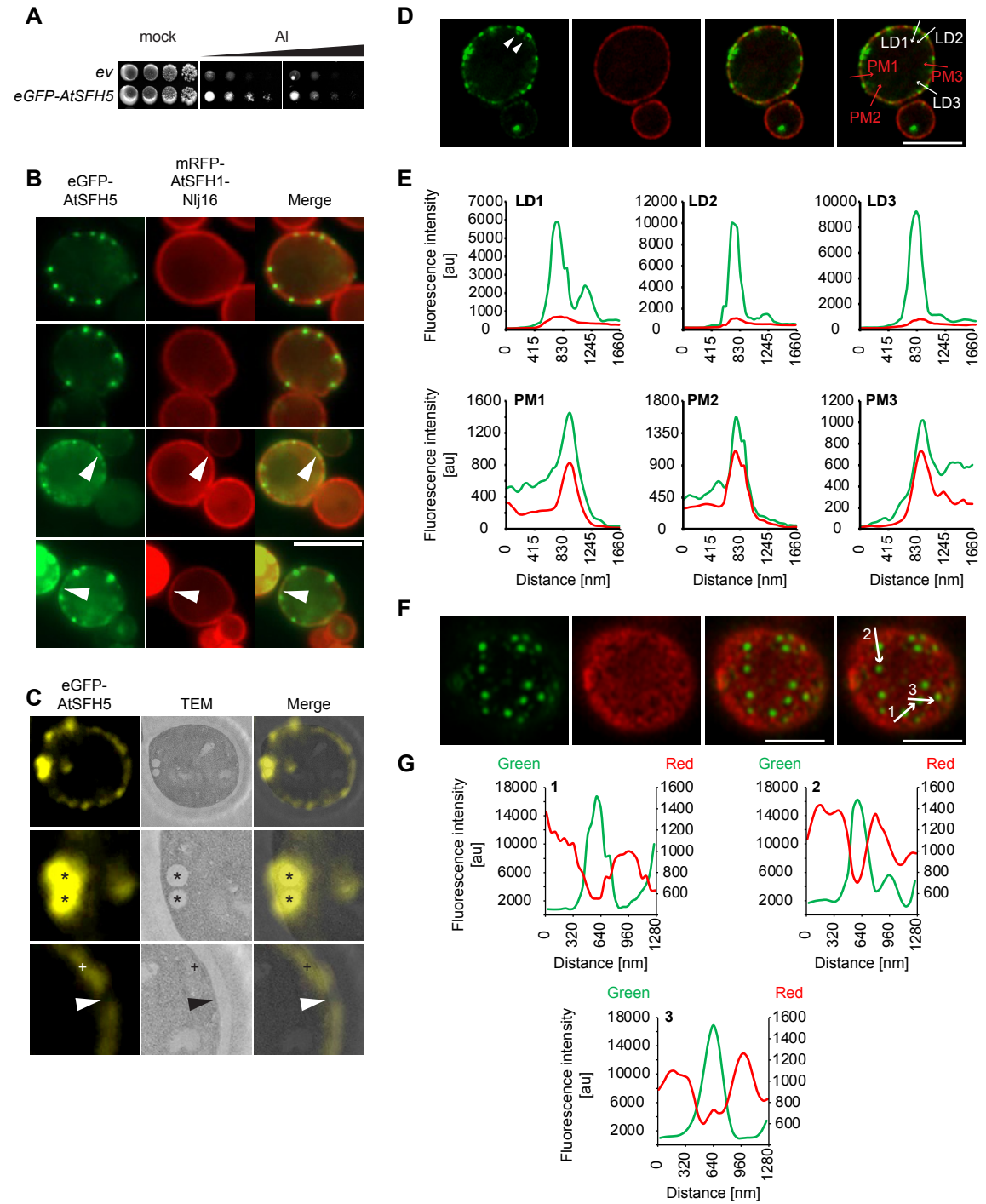
A
mock
Al
ev
eGFP-AtSFH5
B
eGFP-AtSFH5
mRFP-AtSFH1-Nlj16
Merge
C
eGFP-AtSFH5
TEM
Merge
D
LD1
LD2
PM1
PM3
LD3
PM2
E
Fluorescence intensity [au]
LD1
LD2
LD3
PM1
PM2
PM3
Distance [nm]
F
1
2
3
G
Green
Red
Fluorescence intensity [au]
Distance [nm]

Figure 8

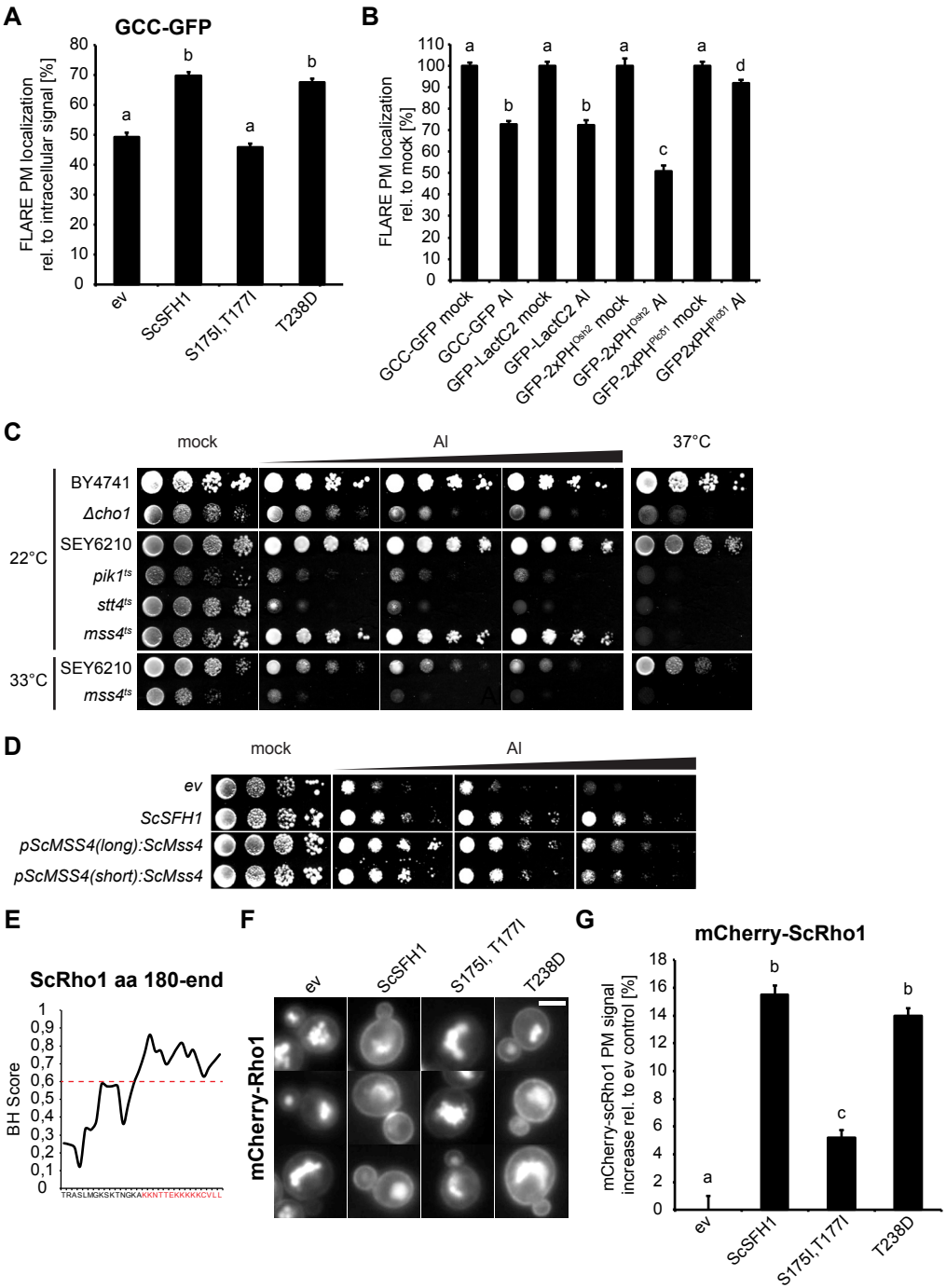
A
GCC-GFP
FLARE PM localization rel. to intracellular signal [%]
ev
ScSFH1
S175I,T177I
T238D
B
FLARE PM localization rel. to mock [%]
GCC-GFP mock
GCC-GFP AI
GFP-LactC2 mock
GFP-LactC2 AI
GFP-2xPH Osh2 mock
GFP-2xPH Osh2 AI
GFP-2xPH Plc81 mock
GFP2xPH Plc81 AI
C
mock
AI
37°C
22°C
BY4741
Δcho1
SEY6210
pik1ts
stt4ts
mss4ts
33°C
SEY6210
mss4ts
D
mock
AI
ev
ScSFH1
pScMSS4(long):ScMss4
pScMSS4(short):ScMss4
E
ScRho1 aa 180-end
BH Score
TRASLMGKSKTNGKAKKNTTEKKKKKCVLL
F
ev
ScSFH1
S175I, T177I
T238D
mCherry-Rho1
G
mCherry-ScRho1
mCherry-scRho1 PM signal increase rel. to ev control [%]
ev
ScSFH1
S175I,T177I
T238D

Figure 9

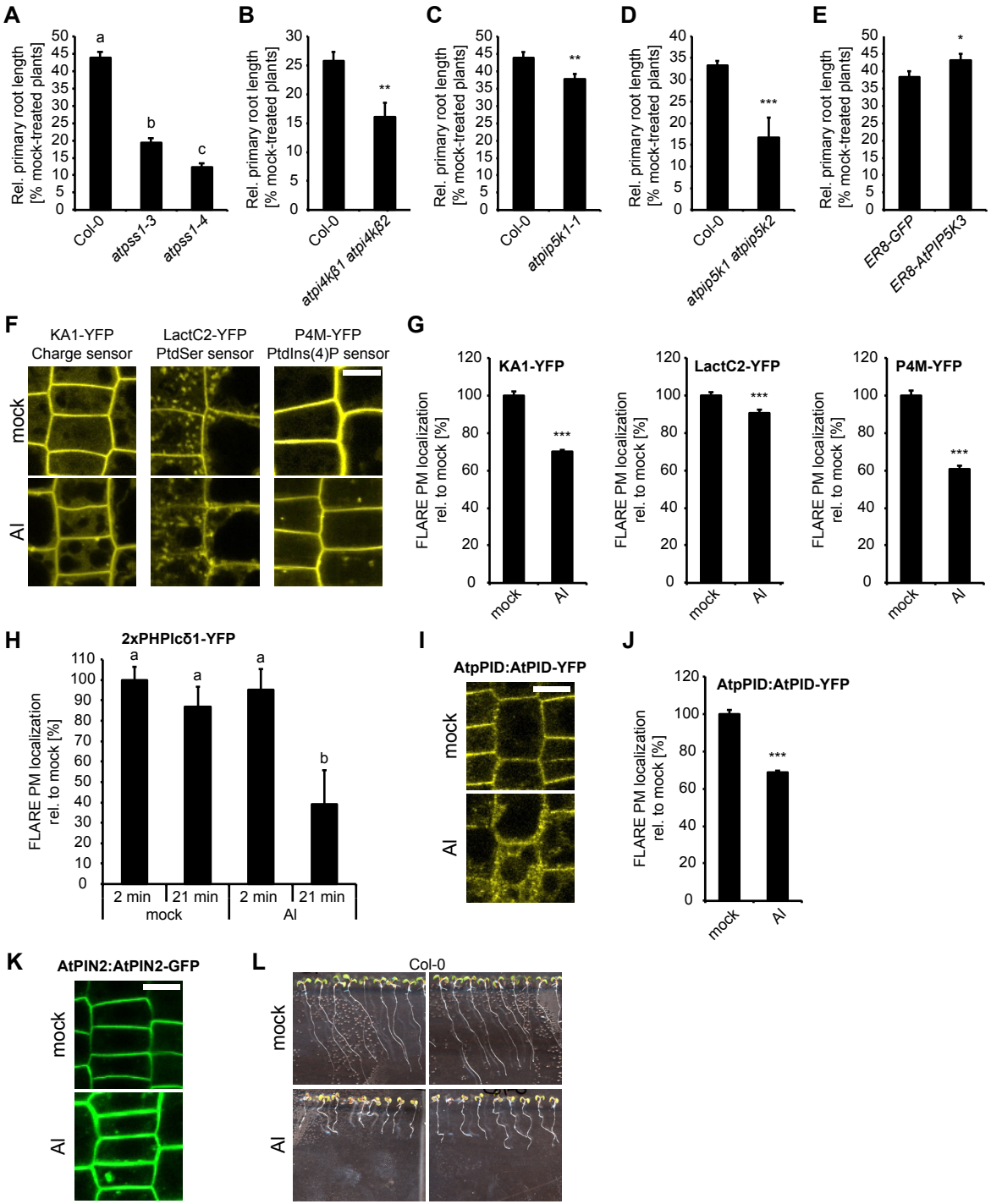
A
Rel. primary root length [% mock-treated plants]
Col-0
atpss1-3
atpss1-4
B
atpi4kβ1 atpi4kβ2
C
atpip5k1-1
D
atpip5k1 atpip5k2
E
ER8-GFP
ER8-AtPIP5K3
F
KA1-YFP Charge sensor
LactC2-YFP PtdSer sensor
P4M-YFP PtdIns(4)P sensor
mock
Al
G
KA1-YFP
LactC2-YFP
P4M-YFP
FLARE PM localization rel. to mock [%]
H
2xPHPlcδ1-YFP
2 min
21 min
I
AtpPID:AtPID-YFP
J
K
AtPIN2:AtPIN2-GFP
L
Col-0

Figure 10

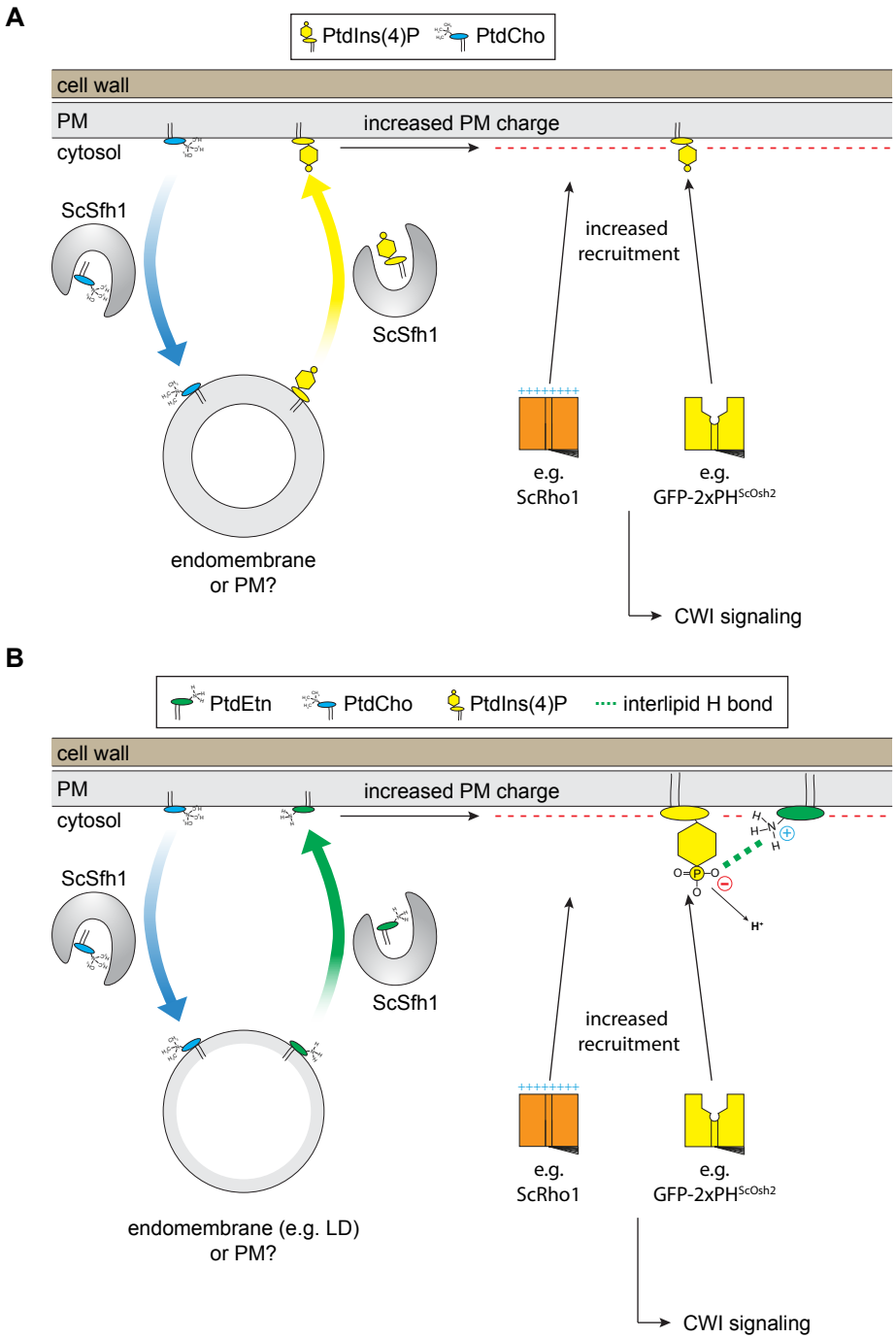
A
PtdIns(4)P
PtdCho
cell wall
PM
cytosol
increased PM charge
ScSfh1
ScSfh1
increased
recruitment
e.g.
ScRho1
e.g.
GFP-2xPH ScOsh2
endomembrane
or PM?
CWI signaling
B
PtdEtn
PtdCho
PtdIns(4)P
interlipid H bond
cell wall
PM
cytosol
increased PM charge
ScSfh1
ScSfh1
increased
recruitment
e.g.
ScRho1
e.g.
GFP-2xPH ScOsh2
endomembrane (e.g. LD)
or PM?
CWI signaling

Figure 11

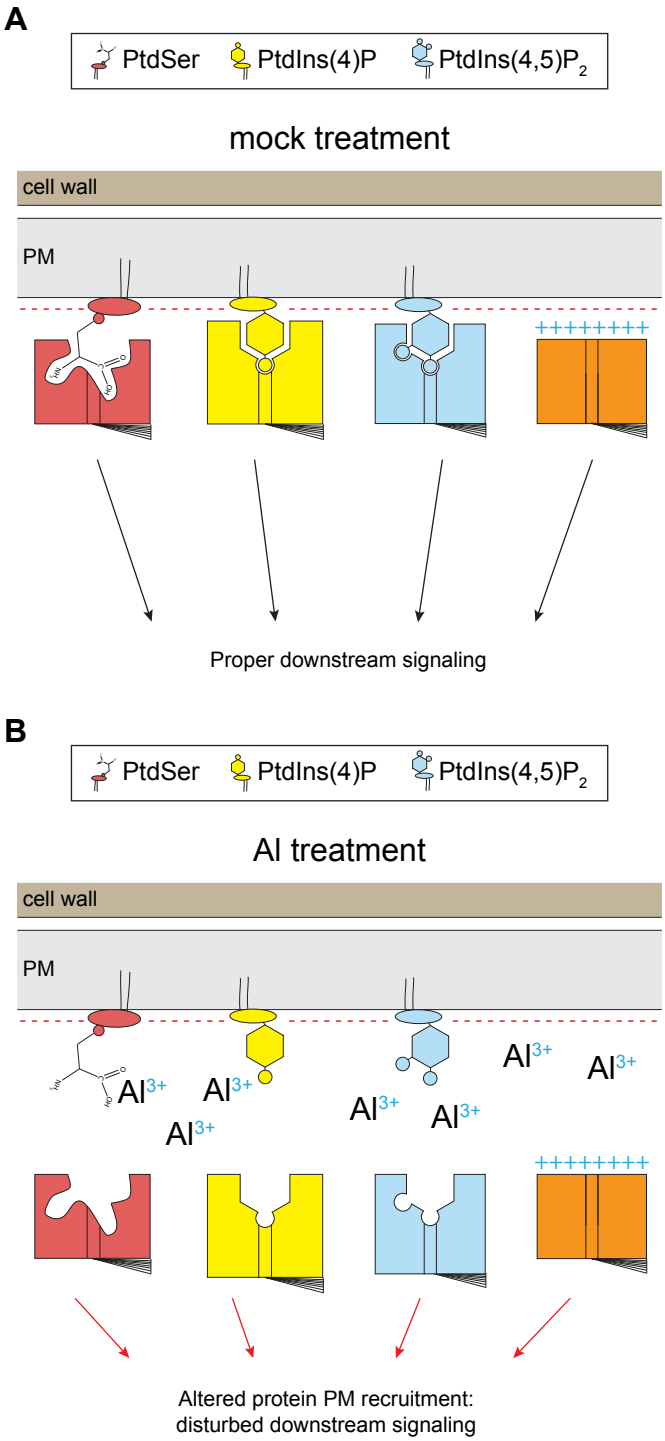
A
PtdSer
PtdIns(4)P
PtdIns(4,5)P2
mock treatment
cell wall
PM
Proper downstream signaling
B
PtdSer
PtdIns(4)P
PtdIns(4,5)P2
Al treatment
cell wall
PM
Al3+
Al3+
Al3+
Al3+
Al3+
Al3+
Altered protein PM recruitment:
disturbed downstream signaling

Figure S1

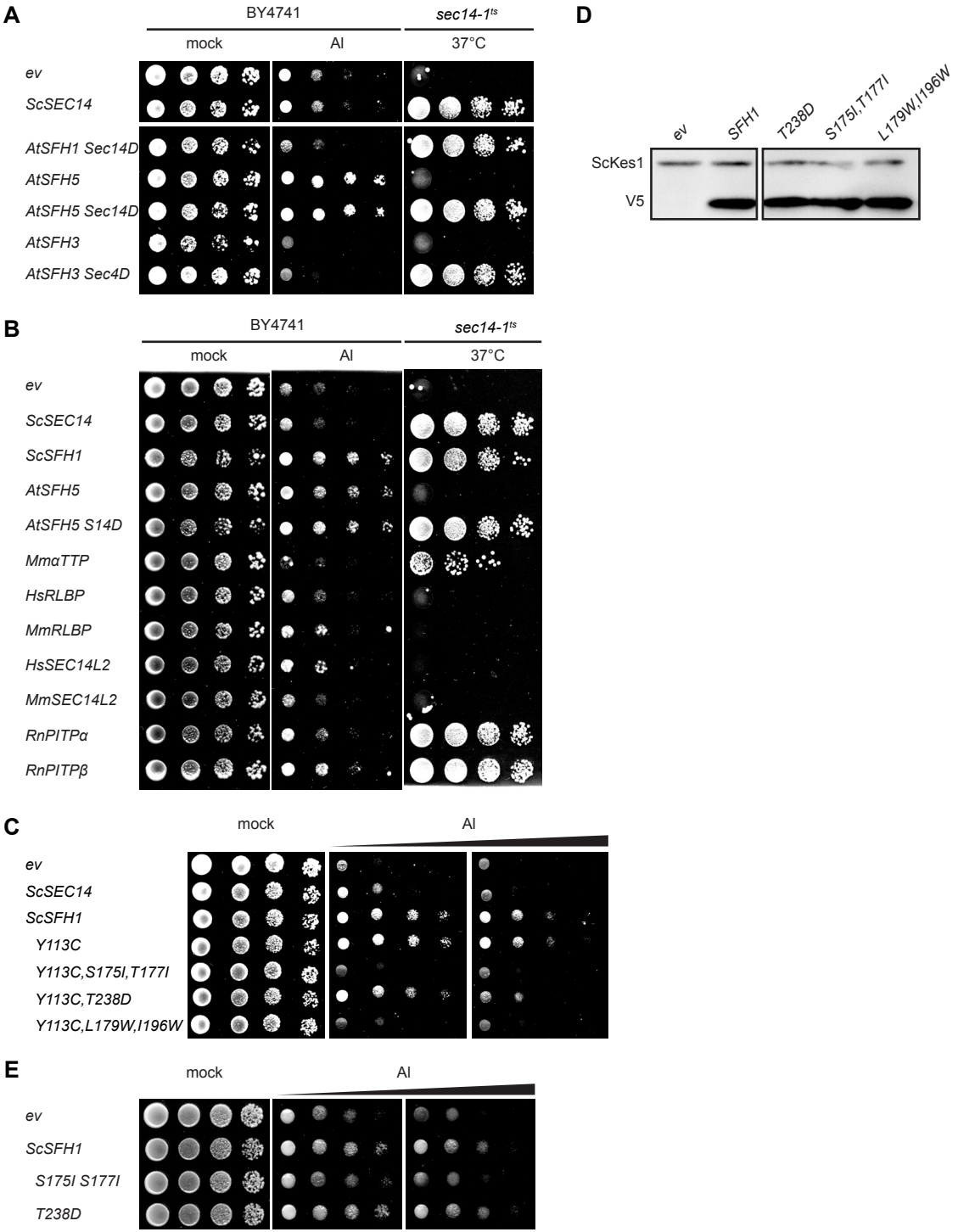
A
BY4741
sec14-1ts
mock
AI
37°C
ev
ScSEC14
AtSFH1 Sec14D
AtSFH5
AtSFH5 Sec14D
AtSFH3
AtSFH3 Sec4D
B
BY4741
sec14-1ts
mock
AI
37°C
ev
ScSEC14
ScSFH1
AtSFH5
AtSFH5 S14D
MmαTTP
HsRLBP
MmRLBP
HsSEC14L2
MmSEC14L2
RnPITPα
RnPITPβ
C
mock
AI
ev
ScSEC14
ScSFH1
Y113C
Y113C,S175I,T177I
Y113C,T238D
Y113C,L179W,I196W
D
ev
SFH1
T238D
S175I,T177I
L179W,I196W
ScKes1
V5
E
mock
AI
ev
ScSFH1
S175I S177I
T238D

Figure S2

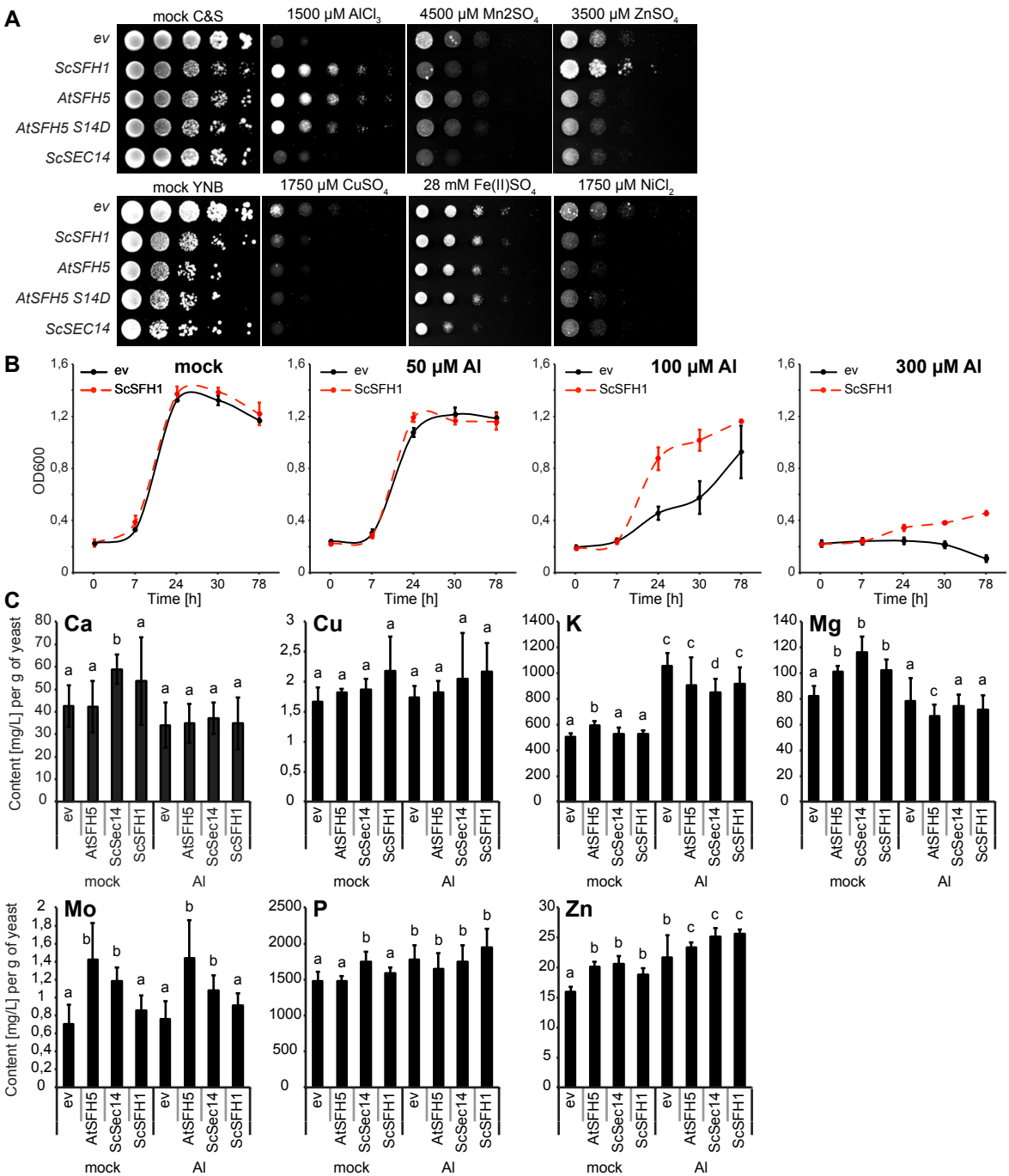
A
mock C&S
1500 µM AlCl3
4500 µM Mn2SO4
3500 µM ZnSO4
mock YNB
1750 µM CuSO4
28 mM Fe(II)SO4
1750 µM NiCl2
ev
ScSFH1
AtSFH5
AtSFH5 S14D
ScSEC14
B
mock
50 µM Al
100 µM Al
300 µM Al
OD600
Time [h]
C
Ca
Cu
K
Mg
Mo
P
Zn
Content [mg/L] per g of yeast
ev
AtSFH5
ScSec14
ScSFH1
mock
Al

Figure S3

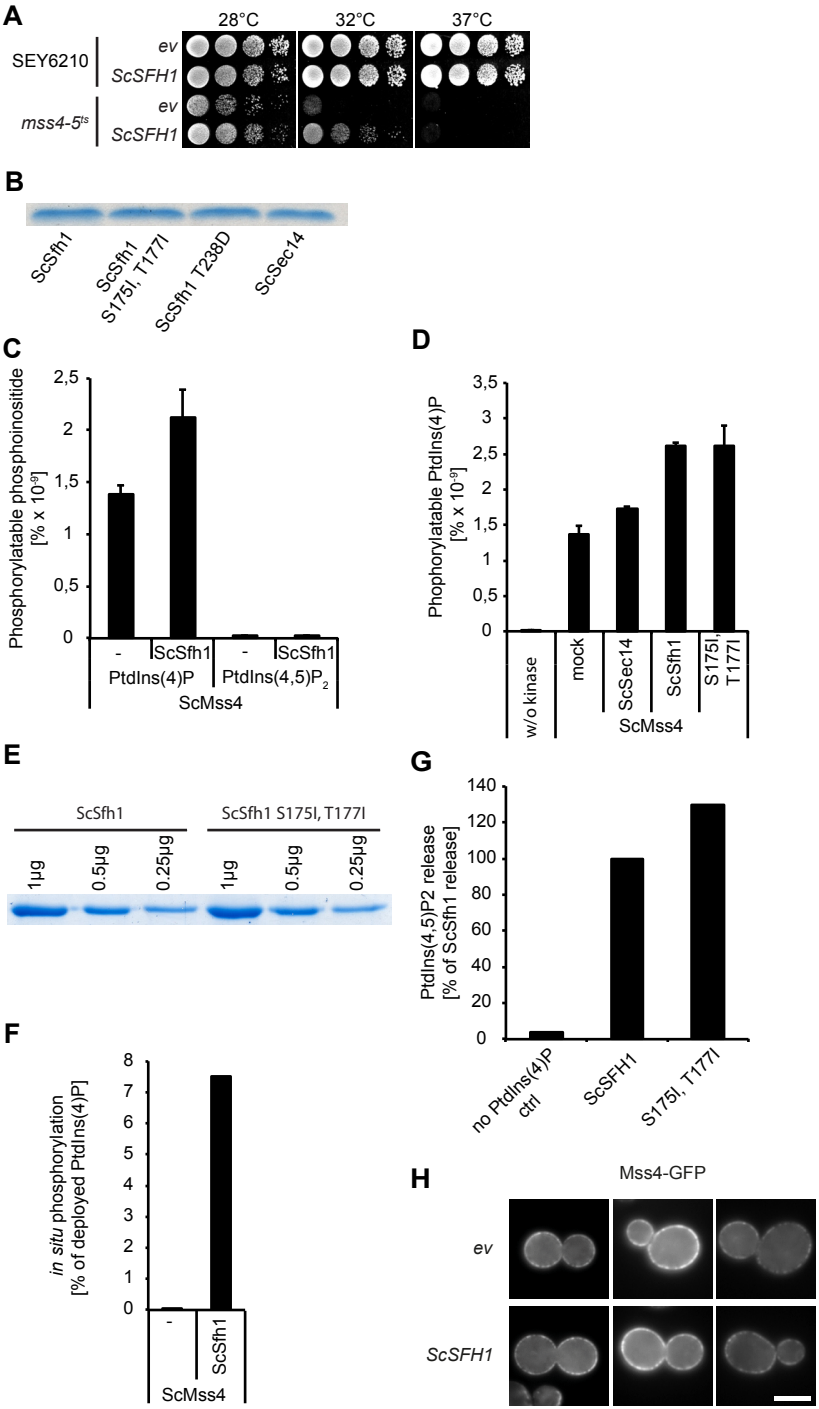
A
28°C
32°C
37°C
SEY6210
ev
ScSFH1
mss4-5ts
ev
ScSFH1
B
ScSfh1
ScSfh1 S175I, T177I
ScSfh1 T238D
ScSec14
C
Phosphorylatable phosphoinositide [% x 10-3]
2,5
2
1,5
1
0,5
0
-
ScSfh1
-
ScSfh1
PtdIns(4)P
PtdIns(4,5)P2
ScMss4
D
Phophorylatable PtdIns(4)P [% x 10-3]
3,5
3
2,5
2
1,5
1
0,5
0
w/o kinase
mock
ScSec14
ScSfh1
S175I, T177I
ScMss4
E
ScSfh1
ScSfh1 S175I, T177I
1µg
0.5µg
0.25µg
1µg
0.5µg
0.25µg
F
in situ phosphorylation [% of deployed PtdIns(4)P]
8
7
6
5
4
3
2
1
0
-
ScSfh1
ScMss4
G
PtdIns(4,5)P2 release [% of ScSfh1 release]
140
120
100
80
60
40
20
0
no PtdIns(4)P ctrl
ScSFH1
S175I, T177I
H
Mss4-GFP
ev
ScSFH1

Figure S4

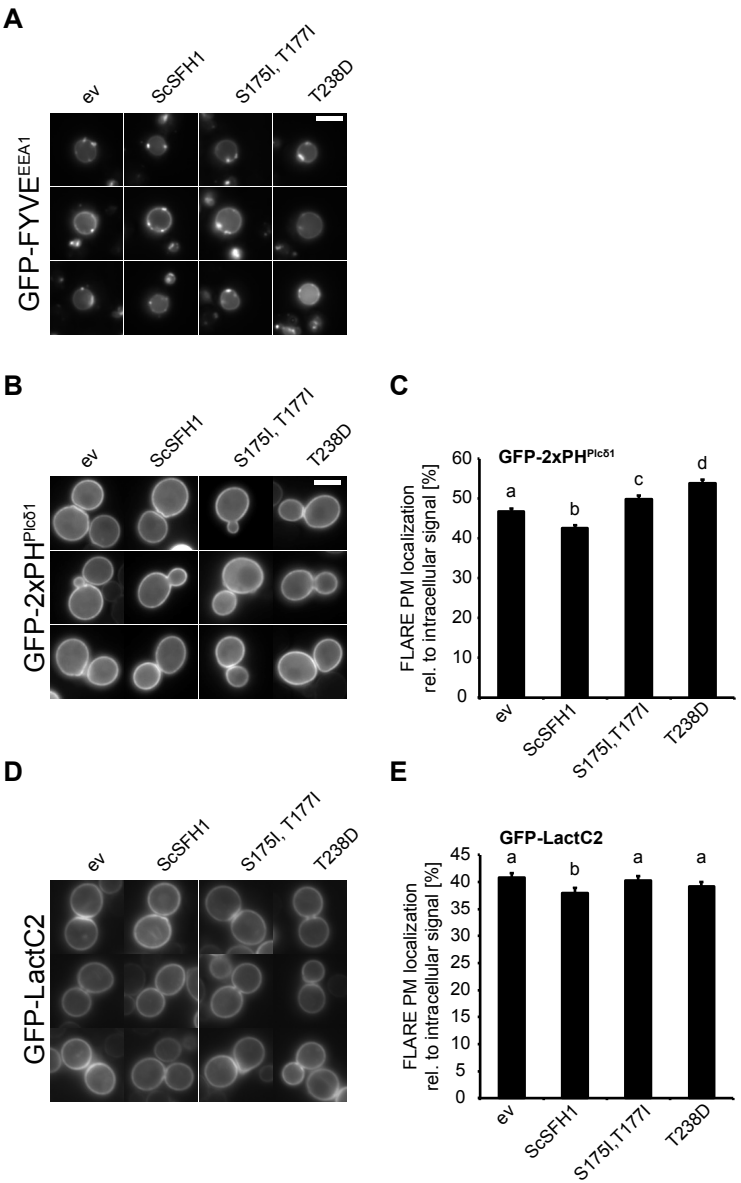
A
ev
ScSFH1
S175I, T177I
T238D
GFP-FYVE^EEA1
B
GFP-2xPH^Plcδ1
C
GFP-2xPH^Plcδ1
FLARE PM localization rel. to intracellular signal [%]
a
b
c
d
D
GFP-LactC2
E
GFP-LactC2

Figure S5

A

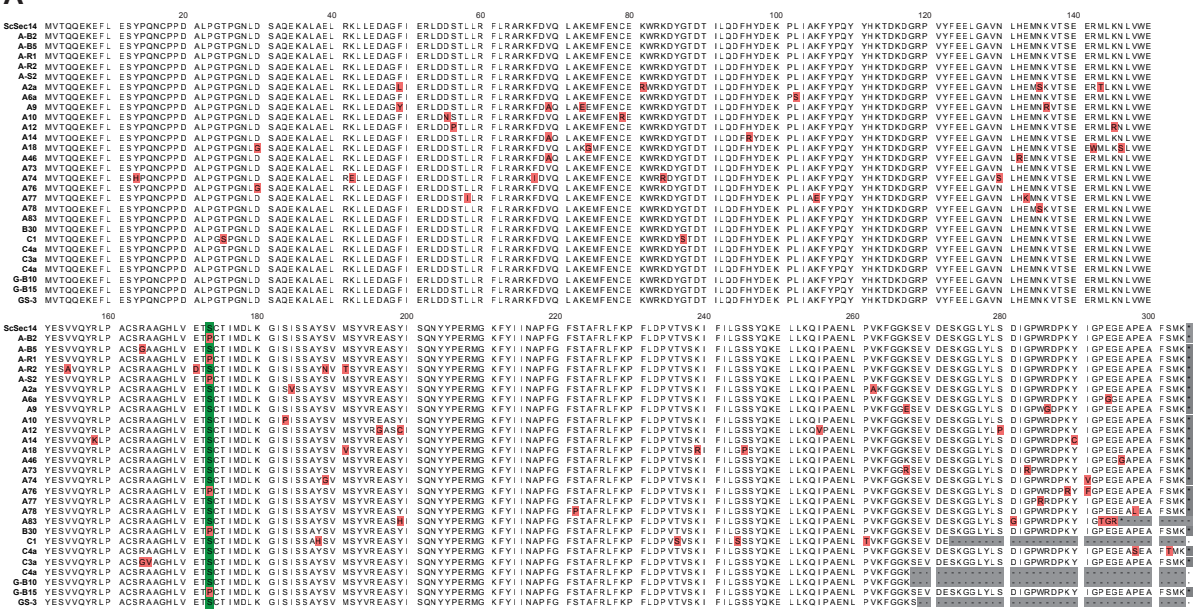

B

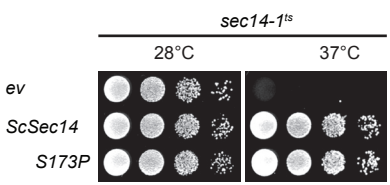

Figure S6

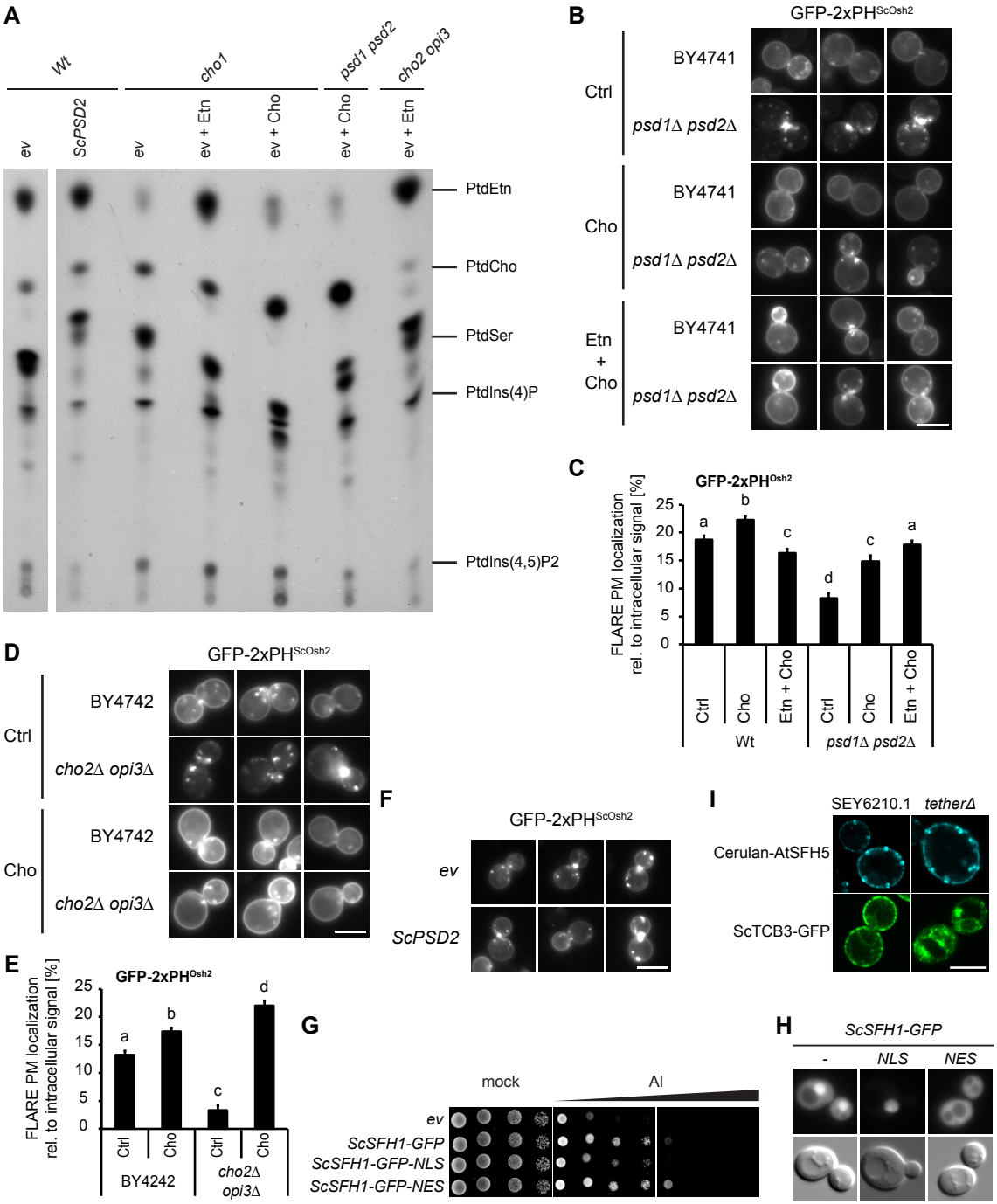
A
Wt
cho1
psd1 psd2
cho2 opi3
ev
ScPSD2
ev
ev + Etn
ev + Cho
ev + Cho
ev + Etn
PtdEtn
PtdCho
PtdSer
PtdIns(4)P
PtdIns(4,5)P2
B
GFP-2xPHScOsh2
Ctrl
Cho
Etn + Cho
BY4741
psd1Δ psd2Δ
C
GFP-2xPHOsh2
FLARE PM localization rel. to intracellular signal [%]
Ctrl
Cho
Etn + Cho
Wt
psd1Δ psd2Δ
D
GFP-2xPHScOsh2
Ctrl
Cho
BY4742
cho2Δ opi3Δ
E
GFP-2xPHOsh2
FLARE PM localization rel. to intracellular signal [%]
BY4242
cho2Δ opi3Δ
F
GFP-2xPHScOsh2
ev
ScPSD2
G
mock
AI
ev
ScSFH1-GFP
ScSFH1-GFP-NLS
ScSFH1-GFP-NES
H
ScSFH1-GFP
-
NLS
NES
I
SEY6210.1
tetherΔ
Cerulan-AtSFH5
ScTCB3-GFP

Figure S7

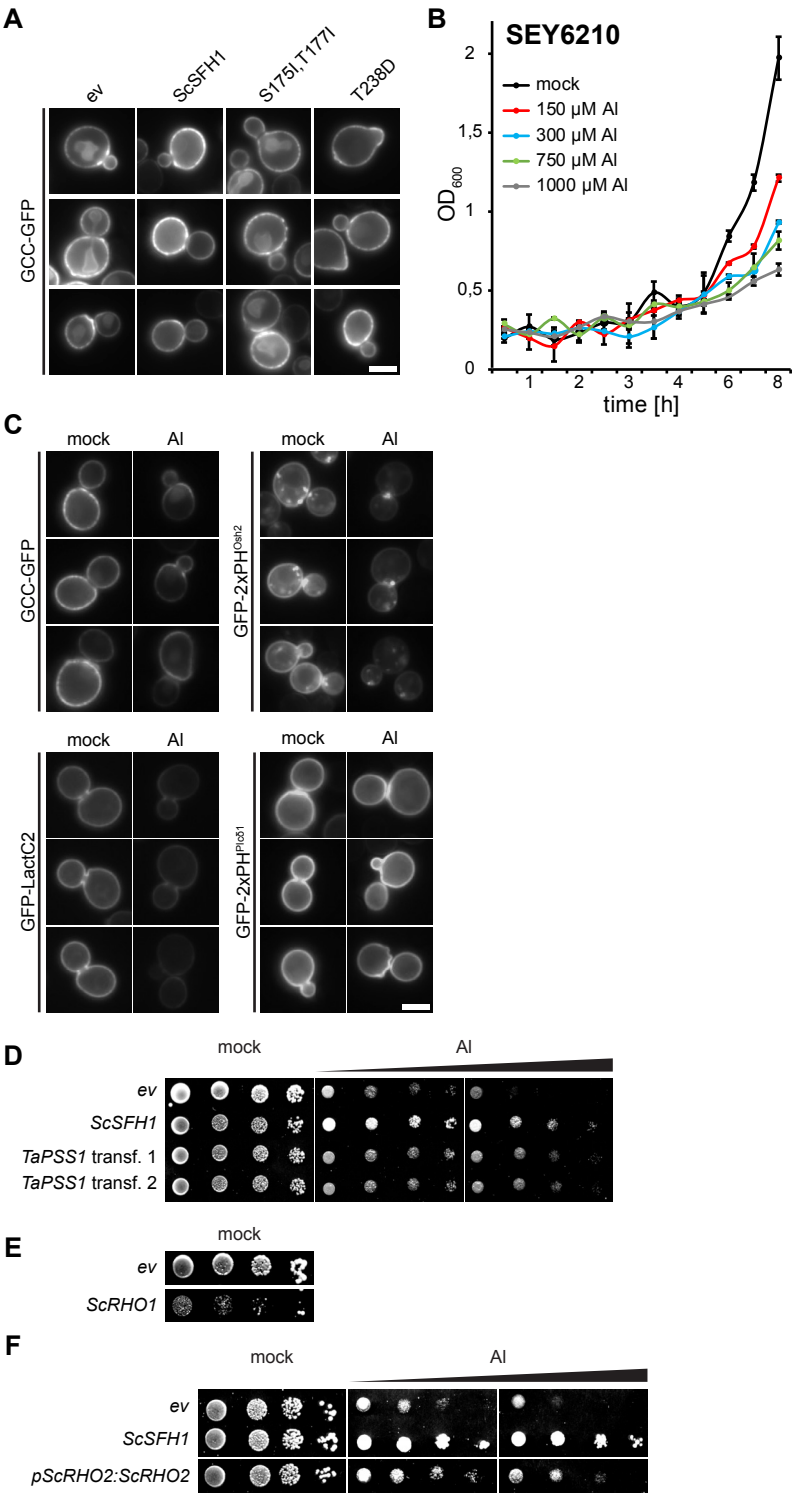
A
ev
ScSFH1
S175I,T177I
T238D
GCC-GFP
B
SEY6210
mock
150 µM Al
300 µM Al
750 µM Al
1000 µM Al
OD600
time [h]
C
mock
Al
GCC-GFP
GFP-2xPHOsh2
GFP-LactC2
GFP-2xPHPhs1
D
mock
Al
ev
ScSFH1
TaPSS1 transf. 1
TaPSS1 transf. 2
E
mock
ev
ScRHO1
F
mock
Al
ev
ScSFH1
pScRHO2:ScRHO2

Figure S8

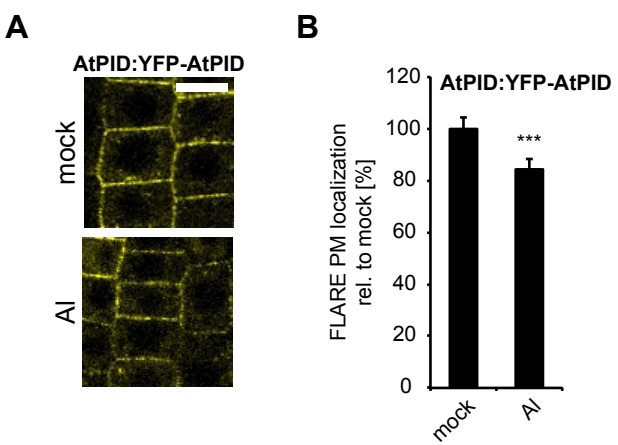
A
AtPID:YFP-AtPID
mock
AI
B
AtPID:YFP-AtPID
FLARE PM localization rel. to mock [%]
120
100
80
60
40
20
0
***
mock
AI

Table S1: Al screen with Arabidopsis cDNA library.

	Screen ID	Locus	Name	Description (source: Araport11)
1	Alr3, Alr4	AT1G52300	N/A	Zinc-binding ribosomal protein family protein
2	Alr17	AT4G24160	N/A	Encodes a soluble lysophosphatidic acid acyltransferase with additional triacylglycerol lipase and phosphatidylcholine hydrolyzing enzymatic activities. Plays a pivotal role in maintaining the lipid homeostasis by regulating both phospholipid and neutral lipid levels
3	Alr23	AT4G24280	CHLOROPLAST HEAT SHOCK PROTEIN 70-1, CPHSC70-1	Involved in protein import into chloroplasts during early developmental stages. The mRNA is cell-to-cell mobile.
4	Alr65	AT5G14050	N/A	Transducin/WD40 repeat-like superfamily protein
5	Alr29, Alr38, Alr39	AT1G04550	BDL, BODENLOS, IAA12, INDOLE-3-ACETIC ACID INDUCIBLE 12	IAA12/BDL plays a role in auxin-mediated processes of apical-basal patterning in the embryo. bdl mutants lack a primary root meristem
6	AtAlr35, AtAle56	AT5G15780	N/A	Pollen Ole e 1 allergen and extensin family protein
7	AtAlr42	AT4G33010	ATGLDP1, GLDP1, GLYCINE DECARBOXYLASE P-PROTEIN 1	Glycine decarboxylase P-protein 1
8	AtAlr54	AT1G75370	ATSFH5, ARABIDOPSIS THALIANA SEC FOURTEEN HOMOLOG 5	Sec14p-like phosphatidylinositol transfer family protein
9	AtAlr55	AT1G30650	AR411, ATWRKY14, WRKY DNA-BINDING PROTEIN 14, WRKY14	Member of WRKY Transcription Factor; Group II-e
10	AtAlr59	AT5G22830	ATMGT10, GMN10, MAGNESIUM (MG) TRANSPORTER 10	Transmembrane magnesium transporter that is essential for chloroplast development and photosynthesis. One of nine family members

Table S2: Hits of the genome wide screen.

Category	Gene ID	Standard Name	References
Lipid metabolism			
	YLR056W	ERG3	C-5 sterol desaturase; glycoprotein that catalyzes the introduction of a C-5(6) double bond into episterol, a precursor in ergosterol biosynthesis; transcriptionally down-regulated when ergosterol is in excess; mutants are viable, but cannot grow on non-fermentable carbon sources; substrate of HRD ubiquitin ligase; mutation is functionally complemented by human SC5D
	YMR207C	HFA1	Mitochondrial acetyl-coenzyme A carboxylase; catalyzes production of malonyl-CoA in mitochondrial fatty acid biosynthesis; relocalizes from mitochondrion to cytoplasm upon DNA replication stress; genetic and comparative analysis suggests that translation begins at a non-canonical (Ile) start codon at -372 relative to the annotated start codon
	YKL212W	SAC1	Phosphatidylinositol phosphate (PtdInsP) phosphatase; involved in hydrolysis of PtdIns[4]P in the early and medial Golgi; regulated by interaction with Vps74p; ER localized transmembrane protein which cycles through the Golgi; involved in protein trafficking and processing, secretion, and cell wall maintenance; regulates sphingolipid biosynthesis through the modulation of PtdIns(4)P metabolism
	YDL052C	SLC1	1-acyl-sn-glycerol-3-phosphate acyltransferase; catalyzes the acylation of lysophosphatidic acid to form phosphatidic acid, a key intermediate in lipid metabolism; enzymatic activity detected in lipid particles and microsomes
	YGR157W	CHO2	Phosphatidylethanolamine methyltransferase (PEMT); catalyzes the first step in the conversion of phosphatidylethanolamine to phosphatidylcholine during the methylation pathway of phosphatidylcholine biosynthesis
Trafficking / Sorting			
	YAL002W	VPS8	Membrane-binding component of the CORVET complex; involved in endosomal vesicle tethering and fusion in the endosome to vacuole protein targeting pathway; interacts with Vps21p; contains RING finger motif
	YLR025W	SNF7	One of four subunits of the ESCRT-III complex; involved in the sorting of transmembrane proteins into the multivesicular body (MVB) pathway; recruited from the cytoplasm to endosomal membranes; ESCRT-III stands for endosomal sorting complex required for transport III
	YNL297C	MON2	Protein with a role in endocytosis and vacuole integrity; peripheral membrane protein; interacts with and negatively regulates Arl1p; localizes to the endosome; member of the Sec7p family of proteins
	YOR132W	VPS17	Subunit of the membrane-associated retromer complex; essential for endosome-to-Golgi retrograde protein transport; peripheral membrane protein that assembles onto the membrane with Vps5p to promote vesicle formation; required for recruiting the retromer complex to the endosome membranes
	YJL204C	RCY1	F-box protein involved in recycling endocytosed proteins; involved in recycling plasma membrane proteins internalized by endocytosis; localized to sites of polarized growth; direct interaction with C-terminal cytoplasmic region of Drs2p plays an important role for Drs2p function in endocytic recycling pathway
	YLR261C	VPS63	Putative protein of unknown function; not conserved in closely related Saccharomyces species; 98% of ORF overlaps the verified gene YPT6; deletion causes a vacuolar protein sorting defect; decreased levels of protein in enolase deficient mutant
	YPL051W	ARL3	ARF-like small GTPase of the RAS superfamily; required for recruitment of Arl1p, a GTPase that regulates membrane traffic, to the Golgi apparatus; NatC-catalyzed N-terminal acetylation regulates Golgi membrane association mediated by interaction with membrane receptor, Sys1p; similar to ADP-ribosylation factor and orthologous to mammalian ARFRP1
	YDR495C	VPS3	Component of CORVET membrane tethering complex; cytoplasmic protein required for the sorting and processing of soluble vacuolar proteins, acidification of the vacuolar lumen, and assembly of the vacuolar H+-ATPase
	YDR136C	VPS61	Dubious open reading frame; unlikely to encode a functional protein, based on available experimental and comparative sequence data; not conserved in closely related Saccharomyces species; 4% of ORF overlaps the verified gene RGP1; deletion causes a vacuolar protein sorting defect
	YBL007C	SLA1	Cytoskeletal protein binding protein; required for assembly of the cortical actin cytoskeleton; interacts with proteins regulating actin dynamics and proteins required for endocytosis; found in the nucleus and cell cortex; has 3 SH3 domains
	YDR484W	VPS52	Component of the GARP (Golgi-associated retrograde protein) complex; GARP is required for the recycling of proteins from endosomes to the late Golgi, and for mitosis after DNA damage induced checkpoint arrest; involved in localization of actin and chitin; members of the GARP complex are Vps51p-Vps52p-Vps53p-Vps54p
CWI			
	YOR008C	WSC1	Sensor-transducer of the stress-activated PKC1-MPK1 kinase pathway; involved in maintenance of cell wall integrity; required for mitophagy; involved in organization of the actin cytoskeleton; secretory pathway Wsc1p is required for the arrest of secretion response
	YLR332W	MID2	O-glycosylated plasma membrane protein; acts as a sensor for cell wall integrity signaling and activates the pathway; interacts with Rom2p, a guanine nucleotide exchange factor for Rho1p, and with cell integrity pathway protein Zeo1p; MID2 has a paralog, MTL1, that arose from the whole genome duplication
	YLR371W	ROM2	Guanine nucleotide exchange factor (GEF) for Rho1p and Rho2p; mutations are synthetically lethal with mutations in rom1, which also encodes a GEF; Rom2p localization to the bud surface is dependent on Ack1p; ROM2 has a paralog, ROM1, that arose from the whole genome duplication
	YNR047W	FPK1	Ser/Thr protein kinase; phosphorylates several aminophospholipid translocase family members, regulating phospholipid translocation and membrane asymmetry; phosphorylates and inhibits the protein kinase Akl1p, stimulating endocytosis; phosphorylates and inhibits upstream inhibitory kinase, Ypk1p; localizes to the cytoplasm, early endosome/TGN, the plasma membrane and the shmoo tip; redundant role with KIN82 in the mating pheromone response; activity stimulated by MIPC, a complex sphingolipid
	YJL095W	BCK1	MAPKKK acting in the protein kinase C signaling pathway; the kinase C signaling pathway controls cell integrity; upon activation by Pkc1p phosphorylates downstream kinases Mkk1p and Mkk2p; MAPKKK is an acronym for mitogen-activated protein (MAP) kinase kinase kinase
	YHR030C	MPK1	Serine/threonine MAP kinase; coordinates expression of all 19S regulatory particle assembly-chaperones (RACs) to control proteasome abundance; involved in regulating maintenance of cell wall integrity, cell cycle progression, nuclear mRNA retention in heat shock, septum assembly; required for mitophagy, pexophagy; affects recruitment of mitochondria to phagophore assembly site; plays role in adaptive response of cells to cold; regulated by the PKC1-mediated signaling pathway
	YKL161C	MLP1	Protein kinase; implicated in Slt2p mitogen-activated (MAP) kinase signaling pathway; interacts with numerous components in the mating pheromone and CWI MAPK pathways; associates with Rlm1p; KDX1 has a paralog, SLT2, that arose from the whole genome duplication
	YJR075W	HOC1	Alpha-1,6-mannosyltransferase; involved in cell wall mannan biosynthesis; subunit of a Golgi-localized complex that also contains Anp1p, Mnn9p, Mnn11p, and Mnn10p; identified as a suppressor of a cell lysis sensitive pkc1-371 allele

Category	Gene ID	Standard Name	References
Cell cycle / Cytosceleton			
	YGR080W	TWF1	Twinfilin; highly conserved actin monomer-sequestering protein involved in regulation of the cortical actin cytoskeleton; coordinates actin filament severing and monomer sequestering at sites of rapid actin turnover; composed of two cofilin-like regions, stimulates actin depolymerization as does the mouse homolog, mTwf1
	YEL029C	BUD16	Putative pyridoxal kinase; a key enzyme involved in pyridoxal 5'-phosphate synthesis, the active form of vitamin B6; required for genome integrity; involved in bud-site selection; similarity to yeast BUD17 and human pyridoxal kinase (PDXK)
	YEL036C	ANP1	Subunit of the alpha-1,6 mannosyltransferase complex; type II membrane protein; has a role in retention of glycosyltransferases in the Golgi; involved in osmotic sensitivity and resistance to aminonitrophenyl propanediol
	YER124C	DSE1	Daughter cell-specific protein; may regulate cross-talk between the mating and filamentation pathways; deletion affects cell separation after division and sensitivity to alpha-factor and drugs affecting the cell wall; relocalizes from bud neck to cytoplasm upon DNA replication stress
	YNL080C	EOS1	Protein involved in N-glycosylation; deletion mutation confers sensitivity to oxidative stress and shows synthetic lethality with mutations in the spindle checkpoint genes BUB3 and MAD1; YNL080C is not an essential gene
	YDR364C	CDC40	Pre-mRNA splicing factor; important for catalytic step II of pre-mRNA splicing and plays a role in cell cycle progression, particularly at the G1/S phase transition; required for DNA synthesis during mitosis and meiosis; has WD repeats; thermosensitivity of the cdc40 null mutant is functionally complemented by a chimeric construct containing the N-terminal 156 amino acids of yeast Cdc40p fused to the C-terminal two thirds (297 amino acids) of human CDC4
Transcription / Translation			
	YMR216C	SKY1	SR protein kinase (SRPK); involved in regulating proteins involved in mRNA metabolism and cation homeostasis; similar to human SRPK1
	YPL254W	HFI1	Adaptor protein required for structural integrity of the SAGA complex; a histone acetyltransferase-coactivator complex that is involved in global regulation of gene expression through acetylation and transcription functions
	YKL009W	MRT4	Protein involved in mRNA turnover and ribosome assembly; required at post-transcriptional step for efficient retrotransposition; localizes to the nucleolus
	YKL054C	DEF1	RNAPII degradation factor; forms a complex with Rad26p in chromatin, enables ubiquitination and proteolysis of RNAPII present in an elongation complex; mutant is deficient in Zip1p loading onto chromosomes during meiosis
	YDR207C	UME6	Rpd3L histone deacetylase complex subunit; key transcriptional regulator of early meiotic genes; involved in chromatin remodeling and transcriptional repression via DNA looping; binds URS1 upstream regulatory sequence, represses transcription by recruiting conserved histone deacetylase Rpd3p (through co-repressor Sin3p) and chromatin-remodeling factor Isw2p; couples metabolic responses to nutritional cues with initiation and progression of meiosis
	YGL173C	KEM1	Evolutionarily-conserved 5'-3' exonuclease; component of cytoplasmic processing (P) bodies involved in mRNA decay; enters the nucleus and positively regulates transcription initiation and elongation; involved in microtubule-mediated processes, filamentous growth, ribosomal RNA maturation, and telomere maintenance; negative regulator of autophagy; activated by the scavenger decapping enzyme Dcs1p; expression regulated by Ash1p in rich conditions
	YDL075W	RPL31A	Ribosomal 60S subunit protein L31A; associates with karyopherin Sxm1p; loss of both Rpl31p and Rpl39p confers lethality; homologous to mammalian ribosomal protein L31, no bacterial homolog; RPL31A has a paralog, RPL31B, that arose from the whole genome duplication
	YOR369C	RPS12	Protein component of the small (40S) ribosomal subunit; homologous to mammalian ribosomal protein S12, no bacterial homolog
	YNR052C	POP2	RNase of the DEDD superfamily; subunit of the Ccr4-Not complex that mediates 3' to 5' mRNA deadenylation
	YJR055W	HIT1	Protein involved in C/D snoRNP assembly; regulates abundance of Rsa1p; required for growth at high temperature; similar to human ZNHIT3
	YDR138W	HPR1	Subunit of THO/TREX complexes; this complex couple transcription elongation with mitotic recombination and with mRNA metabolism and export, subunit of an RNA Pol II complex; regulates lifespan; involved in telomere maintenance; similar to Top1p
	YBL093C	ROX3	Subunit of the RNA polymerase II mediator complex; associates with core polymerase subunits to form the RNA polymerase II holoenzyme
	YMR263W	SAP30	Component of Rpd3L histone deacetylase complex; involved in silencing at telomeres, rDNA, and silent mating-type loci; involved in telomere maintenance
	YBR095C	RXT2	Component of the histone deacetylase Rpd3L complex; possibly involved in cell fusion and invasive growth; relocalizes to the cytosol in response to hypoxia
	YDR500C	RPL37B	Ribosomal 60S subunit protein L37B; required for processing of 27SB pre-rRNA and formation of stable 66S assembly intermediates; protein abundance increases in response to DNA replication stress; homologous to mammalian ribosomal protein L37, no bacterial homolog; RPL37B has a paralog, RPL37A, that arose from the whole genome duplication
	YMR263W	SAP30	Component of Rpd3L histone deacetylase complex; involved in silencing at telomeres, rDNA, and silent mating-type loci; involved in telomere maintenance
	YHR178W	STB5	Transcription factor; involved in regulating multidrug resistance and oxidative stress response; forms a heterodimer with Pdr1p; contains a Zn(II)2Cys6 zinc finger domain that interacts with a pleiotropic drug resistance element in vitro
	YDR289C	RTT103	Protein involved in transcription termination by RNA polymerase II; interacts with exonuclease Rat1p and Rai1p; has an RPR domain (carboxy-terminal domain interacting domain); also involved in regulation of Ty1 transposition
	YDR025W	RPS11A	Protein component of the small (40S) ribosomal subunit; homologous to mammalian ribosomal protein S11 and bacterial S17; N-terminally propionylated in vivo; RPS11A has a paralog, RPS11B, that arose from the whole genome duplication
Amino acid transport / Metabolism			
	YBR068C	BAP2	High-affinity leucine permease; functions as a branched-chain amino acid permease involved in uptake of leucine, isoleucine and valine; contains 12 predicted transmembrane domains; BAP2 has a paralog, BAP3, that arose from the whole genome duplication
	YBR069C	TAT1	Amino acid transporter for valine, leucine, isoleucine, and tyrosine; low-affinity tryptophan and histidine transporter; overexpression confers FK506 and FTY720 resistance; protein abundance increases in response to DNA replication stress
	YCR027C	RHB1	Putative Rheb-related GTPase; involved in regulating canavanine resistance and arginine uptake; member of the Ras superfamily of G-proteins

Category	Gene ID	Standard Name	References
Chaperon function			
	YLR369W	SSC2	Mitochondrial hsp70-type molecular chaperone; required for assembly of iron/sulfur clusters into proteins at a step after cluster synthesis, and for maturation of Yfh1p, which is a homolog of human frataxin
	YPL106C	SSE1	ATPase component of heat shock protein Hsp90 chaperone complex; serves as nucleotide exchange factor to load ATP onto the SSA class of cytosolic Hsp70s; plays a role in prion propagation and
Spermidine / Spermine biosynthesis			
	YOL052C	SPE2	S-adenosylmethionine decarboxylase; required for the biosynthesis of spermidine and spermine; cells lacking Spe2p require spermine or spermidine for growth in the presence of oxygen but not when grown
Mitochondrial fusion			
	YDR470C	UGO1	Outer membrane component of the mitochondrial fusion machinery; binds to Fzo1p and Mgm1p to link these two GTPases during mitochondrial fusion; involved in fusion of both the outer and inner
Proteins of unknown function			
	YHR151C	MTC6	Protein of unknown function; mtc6 is synthetically sick with cdc13-1; SWAT-GFP and mCherry fusion proteins localize to the vacuole while SWAT-GFP fusion also localizes to the endoplasmic reticulum
	YER156C	N/A	Putative protein of unknown function; interacts with Hsp82p and copurifies with Ipl1p; expression is copper responsive and downregulated in strains deleted for MAC1, a copper-responsive transcription
Dubious open reading frame			
	YGL007W	BRP1	Putative protein of unknown function; conserved among S. cerevisiae strains; located in the upstream region of PMA1; deletion leads to polyamine resistance due to downregulation of PMA1
	YDR024W	FYV1	Dubious open reading frame; unlikely to encode a functional protein, based on available experimental and comparative sequence data; not conserved in closely related Saccharomyces species; mutation
	YLR338W	OPI9	Dubious open reading frame; unlikely to encode a functional protein, based on available experimental and comparative sequence data; partially overlaps the verified ORF VRP1/YLR337C
	YNL120C	N/A	Dubious open reading frame; unlikely to encode a functional protein, based on available experimental and comparative sequence data; deletion enhances replication of Brome mosaic virus in S. cerevisiae, but
	YJL175W	N/A	Dubious open reading frame unlikely to encode a functional protein; deletion confers resistance to cisplatin, hypersensitivity to 5-fluorouracil, and growth defect at high pH with high calcium; overlaps gene
	YJR018W	N/A	Dubious open reading frame; unlikely to encode a functional protein, based on available experimental and comparative sequence data
	YDR433W	N/A	Dubious open reading frame; unlikely to encode a functional protein, based on available experimental and comparative sequence data

Table S3: Yeast strains used in this study.

	Strain	Genotype	Reference
1	BY4741	MATa his3Δ1 leu2Δ0 met15Δ0 ura3Δ0	Euroscarf KO collection
2	*sec14-1ts (CTY1-1A)*	MAT***a*** *ura3-52 lys2- 801 ∆his3-200 sec14-1ts*	Bankaitis et al., 1989
3	*pkc1-3ts (TSARRAY#541)*	MATa pkc1-3::KanR; his3Δ1 leu2Δ0 ura3Δ0 met15Δ0	received from Charly Boone
4	*sfh1 (Y7092, SN#3729)*	MATalpha ykl091cΔ0::natMX4 can1Δ0::STE2pr-Sp_HIS5 lyp1Δ0 his3Δ1 leu2Δ0 ura3Δ0 met15Δ0 LYS2+	received from Charly Boone
5	*BY4741 (Kan array, DMA#2810)*	MATa ykl091cΔ0::kanMX4 his3Δ1 leu2Δ0 ura3Δ0 met15Δ0	received from Charly Boone
6	*pkc1-3ts Y9687 TS-Query (TSQUERY#541)*	MATalpha pkc1-3::NatR can1Δ::STE2pr-Sp_his5 lyp1Δ::STE3pr-LEU2	received from Charly Boone
7	BY4741 *wsc1Δ*	MATa; ura3Δ0; leu2Δ0; his3Δ1; met15Δ0; YOR008c::kanMX4	Euroscarf KO collection
8	BY4741 *wsc2Δ*	MATa; ura3Δ0; leu2Δ0; his3Δ1; met15Δ0; YNL283c::kanMX4	Euroscarf KO collection
9	BY4741 *wsc3Δ*	MATa; ura3Δ0; leu2Δ0; his3Δ1; met15Δ0; YOL105c::kanMX4	Euroscarf KO collection
10	BY4741 *mid2Δ*	MATa; ura3Δ0; leu2Δ0; his3Δ1; met15Δ0; YLR332w::kanMX4	Euroscarf KO collection
11	BY4741 *mtl1Δ*	MATa; ura3Δ0; leu2Δ0; his3Δ1; met15Δ0; YGR023w::kanMX4	Euroscarf KO collection
12	BY4741 *rom1Δ*	MATa; ura3Δ0; leu2Δ0; his3Δ1; met15Δ0; YGR070w::kanMX4	Euroscarf KO collection
13	BY4741 *rom2Δ*	MATa; ura3Δ0; leu2Δ0; his3Δ1; met15Δ0; YLR371w::kanMX4	Euroscarf KO collection
14	BY4741 *tus1Δ*	MATa; ura3Δ0; leu2Δ0; his3Δ1; met15Δ0; YLR425w::kanMX4	Euroscarf KO collection
15	BY4741 *sac7Δ*	MATa; ura3Δ0; leu2Δ0; his3Δ1; met15Δ0; YDR389w::kanMX4	Euroscarf KO collection
16	BY4741 *bck1Δ*	MATa; ura3Δ0; leu2Δ0; his3Δ1; met15Δ0; YJL095w::kanMX4	Euroscarf KO collection
17	BY4741 *mkk1Δ*	MATa; ura3Δ0; leu2Δ0; his3Δ1; met15Δ0; YOR231w::kanMX4	Euroscarf KO collection
18	BY4741 *mkk2Δ*	MATa; ura3Δ0; leu2Δ0; his3Δ1; met15Δ0; YPL140c::kanMX4	Euroscarf KO collection
19	BY4741 *mpk1Δ*	MATa; ura3Δ0; leu2Δ0; his3Δ1; met15Δ0; YHR030c::kanMX4	Euroscarf KO collection
20	BY4741 *mlp1Δ*	MATa; ura3Δ0; leu2Δ0; his3Δ1; met15Δ0; YKL161c::kanMX4	Euroscarf KO collection
21	MML550	MATα leu2–3,112 ura3–52 trp1 his4 can1y; Pkc1GFP	Vilella et al., 2005
22	BY4742 *cho2Δ opi3Δ*	MATa his3Δ1 leu2Δ0 lys2Δ0 ura3Δ0 cho2::KanMX opi3::LEU2	Dowd et al., 2001
23	BY4742 *psd1Δ psd2Δ*	MATa his3Δ1 leu2Δ0 met15Δ0/lys2Δ0 ura3Δ0 psd1::KanMX psd2:URA3	Gift from Mesut Bilgin
24	SEY6210	MATalpha leu2-3,112 ura3-52 his3Δ200 trp1-Δ901 lys2-801 suc2-Δ9	Robinson et al., 1988
25	*pik1ts (AAY104)*	SEY6210 except pik1Δ::HIS3 and harboring pRS314pik1-83	Audhya et al., 2000
26	*stt4ts (AAY102)*	SEY6210 except stt4Δ::HIS3 and harboring pRS415stt4-4	Audhya et al., 2000
27	*mss4ts (AAY202)*	SEY6210 mss4Δ::HIS3 and harboring YCplac111mss4ts-102	Stefan et al., 2002
28	*mss4-5*	MATalpha mss4Δ::KanMX ura3-52 his3-Δ200 ade pRS315(mss4-5ts)	Nile et al., 2013
29	*rho1ts (AAY606)*	SEY6210 except rho1Δ::HIS3 carrying pRS316rho1V43T	Audhya et al., 2002
30	SEY6210.1	MATa leu2-3,112 ura3-52 his3Δ200 trp1-Δ901 lys2-801 suc2-Δ9	Manford et al., 2012
31	*tetherΔ*	SEY6210.1 ist2∆::HISMX6 scs2∆::TRP1 scs22∆::HISMX6 tcb1∆::KANMX6 tcb2∆::KANMX6 tcb3∆::HISMX6 ire1∆::NATMX	Manford et al., 2012

Table S4: Plasmids used in this study.

	Plasmid Name	Source
1	pDR195	Rentsch et al., 2005
2	pDR195-ScSEC14-V5	Schaaf et al., 2008
3	pDR195-ScSEC14^{S173P}-V5	This study
4	pDR195-ScSFH1-V5	Schaaf et al., 2011
5	pDR195-ScSFH1^{T238D}-V5	This study
6	pDR195-ScSFH1^{S175I,T177I}-V5	This study
7	pDR195-ScSFH1^{L179W,I196W}-V5	This study
8	pDR195-ScSFH1^{Y113C,T238D}-V5	Schaaf et al., 2011
9	pDR195-ScSFH1^{Y113C,S175I,T177I}-V5	Schaaf et al., 2011
10	pDR195-ScSFH1^{Y113C,L179W,I196W}-V5	Schaaf et al., 2011
11	pDR195(LEU2)	This study
12	pDR195(LEU2)-ScSFH1-V5	This study
13	pDR195(LEU2)-ScSFH1^{T238D}-V5	This study
14	pDR195(LEU2)-ScSFH1^{S175I,T177I}-V5	This study
15	pDR195-ScSFH2	This study
16	pDR195-ScSFH3	This study
17	pDR195-ScSFH4	This study
18	pDR195-ScSFH5	This study
19	pDR195-AtSFH1_Sec14D	This study
20	pDR195-AtSFH3	This study
21	pDR195-AtSFH3_Sec14D	This study
22	pDR195-AtSFH5	This study
23	pDR195-AtSFH5_Sec14D	This study
24	pAG414GPD-eGFP-AtSFH5	This study
25	pAG425GPD-Cerulean-AtSFH5	This study
26	pDR195-MmαTTP	This study
27	pDR195-HsRLBP	This study
28	pDR195-MmRLBP	This study
29	pDR195-HsSEC14L2	This study
30	pDR195-MmSEC14L2	This study
31	pDR195-RnPITPα	This study
32	pDR195-RnPITPβ	This study
33	pDR195-ScPSD1	This study
34	pDR195-ScPSD2	This study
35	pDR195-ScMSS4prom(short):MSS4	This study
36	pDR195-ScMSS4prom(long):MSS4	This study
37	pDR195-pScRHO1:RHO1	This study
38	pC-186_pRHO2:ScRHO2	Madaule et al., 1987
39	pCS321: pRS416_MSS4prom:MSS4-GFP	Audhya et al., 2003
40	pRS424-GFP-2xPH(Osh2)	Stefan et al., 2011
41	pRS424-GFP-FYVE(EEA1)	Burd et al., 1998
42	pRS426-GFP-2×PH(PLCd)	Stefan et al., 2002
43	pRS416-GFP-LactC2	Fairn et al., 2011
44	pRS414-AHSpo20(51-91)-GCCGMAP210 (39-377)-GFP	Horchani et al., 2014
45	pRS415-mCherry-P4C	Gift from Chris Stefan

46	pRS415-TCB3-GFP (pAM43)	Manford et al., 2012
47	pBP73-G: pRS416-GFP-P4C	Luo et al., 2015
48	YCpLac11-mCherry-Rho1	Fernandez-Acero et al., 2015
49	pDR199-mRFP-AtSFH1-Nlj16	Gift from Marília de Campos
50	pDR195-TaPSS1	This study
51	pET28-ScSFH1	Schaaf et al., 2008
52	pET28-ScSFH1^{T238D}	This study
53	pET28-ScSFH1^{S175I,T177I}	This study
54	pET28-ScSec14	Schaaf et al., 2008

Supplemental References

1. Rentsch D, Laloi M, Rouhara I, Schmelzer E, Delrot S, Frommer WB. NTR1 encodes a high affinity oligopeptide transporter in Arabidopsis. Febs Lett. 1995;370(3):264-8.
2. Schaaf G, Ortlund EA, Tyeryar KR, Mousley CJ, Ile KE, Garrett TA, et al. Functional anatomy of phospholipid binding and regulation of phosphoinositide homeostasis by proteins of the sec14 superfamily. Mol Cell. 2008;29(2):191-206.
3. Schaaf G, Dynowski M, Mousley CJ, Shah SD, Yuan PH, Winklbauer EM, et al. Resurrection of a functional phosphatidylinositol transfer protein from a pseudo-Sec14 scaffold by directed evolution. Mol Biol Cell. 2011;22(6):892-905.
4. Audhya A, Emr SD. Regulation of PI4,5P2 synthesis by nuclear-cytoplasmic shuttling of the Mss4 lipid kinase. Embo J. 2003;22(16):4223-36.
5. Fairn GD, Schieber NL, Ariotti N, Murphy S, Kuerschner L, Webb RI, et al. High-resolution mapping reveals topologically distinct cellular pools of phosphatidylserine. The Journal of cell biology. 2011;194(2):257-75.
6. Stefan CJ, Audhya A, Emr SD. The yeast synaptojanin-like proteins control the cellular distribution of phosphatidylinositol (4,5)-bisphosphate. Mol Biol Cell. 2002;13(2):542-57.
7. Horchani H, de Saint-Jean M, Barelli H, Antonny B. Interaction of the Spo20 Membrane-Sensor Motif with Phosphatidic Acid and Other Anionic Lipids, and Influence of the Membrane Environment. Plos One. 2014;9(11).
8. Burd CG, Emr SD. Phosphatidylinositol(3)-phosphate signaling mediated by specific binding to RING FYVE domains. Mol Cell. 1998;2(1):157-62.
9. Luo X, Wasilko DJ, Liu Y, Sun J, Wu X, Luo ZQ, et al. Structure of the Legionella Virulence Factor, SidC Reveals a Unique PI(4)P-Specific Binding Domain Essential for Its Targeting to the Bacterial Phagosome. PLoS Pathog. 2015;11(6):e1004965.
10. Fernandez-Acero T, Rodriguez-Escudero I, Molina M, Cid VJ. The yeast cell wall integrity pathway signals from recycling endosomes upon elimination of phosphatidylinositol (4,5)-bisphosphate by mammalian phosphatidylinositol 3-kinase. Cell Signal. 2015;27(11):2272-84.
11. Madaule P, Axel R, Myers AM. Characterization of two members of the rho gene family from the yeast Saccharomyces cerevisiae. Proceedings of the National Academy of Sciences of the United States of America. 1987;84(3):779-83.

Data S1: Information about PixelAnalysis.

Introduction

In order to partially automate the collection of membrane/intracellular fluorescence ratios in micrographs of fluorescently labelled cells a small program was developed in MATLAB 2016a (The MathWorks Inc., Natick, MA, USA). The program's main feature is the automatic identification of membrane and intracellular regions in cells with bright membrane (= high pixel intensity) and dark intracellular (= low pixel intensity).

The program features an intuitive UI and straight-forward operation with only simple user interaction. After a (high-resolution) digital image of cells has been imported to the program, the user can manually select a linear region of interest (ROI) across a single cell or between cells in the micrograph. The pixel intensities along this ROI are then analyzed in order to automatically discover membrane peaks and intracellular regions in the pixel intensity profile. In order to calculate the membrane/intracellular fluorescence ratios, first the pixel intensity of the intracellular region is determined by calculating the average intensity of all pixels in the intracellular region. The average intensity of the membrane is determined analogously by calculating the average intensity of the "right" and "left" membrane peaks. Finally, the membrane/intracellular fluorescence ratio is calculated by dividing average membrane pixel intensity by average intracellular pixel intensity.

Background Information

In order to prepare the micrograph for automatic identification of membrane peaks and intracellular regions the overall image is first converted to grayscale. Then, the image is sharpened; brightness and contrast are adjusted in order to reduce noise in the micrograph. For a finer resolution and easier downstream processing, the image is interpolated to a five-fold resolution. After the user has selected a ROI, an index is assigned to each pixel along the one-dimensional ROI line. The intensities of these pixels constitute the original data, which is stored for further use downstream.

In order to find the index of the membrane peaks and the start and end indexes of the cytosol region, the pixel data along the ROI line is processed further. First, a continuous graph is created from the raw pixel intensity values along the ROI by interpolating a spline between the discrete pixel values. Next, a 0.8 order fractional derivative is calculated using `fgl_deriv()`, a MATLAB function for fractional derivatives developed by Jonathan Hadida

(MathWorks File Exchange #45982; https://www.mathworks.com/matlabcentral/fileexchange/45982-fractional-derivative). This derivative is then integrated again using MATLAB's `trapz()` function which implements a trapezoidal numerical integration method. Subsequently, noise is reduced by applying a median filter to the data.

In order to find membrane peak candidates, MATLAB's `findpeaks()` function is used to detect local maxima in the resulting graph with the requirement that they are higher than the background noise and have a certain minimum prominence. The actual membrane peaks are then selected from the candidates by looking for the peaks with the highest slopes towards left or right (i.e. versus background), respectively. Using the indexes of the automatically discovered membrane peaks, each peak's original pixel intensity is then obtained from the original data (see above).

When analyzing pixel intensities across single cells, the cytosol pixels are required to be located between the two membrane peaks. During analyses it became evident that there usually are several small peaks in the pixel intensities between membrane peak and cytosol baseline. The first small peak with an intensity below 75 % of the highest membrane peak's intensity is declared to be the start (and end, respectively) of the cytosol region. The cytosol region is made up of all the pixels between the start and end pixel. Analogous to the treatment of the peaks, the original raw pixel data of each pixel in the membrane region is obtained by index.

When analyzing pixel intensities between cells, the automatic discovery of membranes and cytosol is performed in a similar way as described above. However, it is assumed that the ROI line starts in the first cell's cytosol and ends in the second cell's cytosol with the membranes of both directly adjacent cells being somewhere in between. Thus, when the membranes have been detected as described, the cytosol region is assumed to be in the pixels from ROI start to first membrane and from second membrane to ROI end.

The original pixel intensities of membrane and cytosol are then each averaged, and the membrane/cytosol intensity ratio is calculated. For each automatic processing step a graph is displayed for the user indicating where membrane peaks and cytosol region have been detected automatically. If the automatic detection is suboptimal, the user can freely change the position of each peak and the start and end position of the cytosol region.

Usage

The program can be executed on any Windows 64-bit system using the binaries provided here. During installation the installer will offer to download a free MATLAB runtime environment for the program. Users who have a MATLAB license of their own – including all

required toolboxes (Signal Processing Toolbox, Image Processing Toolbox) – can also execute the program from source.

After the program has been started, first import a digital micrograph. Generally, any image format should work (e.g. TIFF, JPG, BMP) but it is recommended that a high-quality, high-resolution image is used for analyses. Next, select whether automatic analyses should be performed across a single cell (e.g. yeast cells) or between two adjacent cells in a tissue. When analyzing across single cells it is recommended that each cell is surrounded by a dark background. Press the “Analyze Cells” button and start placing ROI lines in the micrograph displayed in the newly created image window. For this, click the left mouse button once to select a start point for the ROI line, keep the mouse button pressed, move the mouse cursor to the position where the ROI line should end and release the button. Double click on the ROI line to confirm the selection or drag the line around the image to place it somewhere else. After the ROI line is confirmed a new window displaying a graph will open. In this window the intensities of the pixels along the ROI line are displayed in blue with the start point of the ROI line being on the left-hand side, the end point being on the right-hand side. The automatically detected membrane peaks and the cytosol region are displayed in red on the graph. There is no need to confirm the ROI line – the intensity ratio is saved in the background. Continue by drawing a new ROI line in the image. Alternatively, the last ROI line can also be discarded entirely by clicking the “Discard Last” button. By clicking the “Analyze Manually” button the membrane peaks and cytosol region can also be selected manually in the graph window. In both cases, by clicking “Analyze Cells” ROI line can be placed in the image window again. In the end, the intensity ratio data can be exported in a CSV file by clicking the “Save Data” button. Additionally, a version of the originally imported micrograph with all the ROI lines drawn on it and all pixel intensity graphs which were used to calculate these ratios are exported for reference – every graph and ROI line being numbered. In order to quit the program, simply click the “Quit” button.

A new micrograph can be imported by simply clicking the “Load Image” button – it is not necessary to close the application in between images. When a new image is imported, the previous image’s data will be stored in a user-selected directory before the new image is displayed.